UNIVERSITE MATIERE BRETAGNE MOLECULES LOIRE ET MATERIAUX

UNIVERSITÉ DE NANTES

THESE DE DOCTORAT DE

L'UNIVERSITE DE NANTES
COMUE UNIVERSITE BRETAGNE LOIRE

ECOLE DOCTORALE N° 596
Matière, Molécules, Matériaux
Spécialité : Physique

Par
Maddalena MAIETTA

Radioprotection aspects associated to radionuclides for medical applications

Thèse présentée et soutenue à l'Université de Nantes, le 13 Décembre 2018
Unité de recherche : Laboratoire Subatech - UMR 6457
Thèse N° :

Rapporteurs avant soutenance :

Helmut Vinke Professeur, Université de Graz (Graz, Autriche);
Chercheur, Organisation Européenne pour la Recherche Nucléaire (CERN), Genève (Suisse)
Daniel Cussol Directeur de recherche, Centre National de la Recherche Scientifique (CNRS),
Université de Caen Normandie (Caen, France), Laboratoire de physique corpusculaire de Caen

Composition du Jury :

Président :
Ulli Köster Chercheur, Institut Laue-Langevin, Grenoble (France)

Examinateurs :
Thierry Stora Chercheur, Organisation Européenne pour la Recherche Nucléaire (CERN), Genève (Suisse)
Nunzio Burgio Chercheur, Ente Nazionale Energie Alternative (ENEA), Centre de recherche Casaccia – Rome (Italy)

Dir. de thèse :
Ferid Haddad Professeur, Université de Nantes, SUBATECH. Directeur, GIP ARRONAX (France)

Co-dir. de thèse:
Sébastien Avila PhD, Ingénieur, Lemer Pax Company (France)
Arnaud Cadiou Ingenieur, Laboratoires Subatech (France)

Contents

Introduction **1**

1 The Radionuclides in Medicine **5**
1.1 Historical overview . . . 5
1.2 The main principles of radioactivity . . . 8
1.2.1 The Bateman Equation . . . 10
1.2.2 Radioactive equilibrium . . . 11
1.2.3 Types of radioactive decay . . . 13
1.2.4 Radiation-Matter interaction . . . 15
1.3 Dose Quantities in Radiological Protection . . . 26
1.4 Methods for Dose calculations . . . 30
1.4.1 The MCNPX Method . . . 32
1.5 The radioprotection principles . . . 33
1.6 The characteristics of the radionuclides in medicine . . . 35
1.7 The places of production . . . 37

2 The transport of radionuclides for medicine: a type B container as case study **41**
2.1 The risks in the transport of radioactive materials and the Regulation . . . 43
2.2 The safety aspects during the transport . . . 43
2.3 General characteristics and classification of the packages . . . 44
2.4 The design of a package for RAM transport . . . 48
2.5 The ColiBRI-30 . . . 50
2.5.1 Specifications of the package . . . 50
2.5.2 The iterative process in this design . . . 54
2.5.3 Technical description of the package . . . 62
2.5.4 The contents and the calculation of the activities to transport . . . 64
2.5.5 The Finite Element Analysis for the design's validation of the Overpack . . . 81
2.5.6 Results of the Finite element Analysis . . . 86
2.5.7 The regulatory tests planning . . . 99
2.5.8 Administrative steps for the approval . . . 100
2.6 Conclusions . . . 101

3 The Radioprotection after the collection: the waste management **105**
3.1 Radioactive waste: definition and classification . . . 106
3.1.1 The situation in France . . . 108
3.2 The basic principles of Activation . . . 110
3.3 The ARRONAX Cyclotron . . . 112
3.4 The study of the materials' activation in the ARRONAX bunker . . . 114
3.4.1 The irradiation device . . . 115
3.4.2 The software ActiWiz . . . 116
3.4.3 The fluence simulation with MCNPX . . . 119
3.5 Examples of application . . . 128
3.5.1 The analysis of the rabbit . . . 131
3.6 Conclusions and future perspectives . . . 145

4 Calculation of Transport limits with the Q-System **147**
4.1 Introduction and background . . . 147
4.2 Methodology for calculating A_1 and A_2 defined by IAEA . . . 150
4.2.1 The basis of the Q-System . . . 150
4.2.2 Calculation of Q_A: External dose due to photons . . . 151
4.2.3 Calculation of Q_B: External dose due to beta emitters . . . 152
4.2.4 Calculation of Q_C : Internal dose via inhalation . . . 153
4.2.5 Calculation of Q_D: Skin contamination and ingestion dose . . . 154
4.2.6 Calculation of Q_E: External exposure in air . . . 155
4.2.7 Special considerations . . . 155
4.3 Calculation of A_1 and A_2 with Monte Carlo method . . . 156
4.3.1 Calculation of Q_A with the MC . . . 158
4.3.2 Calculation of Q_B with the MC . . . 160
4.3.3 Calculation of Q_D with the MC . . . 162
4.3.4 Example of application: Calculation of the Q-values for Y-90 . . . 163
4.3.5 Results of the A_1 and A_2 limit with the Monte Carlo technique . . . 169
4.4 Conclusions and Future perspectives . . . 175

Conclusions **177**

A The Isotope's collection: a study on the MEDICIS collection point **183**
A.1 The CERN-MEDICIS facility . . . 184
A.2 The Isotope collection in MEDICIS . . . 185
A.2.1 The main principles/ ideas . . . 185
A.3 The original project . . . 188
A.3.1 The layout . . . 188
A.4 The actual system . . . 192
A.5 Conclusions . . . 194

B **197**
B.1 Dictionary of RAM transport . . . 197
B.2 The basic principles of the Finite element analysis (FEA) . . . 199
B.2.1 The ANSYS simulation: a description of the basic steps . . . 200
B.3 Tables of physical characteristics of the materials involved in the FEA of the ColiBRI-30 204
B.3.1 Mechanical data of the ColiBRI's screws . . . 204
B.3.2 Engineering data for Thermal calculations . . . 205
B.3.3 Engineering data for Mechanical calculations . . . 206

C **207**
C.1 Tables with MCNPX results for monoenergetic source particles . . . 207
C.1.1 For Q_A calculations . . . 207
C.1.2 For Q_B calculations . . . 209
C.1.3 For Q_D calculations . . . 210
C.2 Example of MCNPX code for beta dose calculation . . . 212

Bibliography **215**

Acknowledgements **221**

Introduction

The development of the so-called theragnostic approach, in which imaging information are used to define the therapeutic strategy, is driving the increasing use of radionuclides in nuclear medicine.
Each radionuclide has its own way of production. They are generally extracted from stable or radioactive target bombarded with a particle beam. Implanted on solid or liquid samples, the radionuclides are transported to the radiopharmacy.
Here the radionuclide is chemically bound to a stable molecule or compound chosen for its ability to localize in a specific organ system. The combination of the radionuclide bound to a molecule or compound is known as a radiopharmaceutical. The last phase of this cycle consists in the human injection for treatments in hospitals or in animals for preclinical studies.
In each phase of the radionuclides production chain the workers shall guarantee that all operations are arranged to fulfill all requirements and regulations to keep the dose as low as reasonably achievable. This is the main principle of the radioprotection, generally called ALARA using the acronym. The justification and the optimization of the procedures are necessary to limit and prevent accidents.

For the radionuclides to use in nuclear medicine, production sites are different from radiopharmacy site and/or hospital. A transport of radioactive material is then needed. In biomedical applications, type A containers are used most of the time to ship radiopharmaceuticals as for example for the FDG transportation.
It is important to verify that needed activities do not exceed the values defined for type A or industrial packages by the International Atomic Energy Agency (IAEA).
IAEA Regulation establish, for each radionuclide, a limit in activity that it is possible to transport with a type A package, called A1 (for special form sources, i.e. certified perfectly sealed and encapsulated sources) and A2 (for non-special form sources). This limit can be easily reached if the activity to transport is high or if the radionuclide of interest is "exotic", which mean that no calculation where done and a low and generic limit was fixed. This latter case exists for some of the non-conventional radionuclide of interest in medicine. When the source exceeds those values, a type B container is needed. There is then a need for the development of a new container to transport them safely according to the international regulations.
The type B used for medical radionuclides shall be not only safe but also compact and easy to handle in sites like radiopharmacy, characteristics not found in the typical tybe B used for the transport of the spent fuel.
The main scope of this PhD is the design of a new type B container for the transport of medical isotopes. The IAEA Regulation defines a set of design and performance requirements that the new packages must comply with in order to obtain the homologation. Before any container for transporting nuclear materials is given a license for its use, a safety submission has to be approved by the designated competent authority. It must demonstrate that the package satisfies all the regulations for the transport of nuclear materials and explain all the theoretical studies done on the package. Moreover specific test must be performed on it, simulating, for the Type B, accidental and normal conditions of transport. The design phase is characterized by the use of finite element analysis to simulate the regulatory test conditions and adjust the shape and the material characteristics. In this way it is possible to validate and assure the good performance of the package in-silico before the (more expensive) real tests.

For some isotopes the transportation limits are not available or tabulated and general values are used to limit the activity to transport. In most cases they are very conservative quantities and their estimate is not based on specific calculations. In some other cases, the listed limits seem to be too conservative and their calculation is based on old nuclear databases or empiric or complex formulae.
The non-tabulated values, and in general the A1/A2 limit, can be evaluated following the so-called

Q-system. An objective of the present work is the research of new limits using Monte Carlo techniques, and in particular the software MCNPX ,to evaluate dose rate values in different regulatory scenarios.

The previous works are perfectly included in a wider framework characterizing this PhD. It is connected to the study of different aspects of the radiation protection of the workers during the phases of the radionuclides production. In particular some aspects of the collection phase and the post-collection have been analyzed.
In the first year of this PhD a joint group CERN-Lemer Pax-Arronax has been involved on the design of the collection chamber for the CERN-MEDICIS, a brand new off line separation facility connected to the preexisting ISOLDE. The main steps of the collection procedures and a layout of the collection point have been detailed in a specification documents, including the operational steps and the radioprotection requirements.

The process of radionuclides' production and collection has as main consequence the production of highly activated materials to be treated and disposed as waste. This is an important task in the management of a facility both during his lifetime and during the decommissioning phase.
The disposal of radioactive waste shall follow the laws and the guidelines imposed by the single countries. In general to establish the sorting center and the type of treatment to apply before the storage, a precise identification of the radionuclide inventory and its activity level is necessary.
A tool for a proper definition of the level of hazard has been recently developed at CERN. This software, called ActiWiz, can be customized for irradiation scenarios different from the ones found at the CERN accelerator complex. This tool has been applied to one of the bunkers of the Arronax Cyclotron and in particular tested with real radioactive objective.

This research project has been supported by a Marie Sklodowska-Curie Innovative Training Network Fellowship of the European Commission's Horizon 2020 Programme under contract number 642889, "MEDICIS-PROMED". It is under the supervision of the Lemer Pax Company, the GIP Arronax and the Subatech Laboratory.
MEDICIS-Promed has the scope to train a new generation of 15 entrepreneurial scientists, which will be able to bridge the different disciplines across fundamental research institutions, private companies and hospitals. All enrolled in PhD fellowship with different subjects and different sectors of the research, the students attended specialized schools and shared their knowledges during the organized training meetings. Thanks to periods called of "secondments", they also had the possibility to spend time in another Institution partner of the Network for at least three months.
The present work, in particular, benefited from the collaboration with CERN.

The plan of the thesis

The scope of this thesis work is to investigate several aspects of the radioprotection of the public and the workers during the cycle of the radionuclide production. In particular four main subjects, corresponding to the arguments treated in each chapter, can be highlighted:

1. The work starts with the clarification of all the phenomenae involved in the interaction of the particles with matter. The rules and the limit to use in radioptoection are highlighted in the Chapter 1. The radionuclides to use in nuclear medicine have specific physical and chemical characteristics. They may be produced with different techniques and particles accelerators.

2. The objective of the Chapter 2 is the detailed explanation of the **design of a new shielded container** for the transport of the irradiated sources. This study started with the identification of the radionuclides to transport and the specifications a new package must comply with. The design made use of two main techniques to asses the optimal performance of the package: Monte Carlo simulations for the radiosafety study and Finite Element Analysis for the mechanical and thermal assessments. The process of the design ended with the planning of experimental tests to perform on the package and with the redaction of the safety documents and technical reports to submit to the authorities.
3. The phase of the shipment is highly regulated. IAEA defines for each isotope a **limit of activity** it is possible to transport with the different type of package. As said before, in some cases those values are not tabulated and generic ones are used. Those limits depend on the hazard of the type of particle and energy emitted in the decay and can be properly calculated with Monte Carlo techniques. This study has been done for several radionuclides of interest for nuclear medicine and it is detailed in the Chapter 3.
4. The work with radioactivity leads to the **materials and tools activation**. The particular case of the Arronax Cyclotron will be discussed in the Chapter 4 as well as the application of the software ActiWiz as tool to predict and analyze the waste with some examples of application.

The Appendix A analyzes an example of the **collection** phase, in particular the one taking place in the recently commissioned CERN facility called Medicis. The devices and the beam instrumentation used for these purposes shall limit the dose to the personnel and possibly the human intervention. The main principles of the proposed design and the actual device are presented.

1 The Radionuclides in Medicine

Contents

1.1 Historical overview **5**
1.2 The main principles of radioactivity **8**
1.2.1 The Bateman Equation 10
1.2.2 Radioactive equilibrium 11
1.2.2.1 Radionuclide generator 11
1.2.3 Types of radioactive decay 13
1.2.4 Radiation-Matter interaction 15
1.2.4.1 Non Charged Particles: Photons 15
1.2.4.2 Non Charged Particles: Neutrons 19
1.2.4.3 Charged Particles 23
1.3 Dose Quantities in Radiological Protection **26**
1.4 Methods for Dose calculations **30**
1.4.1 The MCNPX Method 32
1.5 The radioprotection principles **33**
1.6 The characteristics of the radionuclides in medicine **35**
1.7 The places of production **37**

In this chapter an overview on the medical physics history is presented with also an explanation of the reasons and the needs of radionuclides for medical purposes.
The physical and chemical factors that guide the choice of the right radioisotope are presented in the first sections as well as some basic details on how they are produced.
The second part of this chapter is dedicated to the definition of several quantities used in radioprotection and set by the International Commission on Radiation Units and Measurements (ICRU) for public and workers. These quantities have been used extensively during this work. This work has the scope to show the radioprotection constraints and the methods used to deal with potential hazards in the different steps of the radionuclide collection. This is done always keeping an eye on the Regulation and radiological limits imposed other than the good practices of work.

1.1 Historical overview

As the development of any other fields of science, the history of nuclear medicine and of the physics at its base, is a complex topic involving the contributions from a large number of scientists, engineers,

and physicians, filled with names of Nobel Price winners.
The origins of nuclear medicine can be traced back to the last years of the19^{th} century with the discovery of radioactivity by Henri Becquerel (1896) and of the radium by Marie and Pierre Curie (1898) [1]. These developments came right after the discovery of X rays in 1895 by Wilhelm Roentgen. They were quickly adopted for medical applications and used to make images in which the radiation was transmitted through the body and imprinted into photographic plates. This allowed doctors to see for the first time "inside" the human body noninvasively, particularly useful for the imaging of bone. X-rays soon became the method of choice for producing radiographs because images could be obtained more quickly and with better contrast than those provided by radium or other naturally occurring radionuclides available at that time. Even if the field of the diagnostic X-ray imaging rapidly gained acceptance, nuclear medicine had to wait some years for further developments.

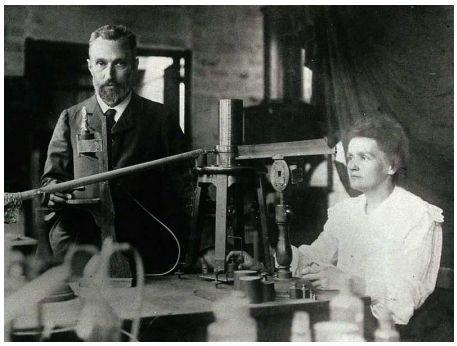



Figure 1.1: On the left Pierre and Marie Curie in their Laboratory. On the right an image of the Roentgen laboratory.

The biologic foundations of nuclear medicine can be set between 1910 and 1945. In 1923, Georg de Hevesy developed the principles of the radiotracer approach [2] and was the first to apply them to a biologic system, studying the absorption and translocation of radioactive lead nitrate in plants [3]. The first human study employing radioactive tracers was probably that of Blumgart and Weiss (1927) [4], who injected an aqueous solution of radon intravenously and measured the transit time of the blood from one arm to the other using a cloud chamber as the radiation detector. In the 1930s, with the invention of the cyclotron by Lawrence it became possible to artificially produce new radionuclides, extending in this way the range of biologic processes that could be studied [5]. Once again, de Hevesy was at the forefront of using these new radionuclides to study biologic processes in plants and in red blood cells. Finally, at the end of the Second World War, the nuclear reactor facilities that were developed as part of the Manhattan Project started to be used for the production of radioactive isotopes in quantities sufficient for medical applications.
In 1950s the development of technology allowed to obtain images of the distribution of radionuclides in the human body with more advanced methods. Major milestones included the development of the rectilinear scanner in 1951 by Benedict Cassen [6] and the Anger camera, the forerunner of all modern nuclear medicine single-photon imaging systems, developed in 1958 by Hal Anger [7]. In 1951, the use of positron emitters and the advantageous imaging properties of these radionuclides also were described by Wrenn and coworkers [8].
Until the early 1960's, nuclear medicine primarily used I-131 in the study and diagnosis of thyroid disorders and an assortment of other radionuclides that were individually suitable for only a few specific organs. The use of Tc-99m for imaging in 1964 by Paul Harper and colleagues [9] changed this line and was a major turning point for the development of nuclear medicine. Today Tc-99m is still the most widely used radionuclide in nuclear medicine applications [10]. An important development was

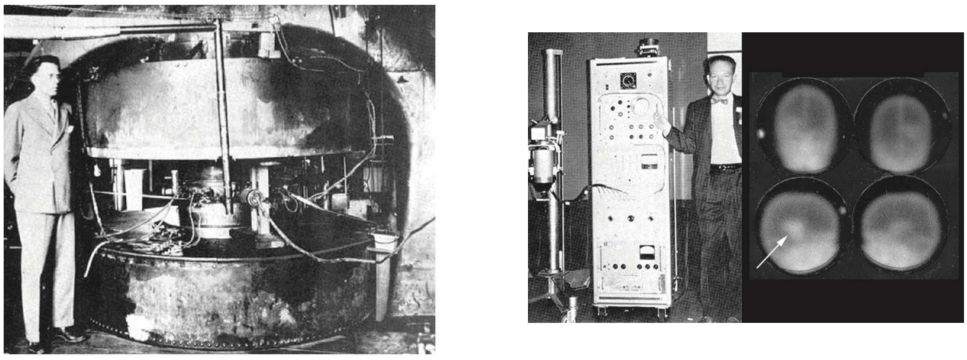

Figure 1.2: On the left Ernest O. Lawrence standing next to his invention, the first cyclotron (Berkeley, CA) [11]. On the right Anger with the first gamma camera in 1958 and a Tc-99m brain scan of a patient (Vanderbilt University Hospital, 1971) [12]. A glioma is indicated by an arrow in one of the views [13].

done in the 70's in the field of the mathematics used to reconstruct tomographic images from a set of angular views around the patient. This revolutionized the whole field of medical imaging (leading to CT, PET, SPECT and MRI) because it replaced the two-dimensional representation of the three-dimensional radioactivity distribution, with a true three-dimensional representation. This allowed the development of PET by Phelps and colleagues and SPECT by Kuhl and colleagues and marked the start of the modern era of nuclear medicine [14].
The birth and the technical improvement of imaging techniques supported the studies on new radiotracers. In 1978 Dr Tatsuo Ido and his colleagues of the Brookhaven National Laboratory, published their results on the synthesis of the tracer composed by glucose labeled with F-18 (FDG, fluorideoxy-glucose) [15]. This substance is still the most adopted $\beta+$ emitter used to study the glucose metabolism in neurology, oncology and cardiology. FDG is a molecule with structure close to the glucose and can be captured by tumor cells, most of the time high consumer of sugar. The presence of a radioactive marker allows the localization of the substance, and then the tumor, from the detection of the emitted gamma rays.
The modern nuclear medicine is characterized by many studies aiming to merge therapy and diagnostic imaging properties. This is the environment of the so called "theranostic". Even if this term has been coined in 1998 (by John Funkhouser) [16], in practice this concept dates back more than 60 years. In 1941, Saul Hertz was the first to use I-131 also for therapeutic purposes in patients with hyperthyroidism and later for those with thyroid cancer [17]. In 1951, the U.S. Food and Drug Administration (FDA) approved sodium iodide for use in patients with thyroid disease.
In a specific diagnostic test the imaging radionuclide can show a particular molecular target on a tumor, allowing a therapy agent to specifically target that receptor. The fusion of imaging and therapy allows also to follow the patient response during the therapy.
More recently the principle of theranostic has been applied to neuroendocrine tumors using compounds specifically targeting somatostatin receptors for example with the use of the pair Ga-68 DOTATATE (PET imaging)/Lu-177 DOTATATE (therapy) [18]. Over the past few years, further development in this field has seen an increasing number of theranostic treatments being made available. Other possible pairs of radionuclides for such theranostic approach are Tc-99m/Re-186, Sc-44/Sc-47 or Cu-64/Cu-67.

1.2 The main principles of radioactivity

It is important at this first stage to recall some basic concepts of radioactivity, defining concepts that will be used later in this work.
Radioactivity is a spontaneous process by which an unstable nucleus (parent) emits radiation (particle or electromagnetic radiation) and transforms into a more stable nucleus (daughter) that may or may not be stable. The unstable daughter nucleus will decay through a further decay series until a stable nuclear configuration is reached.
All radioactive processes are governed by the same formalism based on two main quantities [19]:

- The **radioactive decay constant** λ that is the characteristic parameter for each radioactive decay process with dimensions of reciprocal time (s^-1);
- The **activity A(t)**, representing the total number of decays (or disintegrations) per unit time and measured in Becquerel (1 Bq= 1 disintegration/s). The old unit of activity, the curie (Ci), was initially defined as the activity of 1 g of ^{226}Ra (1 Ci = 3.7 x 10^{10} s^{-1}).

Those two quantities are linked in the following formula:

$$A(t) = \lambda N(t) \tag{1.1}$$

where N(t) is the number of identical radioactive atoms at the time t.
Let's consider the simpler transformation of an unstable parent P into a stable daughter D with decay constant λ_P. The rate of depletion of the number of radioactive parent nuclei, N_P, is equal to the activity of radioactive parent, A_P(t), at time t:

$$\frac{dN_P}{dt} = -A_P(t) = -\lambda_P N_P(t)$$

This differential equation for N_P can be written in integral form as follow:

$$\int_{N_P(0)}^{N_P(t)} \frac{dN_P}{N_P} = -\int_0^t \lambda_P dt$$

with $N_P(0)$ is the initial condition represented by the radioactive parent nuclei at the time t=0.
Assuming λ_P constant, the equation 1.2 can be solved as:

$$N_P(t) = N_P(0)e^{-\lambda_P t}$$

And using the equation 1.1 defining the activity:

$$A_P(t) = \lambda_P N_P(t) = \lambda_P N_P(0)e^{-\lambda_P t} = A_P(0)e^{-\lambda_P t} \tag{1.2}$$

with $A_P(0)$ the initial activity of the radioactive substance.
The characterization of a given radioactive parent substance P make use of two special time periods called half-life ($T_{1/2}$) and mean or average life τ.
The **half-life** $(T_{1/2})_P$ of a radioactive substance P is the time during which the number of radioactive nuclei of the substance decays to half of the initial value $N_P(0)$ present at time t = 0. In the same way it can be also stated that in the time of one half-life the activity A_P(t) of a radioactive substance P decreases to one half of its initial value $A_P(0)$.

$$N_P[t = (T_{1/2})_P] = \frac{1}{2}N_P(0) = N_P(0)e^{-\lambda_P (T_{1/2})_P}$$
$$A_P[t = (T_{1/2})_P] = \frac{1}{2}A_P(0) = A_P(0)e^{-\lambda_P (T_{1/2})_P}$$

From the previous equations it is possible to obtain the relationship between the decay constant and the half-life:

$$\lambda_P = \frac{ln2}{(T_{1/2})_P} = \frac{0.693}{(T_{1/2})_P}$$

Mean (average) life τ_P of a radioactive parent P is defined as the time required for the number N_P of radioactive atoms (or its activity A_P) to fall to 1/e = 0.368 of the initial number of nuclei $N_P(0)$ (or of the initial activity $A_P(0)$):

$$N_P(t = \tau_P) = \frac{1}{e} N_P(0) = 0.368 N_P(0) = N_P(0) e^{-\lambda_P \tau_P}$$
$$A_P(t = \tau_P) = \frac{1}{e} A_P(0) = 0.368 A_P(0) = A_P(0) e^{-\lambda_P \tau_P}$$

Comparing the second and the fourth member of the previous equation, it may be noted that the exponential factor $e^{-\lambda_P \tau_P}$ shall be equal to 1/e= e^{-1}. Thus, $-\lambda_P \tau_P = 1$, and:

$$\lambda_P = \frac{1}{\tau_P} = \frac{ln2}{(T_{1/2})_P}$$

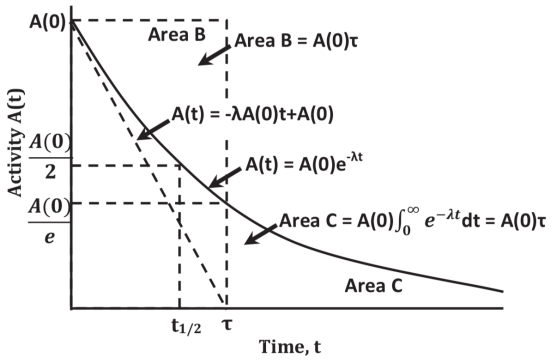

Figure 1.3: Activity A(t) plotted versus time t for a simple decay of a radioactive parent P into a its daughter D [20].

The radioactive decay of parent P into stable daughter D, discussed up to now is the simplest radioactive decay process. It is possible indeed that the radioactive parent P decays with constant λ_P into a radioactive (unstable) daughter D. This decay is followed by the one of the daughter with decay constant λ_D into another stable or unstable nucleus, called G. This results in a radioactive decay series ending with a final stable product.
In this case the decay of the parent P follows the law described by the Eq.1.2 and 1.2.
The rate of change of the number of daughter nuclei, however, is more complicated and consists of two components: one being the supply of new daughter nuclei D through the decay of P and the other coming from the loss of daughter nuclei D from the decay in G.

$$\frac{dN_D(t)}{dt} = \lambda_P N_P(t) - \lambda_D N_D(t) = \lambda_P N_P(0) e^{-\lambda_P t} - \lambda_D N_D(t)$$

Assuming as initial conditions the number of parent nuclei $N_P(t=0) = N_P(0)$ and the absence of daughters at the time t=0 ($N_D(t=0) = 0$), the solution of the previous differential equation is:

$$N_D(t) = N_P(0) \frac{\lambda_P}{\lambda_D - \lambda_P} [e^{-\lambda_P t} - e^{-\lambda_D t}]$$

Recognizing that the activity of the daughter is given by $\lambda_D N_D$, and using the Eq1.2, it is possible to obtain the following expression:

$$A_D(t) = N_P(0)\frac{\lambda_D\lambda_P}{\lambda_D - \lambda_P}[e^{-\lambda_P t} - e{-\lambda_D t}] = A_P(0)\frac{\lambda_D}{\lambda_D - \lambda_P}[e^{-\lambda_P t} - e^{-\lambda_D t}] \tag{1.5}$$

where $A_D(t)$ and $A_D(0)$ are respectively the activity of the daughter nuclei at the time t and 0. While the parent nuclei follow the exponential law of decay, the daughter's activity starts at 0, then initially rises with time t, reaching a maximum at a characteristic time $t=(t_{max})_D$, and then diminishing to reach 0 at $t=\infty$. The time for the daughter to reach the maximum activity (t_{max}) can be determined by differentiating the Eq.1.5 and setting it equal to zero:

$$(t_{max})_D = \frac{ln\frac{\lambda_P}{\lambda_D}}{\lambda_P - \lambda_D}$$

Again, the daughter D may decay in a radioactive one, G, and another series of differential equations will results for the description of its abundance with time. In particular:

$$\frac{N_G}{dt} = \lambda_D N_D - \lambda_G N_G$$

And from this, using the previous solutions:

$$N_G(t) = N_P(0)\lambda_P\lambda_D[\frac{e^{-\lambda_P t}}{(\lambda_D - \lambda_P) + (\lambda_G - \lambda_P)} + \frac{e^{-\lambda_D t}}{(\lambda_P - \lambda_D) + (\lambda_G - \lambda_D)} + \frac{e^{-\lambda_G t}}{(\lambda_P - \lambda_G) + (\lambda_D - \lambda_P)}]$$

The mathematical model describing abundances and activities in a decay chain as a function of time, based on the decay rates and initial abundances, is known as Bateman model or equation.

1.2.1 The Bateman Equation

The solutions for first three members of a radioactive series presents a recursion of similar terms, which has been generalized into a series of expressions known as the Bateman equations [21] [22]. If it is assume that at t = 0 only the parent substance is present, the number of atoms of any member of the chain at a subsequent time t is given by:

$$N_n(t) = C_1 e^{\lambda_1 t} + C_2 e^{\lambda_2 t} + C_3 e^{\lambda_3 t} + ... + C_n e^{\lambda_n t}$$

where the n-th constant C_n is:

$$C_n(t) = N_1(0)\frac{\lambda_1\lambda_2...\lambda n - 1}{(\lambda_1 - \lambda_n)(\lambda_2 - \lambda_n)...(\lambda_{n-1} - \lambda_n)}$$

These relationships can be further simplified using product notation obtaining the following general expression valid for any member of the decay series:

$$N_i(t) = N_1(0)\prod_{i=1}^{n-1}\lambda_i \sum_{i=1}^{n}\frac{e^{-\lambda_1 t}}{\prod_{i=1}^{n}(\lambda_n - \lambda_i)}$$

1.2.2 Radioactive equilibrium

In many parent P → daughter D → grand-daughter G relationships, after a certain time t the parent and daughter activities reach a constant ratio independent from the time. This condition is known as *radioactive equilibrium* and can be analyzed by examining the behavior of the activity ratio [19]:

$$\frac{A_D(t)}{A_P(t)} = \frac{\lambda_D}{\lambda_D - \lambda_P}[1 - e^{-(\lambda_D - \lambda_P)t}] \tag{1.6}$$

Three possible cases can be highlighted:

- The half-life of the daughter exceeds that of the parent: $(T_{1/2})_D > (T_{1/2})_P$ resulting in $\lambda_D < \lambda_P$. The activity ratio at the Eq.1.6 can be written as:

$$\frac{A_D(t)}{A_P(t)} = \frac{\lambda_D}{\lambda_P - \lambda_D}[e^{(\lambda_P - \lambda_D)t} - 1] \tag{1.7}$$

  The ratio of activities increases exponentially with time t, indicating that *no equilibrium* between the parent activity $A_P(t)$ and daughter activity $A_D(t)$ will be reached.

- The half-life of the daughter is shorter than that of the parent: $(T_{1/2})_D < (T_{1/2})_P$.
  The activity ratio at large t becomes constant and is then independent of time. This case is called of *transient equilibrium*.

$$\frac{A_D(t)}{A_P(t)} = \frac{\lambda_D}{\lambda_P - \lambda_D} = const > 1 \tag{1.8}$$

- The half-life of the daughter is much shorter than that of the parent: $(T_{1/2})_D \ll (T_{1/2})_P$. For relatively large time t» t_{max}, the Eq.1.8 simplifies to:

$$\frac{A_D(t)}{A_P(t)} \approx 1 \tag{1.9}$$

  The case in which the activity of the parent is identical to the one of the daughter is known as *secular equilibrium*.

1.2.2.1 Radionuclide generator

The conditions of transient equilibrium is of particular importance in nuclear medicine since it constitutes the physical base of the radionuclide generators.
As it has been shown previously, in case of secular equilibrium once the activity of the daughter reach the maximum value, after the time t_{max}, the ratio at the Eq.1.6 between the two radionuclides remains constant and both appear to decay with the same half-life of the parent.
Once equilibrium has been achieved between the parent and daughter activities, it can be cut by chemical separation (with a process called "milking" of the daughter nuclide) of the two radionuclides which will be followed by regrowth of the product radioactivity as new atoms are produced by transformation of the parent.
Generally the parent and the daughter radionuclides belong to two different chemical element with different chemical properties. The chemical separation is made with the use of resins able to adsorb the parent and not the radionuclides daughter,
This kind of devices allow to create and continuously generate the daughter radionuclides which is the

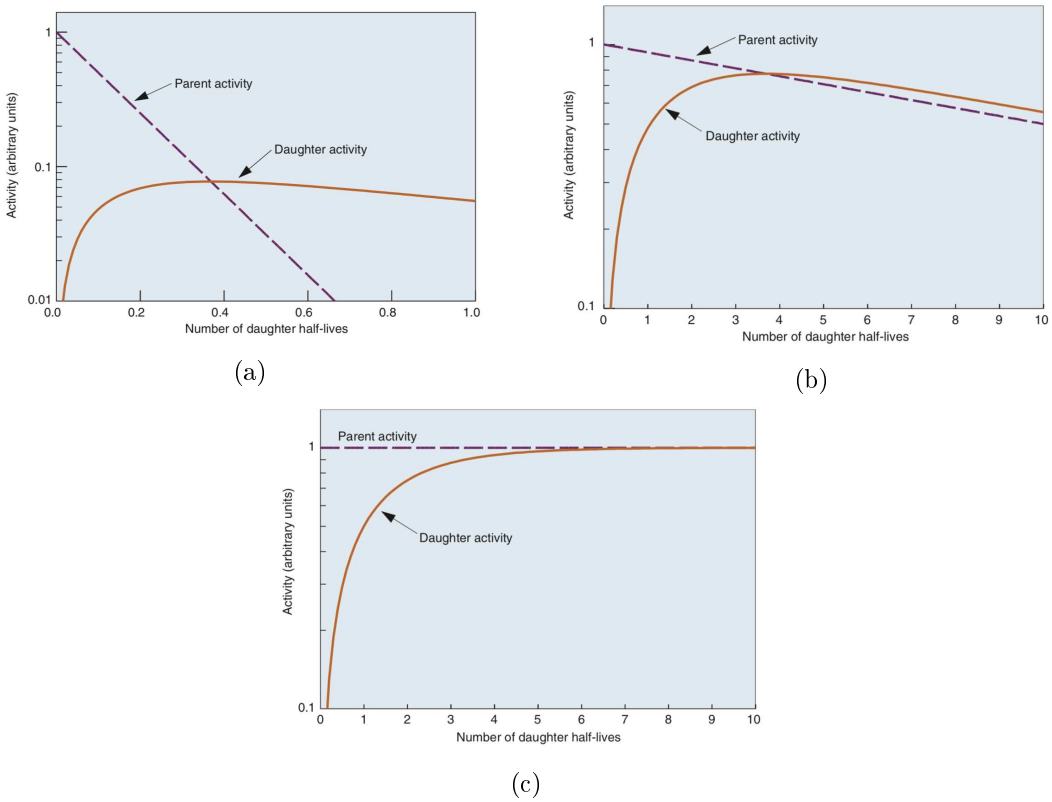

Figure 1.4: Types of parent-daughter nuclide equilibrium. a) No equilibrium, b) transient equilibrium, c) secular equilibrium [13].

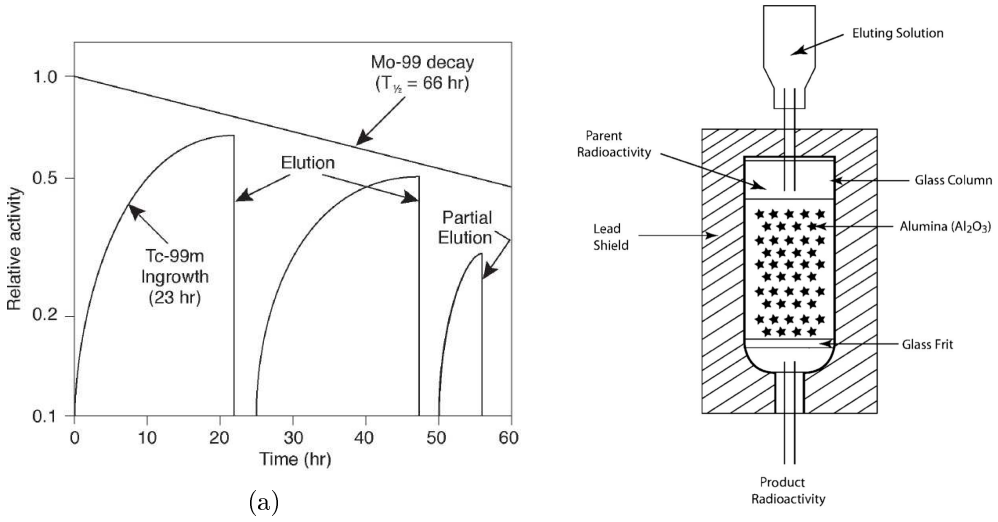

Figure 1.5: a) Regeneration of the Tc-99m at each elution within 23h, time to obtain the max Tc-99 activity. b) Schematics of a generator [20].

one used for medical purposes.
The most famous example is given by the Mo-99/Tc-99m generator (Fig.1.5a).

Tc-99 is the most used radionuclides adopted for SPECT imaging. Its short half-life (6.01 h) makes

the procurement and the logistic complex if not produced by a generator, starting from the β- decay of the long-lived Mo-99 (65.94 h).
Applying the decay equations described above, the maximum activity of the Tc-99m coming from the decay of Mo-99 is reached in about 23 hours. At this time it is possible to elute the generator and extract the Tc-99m, eliminating its activity from the resin.
A typical generator consists of a glass column filled with a suitable exchange material such as alumina (Al_2O_3) held in place with a porous glass disk and enclosed in a lead shield (Fig.1.5b) [20]. The parent radionuclide is adsorbed on the top of the alumina and the product is also retained in the matrix until it is separated from the parent radionuclide eluting with a solution that leaches the daughter radionuclide without removing the parent.

1.2.3 Types of radioactive decay

The most important radioactive decay modes are: alpha (α) decay, beta decay (including the three subprocess $\beta+$, β- and electron capture ε), and isomeric transition (IT) or internal conversion (IC), spontaneous fission (sf), proton (p) or neutron (n) decay.
Most of the previous processes are also followed by gamma emissions or radiation coming from atomic rearrangement.
The first three types of decay are the most useful in nuclear medicine since the particles emitted have short range and are able to release their energy in distances comparable with the cellular length.

- **Alpha decay:**
  In decay by α particle emission, the nucleus ejects an α particle, which consists of two neutrons and two protons (essentially a $^4_2$He nucleus). Using a standard notation it can be represented as [23]:
  $$^A_Z X \longrightarrow ^{A-4}_{Z-2} Y + \alpha \tag{1.10}$$
  The α particle is emitted with kinetic energy usually between 4 and 8 MeV. Although quite energetic α particles have very short ranges in solid matter. For example a particle with 5 MeV has a range in the soft tissue of 4,46E+01μm.
  Decay by α emission results in a transmutation of elements that is not isobaric. Atomic mass is decreased by 4. This process is common among very heavy elements that must lose mass to achieve nuclear stability. Heavy, naturally occurring radionuclides such as U-238 and its daughter products undergo a series of decays involving α and β particle emissions to transform into lighter and stable nuclides.

- **Beta- decay:**
  Radioactive decay by β- emission is a process in which a neutron in the nucleus is transformed into a proton and an electron. Schematically, the process is the following:
  $$n \longrightarrow p + e^- + \bar{\nu} + energy$$
  The electron (e^-) and the antineutrino ($\bar{\nu}$) are ejected from the nucleus and carry away the energy released in the process as kinetic energy. The electron is called β- particle. The neutrino is a particle having no mass (or a quasi-null mass) nor electrical charge. It undergoes virtually no interactions with matter and therefore is very difficult to detect [23]. Its practical consequence is to carry away some of the energy released in the decay process.
  Decay by β- emission may be represented in standard nuclear notation as:
  $$^A_Z X \longrightarrow ^A_{Z+1} Y + e^- + \bar{\nu}$$

The parent radionuclide and daughter product represent different chemical element since the atomic number increases by one. Thus β- decay results in a transmutation of elements. On the other hand the mass number A remains unchanged because the total number of nucleons in the nucleus is preserved. This is therefore an isobaric decay mode.
Some radionuclides of medical interest that undergo β- decay include I-131, Xe-133, and Cs-137.

- **Beta+ decay:**
In radioactive decay by positron emission, a proton in the nucleus is transformed into a neutron and a positively charged electron. The positively charged electron, or positron ($\beta+$), and a neutrino are ejected from the nucleus:

$$p \longrightarrow n + e^{+} + \nu + energy$$

After ejection from the nucleus, the positron loses its kinetic energy colliding with atoms of the surrounding matter and comes to rest, usually within a few millimeters from its origin in body tissues. Moreover the positron and an electron temporarily form a system called "positronium" with lifetime of approximately 10^{-10} sec. The positron then combines with the negative electron in an annihilation reaction, in which their masses are converted into energy. The mass - energy equivalent of each particle is 0.511 MeV. This energy appears in the form of two 0.511 MeV annihilation photons leaving the site of the event in two opposite directions due to the conservation of the momentum.
There is a minimum transition energy requirement of 1.022 MeV (the double of the electron mass) before a $\beta+$ decay can occur. This requirement may be understood evaluating the difference between the atomic mass of the parent and the daughter atoms. In $\beta+$ decay, a positron is ejected from the nucleus. This reduces the atomic number by one. The daughter atom has an excess electron that it must releases to reach its ground state. Thus two particles are emitted from the atom during $\beta+$ decay, and because the rest mass energy of an electron or a positron is 0.511 MeV, a total transition energy of 1.022 MeV is required.
Positron emitters are useful in nuclear medicine because two photons are generated per nuclear decay event. Furthermore, the precise directional relationship between the annihilation photons permits the use of coincidence counting techniques, the base of the PET imaging method.
In standard notation [23]:

$$^{A}_{Z}X \longrightarrow ^{A}_{Z-1}Y + e^{+} + \nu$$

It is then another isobaric decay mode, with a transmutation of elements. Examples of $\beta+$ emitters are N-13, O-15 or F-18.

The beta decays have three "bodies" in the final state: the recoil daughter nucleus, the $e^{\pm}$, and a neutrino. The daughter nucleus is much more massive than the leptons, therefore, the leptons carry off most of the energy. Consequently the emerging electron does not have a fixed energy, but its kinetic energy results in a continuum distribution, that (generally) peaks at small energies, and reaches the so-called β-endpoint.
Beta particles presents measurement problems for nuclear medicine applications.
These arise from the fact that they can penetrate only relatively small thicknesses of solid materials (es. for E=1 MeV the projected range in soft tissue is 4,2 mm).

- **Electron capture:**
Electron capture (EC) is a process called sometimes "inverse β- decay". An orbital electron is

"captured" by the nucleus and combines with a proton to form a neutron:

$$p + e^- \longrightarrow n + \nu + energy$$

The neutrino is emitted from the nucleus and carries away the transition energy. Since an electron of the orbital shell is used, the energy is compensated by the emission od characteristic X-rays and Auger electrons, which are emitted by the daughter product when the resulting orbital electron vacancy is filled.

$$e^- + {}^A_Z X \longrightarrow {}^A_{Z-1}Y + \nu$$

Like β- decay it is an isobaric decay mode leading to a transmutation of elements.
EC decay results frequently in a daughter nucleus in an excited or metastable state. A consequent γ ray (or conversion electron) may be emitted when the daughter assume the ground state. This process is called (EC, γ) decay.
Important EC and (EC, γ) radionuclides in nuclear medicine include ^{57}Co, ^{67}Ga, ^{111}In, ^{123}I, ^{125}I, and ^{201}Tl.

- **Gamma decay and Internal conversion:**
  The daughter nucleus of a radioactive parent may be formed in an excited state.
  Sometimes the excited state is relatively stable and it is called metastable or isomeric state. The decay of the excited state by the emission of a γ ray is called a gamma decay.
  Metastable radionuclides are of great importance in nuclear medicine. Due to their relatively long lifetimes, it is possible in some cases to separate them from their radioactive parent and obtain a relatively "pure" source of γ rays. This is the principles on which the Tc-99m generator are based.

  An alternative to γ ray emission is internal conversion. In this process, the nucleus decays transferring energy to an orbital electron, which is ejected instead of the γ ray and called conversion electron. These electrons usually originate from one of the inner shells (K or L), provided that the gamma energy is sufficient to overcome the binding energy of that shell. The orbital vacancy created by internal conversion is filled by an outer shell electron, accompanied by emission of characteristic X-rays or Auger electrons.

1.2.4 Radiation-Matter interaction

In radioactive decay processes, particles or electromagnetic radiation are emitted from the nucleus, leading to different effects when interacting with matter and thus with human tissues.
The emitted particles can be divided in two main classes: non charged particles (including photons and neutrons) and charged particles (alpha and beta radiation).
For both classes of particles it is possible to highlight common phenomena of radiation-matter interaction.

1.2.4.1 Non Charged Particles: Photons

The principal modes by which photons interact with matter to be attenuated and to deposit energy are by the photoelectric effect, the Compton effect, and pair production. Photons also undergo Rayleigh scattering, Bragg scattering, photodisintegration, and nuclear resonance scattering; however, these result in negligible attenuation or energy deposition and can generally be ignored for purposes of radiation protection.

1. **Rayleigh (coherent) scattering:**
   it is a type of scattering interaction that occurs between a photon and an atom as a whole. Because of the great mass of an atom, very little recoil energy is absorbed by the atom. The photon is therefore deflected with essentially no loss of energy.

2. **Photoelectric effect:**
   It is an atomic absorption process in which an atom absorbs totally the energy of an incident photon. The energy absorbed is used to eject an orbital electron from the atom, called photoelectron. The electron is ejected with an energy equal to that of the one of the incoming photon, $h\nu$, minus the binding energy of the electron in its particular orbit, an energy that must be overcome to free the electron from the atom. Since a vacancy is created in the electron shell, a characteristic X-ray will also be emitted. The kinetic energy of the ejected electron and the X-ray produced are almost always absorbed in the medium where photoelectric absorption occurs typically with another photoelectric interaction for the second.
   The photoelectric absorption coefficient τ is a function of the atomic number Z of the absorbing material (generally related to the density ρ of the absorbing medium) and the energy of the radiation as follows:
   $$\tau \cong \frac{Z^5}{E^3}$$
   It is evident that photoelectric absorption is most pronounced in high-Z materials and for low-energy photons (less than 0.5 MeV).

3. **Compton effect:**
   Compton scattering involves a collision between a photon and a "free" or very loosely bound electron in which a part of the energy of the photon is imparted to the electron. The scattered photon emerges from the collision in a new direction and with reduced energy and increased wavelength. The change in wavelength, $\lambda - \lambda'$ commonly called Compton shift, is determined only by the scattering angle [20]:
   $$\lambda - \lambda' = \frac{h}{m_0 c}(1 - cos\theta) = 0.024264(1 - cos\theta)$$
   The term h/m_0c, called the Compton wavelength, has the value $2.4264*10^{-10}$ cm.
   Energy transfer to the recoiling electron is the most important consequence of the Compton interactions since it will be absorbed locally to produce radiation dose.
   The Compton interaction coefficient, σ, is determined by electron density (which is directly related to Z) and inversely proportional to the energy E:
   $$\sigma \cong const. \times \frac{Z}{E}$$
   Compton scattering interaction is then especially important for gamma rays of medium energy (0.5-5.0 MeV) and, for low Z materials such as tissue, it can be the dominant mechanism of interaction down to 30 keV.

4. **Pair production:**
   This phenomenon is relevant for high-energy (>1.022 MeV) photons. They can interact with the strong electromagnetic field surrounding a nucleus and their energy can be converted into a pair of electron masses, one negatively charged (electron) and the other positively charged (positron). Pair production is a classic example of Einstein's special theory of relativity in which

the pure energy of the photon is converted into two electron masses. Since energy is conserved the positron and electron share the energy left (hν -1.022) after the electron masses have been formed, appearing as kinetic energy of the e^+ and e^- pair. Actually this energy is not shared equally: the positively charged nucleus repels the positive charge of the positron which provides an extra "kick", while the electron is attracted and thus slowed down with a decrease in its kinetic energy.
However this slight difference in energy is of little consequence in radiation dosimetry or detection since the available energy, hν - 1.022 MeV, will be absorbed in the medium with the same average result regardless of how it is shared.
The positron will exist as a separate particle as long as it has momentum and kinetic energy. It will interact with a negatively charged electron forming for a brief moment a particle called "positronium" which vanishes yielding two 0.511 MeV photons.
The pair production interaction coefficient k is proportional to the square of the atomic number Z for photons with energy greater than 2 x 0.511 MeV (the energy required to form an electron-positron pair):

$$k \cong constant \times Z^2(E - 1.022MeV)$$

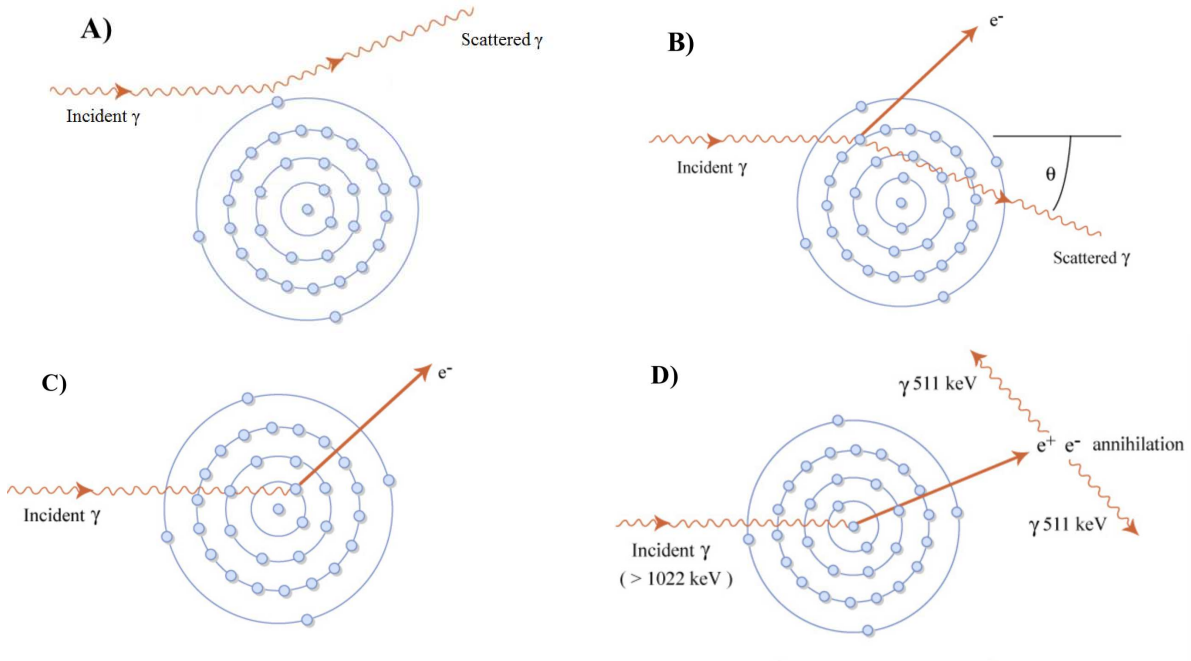

Figure 1.6: Schemes of the principal phenomenae of photon interaction with matter: A) Rayleigh scatering, B) Compton scattering, C) Photoelectric effect, D) Pair Production [13].

Those phenomena are relevant for dosimetric and radioprotection purposes since they result in the transfer of energy to electrons, which in their turn impart that energy to matter along their tracks.
The relative importance of Compton effect, photoelectric effect, and pair production depends on the energy of the photon and on the atomic number of the absorbing material (Fig.1.7). Photoelectric effect is dominant at the lower photon energies, the Compton effect takes over at medium energies, and pair production at the higher energies (above 1MeV). The dependence of those effects on Z of the absorbing material is directly connected to the choice of the shield to use: higher is the atomic number Z, higher is the probability/coefficient of absorption for gammas.

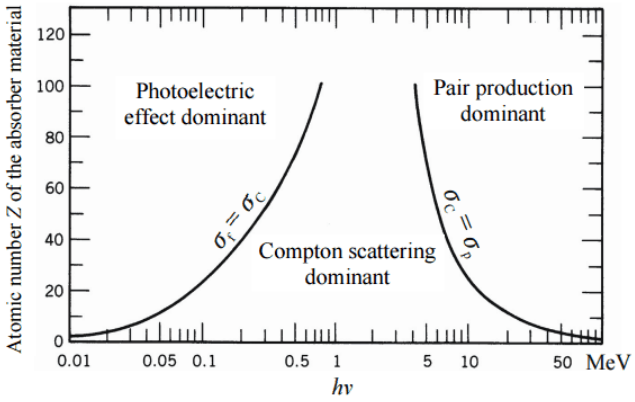

Figure 1.7: Graph representing the regions of Z and E in which each interaction predominates. The curves show where two kinds of interactions are equally probable [24].

The change in intensity (I) of a photon beam by an absorber is expressed mathematically as a decreasing function with thickness (x) of absorber (Fig.1.8):

$$\frac{dI}{dx} = -\mu I$$

where the constant of proportionality μ is the total attenuation coefficient of the medium for the photons of interest.
Considering the beam monoenergetic and the photons attenuated under conditions of "good geometry" (i.e., the beam is narrow and contains no scattered photons), then intensity I(x) of photons penetrating an absorber of thickness x (and without interaction in the medium) is found by integrating the previous equation:

$$\int_{I_0}^{I(x)} \frac{dI}{I} = \int_0^x -\mu dx$$

where I(0) is the beam intensity before entering the absorber. The previous yield to:

$$ln(I(x)) - ln(I(0)) = -\mu x$$

Or rearranging it in exponential form:

$$I(x) = I(0)e^{-\mu x} \tag{1.11}$$

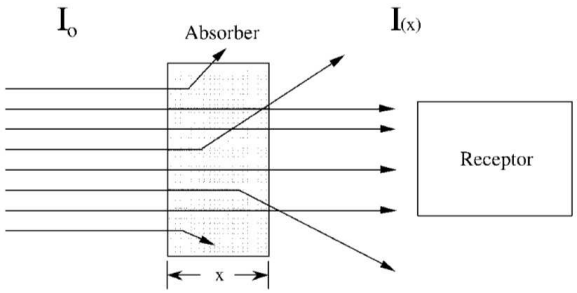

Figure 1.8

The linear attenuation coefficient μ is the probability of interaction per unit distance in an absorbing medium. It can be seen as the analogous of the radioactive disintegration constant λ, which expresses

the probability of transformation of radioactive atoms per unit time. The exponential relationship for photon absorption suggests that, theoretically, a complete absorption of a beam of photon never occurs, but in a practical sense the exponential attenuation and/or absorption can be used to reduce most the beam intensities to imperceptible levels.
The relationship between beam intensity and the attenuation coefficient (Eq.1.11) is valid for photoelectric, Compton, and pair production interactions. The attenuation coefficient is then the sum of the three coefficient relative to the type of interaction:

$$\mu = \tau + \sigma + k$$

The coefficient μ (with unit of cm^{-1}) is the sum of the coefficients of individual interaction processes, each of which is a function of the gamma ray energy, the atomic number, and the mass and density of the absorbing medium. If other processes have significant effect on the absorption of a beam of photons, these would need to be accounted and contribute to an increase of μ or accomplished by a separate exponential terms.
Radiation exposure or absorbed dose from photons are connected to the amount of energy deposited by the various photon interactions as they traverse a medium. Some interactions produce radiant energy that carries energy out of the medium, as for example Compton scattered photons, bremsstrahlung from high-energy recoil electrons, annihilation radiation, and characteristic X-rays.
The attenuation coefficient μ cannot be used to determine energy deposition. Consequently, a linear energy absorption coefficient, μ_{en}, has been defined:

$$\mu_{en} = \mu - (\sigma_s + \text{other probabilities of interaction})$$

Generally the mass energy absorption coefficient μ_{en}/ρ with units of cm^2/g is the most useful form for determining radiation exposure or dose when a flux of x-rays or gamma rays is known or can be determined.
Most radiation protection works are done with the total attenuation coefficient μ (for radiation shielding) or the total mass energy absorption coefficient μ_{en}/ρ (for radiation dose calculations) instead of coefficients for the individual interactions.
The Fig.1.9 represents an example of how the attenuation of photons varies considerably with photon energy and Z of the absorbing medium. Two materials are taken as example: water, with low Z and density and composition similar to the human tissues, and lead, high Z absorber generally used for γ-shielding purposes.
For water at low energies (<15 keV), the photoelectric effect is the main type of interaction. As the photon energy increases, τ drops rapidly and Compton scattering interactions (σ) become dominant at about 100 keV in water and at about 500 keV in lead. The Compton scattering effect remains dominant up to several hundred keV where it decreases with energy until pair production becomes the dominant process.
In lead, the photoelectric effect is the dominant interaction at low energies. The importance of this effect decreases rapidly with increasing photon energy, but rises again when the photon energy is sufficient to eject a photoelectron from the K shell of the atom. For photon energies above a few hundred keV, Compton scattering interactions dominate and continue to do so until photon energies are well above the 1.022 MeV, pair production threshold.

1.2.4.2 Non Charged Particles: Neutrons

Another type of uncharged particle is represented by neutrons. Before the interaction of neutrons with matter can be discussed, the different types of neutrons, according to their energies or speeds, must first be classified:

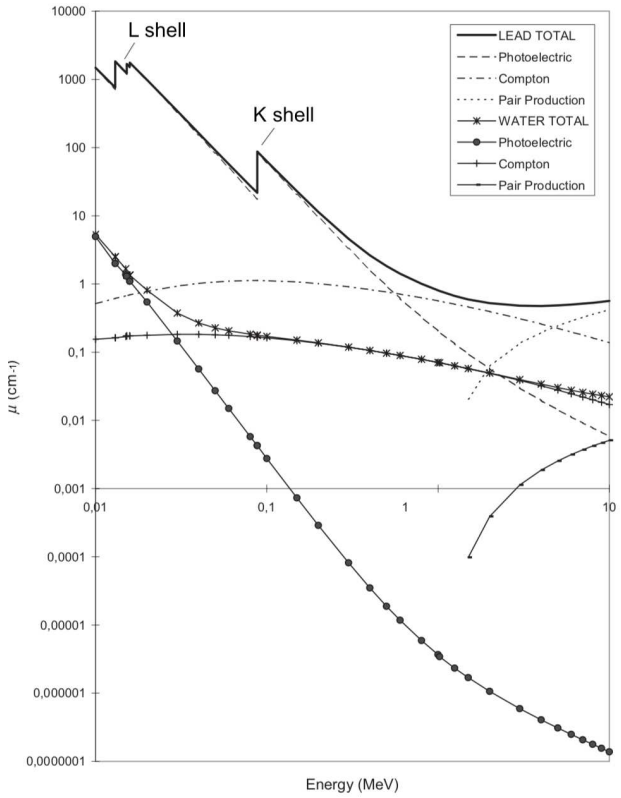

Figure 1.9: Photon attenuation coefficients for a low-Z material (water) and an high-Z absorber (lead) with relative contributions of photoelectric, Compton, and pair production interactions vs. photon energy [20].

Class	Energy
Cold	<1 meV
Thermal	< 0.5 eV
Epithermal	0.5 eV - 50 keV
Fast	> 50 keV
Medium energy	> 1 MeV
High energy	> 10 MeV

Since neutrons are electrically neutral, they can interacts only weakly with matter.
Contrary to X-rays, which interact dominantly with the electron shell of the atom, the neutrons reacts mostly with the nucleus.
Radiation protection for neutrons involves three types of interactions: elastic scattering, inelastic scattering, and capture.

1. **Elastic scattering (n,n):** In those interactions the neutron shares its initial kinetic energy with the target nucleus, which suffers only a recoil and is not left in an excited state. The kinetic energy of the recoil nucleus plus kinetic energy of the neutron after interaction is equal to the kinetic energy of the incident neutron, so the total kinetic energy in the system remains constant.

2. **Inelastic scattering (n,n'), (n,nγ):** Here the scattered neutron and the recoil nucleus have less energy than the one of the incident neutron. The nucleus is then left in an excited state.

In the (n,nγ) process, the excitation energy is released by the nucleus through the emission of gamma ray, whereas in the (n,n') process the nucleus remains in a metastable state.

3. **Radiative capture or (n,γ) reaction:** In this process the target nucleus captures the incident neutron and forms a compound nucleus. The mass number of an element is increased by one unit due to the addition of a neutron. The excitation energy induced by the extra neutron is released by gamma radiation. The element remains the same since the atomic number Z does not change, but the product of the reaction, which is often radioactive, is shifted to the right of the line of stable nuclides on the chart of the nuclides.
These types of reaction are commonly used in nuclear power plant to produce artificial radioactive nuclides.

4. **Charged particles emission (CPE):** These are reactions in which the compound nucleus that is formed breaks up by the emission of a charged particle such as a proton (n,p) or alpha particle (n,α). Such reactions usually require energetic neutrons to expel a particle from a nucleus.
When a proton in the nucleus is replaced by a neutron the mass number is not changed, but the charge is decreased by one unit and the atom is moved below the line of stability on the chart of the nuclides.

5. **Fission:** Interaction of neutrons with fissile nuclei may cause the formation of a compound nucleus which then splits into two fission fragments and one or more neutrons. Fission may occur in several isotopes of Th, U, Np, Pu and higher actinides when irradiated with neutrons. Common reactor fuel materials include ^{235}U, ^{239}Pu (and some ^{241}Pu).
Depending on the element of the target, the energy of the neutrons inducing the fission may vary: some acinides fission when irradiated with slow neutrons, while other elements, like lead or bismuth, may fission when irradiated with high energy neutron ($>$ 100 MeV).

The Fig.1.10 summarizes the possible neutron interaction depending on the energy range.

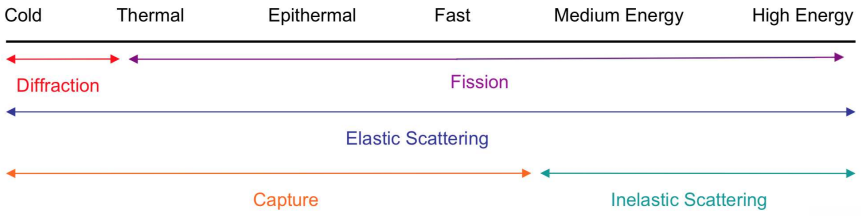

Figure 1.10: Dominant neutron interaction in typical range of energies.

The two most important properties of neutrons relative to radiation protection are the probability of interaction in a medium, denoted by the cross-section (σ) and the energy transferred to or deposited in the medium.
In particular the cross-sections are directly related to neutron energy and the absorbing medium. It is the probability that neutron-target interactions will occur. Neutron cross sections are related to the geometric dimension of the target nucleus. Therefore, cross sections are typically expressed in cm^{-2} or barns=10^{-24} cm^2. The cross section for a given nuclear interaction is also dependent on other factors, such as the speed of the neutron, the type of interaction, and the stability of the target nucleus. Cross sections are typically defined for specific nuclear reactions and for the overall probability of nuclear reaction (σ_t) with a target nucleus (elastic or inelastic scattering, capture or fission):

$$\sigma_t = \sigma_{es} + \sigma_{is} + \sigma_c + \sigma_f$$

The cross section definition focused on the interaction of neutron with a single target nucleus is known also as microscopic cross section. It is useful for understanding the fundamental interaction processes for neutrons and matter. However, the attenuation of neutrons in shielding material, is generally discussed through the macroscopic cross section (Σ):

$$\Sigma_t = N\sigma_t$$

where σ_t is the total microscopic cross section and N is the atom density of the target material, defined as:

$$N = \frac{\rho N_A n}{M}$$

where ρ is the density of the composite material, M is the molecular weight of the material, N_A is Avagadro's number, and n is the number of atoms of the element in the molecule.
The intensity of a neutron beam, I(x), passing through a target material of thickness x can be expressed using a law similar to the one used for the photons:

$$I(x) = I(0)e^{-N\sigma_t x} \qquad \text{or} \qquad I(x) = I(0)e^{-\Sigma_t x}$$

This formulae allow the calculation of the fraction of neutrons, at a given energy, that will go through a thickness (x) of a given target or shielding material without undergoing any type of scattering or capture interaction.
In other words, Σ_t can be thought as the probability per unit path length that a neutron will undergo an interaction as it moves through an absorber and be removed from the beam either by absorption or scattering. Indeed it is connected to the mean free path (mfp) of the neutron, i.e. the average distance a neutron of a given energy will travel before it undergoes an interaction:

$$\text{mfp} = \frac{1}{\Sigma_t}$$

As for the photons, it is possible to define a neutron mass coefficient (cm^2/g) by dividing Σ_t by the density of the absorber:

$$\text{Neutron mass coefficient} = \frac{\Sigma_t}{\rho}$$

The choice of the good shielding material for neutrons shall take into account the energy/spectra of the neutron beam and the relative phenomena occurring when it interacts with the absorbing materials. It could be a good option to built the neutron shield as a multi-layer object, following a three-step logical chain:

- Fast and high energy neutrons are characterized by high scattering cross section. In low Z materials a larger fraction of neutron energy may be lost in the collision. So the first step, can consist in using hydrogenated materials, like paraffine or PMMA, to induce scattering reactions, which slow down or moderate the neutron to thermal energies.

- For thermal neutrons, elements with high capture cross sections are often dispersed in low Z shielding material to absorb the moderated/thermalized neutrons. Borated polyethylene, layers of B_4C and aluminum, boron-aluminum alloys, and boric acid or gadolinium mixed with water or paraffine are examples of materials commonly used for this purpose.

- Neutron shielding may also incorporate, as last layer, high atomic weight elements to reduce dose from gamma radiation emitted with the neutron capture. Lead, bismuth, and tungsten are often used due to their high density, good gamma attenuation characteristics, and relatively benign activation products.

This three step chain is valid in particular for neutrons in the energy range of a nuclear power plant (10 MeV) or a bit higher.

1.2.4.3 Charged Particles

Charged particles lose their energy in a manner that is completely different from that of uncharged radiations (gamma or neutron).
Being surrounded by a Coulomb electric force field, they can interact with one or more electrons or with the nucleus of practically every atom encounters in matter.

Heavy charged particles:
A heavy charged particle traversing matter loses energy primarily through the ionization and excitation of atoms.
The collisions may involves electrical forces of attraction or repulsion or actual mechanical contact.
In the first case, a charged particle passing near an atom exerts electrical forces on the orbital electrons of that atom. The strength of the forces may be sufficient to cause an orbital electron to be separated from the atom, thus causing its ionization. Part of the projectile particle energy is used to overcome the binding energy of the electron to the atom, and the remainder is given to the ejected secondary electron as kinetic energy.
In the second case, the incident particle will interact primarily with a single atomic electron (effect know as "hard" or "knock-on collision"), which is then ejected from the atom with considerable kinetic energy. The ejected electron may be sufficiently energetic to cause secondary ionizations on its own (Delta (δ) ray). Ionization involving an inner electronic shells eventually leads to the emission of characteristic X-rays or Auger electrons.
Heavy charged particles travel an almost straight path through matter since any deflection in electron collisions is negligible.
The key parameter to study the interaction of charged particle with the matter is the mass collision stopping power. It can be defined as the expectation value of the rate of energy loss per unit of path length x by a charged particle of type Y and kinetic energy T, in a medium of atomic number Z:

$$\left(\frac{dT}{dx}\right)_{Y,T,Z}$$

In particular, using the H.A. Bethe relativistic formula:

$$-\left(\frac{dT}{dx}\right)_{coll} = \frac{4\rho\pi r_e^2 mc^2 z^2 Z N_A}{\beta^2 A}\, ln\frac{2mc^2\beta^2}{I(1-\beta^2)} - \beta^2$$

where mc^2 is the rest energy of the electron, r_e is the classical electron radius, z is the charge of the heavy charged particle, Z and A are the atomic number and the atomic mass of the target atom with density ρ, N_A os the Avogadro costant and I is the mean excitation energy of the medium, β=v/c is the ratio of particle velocity to the velocity of light.
The Bethe formula cannot well reproduce experimental data in low energy region, below few hundred keV. Under these conditions, interactions involving electron capture and loss by moving ions become the biggest component of the energy loss process. To take these effects into account, the Bethe's formula shall include various correction terms (Bethe-Bloch-Sternheimer formula):

$$-\left(\frac{dT}{dx}\right)_{coll} = \frac{2\rho\pi r_e^2 mc^2 z^2 Z N_A}{\beta^2 A}\, ln\frac{2mc^2\beta^2}{I^2(1-\beta^2)} - 2\beta^2 - \delta - 2\frac{C}{Z}$$

with δ a density correction factor and C the shell correction important for small particle velocities.
The dT/dx curve following Bethe-Bloch-Sternheimer is characterized by three regions (Fig.1.11):

1. At low energies a $(1/\beta)^2$ drop to a minimum. Particles at this point are called "minimum ionising particle".
2. At higher energies a logarithmic rise follows.
3. At very high energies a plateau is reached.

The energy loss is often given as $1/\rho$ dT/dx with the length in [cm] and the density in [g/cm^3]). The

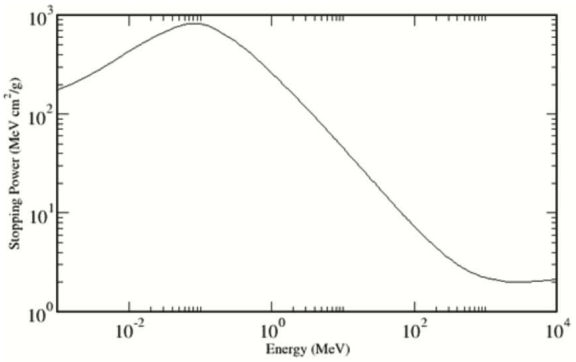

Figure 1.11: Mass collision stopping power of liquid water for protons (from NIST).

plot of the specifc energy loss along the track of a charged particle is called Bragg curve (1.12). The energy deposition near the end of the range enhances and forms the sharp peak called the Bragg peak, which is characteristic of heavy charged particles.

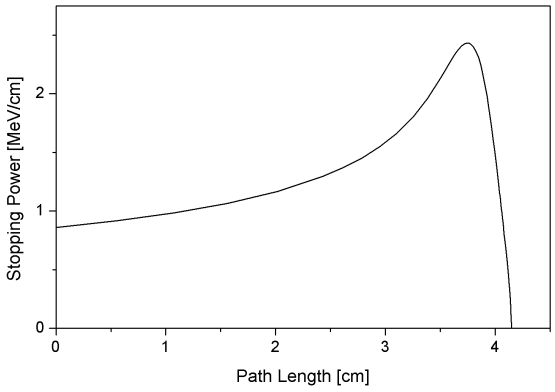

Figure 1.12: Example of Bragg curve for alphas particles of 5,5 MeV in air.

This behavior is used in particle therapy of cancer to concentrate the effect of light ion beams on the tumor region, minimizing the effect on the surrounding healthy tissue.

Electrons:
Electrons and positrons lose energy almost continuously when being slowed down in matter and may interact with:

- the nucleus of an atom;
- the orbital electrons of an atom.

Moreover, interactions may be:

- elastic, resulting in no loss of energy;
- inelastic, where the kinetic energy of the incident electron changes.

Elastic collisions with the nucleus result in scattering of the electron with no loss of energy. The amount of scattering that occurs is dependent on the atomic number of the nucleus (higher atomic numbers cause more scattering).
Elastic collisions with the orbital electrons of an atom, also leading to scattering of the incident electron but no transfer of energy.
Inelastic collisions with orbital electrons result in transfer of energy from the incident electron to the orbital electron. If this energy is sufficient for the electron to ascend to a higher shell, the atom assumes an excited state. The space in the lower shell is rapidly filled by another orbital electron, which releases a photon. This one may generate characteristic X-rays if the binding energy of the shell is sufficiently large (as in heavy elements like lead or tungsten), or visible light for less tightly bound electrons.
If sufficient energy is transferred to an orbital electron it may be able to escape the atom, leaving the atom ionised. The freed electron may cause further ionisations before it loses its energy and is captured by an atom.
Inelastic collisions with the nucleus result in Bremsstrahlung, German word for "braking radiation". As the electron interacts with the nucleus, it slows down and changes direction. The energy that is lost by the electron is released as a photon.

The total energy loss in case of electron is then coming from collisions and from radiation (which dominates at high energies):

$$\left(\frac{dT}{dx}\right) = \left(\frac{dT}{dx}\right)_{coll} + \left(\frac{dT}{dx}\right)_{rad} \tag{1.12}$$

Collision losses are similar to those for heavy charged particles except for some differences:

- For electrons the indistinguishability of final state electrons in scattering processes must be taken into account;
- For positrons annihilation effects shall be considered.

Accounting for these effects it is possible to obtain a version of the Bethe-Bloch equation (extended by Sternheimer) for electrons and positrons:

$$-\left(\frac{dT}{dx}\right)_{coll} = 2\rho\pi r_e^2 mc^2 z^2 \frac{Z}{A}\frac{1}{\beta^2}\,[ln\frac{\tau^2(\tau+2)}{2(I/m_e c^2)^2} - F(\tau) - \delta(\beta) - 2\frac{C(I,\beta)}{Z}]$$

where τ is the kinetic energy of the primary electron and the function F(τ) is different for electron and positron:

$$F(\tau)_{electron} = 1 - \beta^2 + \frac{\frac{\tau^2}{8} - (2\tau+1)ln2}{(\tau+1)^2}$$

$$F(\tau)_{positron} = 2\,ln2 - \frac{\beta^2}{12}\,[23 + \frac{14}{\tau+2} + \frac{10}{(\tau+2)^2} + \frac{4}{(\tau+2)^3}]$$

Below 100 keV, the term outside the brackets is the most important. The factor $1/\beta^2 = c^2/v^2$ makes the stopping power nearly inversely proportional to the kinetic energy. For energies above 100 keV, β is essentially 1 and the term in front becomes nearly constant. The terms inside the square bracket increase slowly with energy and the stopping power passes through a minimum in the neighborhood of 1 MeV.

The factor before the brackets contains the number of electrons per unit mass, given by $N_A(Z/A)$. since Z/A is 0.5 or slightly less for all materials, except hydrogen, the mass stopping power decreases only slightly as atomic number increases.

The second term of the Eq.1.12 is related to the energy loss by Bremsstrahlung for a charge of mass m, charge number z and energy E:

$$-\Big(\frac{dT}{dx}\Big)_{rad} = 4\alpha N_A \frac{Z^2}{A} z^2 \Big(\frac{1}{4\pi\varepsilon_0}\frac{e^2}{mc^2}\Big)^2 E\, ln\frac{183}{Z^{\frac{1}{3}}}$$

where Z and A are respectively the atomic number and mass of the medium.
The dependence on the reciprocal of the squared mass of the projectile suggests that Bremsstrahlung is more relevant for light particles, such as electrons. The size of the decrease depends on the particle velocity due to the influence of the β^2 terms in the parenthesis.

1.3 Dose Quantities in Radiological Protection

This paragraph collects the definitions of some of the most important radioprotection quantities that will also be used in other parts of the present work.
They have been designed by ICRP and ICRU (International Commission on Radiation Units and Measurements) to meet the need to protect human beings, public and workers, from the effect of radiations.
There are two types of quantities defined for specific use in radiological protection (Fig.1.13): Protection quantities (from ICRP and used for assessing the exposure limits) and Operational quantities (from ICRU and intended to provide a reasonable estimation for the protection quantities).
Those definitions require a quantitative description of radiation fields and of the exposure of the human body [24]. Similar considerations apply to protection of other biological organisms. While radiation fields can be well described by physical quantities such as particle fluence or air kerma in free air, the description of the exposure of humans must also include information about the biokinetics of radionuclides and other parameters of the human body.

Kerma, K

Kerma is an acronym for "kinetic energy released in matter". It is a non-stochastic quantity applicable to indirectly ionizing radiations such as photons and neutrons. It quantifies the average amount of energy transferred from indirectly ionizing radiation to directly ionizing radiation without concern as to what happens after this transfer. The energy of uncharged particles is imparted to matter in a two stage process. In the first stage, the photon (or neutron) transfer energy to the secondary charged particles (electrons) through various photon (or neutron) interactions (the photoelectric effect, the Compton effect, pair production, etc.). In the second stage, the charged particle transfers energy to the medium through atomic excitations and ionizations.
Kerma is defined as:

$$K = \frac{d\varepsilon_{tr}}{dm} \tag{1.13}$$

where $d\varepsilon_{tr}$ is the sum of the initial kinetic energies of all charged ionizing particles freed by uncharged ionizing particles in a material of mass dm. The SI unit of kerma is the Joule per kilogram (J/kg), termed Gray (1Gy = 1J/kg).
As said, the energy transferred to electrons by photons can be expended in two distinct ways: through

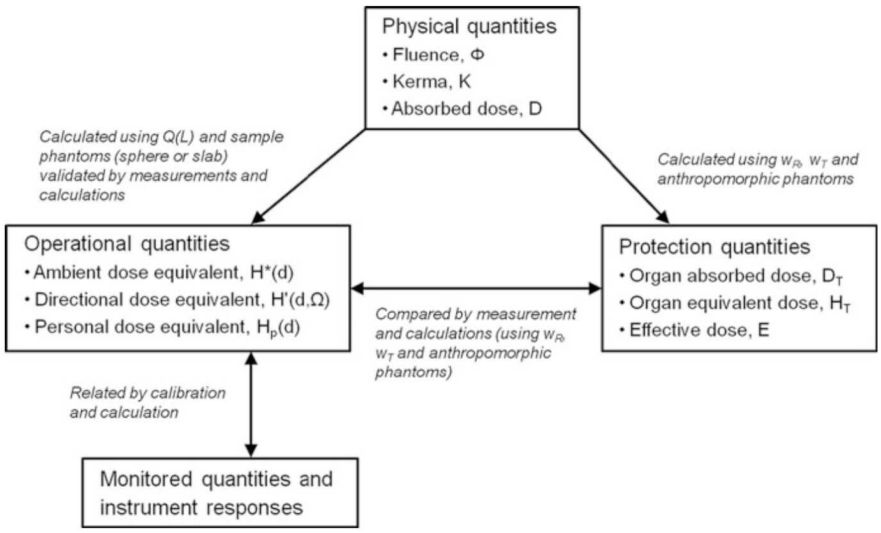

Figure 1.13: Relationship between physical protection and operational quantities [25].

collision interactions (soft collisions and hard collisions) or through radiative interactions (Bremsstrahlung and electron-positron annihilation).
The total kerma is therefore usually divided into two components: the collision kerma K_{col} and the radiative kerma K_{rad}:

$$K = K_{col} + K_{rad} \tag{1.14}$$

Absorbed Dose, D

Defined as the ratio of mean energy , $d\varepsilon$, imparted by ionising radiation in a volume element and the mass, dm, of the matter in that volume [26]:

$$D = \frac{d\varepsilon}{dm} \tag{1.15}$$

This definition does not reflect the random fluctuations of the interaction events in tissue despite the origin from the mean value of the stochastic quantity of energy. The Dose is a point quantity. It should be recognized that the physical process does not allow dm to approach zero in the mathematical sense [24]. The unit of absorbed dose is the Gray (Gy).

Radiation Weighting Factor, W_R

It is a dimensionless variable weighting factor to be applied to the absorbed dose to provide an estimate of the relative human hazard of different types and energies of ionizing radiations. Values of W are selected from experimental values of the Relative Biological Effectiveness (RBE), which is the ratio of X- or γ-ray dose to that of the radiation in question giving the same kind and degree of biological effect. These values are presented in the Tab.1.1.

Equivalent Dose, H

This concept takes into account the nature of radiations in a refinement of the Absorbed Dose. Indeed the Equivalent Dose is obtained by multiplying the absorbed dose for the radiation weighting factor. So it reflects the difference in the nature of the radiations and the severity of the biological damages

Radiation	Energy	W_R (formerly Q)
X-rays, Gamma rays, Beta particles, Muons		1
Neutrons	$<$ 1 MeV 1 MeV - 50 MeV $>$ 50 MeV	$2.5 + 18.2\ e^{-[ln(E)]^2/6}$ $5.0 + 17.0\ e^{-[ln(2E)]^2/6}$ $2.5 + 3.25\ e^{-[ln(0{,}04E)]^2/6}$
Protons, charged pions		2
Alpha particles, Nuclear fission products Heavy nuclei		20

Table 1.1: Radiation weighting factors W_R (formerly termed Q factor) used to represent relative biological effectiveness according to ICRP report 103 [26].

they can cause:

$$H_T = \sum_R W_R \cdot D_{T,R} \tag{1.16}$$

where, H_T is the Equivalent Dose absorbed by the tissue T, $D_{T,R}$ is the absorbed dose in grays (Gy) in tissue T due to the radiation type R and W_R is the radiation weighting factor.
The SI unit of measure for equivalent dose is the Sievert (Sv), defined as one Joule per kg.

Effective Dose, E

It is a biological dose quantity commonly used in radioprotection, as it determines how dangerous an individual's exposure to radiations can be. It takes into consideration not only the nature of the incoming radiation but also the sensitivities of the body parts affected through the use of adimensional weighting factors for different tissues, W_T, reported in the Tab.1.2.

It represents the stochastic health risk to the whole body, which is the probability of cancer induction and genetic effects, of low levels of ionising radiation.The unit of the effective dose is the Sievert, the same unit used for the equivalent dose absorbed locally by an organ. The ICRP defines the Effective dose as:

$$E = \sum_T W_T \cdot H_T = \sum_T W_T \sum_R W_R \cdot D_{T,R} \tag{1.17}$$

where: E is the effective dose to the entire organism, H_T is the equivalent dose absorbed by tissue T, W_T is the tissue weighting factor defined by regulation, W_R (Tab.1.2) is the radiation weighting factor (Tab.1.1).

Exposure, X

It is defined by the ICRU [27] as the ratio:

$$X = \frac{dQ}{dm} \tag{1.18}$$

where the value of dQ is the absolute value of the total charge of the ions of one sign produced in air when all the electrons and positrons liberated by photons in air of mass dm are completely stopped in air.

Organs	Tissue weighting factors
Gonads	0.08
Red Bone Marrow	0.12
Colon	0.12
Lung	0.12
Stomach	0.12
Breasts	0.12
Bladder	0.04
Liver	0.04
Oesophagus	0.04
Thyroid	0.04
Skin	0.01
Bone surface	0.01
Salivary glands	0.01
Brain	0.01
Remainder of body	0.12
Total	1.00

Table 1.2: Weighting factors for different tissues [26].

Equivalent Ambient Dose, H*(d)

For the purposes of routine radiation protection, it is desirable to characterize the potential irradiation of individuals in terms of a single dose equivalent quantity that would exist in a phantom approximating the human body. The phantom selected is the so-called ICRU sphere made of 30 cm diameter tissue-equivalent plastics. The Equivalent Ambient Dose, H*(d), at a point in a radiation field is the dose equivalent that would be produced by the corresponding expanded and aligned field at a depth d in the ICRU sphere, on the radius opposing the direction of the aligned field Fig.1.14.

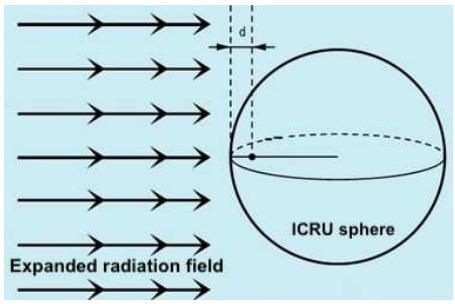

Figure 1.14: Scheme for the definition of H*(d).

For strongly penetrating radiations a reference depth, d, of 10 mm was recommended (H*(10)). Instead, H*(0.07) is applied for monitoring weakly penetrating radiation, like beta or alpha particles and for the monitoring of the doses to the extremities from all kind of ionising radiation.

1.4 Methods for Dose calculations

The Absorbed Dose and the Dose rate are two basic radioprotection quantities.
An accurate analysis and forecast is necessary when a new experiment or a new device must be installed in radiation areas. Moreover calculations are fundamental to plan shielding material, thickness and position to respect the operational limits.
Radiation measurements and investigations of radiation effects require various specifications of the radiation field at the point of interest. The quantity used to define and characterize the radiation field are fluence and fluence rate [24], from which the energy fluence or energy fluence rate can be determined.

- **Fluence and Fluence rate:**
  Fluence Φ is defined as the number dN of particles incident on a sphere of cross-sectional area da during a time interval extending from an arbitrary starting time t_0 to a later time t_{max}. It is generally expressed in m^{-2} or cm^{-2}:
  $$\Phi = \frac{dN}{da}$$
  The fluence may be defined for all values of t in the interval (t, t_{max}) by the fluence rate ($m^{-2}s^{-1}$ or $cm^{-2}s^{-1}$) as:
  $$\phi = \frac{d\Phi}{dt} = \frac{d}{dt}\frac{dN}{da}$$
- **Energy fluence and energy fluence rate:**
  Energy fluence Ψ is defined as the total energy dE carried by the incident particles on a sphere of cross-sectional area da during a time interval extending from an arbitrary starting time t_0 to a later time t_{max}. In other words it is the amount of radiation energy delivered to a unit area and in a certain range of time.
  $$\Psi = \frac{dE}{da}$$
  which is usually expressed in units of J m^{-2} or J cm^{-2}.
  As for the fluence rate, the energy fluence rate may define the energy fluence by for all values of t in the interval (t, t_{max}):
  $$\psi = \frac{d\Psi}{dt} = \frac{d}{dt}\frac{dE}{da}$$
  In case all the particles have the same energy E, the energy fluence Ψ is equal to ΦE.

Once these two quantities are known it is possible to connect the radiation field to the dosimetric quantities.

Relation of kerma to energy fluence for Photons
For mono-energetic photons the total kerma K (radiative + collisional) at a point in a medium is related to the energy fluence ψ in the medium by the following equation:

$$K = \psi(\frac{\mu_{tr}}{\rho})_{Z,E} \tag{1.19}$$

where (μ_{tr}/ρ) is the mass-energy transfer coefficient of the medium, characteristic of the photon energy E and the atomic number Z of the matter. For poly-energetic beams, similarly as above, spectrum-averaged mass-energy transfer coefficients can be used in conjunction with total energy fluence to

obtain the total kerma:

$$K = \int_0^{E_{max}} \psi'(E)(\frac{\mu_{tr}}{\rho})_{Z,E} dE \tag{1.20}$$

where $\psi'(E)$ is the differential distribution of photon energy fluence, in units of J m^{-2} MeV^{-1}.

Relation of kerma to fluence for Neutrons:
Equations 1.19 and 1.20 could be applied to neutrons as well. Usually neutron fields are described in terms of fluence, instead of energy fluence as is usually the case with photons. Thus a quantity called the kerma factor F_n is tabulated for neutrons:

$$(F_n)_{E,Z} = (\frac{\mu_{tr}}{\rho})_{Z,E} E \tag{1.21}$$

the kerma can be written as:

$$K = \phi(F_n)_{E,Z} = (\frac{\mu_{tr}}{\rho})_{Z,E} E\phi \tag{1.22}$$

If neutrons have an energy spectrum of particle fluence, the previous equation can be replaced by:

$$K = \int_0^{E_{max}} \phi'(E)(F_n)_{E,Z} dE \tag{1.23}$$

Relation of exposure to energy fluence:
Generally, the transfer of energy (kerma) from the photon beam to charged particles at a particular location does not lead to the absorption of energy by the medium (absorbed dose) at the same location. This is due to the non-zero range of the secondary electrons released through photon interactions.Since radiative photons mostly escape from the volume of interest, one relates absorbed dose usually to collision kerma.
Collisional kerma can in turn be connected to the exposure X, multiplying it by (e/W_{air}), the number of coulombs of charge created per joule of energy deposited (33,97 J/C). In this way it is possible to obtain the charge created per unit mass of air (or exposure):

$$X = K_{coll,air}(\frac{e}{W_{air}}) = \psi(\frac{\mu_{en}}{\rho})_{air} (\frac{e}{W_{air}})$$

If a spectrum of photon energy fluence is present and the energy-absorption coefficient as a function of photon energy E for air the previous equation shall be integrated:

$$X = \int_0^{E_{max}} \psi'(E)(\frac{\mu_{en}}{\rho})_{E,air} (\frac{e}{W_{air}}) dE$$

Relation of fluence to dose:
In case of electrons (or a charged particle), under the conditions that radiative photons escape the volume of interest and secondary electrons are absorbed on the spot (charged particle equilibrium of secondary electrons), the absorbed dose to medium D is related to the electron fluence Φ in the medium as follows:

$$D = \Phi(\frac{S_{coll}}{\rho})$$

where (S_{col}/ρ) is the mass collision stopping power of the medium at the energy of the electron. Because of electron slowing down, even for a monoenergetic starting electron, there is generally an electron fluence spectrum in the medium and it is more correct evaluate D as:

$$D = \int_0^{E_{max}} \Phi(E)(\frac{dT}{dx\rho}_c)(E) dE$$

The methods used to estimate the Dose (and/or the Equivalent Ambient Dose) can be divided in two main categories: **Deterministic** and **Monte Carlo Methods**.
In the first case, equations and analytical formulae are used to describe the average behaviour of the particle population.
The advantage of the deterministic methods consists mainly in the rapidity of the reponse. A disadvantage is related to the use of build-up factors normally extrapolated from high to low energies or with unknown geometrical conditions, which can lead to significant errors in the results.
Commercial software are for example MicroShield [28] or Nucleonica [29], used also in this work for some application. They are characterized by a practical user-interface that allows the definition of simple geometries to approximate the elements of the problem (mainly sources, detector and shield).
In Monte Carlo calculations, the required physical quantities are estimated by generating a number of typical particle tracks. At each stage the position of the next collision, the type of interaction, and the energy and direction of the resulting particles are all sampled from known physical laws by choosing random numbers. In this way a particle in the calculation follows the same procedure as it would experience in reality. By recording properties of the tracks which reach the regions of interest for a given number of samples, it is possible to estimate an average quantity such as Dose rate.
MC calculations have the advantage of being applicable to any geometry and to be able to use updated nuclear data. Its accuracy is limited only by the knowledge of the cross-section data.
Example of MC software are FLUKA [30], MCNP [31] or RayXpert [32]. The last two methods have been used in the present work.

1.4.1 The MCNPX Method

MCNPX 5.0 [31] has been the software mainly used in this PhD work. General-purpose, continuous-energy, generalized-geometry, time-dependent, Monte Carlo radiation-transport code designed to track many particle types over broad ranges of energies.
It calculates the absorbed dose on the basis of the so-called "KERMA approximation": the Kinetic energy transferred to charged particles is assumed to be locally deposited. The conditions under which the KERMA approximation is valid are the following:

- Low-energy photons (secondary electrons have very short range);
- Charged Particle Equilibrium (CPE) or at least transient CPE exists: range of primary radiation is higher than the one of the secondary particles;
- Radiative losses in medium are negligible.

Charged particle equilibrium (CPE) exists for the volume V if each charged particle of a given type and energy leaving V is replaced by an identical particle of the same energy entering (in terms of expectation values). In this case the Kerma is equal to the Dose [20].
MCNPX uses three basic approaches to calculate the dose, each one connected to different options called "Tallies" (tallying is the process of scoring the parameters of interest, i.e. providing the required answers):

1. Track Length Heating Method: it uses F4/FM4 or F6 Tallies (Kerma approximation) for a specified cell;
2. *F8 Tally: it evaluates the energy deposited in the selected cell. It furnishes rigorous dosimetry for situations where Kerma approximation does not hold. This option is valid only for photons and electrons;
3. Fold in Fluence to Dose Conversion Function using DE/DF cards (options) associated to F5 or F4 Tally. Valid typically for whole body irradiation. Flux to dose rate conversion factors are

furnished in the Appendix G of the MCNPX manual. They can be used as alternative to the Dose card.

The methods selected in this work are the number 1 and 2. In both cases the detector is a cell composed of water or air depending if the final value is the absorbed dose to the body or the ambient equivalent dose rate. The choice of water is due to the fact that human tissues have in average the same density and composition.
The results of the tally *F8 has the dimension of MeV. To obtain the right dimensions (mSv/h) the steps are the following:

1. Divide by the mass (g) of the detector;
2. Multiply by the activity of the source (Bq = s^{-1});
3. Multiply by the conversion factor c=0.00057678 to obtain the results in mSv/h.

The results of the tally F6 has the dimension of MeV/g, so, to obtain the correct dimensions, it has to be multiplied by the activity and the factor c.
The condition of CPE must be tested using the tallies F6 and *F8: if the two values are the same (after the factors multiplication), so the Dose is equal to the Kerma and the situation of equilibrium is proved. This allow to consider as dose rate the value the one with lower variance.

1.5 The radioprotection principles

The aim of radiation protection is to prevent reliably the effects of radiation.
The safety principles and limitations imposed by the Authorities are based on the famous ALARA principle, acronym used in radiation safety for "As Low As Reasonably Achievable". It is actually a regulatory requirement for all radiation protection programs and integral part of all activities that involve the use of radiation or radioactive materials since it can help preventing overexposures or unnecessary exposures.
The three major principles to maintain the doses As Low As Reasonably Achievable are:

1. **Minimizing exposure time:** methods of reducing the amount of time that is spent in a radiation field include study the possible risk prior to performing any work, rapid transit through the areas of highest radiation levels, preplanning in advance any activities that take place in the radiation field, practicing on mockups of a work area prior to the work to be done in order to improve familiarity with the procedure;
2. **Maximizing distance from the radiation source:** the intensity of a radiation source falls off as the square of the distance from that source. Therefore, doubling the distance reduces the exposure by a factor of four;
3. **Apply a shielding between the operator and the source:** the choice of the shield depends on the type of radiation.
   The Fig.1.15 can be used to summarize the type of shielding to use depending on the type of source. The shielding strategy is driven by the charge, the mass and the energy of the radiation from which one wants to protect for.
   Alpha particles interact strongly with matter, releasing the majority of their energy at the end of their path. Those particles emitted during alpha decay only travel few centimeters in air and are unable to penetrate the outer layer of dead skin cells. On the other hand alpha emitters are capable to cause serious cell damages when ingested.
   Beta particles have smaller mass, so they are able to travel further in air, up to a few meters,

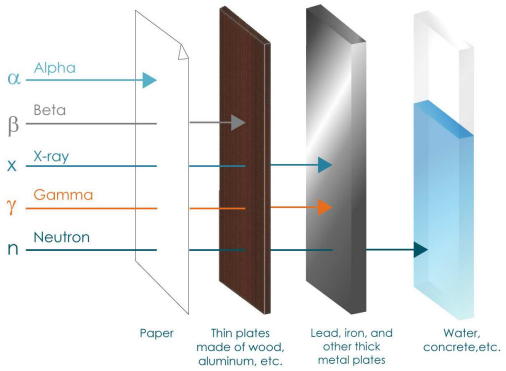

Figure 1.15: Different type of shielding for the type of radiation [33].

and can be stopped by a thick piece of plastic or even a stack of paper. It can penetrate skin a few centimeters, causing damages with an external health risk. Ingestion is also a source of serious damages.
Gamma radiation, having no mass or charge, can travel much further in air than alpha or beta. They can be stopped by a thick or dense layer of material, with high atomic number such as lead or depleted uranium.
Lead is quite ineffective for blocking neutron radiation, since they are uncharged and can simply pass through dense materials. Shielding composed of different layers are preferable: hydrogen and hydrogen-based materials are well-suited to thermalize the neutrons and higher Z meterials are used to capture them (as lead or even the lower Z materials as boron or lithium).

In order to keep the risk of stochastic damage from ionising radiation as low as possible, three general principles have been set out in radiation protection for dealing with ionising radiation. These are based on recommendations from the International Commission on Radiological Protection (ICRP) [26], an independent, international and non-governmental organization, whose mission is to provide recommendations, guides and standards on radiation protection matters.

- **Justification:**
  Every new application of ionising radiation or each new use of radioactive materials must be justified in advance. Moreover activities are permitted only when they are associated with a reasonable benefit for the individual and for society. In this case, "reasonable" means that the benefit outweighs any health detriment possibly caused by the activity.

- **Dose limitation:**
  The Dose to the workers and the public during justified activities must not exceed certain limit values. Different limit values apply for the general population and for persons occupationally exposed to radiation. Dose limits are set so that any continued exposure just above the dose limits would result in additional risks that could be reasonably described as ”unacceptable” in normal circumstances.
  The effective dose limits for ionising radiation are:
  Occupational exposures (exposure of the workers as results of their work activities) following the ICRP recommandations are:

  – 20 mSv per year (averaged over 5 calendar years);
  – with no single year exceeding the 50 mSv;

  - Annual limit to the eye lens of 20 mSv (averaged over a 5 years period with no single year above 50 mSv);
  - Annual dose to hands, feet and skin of 500 mSv.

  Members of the public (for exposure other than occupational and medical):

  - 1 mSv in a year;
  - 15 mSv in a year to the lens of the eye (established in 2013);
  - 50 mSv in a year to the skin

  The dose limits as established by the ICRP (2007) [26] are taken as being above natural background levels. Therefore, it is important that the radiation levels arising from natural background are determined prior to an exposure.

- **Optimisation:**
  If an activity that is connected with radiation exposure and contamination is justified, the principle of optimisation requires that any unnecessary radiation exposure and contamination has to be avoided. The magnitude of individual doses, the number of people exposed and the likelihood of incurring exposures shall be minimized. The optimization is an idea of broad application. At the top level it covers the organizational structure needed to enable the correct allocation of responsibilities. It can also refer to the necessity of a statistical study of risk assessment and apply to procedures designed to prevent or mitigate the consequences of accidents.

1.6 The characteristics of the radionuclides in medicine

Radionuclides are an essential part of medical diagnostic and therapeutic procedures. In combination with imaging devices which register the gamma rays emitted from them, they can be used to study the metabolic processes taking place in various parts of the body.
Radionuclides are most of the time attached as labels to compounds of biomedical interest for nuclear medicine applications, forming the so-called *Radiopharmaceuticals*. Each human organ acts differently from a chemical point of view and can absorb differently specific molecules. The thyroid, for example, takes up iodine, while the brain consumes high quantities of glucose. Once a radioactive form of one of these substances enters the body, it is incorporated into the normal biological processes and excreted in the usual ways. With this knowledge, radiopharmacists are able to attach various radioisotopes to biologically active substances.
For most applications, the radiopharmaceutical is injected into the patient, and the emissions are detected using external imaging or counting systems. Among them the most common used techniques are SPECT (single photon emission computed tomography), and PET (positron emission tomography). The Chart of Nuclides contains hundreds of radionuclides that could conceivably be used for some biomedical applications, either in elemental form or as a radiopharmaceutical. However, the number of radionuclides actually used is much smaller because of various practical considerations.
It is possible to highlight some parameters to choose the correct nuclide for a medical application [34]:

- The **Type and Energy of emissions** from the radionuclide determine the availability of useful photons for counting or imaging. For external detection of a radionuclide introduced in the body, photons in the 50-600 keV energy range are suitable. Very-low-energy photons (< 50 keV) have a high probability of interacting in the body and will not in general escape for external detection. On the other hand these emissions increase the radiation dose to the patient to healthy tissues.

An example of this is I-131, which decays by ($\beta-, \gamma$) emitting a β particle, followed by γ rays at 364 (82%), 637 (6.5%), 284 (5.8%), or 80 keV (2.6%). The γ rays are in an appropriate range for external detection; however, the β- particles contribute to additional dose as compared with radionuclides that decay by (EC,γ).
Radionuclides, mainly beta and alpha emitters, can be also used for therapeutic purposes. In this case the Energy of emission shall be released only to the target and then the range must be compatible with the tumor cell dimensions to avoid damages to healthy tissues. Examples in this field are Lu-177 and Y-90 as beta emitters and Ac-225 or Tb-149 as alpha emitters. At the same time the compound should be localized in the body and it should emit gammas to enable the imaging. Therapeutic and imaging combinations is at the origin of the so-called "Theranostic Radionuclides".

- The **physical half-life** of the radionuclide should be within the range of days (preferably minutes to hours depending on the vector molecule) for clinical applications. If the half-life is too short, there is insufficient time for preparation of the radiopharmaceutical and injection into the patient. An example of this is the positron emitter O-15 ($T_{1/2}$ = 122 sec). This limits O-15-labeled radiopharmaceuticals to simple compounds such as $H_2^{15}O$ and $C^{15}O$ and obliges to perform the PET imaging close to the production sites. On the other hand, if the half-life is too long, an higher portion of the radiation is emitted outside of the examination time, which can result in a high radiation dose to the patient in relation to the number of decays detected during the study. Long-lived radionuclides also can cause problems in terms of storage and disposal at the place of production. An example of a very long-lived radionuclide that is not used in human studies because of half-life considerations is Na-22 ($T_{1/2}$ = 2.6 yr).

- The **Radionuclidic Purity** is defined as the ratio, expressed as a percentage, of the radioactivity of the desired radionuclide to the total radioactivity of the source [35]. Radionuclidic contaminants arise in the production pathway of radionuclides and can be significant in some situations. The effect of these contaminants is to increase the radiation dose to the patient. They may also increase detector dead time, and if the energy of the emissions falls within the acceptance window of the detector system, resulting in incorrect counting rate or pixel intensities in the produced images .

- The **Specific activity** of the radionuclide largely determines the mass of a compound that is introduced for a given radiation dose. Because nuclear medicine relies on the use of pharmacologic tracer doses that do not disturb the biologic system under study, the mass should be low and the specific activity high. At low specific activities, only a small fraction of the molecules in the sample are radioactive and therefore signal producing, whereas the rest of the molecules add to the mass of the compound being introduced, without producing signal. Theoretically, the specific activity of a radionuclide is inversely proportional to its half-life, but in practice, many other factors can determine the actual specific activity of the injected labeled compound, like the abundance of stable isotopes.

- The **Chemical Properties** of the radionuclide also are an important factor. Radionuclides of elements that can easily produce useful precursors (chemical forms that react readily to form a wide range of labeled products) and that can undergo a wide range of chemical syntheses are preferred. Radionuclides of elements that are easily incorporated into biomolecules, without significantly changing their biochemical properties, also are attractive. Examples are C-11, N-13,

O-15, elements that are found naturally in many biomolecules. Metals such as Tc-99m and Ga-67 also are widely used as labels in nuclear medicine, because of the desirable imaging properties of the radionuclide.

- Finally, the **Cost, industrial Constraints and the availability** of a radionuclide should be considered. Sufficient quantities of radionuclide for radiopharmaceutical labeling and subsequent patient injection must be produced at a cost (both materials and labor) consistent with today's health care market.
  Some example of radionuclides satisfying the previous criteria are reported in the Tab.1.3.

Radionuclide	**Decay Mode**	**Principal γ emissions**	**Half-Life**	**Primary Use**
C-11	β+	511 keV	20.4 min	Imaging
N-13	β+	511 keV	9.97 min	Imaging
O15	β+	511 keV	2.03 min	Imaging
F-18	β+	511 keV	110 min	Imaging
P-32	β-	-	14.3 d	Therapy
Ga-67	EC	93, 185, 300 keV	3.26 d	Imaging
Rb-82	β+	511 keV	1.25 min	Imaging
Sr-89	β-	-	50.5 d	Therapy
Y-90	β-	-	3.19h	Therapy
Tc-99m	IT	140 keV	6.02 hr	Imaging
In-111	EC	172, 247 keV	2.83 d	Imaging
I-123	EC	159 keV	13.2 hr	Imaging
I-125	EC	27-30 keV X rays	60.1 d	In vitro assays
I-131	β-	364 keV	8.04 d	Therapy
Sm-153	β-	41, 103 keV	46.7 hr	Therapy
Lu-177	β-	113,208 keV	6.64	Therapy
Re-186	β-	137 keV	3.8 d	Therapy
Tl-201	EC	68-80 keV X rays	3.04 d	Imaging
At-211	EC, α	92, 687 keV	7.21 h	Therapy
Ac-225	α	10 d		Therapy

Table 1.3: Example of radionuclides used in nuclear medicine (EC, electron capture; IT, internal transition).

1.7 The places of production

The radionuclides used in nuclear medicine (for diagnostic imaging and/or therapeutic treatments) are "artificially produced", bombarding nuclei of stable or unstable atoms with subnuclear and nuclear particles with a proper energy. This causes nuclear reactions that convert the nucleus into an unstable (or radioactive) one.
The main places of production for the medical radionuclides are: nuclear reactors and charged particle accelerators.

- ***Reactor production:***
  Nuclear reactors play an important role since many years in providing radionuclides for medical applications. The core of a nuclear reactor contains a quantity of fissionable material, typically natural uranium (U-235 and U-238) enriched in U-235 content. U-235 undergoes spontaneous nuclear fission ($T_{1/2} \sim 7$ x 10^8 years), splitting into lighter nuclear fragments and emitting fission neutrons in the process. This ones stimulate additional fission events when bombarding U-235 and U-238. The most important reaction is the following:

$$^{235}U + n \rightarrow {}^{236}U^* \tag{1.24}$$

  The $^{236}U^*$ nucleus is highly unstable and promptly undergoes nuclear fission, releasing additional fission neutrons. In the nuclear reactor, the objective is to have the fission neutrons emitted in each spontaneous or stimulated fission event inducing, on the average, one additional fission event. This establishes a controlled, self-sustaining nuclear chain reaction.
  Each nuclear fission event results in the release of a large amount of energy (about 220 MeV per fission in case of fissioning nuclei like $^{236}U^*$, $^{240}Pu^*$, $^{242}Pu^*$), most of which is dissipated as thermal energy. Some radionuclides are produced directly in the fission process and can be subsequently extracted by chemical separation from the fission fragments. This is the case of I-131, Xe-133 or for the more famous Mo-99, playing an important role in nuclear medicine as the parent radionuclide in the Mo-99/Tc-99m generator.
  Another way of producing radionuclides consists in the usage of the large neutron flux in the reactor to activate samples placed around the reactor core to induce (n, γ). This is the case for example of Mo-99 and Sn-117m

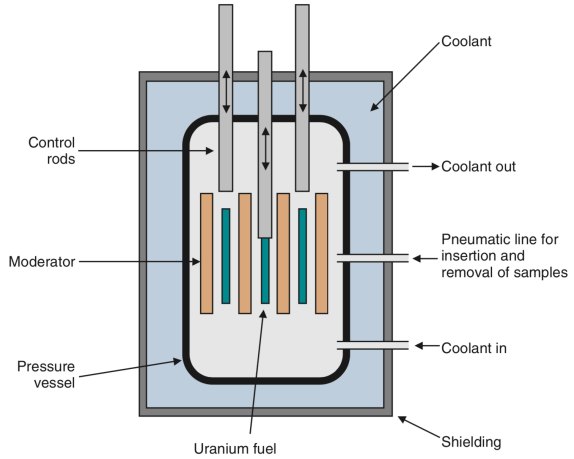

Figure 1.16: Schematic representation of a nuclear reactor [13].

- ***Cyclotron production:***
  Cyclotrons are the most commonly used devices for acceleration of particles to sufficient energies for the required nuclear reactions intended to produce radionuclides to use in nuclear medicine (Fig.1.17).
  Ions are produced in an ion source at the centre of the machine and are accelerated out from the centre by a puller electrode. An high frequency electric field is set through two or more hollow electrodes, called "Dees" due to their semicircular shapes.
  When the ion is emitted from the source, it is accelerated towards the Dee having a opposite

potential. Due to a normal magnetic field, the ion experiences magnetic Lorentz force and moves in a circular path. By the time the ion arrives at the gap between the Dees, the polarity of the Dees gets reversed. Hence the particle is once again accelerated and moves into the other Dee with a greater velocity along a circle of greater radius.
Since the rotational frequency of the particles remains constant as the energy of the particles increases, the diameter of the orbit increases until the particle can be extracted from the outer edge of the machine.
The limit on the energy of a particle is determined on a practical basis by the diameter of the magnet pole face.
Typical beam currents at the target are in the range of 50-100 μA. For cyclotrons using positively charged particles, the beam is electrostatically deflected and directed to the target (this cause some beam loss and the activation of internal part of the cyclotron). In case of use of negative ions, they are passed through a thin carbon foil, which strips off the electrons and converts the charge on the particle from negative to positive. The interaction of the magnetic beam with this positive ion bends its direction of motion outward and onto the target. The negative-ion cyclotron has a beam extraction efficiency close to 100% and requires minimal levels of shielding.
Cyclotrons are used to produce a variety of radionuclides for nuclear medicine. A positive charge is added to the nucleus in most activation processes. Therefore, the products lie in the proton-rich region and tend to decay by EC or $\beta+$ emission. Addition of positive charge to the nucleus changes its atomic number. Therefore cyclotron-activation products are usually carrier free.
Examples of radionuclides produced by cyclotrons are: C-11, O-15, N-13, Ga-67 or the famous F-18. This one is used to produce F-18-fluorodeoxyglucose (FDG).

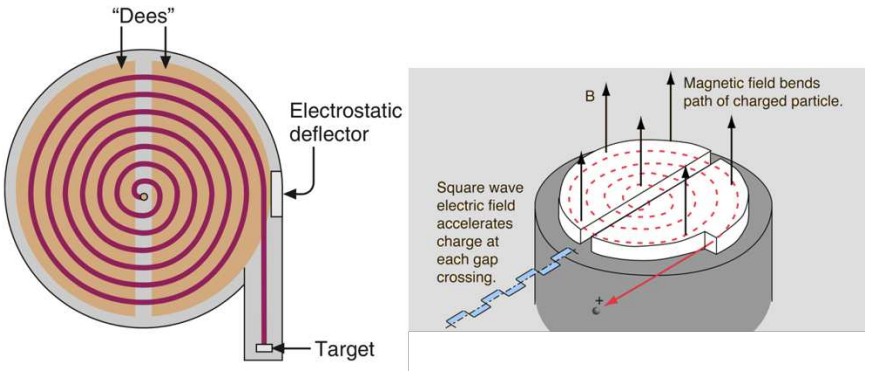

Figure 1.17: Schematic representation of a positive ion cyclotron [13] [36].

- ***Other Accelerators: ISOL Method***
  Accelerators can also be used to produce radionucleides by spallation, fission and fragmentation reactions on target from the irradiation with high energy particle beams.
  With such high energy beam a lot of element are produced. To isolate the nucleide of interest, it is then efficient to use the ISOL technique.
  The products are then ionized, accelerated, mass-separated and transported to experimental stations. Here the desired isotopes are generally implanted on metallic foils. The ISOL (isotope separation on-line) method (Fig.1.18) requires a high-intensity primary beam of light particles from a driver accelerator (or a reactor), and a thick hot target, from which the exotic nuclei formed have to diffuse and effuse into an ion source, for ionisation and extraction [37]. As this method generally results in the formation of a whole host of nuclei, stable and non-stable, it is essential to use mass separators to select specific ions of interest. This is the technique used in

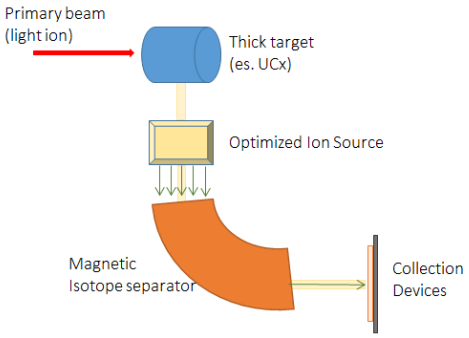

Figure 1.18: Schematic representation of the ISOL technique for the RIB production.

CERN facilities like ISOLDE and MEDICIS. The description of these two accelerators can be found at the Appendix A with particular details on the radionuclides collection principles and tools for the MEDICIS facility.

2

The transport of radionuclides for medicine: a type B container as case study

Contents

2.1 The risks in the transport of radioactive materials and the Regulation . . . 43
2.2 The safety aspects during the transport . . . 43
2.3 General characteristics and classification of the packages . . . 44
2.4 The design of a package for RAM transport . . . 48
2.5 The ColiBRI-30 . . . 50
2.5.1 Specifications of the package . . . 50
2.5.2 The iterative process in this design . . . 54
2.5.3 Technical description of the package . . . 62
2.5.4 The contents and the calculation of the activities to transport . . . 64
2.5.4.1 The Radioprotection study . . . 65
2.5.4.2 The Thermal study . . . 71
2.5.4.3 The simulation model . . . 73
2.5.4.4 Results of the simulations . . . 74
2.5.4.5 The list of isotopes to transport . . . 80
2.5.5 The Finite Element Analysis for the design's validation of the Overpack . . . 81
2.5.5.1 Basic principles of mechanics . . . 82
2.5.5.2 FEA Modelization . . . 85
2.5.6 Results of the Finite element Analysis . . . 86
2.5.6.1 Stacking test . . . 86
2.5.6.2 9m drop tests . . . 88
2.5.6.3 Drop onto a bar . . . 92
2.5.6.4 Drop of the 500 kg mass . . . 96
2.5.7 The regulatory tests planning . . . 99
2.5.8 Administrative steps for the approval . . . 100
2.6 Conclusions . . . 101

The development of new techniques of production of exotic radionuclides to use in systemic radiotherapy and imaging (for example using the so-called matched pairs) yields to the development of new containers to transport them. As stated at the par.1.6 of the first chapter, the radionuclides suitable for nuclear medicine purposes are characterized by short half-life. They are generally produced

in nuclear reactors, cyclotrons or other accelerator facilities and collected on small metallic foils.
Once the samples are irradiated, they shall undergo a series of chemical treatments before being coupled to biological substances to be injected in humans or animals for preclinical studies.
From the place of irradiation the samples containing the desired radionuclide is shipped to a chemical laboratory to be dissolved (generally in acid compounds) if in solid form, and "cleaned" from all the possible impurities and contaminants (this is possible for example through a process called chromatography) before being used. The final product can be then used in the same place of production or it can be shipped again to other places like hospitals, imaging center or other research institutes. Appropriate

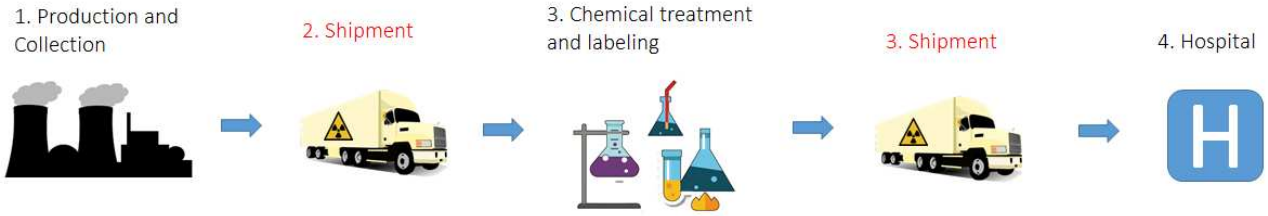

Figure 2.1: Scheme of the path of the medical radionuclides. The phase of the shipment appears. The difference can be found in the level of activities, higher in the first one since it involves also the presence of radioactive contaminants to be cleaned in a second stage.

packages are needed to move the irradiated samples. In the first phase of this path the sample to transport is characterized by a high level of activity, generally due also to the presence of radioactive contaminants collected at the same time.
Due to the hours or days spent for the travel and the needs to take into account the decay of the radionuclides, the activities to transport suitable for the radiopharmaceutical production sometimes exceeds the values defined for the type A containers or industrial packages imposed by the IAEA. This higher hazard involves the use of more complex and safety demanding packages.
Unlike other type of packages, the shipping containers suitable for the transport of high activities, called type B, need the approval of the Regulatory Authorities. It must be proved that they are able to sustain both the normal conditions of transit and accidental situations.
Existing type B packages have been designed on specific requests from the users. Dimensions of the sources, type of radionuclides and activity make available products too specific. Generally type B packages for medical isotopes are drums made of steel [38] or light material like foam or cork.
Many solutions are available for type B containers for waste and spent fuel, but their size make them unsuitable for the transport of small sources like the ones used in nuclear medicine, 10-20 ml ampoules.
One of the main topic of this PhD work has been the design of a new package for the transport of radionuclides to be used in nuclear medicine. The objective has been the design of a container that is compact, easy to handle and suitable for a long list of radionuclides with high activity.
The container has been designed by Lemer Pax in collaboration with the GIP Arronax and the Subatech Laboratories for the theoretical studies.

This chapter is organized as follows. The first paragraphs summarize the main concerns regarding the transport of RadioActive Material (RAM), with some details on the regulatory requirements. The second part of this chapter is fully dedicated to the description of the method used to design a package for RAM transport and in particular to the design of a new type B(U) package for medical radionuclides.
Some of the technical words used in this chapter have been defined at the par.B.1 of the Annex B.

2.1 The risks in the transport of radioactive materials and the Regulation

The transport of radioactive material leads to different risks:

- The risk of **Irradiation** (or External Exposure) of the public and of the workers in case the components of the package ensuring the radiologic protection will fail following an accident;
- The risk of contamination via **Inhalation** or **Ingestion** of radioactive particles (or Internal Exposure) due to the leak of the transported source out of the containment system and the overpack;
- The risk of **Environmental pollution** and the **Chemical risk** (due for example to the creation of toxic or corrosive acids of the uranium hexafloruride in contact with water in case of transport of fissile material);
- The risk of **uncontrolled nuclear chain reaction**, only in case of transport of fissile material;
- **Release of heat**, from substances like irradiated fuel, that can lead to the package's damage and consequent injury to the nearby persons.

Moreover there are several factors that can amplify the risks, like the nature of the radioactive materials transported, their chemical form (solid, liquid or gaseous), their conditioning (powder, non dispersible solid, encapsulated sources) and the activity of the transported substances.
To face all these factors of risk, a Regulation, internationally valid, have been put in place to frame and strictly define the quantity of substances to transport, the characteristics and the requirements for the shipping packages.
The base of the rules in this field have been developed by the International Atomic Energy Agency (IAEA), that collected the standards and the safety norms in the document *"Specific Safety Guide No. SSR-6: Regulation for the safe transport of Radioactive Material - Edition 2012"*, used as reference for this work. The recommendations for the transport of radioactive materials, and in general of dangerous goods, can be found also in several organization's Guides specialized by mode of transport and internationally valid:

- **Route:**
  United Nations Economic Commission for Europe (UNECE, Geneva), European Agreement concerning the International Carriage of Dangerous Goods by Road (ADR);
- **Railway:**
  Intergovernmental Organization for International Carriage by Rail (OTIF, Berne), Regulations Concerning the International Carriage of Dangerous Goods by Rail (RID);
- **Inland waterways:**
  United Nations Economic Commission for Europe (UNECE, Geneva), European Agreement concerning the International Carriage of Dangerous Goods by Inland Waterways (ADN);
- **Air:**
  International Civil Aviation Organization (ICAO, Montreal), Technical Instructions for the Safe Transport of Dangerous Goods by Air (ICAO IT);
- **Maritime:**
  International Maritime Organization (IMO, London), International Maritime Dangerous Goods Code (IMDG).

2.2 The safety aspects during the transport

The radioprotection of the workers and the public is the basic and constant concern in all the Regulations cited above. All the technical aspects, package's design and manipulation, as well as

the optimization actions, find their foundations in the ALARA principle. This principle aims to keep As Low As Reasonably Achievable the dose in the chain of activities involved during the shipments of radioactive material.
Besides the operational dose rate limits for the workers listed in the Chap.1 (par.1.5), two additional radioprotection rules shall be applied during the transport of RAM [39]:

1. The dose rate at contact of the package must not exceed 2 mSv/h. This limit may, however, be increased to 10 mSv/h in the case of the so-called "Exclusive use" (par. 221 and 528 [39]). In the latter case the sender or the consignee can then give specific instructions to limit the presence near the package. For example no intermediate stop from the starting to the delivery point are previewed and also no subsequent addition of RAM to the cargo along the pathway;
2. For road and rail transport, in any case, the dose rate must not exceed 2 mSv/h at contact with the vehicle (or wagon) and must be less than 0.1 mSv/h at 2 meters from the vehicle (or wagon) (par. 573 [39]).

The regulation also sets a limit on the level of contamination of the outer surfaces of packages. It must be less than 4 Bq/cm^2 for beta and gamma emitters and low toxicity alpha emitters (half-life $<$ 10 days), and 0.4 Bq/cm^2 for radioelements emitting high energy alpha particles (which are particularly harmful especially if ingested). Those limits are applicable when averaged over any area of 300 cm^2 of any part of the surface (par.. 508 [39]). In particular this is called ”non- fixed contamination”, since it can be removed from a surface during routine conditions of transport.

2.3 General characteristics and classification of the packages

The safety during the transport lies principally in the choice of the package that should provide an adequate shielding to protect the workers, the environment and the public against the effects of radiations. It should also provide protection against the dispersion of the contents both in normal and/or accidental conditions of transport in case of main radioactive materials.
The principal safety functions of the packages consists in the prevention of the potential risks listed in par.2.1: ensure a protection against ionizing radiation with an adequate shielding, prevent the release of substances out of the package, prevent the occurrence of a nuclear chain reaction (for fissile materials) and provide protection against the thermal release of the contents.
The first level of protection is therefore the robustness of the package, which must ensure the maintenance of security functions, including in the event of a severe accident if the security issues require it.
A list of general safety requirements for all packaging and packages shell be taken into account in the phase of design (par. 607-618 [39]):

- In relationship to the mass, the volume and the shape of the package, it must be designed to be secured during the transport and easily and safely transported, independently by the activity stored in it;
- The lifting systems attached to the package shall not fail and safety factors must be taken into account to cover eventual failures. Moreover any lifting elements shall be removable or rendered incapable of being used during transport;
- The external surface shall be designed as far as practicable, to prevent the retention of water and to be easily decontaminable;
- The chosen materials must be compatible with the radioactive contents;
- Unauthorized operations must be prevented adding safety control elements.

The IAEA foresees a classification of the packages in relation to the activity and the physical form of the radioactive material to transport. For each of them a set of standard performances, design requirements and specific test procedures, are established.
For each radionuclide two activity limits, called A_1 and A_2, have been established to define the quantity of substance to transport in each type of container. A_1 shall mean the activity value for *special form radioactive material* (indispersable solid or sealed capsule), while A_2 is the activity limit for radioactive material *other than special form*. These two A values (given in TBq unit) are used to clearly define the type of the container. Five levels of packages are defined. They are related to the potential hazard of the material to transport and reflects also a difference in the standard requirements.
Here below more details of the different categories.

- *Excepted package*:
  Excepted packages are the ones in which the allowed radioactive contents is restricted to a such low level that the potential hazards are not relevant. Therefore no testing procedure regarding the package design is required. The radiation level at any point on the surface of an excepted package cannot exceed 5 μSv/h (par 516 [39]). This threshold prevents the public from being unnecessary exposed and protects any sensitive photographic material in close proximity from any damages. This value of dose rate gives the limit for the activity to transport. More in particular the activity to transport must be:

  - Lower than A_1 for special form radioactive material for solid sources;
  - Lower than A_2 for all the other radioactive materials for solid sources;
  - Lower than 10^{-1} A_2 for all the other radioactive materials for liquid.

  Due to the very low hazards this type of package does not require approval from the authorities.

- *Industrial package*:
  This type of packages are generally used to transport two kinds of materials, both in a non-easely dispersable form:

  - Material with low activity per unit mass (known as Low Specific Activity or LSA materials), like the common hospital waste;
  - Non-radioactive objects with low level of surface contamination (known as Surface Contaminated Objects or SCO), like fuel cycle machinery or parts of nuclear reactor.

  There are three types of industrial packages (Type IP-1, Type IP-2, and Type IP-3) that are used for LSA and SCO shipments. The requirements that packages have to meet to be classified as industrial packages are listed in the Tab. 2.1. Many normal packages used in industry, such as steel drums or bins, could easily meet the requirements for this category.

- *Type A package*:
  Type A packages are intended to provide a safe and economical means of transport for a well defined, but significant, quantity of radioactive material. It is assumed that this type of package may be damaged during transport activities and that a portion of the content may be released. The radioactive quantity that they can transport is then limited by the regulation and fixed to a value:

  - Lower then A_1 for special form radioactive material;
  - Lower then A_2 for all the other radioactive materials.

Criteria	Requirements
Design Requirements	• General requirements for all packages; • Additional pressure and temperature requirements if transported by air. • Type A additional requirements (only for IP-3).
Test Requirements: Normal Conditions	• Free drop test from 0.3 to 1.2 m, depending on the mass of the package (for IP-2, IP-3); • Stacking or compression test (for IP-2, IP-3); • Penetration test (6 kg bar dropped on the package from 1m, only for IP-3).

Table 2.1: Industrial Package requirements (par. 719-724 [39]).

Type A packages are designed to maintain their integrity under the kind of mishandling which may be encountered in normal transport conditions, for example: falling from vehicles, being dropped during manual handling, being exposed to the weather (i.e. the rain), being struck by a sharp object, or having other packages or cargo stacked on top of it (Tab. 2.2). The homologation of this type of package shall foresee a phase of testing, but the presence of regulatory authorities is not mandatory.

Criteria	Requirements
Design Requirements	• General requirements for all packages. • Additional pressure and temperature requirements if transported by air.
Test Requirements: Normal Conditions	Each of the following test must be preceeded by a water spray test: • Free drop test (from 0.3 to 1.2 m depending on the mass of the package) • Stacking or Compression test • Penetration test (6 kg bar dropped from 1m)

Table 2.2: Type A package requirements (par. 719-724 [39]).



Figure 2.2: Example of Type A package (Posisafe, Lemer Pax) used for the shipment of medical sources.

- *Type B package*:
  Type B packages are required for the transport of highly radioactive materials. For this reason it should be capable of withstanding most accidental conditions, without breach of its containment or an increase in radiation levels for the general public and/or for the personnel involved in rescue or clean-up operations. The activities that it is possible to transport are in this case:

  – higher than A_1 and lower than 3000 A_1 or 10^5 A_2 (whichever is the lower) for special form radioactive material if transported by air;
  – higher than A_2 and lower than 3000 A_2 for all other radioactive material if transported by air.

  The design of a Type B package requires the approval of competent Authorities. Besides the limits of activity to transport and the limits of dose rate at contact with the package, this type of container shall be able to sustain not only normal but also accidental conditions of transport. The Tab.2.3 summarizes the stringent conditions a package must satisfy to obtain an homologation as Type B Package. Additional details on the design path and on the testing conditions will be added in the following paragraphs.

Criteria	**Requirements**
Design Requirements	• General requirements for all packages. • Additional pressure and temperature requirements if transported by air • Type A additional requirements
Test Requirements: Normal Conditions	Each of the following test must be preceded by a water spray test: • Free drop test (from 0,3 to 1.2 m depending on the mass of the package) • Stacking or Compression test • Penetration test (6 kg bar dropped from 1 m)
Test Requirements: Accidental Conditions	Cumulative effect of: • Test of normal conditions of transport; • Free frop test (from 9 m); • Puncture test (drop from 1 m on a rigid bar); • Drop of 500kg mass on the package; • Thermal test (fire of 800°C for 30min); • Immersion in water (15 m for 8 h).

Table 2.3: Summary of the Type B requirements (par. 719-729 [39]).

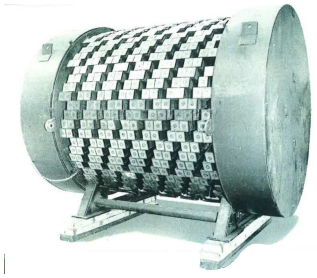

Figure 2.3: Example of Type B package for the transport of spent fuel (Lemer Company).

- *Type C package*:
  They are used to transport radioactive materials with activity higher than the one established for the type B by air. For this reason, they must sustain not only to all the tests established for the Type A and B package but additional safety evidences are needed (Tab.2.4).

Criteria	Requirements
Design Requirements	• General requirements for all packages; • Additional pressure and temperature requirements if transported by air; • Type A additional requirements; • Type B additional requirements (due to internal heat generation and max surface temperature).
Test Requirements: Normal Conditions	Each of the following test must be preceded by a water spray test: • Free drop test (from 0,3 to 1.2 m depending on the mass of the package); • Stacking or Compression test; • Penetration test (6kg bar dropped from 1 m).
Test Requirements: Accidental Conditions	Cumulative effect on one specimen of: • Free drop test (from 9 m); • Puncture test (drop from 1m on a rigid bar); • Drop of 500 kg mass on the package; • Puncture test; • Fire test (immersion in 800°C for 60 min); A separate specimen can be used for: • Impact test (at not less than 90 m/s).

Table 2.4: Summary of the Type C requirements (par. 734-737 [39]).

2.4 The design of a package for RAM transport

The term "design" includes all activities from the specifications of the material to be transported to the drawing and the demonstration that the chosen shape satisfies the national and international legal requirements.
In practice there is a lot of inter-connection between all of these activities which will not necessarily be sequential and most of the time need to be repeated and refined many times before achieving the right combination. It is possible to divide the entire process in five big steps, each of them containing several actions (Fig.2.4):

1. **First step: Specification**
   This phase initiates the design of the package. It consists in the identification of all the requirements the package must comply with, strongly depending on the final scope of the package. The information to collect in this step are:

   (a) the nature and the chemical form of the materials to be transported;
   (b) the maximum activities involved;
   (c) ambient temperature conditions and eventual heat generation due to the decay of the source;
   (d) transport mode (rail, air, naval);

(e) materials to be used, or any material restrictions with the ambient or the source;
(f) the locations where the packaging will be used;
(g) any specific handling and/or operating requirements.

The first two items will determine the package type, i.e. whether it is type C, B, A, IP or Excepted. This immediately reports to the normal and/or accidental conditions of transport it will need to be designed for. Item c) is a limit for the following item d). Items d), e) and f) can impose size and weight limitations and result in constraints on the position, form and shape of lifting and tie-down features for example.

2. **Second step: Design**
The design phase consists in the realization of the technical drawing of the prototype based on the specifications.
Some of the aspects analyzed at this stage are: the shielding definition, the mechanical strength, the thermal design, the radioactive containment and the sealing type, lifting and handling systems, manufacturing ability.
For the definition of some structural elements, and in particular for the choice of the radiological containment system (shield), analytical or Monte Carlo calculations must be done. The scope is to insure that the materials and the chosen geometrical dimensions are sufficient to stay below the dose rate limits prescript by the regulations. Example of tools used for these purposes are Nucleonica, RayXpert or MCNPX.

3. **Third step: In silico testing**
In general, there is not a straight line between the drawing and the prototype realization and the experimental testing phase. It must be noticed that an adequate number of tests carried out directly with one or several prototypes is prohibitive especially when the article and/or the realization of the test themselves are costly.
For this reason in the drawing phase it is possible to integrate calculations and simulations that can describe the behavior of the package in the test conditions specified in the Regulation. This method reduces the incidence of mechanical failures and saves time and money. For this purpose Finite Element Analysis (FEA) could be used. They allow carrying out mechanical and transient thermal analysis on virtual prototypes and provide accurate representation of the deformations.
The basic philosophy of this technique is the following. The finite element method involves modeling the structure using small interconnected elements called, indeed, **finite elements**. A displacement function is associated to each of them. Every interconnected element is linked, directly or indirectly, to every other element through common (or shared) interfaces, including nodes and/or boundary lines and/or surfaces. By using known stress/strain properties for the material composing the structure, it is possible to determine the behavior of a given node in terms of the properties of every other elements in the structure. The total set of equations describing the behavior of each node results in a series of algebraic equations expressed in matrix notation [40]. More information on the FEA and the systematic procedure of simulation with the software ANSYS can be found in Annex B par.B.2.
In the design phase, an iterative process is put in place between the second and the third step listed. Once a first drawing is realized, it is tested with the FEA. The results of the simulations help in the redefinition of structural elements (i.e. insertion of additional reinforcements, modification of the material of the components thickness, etc). The modifications yield to a new simulations set.

4. **Fourth step: Test**
   Practical evidences are required to demonstrate that the prototype can sustain the conditions and the loadings experienced in transport and a schedule of test must be defined. The type of test depends on the package category and the conditions of loading are prescribed by the IAEA regulation. In some cases, and with the consent of the authorities, it may be possible to substitute some test with calculations or FEA simulations. With the same methods, additional test may be required or provided to demonstrate the resistance of special components.

5. **Fifth step: Approval**
   This represent the last step of the chain. It is important to notice that this is a process and not a single event. Approval will need to be gained at different stages of the design progresses from the concept, through the production of calculations supporting the choice of the mechanical drawing and safety, to final design drawings.
   In France the organization in charge of the emission of the homologation and the certificate of agreement is the ASN, Autorité de Sûreté Nucléaire. The developer of a new model of package shall transmit to ASN several documents with in-depth technical justifications, studied in detail with the support of another institution, the IRSN, Institut de Radioprotection et de Sûreté Nucléaire.

The steps described before represent the basic path followed also in the design of the type B package.
The following paragraphs describe in detail all the actions done in the processes of Specification, Design and Testing of the prototype in order to comply with the requirements imposed by IAEA.
In particular the design presented in the paragraph 2.5.1 is the results of an iterative process that made use of the FEA. This method helped to define shape, thickness and positioning of the different elements composing the package. Before giving a complete technical description of the results and of the final shape chosen for the package, the element on which the iterative process are based are presented.
The description and the results of the last chain of tests, relative to the final drawing, are presented in order to prove the good performance of the chosen design.

2.5 The ColiBRI-30

2.5.1 Specifications of the package

The first step in the design of a new package is to establish its main scopes and specifications.

- The container under study is intended to transport medical radionuclides from the place of production, mainly research reactors, large isotope separator facilities or cyclotrons, to the radiopharmacies or chemical laboratories for the treatment of the irradiated sources.

- The container is intended to transport both solid and liquid samples (Fig.2.5).
  The solid sources can be in form of metallic plates (if the irradiated samples come from nuclear reactors or from the CERN-Medicis facility) or in plastic or metallic vials. In the case of reactors, if the irradiation is done immersing the samples in the pools, the metallic foils are placed in quartz ampoules arranged in aluminium tubes. At the end of the irradiation, the tubes are cut and the ampoules extracted.
  The liquid sources are generally included in vials containing radionuclides after a first chemical

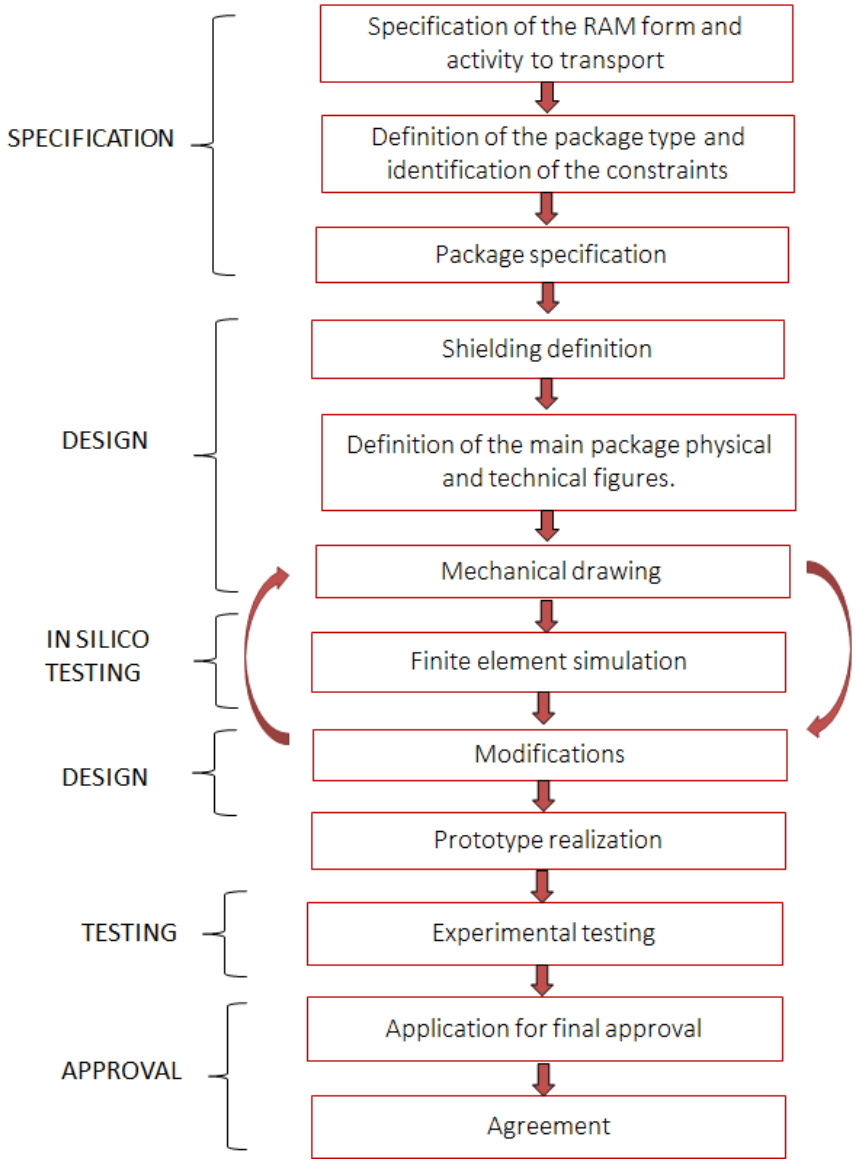

Figure 2.4: Flowsheet for a type B package design and approval process.

treatment. Sometimes for the transport they are placed inside polyethylene layers for additional protection.

- The dimensions of the internal region of the container must be compatible with the ones of the sources to transport: 3 cm of diameter and 7 cm of height are sufficient to allocate vials commonly used for radiopharmaceuticals as well as for the quartz ampoules coming from the nuclear reactors.
- The characteristics of the package's content suggests that the type of radioactive material is "non-special form" since the sources are not sealed and the risk of release (in the confinement system) after an accident must be considered. The limit of activity to transport for this kind of material is imposed by the A_2 values given in the IAEA Regulation for each radionuclide.
- The sources identified for the transport with this package are listed in the Tab.2.5.



Figure 2.5: Pictures of the solid samples: example of sample in quartz ampoule before encapsulation for irradiation at ILL (left) and sample holder of ISOLDE SSP chamber with two Zn coated Au foils (right).

Radionuclide	Half-life	Decay type	Daughter Nuclide	A_2 [TBq]
C-11	20.37 m	ε	B-11	6.00E-01
Sc-47	3.351 d	β	Ti-47	7.00E-01
Cu-61	3.333 h	ε	Ni-61	2.00E-02
Cu-67	2.579 d	β-	Zn-67	7.00E-01
As-71	2.720 d	ε	Ge-71	2.00E-02
As-77	1.618 d	β-	Se-77	7.00E-01
Sr-89	50.57 d	β-	Y-89	6.00E-01
Y-90	64 h	β-	Zr-90	3.00E-01
Nd-140	3.37 d	ε	Pr-140	2.00E-02
Tb-149	4.12 h	ε:83.3% α: 16.7%	Eu-145/ Gd-149	9.00E-05
Sm-153	46.284 h	β-	Eu-153	6.00E-01
Tb-155	5.32 d	ε	Gd-155	2.00E-02
Tb-161	6.89 d	β-	Dy-161	2.00E-02
Yb-166	2.362 d	ε	Tm-166	2.00E-02
Er-169	9.392 d	β-	Tm-169	1.00E+00
Yb-175	4.185 d	β-	Lu-175	9.00E-01
Lu-177	6.65 d	β-	Hf-177	7.00E-01
Re-186	3.7186 d	β-: 92.53% ε: 7.47%	Os-186/ W-186	6.00E-01
At-211	7.214 h	ε: 58.2% α: 41.8%	Po-211/ Bi-207	5.00E-01
Ac-225	10.0 d	α	Fr-211	6.00E-03
Ra-226	1600 y	α	Rn-222	3.00E-03
Ac-227	21.77 y	α	Fr-223	9.00E-05
Re-188	17 h	β-	Os-188	4.00E-01
Th-228	1.9125 y	α	Ra-224	1.00E-03
Th-229	7932 y	α	Ra-225	5.00E-04
W-188	69.78 d	β-	Re-188	3.00E-01

Table 2.5: Radionuclides sources to transport with the Type B package with relative limits of transport defined in the IAEA Regulation. The type of decay and the half-life are also indicated.

These radionuclides are produced in reactors (like for example the Lu-177, thorium isotopes or Y-90) or in cyclotrons (as the copper or the scandium isotopes). The terbium and scandium isotopes can be produced with high activity also in some ISOL facilities, like the CERN-ISOLDE.

The new CERN-Medicis facility started the production of C-11, Cu-67, Er-169 and Ac-225 in testing batches of low activity (up to 100 MBq) and plans to increase it the next future.

- The container under study is intended to be licensed as type B(U), where the notation (U) stands for "Unilateral". It means that the package shall be classified in accordance with the competent Authority certificate of approval issued by the country of origin of the package and that the certification in this jurisdiction is accepted elsewhere without further approvals.

- In order to obtain the certificate of approval by the nuclear French authority (ASN), it must be demonstrated that this design satisfies precise requirements reported in the paragraphs 652-666 of [39] for the type B, other then general requirements listed in the par. 607-618 seen in the section 2.3 and valid for all the types of package.
  Typical specifications associated to the type B, are valid under precise conditions of temperature and pressure (clarified also later in this work). Among them:

  - In absence of insolation the accessible surfaces of the package shall not exceed 50°C, with an ambient temperature of 38°C (par 619);
  - The package to be transported by air shall be capable of withstanding without loss of radioactivity an operative pressure of plus 95 kPa (par. 621);
  - The package must be able to sustain working temperature range of -40° to +70° to prevent potential degradation of package materials (par. 639). This is valid also for the type A;
  - If the containment system is a separate unit, it must be possible to securely closed by a fastening device independent from other part of the package. The fastening device cannot be open unintentionally or by the pressure that can be developed in the package (par. 643);

- The par.2.2 listed the dose rate limits to respect at contact with the package: 2 mSv/h or 10 mSv/h in case of exclusive use.

- A package shall be designed so that the heat generated in it by the radioactive contents shall not, under normal conditions of transport, affect the requirements for the containment and shielding if left unattended for a period of one week (par. 653). This means that the containment system must be effective and keep its integrity for the duration of 7 days.

- As reported in the Tab.2.3, the type B package must be tested to prove it is able to sustain both the normal and accidental conditions, showed in the Fig.2.6. The first are also required for type A containers and are: water spray test, free drop test, stacking test and penetration test. Parameters like the height of the drops may depend on the weight and the content of the package. The second chain of tests includes three different drop tests (to perform with the same package), fire and water immersion of the package.

Besides the requirements imposed by the Regulation, it has been decided to add **other specifications**, coming from discussions with potential users:

1. It shall be easy to manipulate and with a safe but fast opening and closure procedures to limit radiation exposure;
2. Elements for the safe stabilization during the transport must be foreseen to avoid accident coming from the package drop;
3. The weight of the total package must insure manipulation with cranes but also with forklifts. A limit of 100 kg is considered;

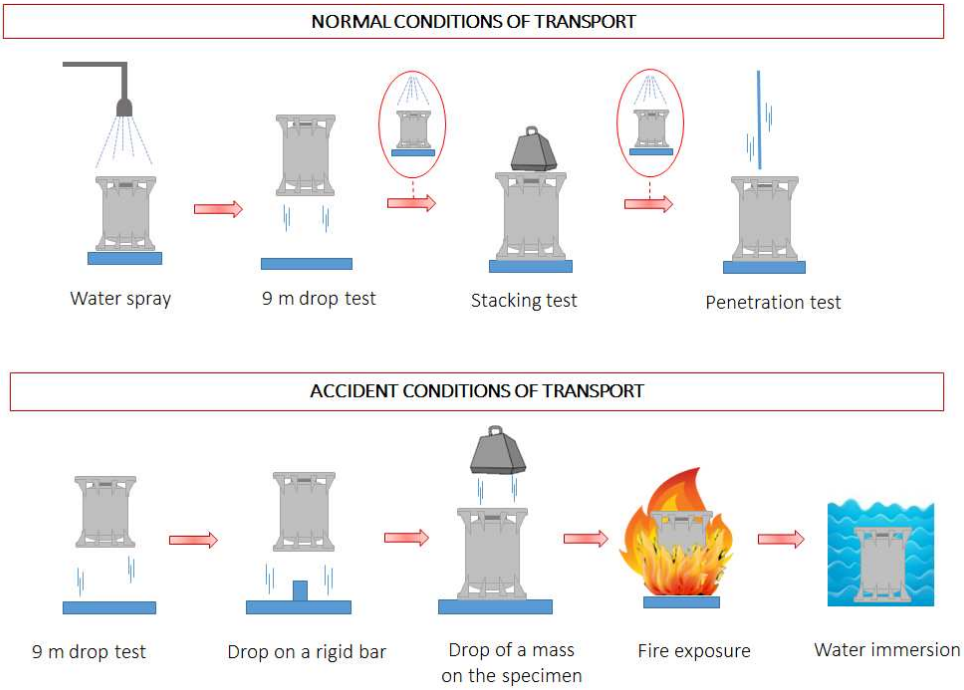

Figure 2.6: Scheme of summary of the normal and accidental conditions test to be performed on the prototype (par. 719-729 [39]).

4. The package should be composed by a shielded removable cask with dimensions and weight allowing the manipulation by hand and with a telemanipulator inside a hotcell. This imposes a limit also on the weight of this element. A value of 20 kg has been chosen as reference;
5. The external surfaces of the package and the inner cask shall be easily decontaminable.

The necessity of fast operations is linked to the short half-life of the RAM to transport, that is the basic characteristic of the radiopharmaceuticals. Fast operations are necessary also to reduce the exposure of the workers involved in these operations (ALARA principle).

The name chosen for this package reflects its scope: **ColiBRI-30**, acronym for "Colis Type B pour RadioIsotopes".

2.5.2 The iterative process in this design

As stated previously, the final design is the result of an iterative process involving the balance of several parameters. Each detail and package component is generally not absolving to only one function and the protection provided against one hazard may affect the margins of safety imposed for another one. The final drawing must be the best compromise, able to solve this chain effect.
The design starts with the definition of all the specifics and the rules the new package must comply with (summarized at the par.2.5.1). Once the first virtual model have been realized it is tested with the finite element analysis. Additions or element modifications lead to another set of simulations and may have effects on the global structural or thermal performance.
In the particular case of the container under study, five versions have been analyzed and subjected to this process.
Before giving the technical details of the final solution adopted and have a look on the results of the last mechanical and thermal test design with the FEA, it is necessary to understand the reasons

and the path that led to them. This will be done observing the consequence of the choices done for materials and shape of the package on the final performance and how they are interconnected. At this stage the discussion is only qualitative.

1. **Choice of the shielding from radiation:**
   This study started with the choice between the two main materials commonly used for shielding purposes (easy to find on the market), lead or tungsten. These two are both very effective against gamma and X-ray radiation due to their high atomic number (Z=82 for Pb and Z=74 for W) but they differenciate for some other aspects:

   - Lead is cheaper and easier to manufacture.
   - Tungsten has density (19.7 g/cm^3) higher than lead (11.3 g/cm^3). This means that a more compact object can be obtained for the same shielding factor.

   As said before, a value of 20 kg for the weight of the shielded package has been chosen as limit in order to allow the manipulation of this object by hand.
   A thickness of W equal to 3.5 cm has been initially implied for the shielding in order to fit this specification. Moreover, based on first calculations, it has been considered as a good compromise for the transport of high activities.
   Considering internal dimensions compatible with the vials of radiopharmaceuticals, the total weight of the removable shielded core is in between 20.3-20.5 kg (depending on the design). The same shielding effect would preview 5 cm of thickness for lead, corresponding to 25-26 kg, then above the specification. For this reason tungsten has been preferred.
   Several mechanical drawings of the shielded container have been produced. Their feasibility, in terms of logistics, manipulation and realization has been studied and discussed with potential users. The Fig.2.7 shows two examples of design. Both have 3.5 cm of tungsten thickness and differentiates in the option of closure/opening of the shield.

   - The design a) shows two metallic rings (one on the main body and one on the lid) closed by three screws. The manipulation in hot cell is possible thanks to holes on the screws that facilitate the use of a proper screwdriver. The lifting of the shielded container is done through the knob of the lid. Since there is not a proper way to examine that the screws have been well fixed, in case the knob fails the container may open.
   - In the design b) the screws were placed on a removable metallic element. The closure is insured by the pressure that they exert on the lid while the tightness is guaranteed by an O-ring placed on the lid base. The lift of the container is done always through the knob. This time the presence of the metallic cage avoids the opening of the container in case the knob fails or in case one of the screw is not fixed. On the other side there is not a recovery lifting system.
   - The design c) is one used for this work, coming from a commercial choice. The Lemer Pax Company is already producing a shielded tungsten container (thickness 3 cm and weight lower then 20 kg) already supplied to nuclear reactors. It overcome all the difficulties connected to the manipulation in the hotcell. Indeed the lid is open and closed thanks to a magnetic tool and secured screwing a safety stainless steel additional lid.
     Together with an overpack made in rigid plastic and foam, this container is certified as type A and its commercial name is PosisafeKL-30® (more details are given later).

   Obviously the choice of the shielding thickness and material is directly connected to the global dimensioning of the overpack. The distance to impose between the shield and the external surface



(a) (b) (c)

Figure 2.7: Examples of studies on the inner shielded container of the type B package.

of the overpack will guarantee a dose rate level below the regulatory limit. With the choice of the Posisafe KL-30, it has been necessary to compensate the smaller thickness of tungsten (3 instead of 3.5) by the distance factor. In particular, a first dimensioning making use of Monte Carlo techniques of dose rate simulation led to the definition of a distance factor of 15-20 cm.

2. **Choice of the material for the fire protection:**
Before any package is given the licence for its use, it must be proved it can resists to thermal shocks. In particular the type B shall resist to normal temperatures of transport, between -40°C and +70°C, and to fire test in which the maximum temperature will be 800°C combined with an ambient temperature of 38°C.
Due to these specifications, it appeared necessary to add to the shielded core another layer of protection to avoid the increase of the temperature inside it and then protect the source from losing their properties at elevated temperatures.

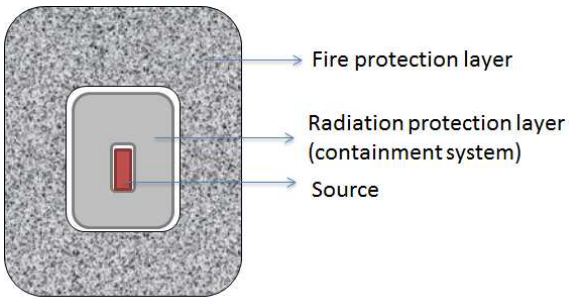

Figure 2.8: Schematics of the layers to preview in the type b package.

The first materials taken into account for the fire protection layer have been: concrete, plaster and ceramic. They all have a low conductivity (a coefficient indicating the property of a material to conduct heat) as shown in Tab.2.6.

On the other hand some negative aspects shall be highlighted. The density of concrete is in the range of 1.75-2.4 g/cm^3 (depending on the composition and the type used [41]). Its use would

Material	Thermal conductivity [W/m K]
Concrete	0.1- 0.7
Plaster	0.2
Ceramics	0.13 - 0.17

Table 2.6: Thermal conductivity of the materials considered in the design of the thermal layer.

correspond in an elevated weight of the overpack. For example a simple cylindrical form of this layer built around the volume occupied by the shielded containment system and with thickness of 15 cm, would results on a weight of around 150 kg. Plaster or ceramics have a lower density (around 0.8-1,2 g/cm^3), resulting in a lower weight of the insulation layer, but they are also poorly resistant to mechanical shocks (resistance to 0.4-2 MPa) and tend to fail by chipping.
One last observation is connected to the difficulties in the simulations of those materials with the finite element methods. They are porous materials and the convective heat transfer in such structures is complex [42].
Moreover, cracks and fractures possibly arising after the drop test, would compromise the performances in the subsequential tests. The impossibility to properly simulate those effects leads to the consideration of other materials.
The need to have lighter and thermal efficient material brought to the choice of insulation wool. In order to select the best product for our purposes research and discussions with manufacturer have been necessary. As shown in the Fig.2.9, the type of wool depends on the range of working temperatures. For this work, alkaline earth silicate (AES) wool is the most appropriate. They consist in amorphous fibers produced by melting a combination of CaO, MgO and SiO_2 [43]. The information and the properties of the chosen wool are reported in Appendix B.

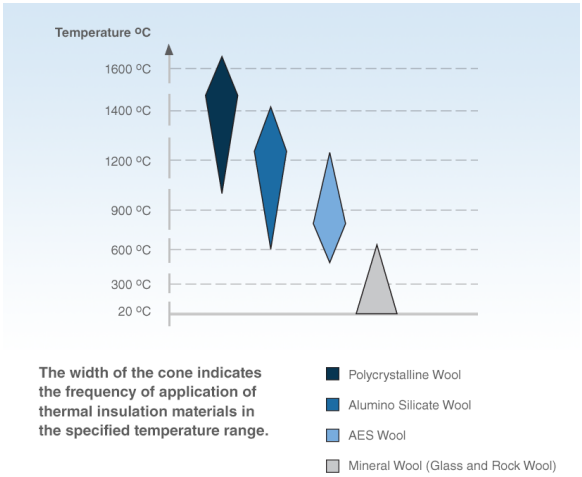

Figure 2.9: Temperature ranges for the application of synthetic insulation wool [43].

Temperature resistance consideration shall be applied also to the choice of the package sealing. Due to the high temperature the package shall sustain, it has been decided to put the sealing on the containment system, the tungsten shield, placed in the inner region of the package. In this way it won't be directly exposed to the high temperature during the test of the accidental

conditions. Beside the working temperature, this decision is influenced by several other factors like the chemical nature of the contents, the frequency of use, the time the package shall remain sealed and the radiation dose. A joint in silicone (VMQ - polysiloxane vinile methyle) can satisfy all the conditions [44]. Its working temperature falls in the range -60°C/+200°C and it is resistant to diluted salt solutions, atmospheric agents and ozone. It also has a good resistance to radiation (max 10^6 Gy).

3. **Shape and materials for the overpack (outer shell):**
The choice of the overpack's shape must fulfill two main functions: protections against the mechanical shocks and definition of a distance factor from the source for dose rate measurements to be done before the shipment. It must be easy to decontaminate and to handle and shall not retain water.
Stainless steel has been chosen as main component of the overpack external shell. It has a good resistance to fire, corrosion and oxidation.
The choice of the shape depends on the items 1 and 2 listed before:

   - The choice of the 3 cm tungsten shield and the idea to use light materials for the fire protection (that do not intervene in the radioprotection) set up the minimum dimensions the overpack must have to guarantee the transport of high activity and dose rates in line with the regulation ($<$ 2 mSv/h at contact with the overpack).
   - Stainless steel is able to sustain high temperature due to its very high melting point (1550°C). As all metal, it has also an elevated heat conduction coefficient (9-12 W/mK). In case of fire test, the elevated heat will flow from the outside to the inner regions of the overpack through the steel surfaces composing it by thermal conduction. An accurate choice of the shape would reduce this effect.

   Other considerations that guided the choice are the following:

   - The total weight is another factor limiting the package dimensions. Massive packages lead to logistic difficulties for manipulation and high transportation costs. A weight of 100 kg has been set as reference to guarantee a good balance between protection, stability, manipulation and shipping costs.
   - The shape of the overpack is also connected to the requirement for the type B to resist to different mechanical drop test (Fig.2.6). It shall be, then. characterized by elements that reinforce the structure and cushion the stresses. Their thickness must be accurately chosen to guarantee the protection of the inner shielded package during the test and at the same time to not contribute massively to the total weight of the package.

Fig.2.10 shows the evolution of the overpack's shape taking into account the previous guidelines. As already stated, the mechanical drawing of the overpack has been an iterative process. The resistance to thermal and mechanical shocks and the limit imposed on the weight have been the three main parameters used at each stage to compare the design and chose the modifications to be made on it. In particular, four shapes have been analyzed and virtually tested before arriving to the final choice.

It is possible to take the Tab.2.7 as reference to track the differences among the design:

I. The first analyzed model has a cylindrical shape with flat bases and a series of reinforcements wings connected to two metallic rings. Once inserted in the mechanism of the finite element analysis, it results in a non adequate performance. From the mechanical point of view, a

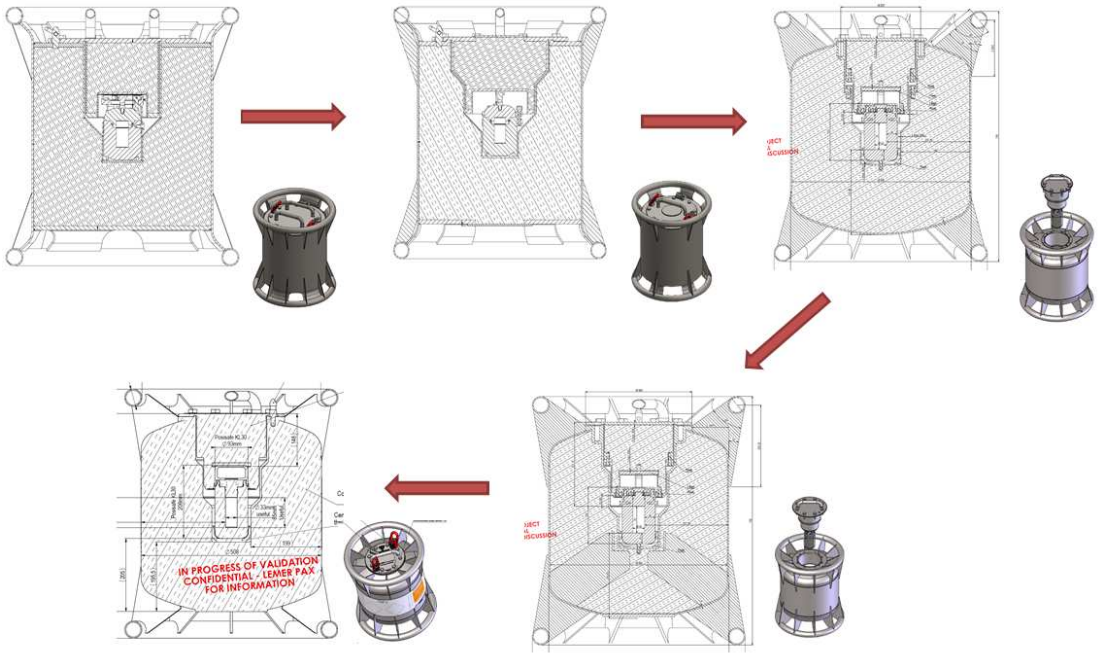

Figure 2.10: Chain of tested projects for the container's overpack (drawings and 3D figures in small).

Number of design	Temperature resistance	Mechanical resistance	In the limit of weight
I	✘	✘	✘
II	✔	✘	✘
III	✔	✘	✔
IV	✘	✔	✘
V	✔	✔	✔

Table 2.7: Comparison of the different design of the overpack.

drop from 9m in an horizontal configuration for example, caused a strong deformation of the internal surfaces due to the stress exercised by the tungsten container. Its weight is 168,4 Kg, higher than the one of the specification.

II. A double cone shape in a second version increased the stability of the inner region during the mechanical drop test (Fig.2.11). However the external reinforcement wings were too thin to avoid the contact of the main body with the target during the impact (Fig.2.12). Other improvements on the shape helped in a gain of weight: the thickness of some elements (base and lid shells) can be reduced without losing in mechanical stability. The weight goes from 168,4 to 138 kg, still higher then the specification limit.
This modifications improved the thermal performance: increasing the metallic path and decreasing the thickness of the surface, the temperature in the internal regions after the 30 min exposition to fire was reduced (Fig.2.13).

III. The top and bottom base are substituted with rounded shells in a third design. This includes also a reinforcement of the wings connecting the main body to the cushioning

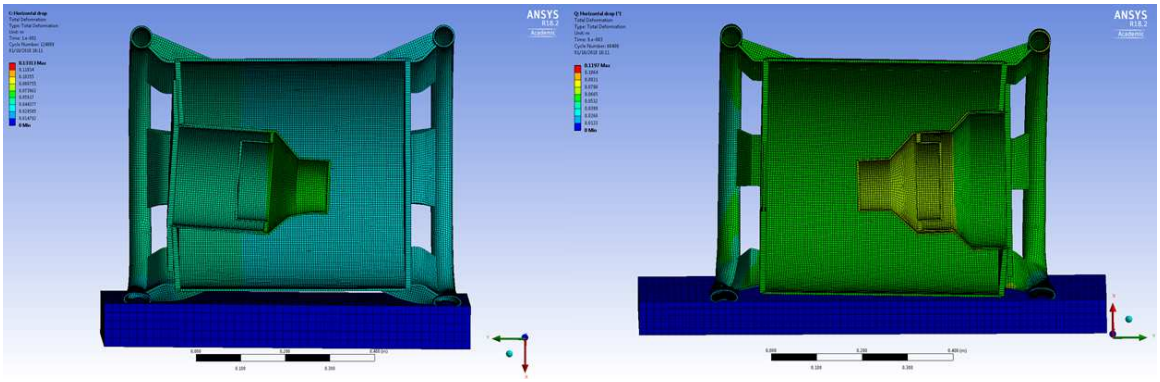

Figure 2.11: Results of the total deformation on the package after a 9m drop test in the horizontal configuration. Design I on the left and design II one on the right.

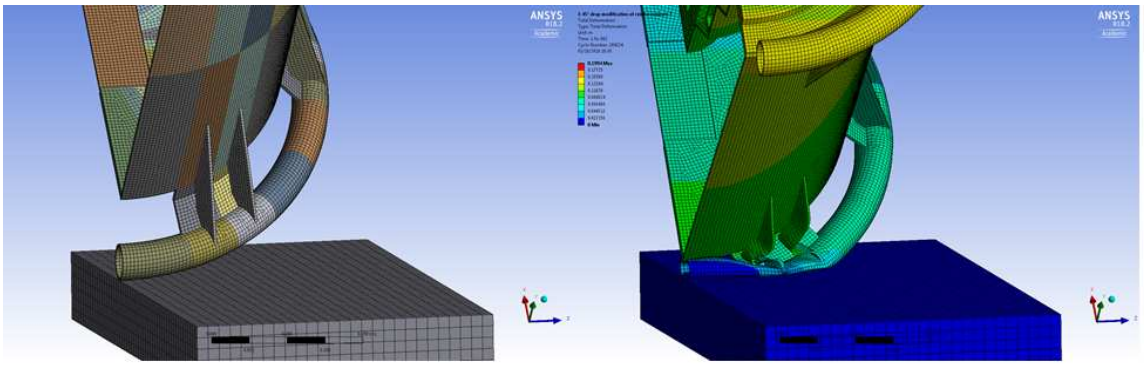

Figure 2.12: Deformation of the steel shell after the 9m drop test for the design II.

rings. The weight decreased from 138 to 112 kg but the width of the internal cone has been reduced to better dispose the lid. The consequences due to the decreased thermal path have been overcome inserting two rings made of PEEK and connected to the metallic internal surfaces of the lid and the main body of the overpack (Fig.2.14). The modifications done didn't show ameliorations during the mechanical drop test. In particular the spherical surface appeared bended inwards due to the weight of the tungsten container after the test (Fig.2.15 and Fig.2.16).

IV. The fourth drawing tried to solve the problem of the base deformations previewing three internal metallic wings. They were inserted to block the tilting and the elongation of the internal surfaces during the mechanical tests. Moreover they are not touching the internal cone in order to not transfer directly the heat. If on one side this design improved the mechanical stability, this massive addition of metallic elements also increased the total weight (122 kg).

V. The last version corresponds to the final adopted solution described in detail in the following paragraphs. The issue of the mechanical stability of the internal metallic surfaces is solved connecting the reinforcement wings to the conic internal shell through a thick (10 mm) stainless steel ring. In this way, during the impact, the elongation force coming from the presence of the tungsten mass is balanced by a reaction force done by the wings connected

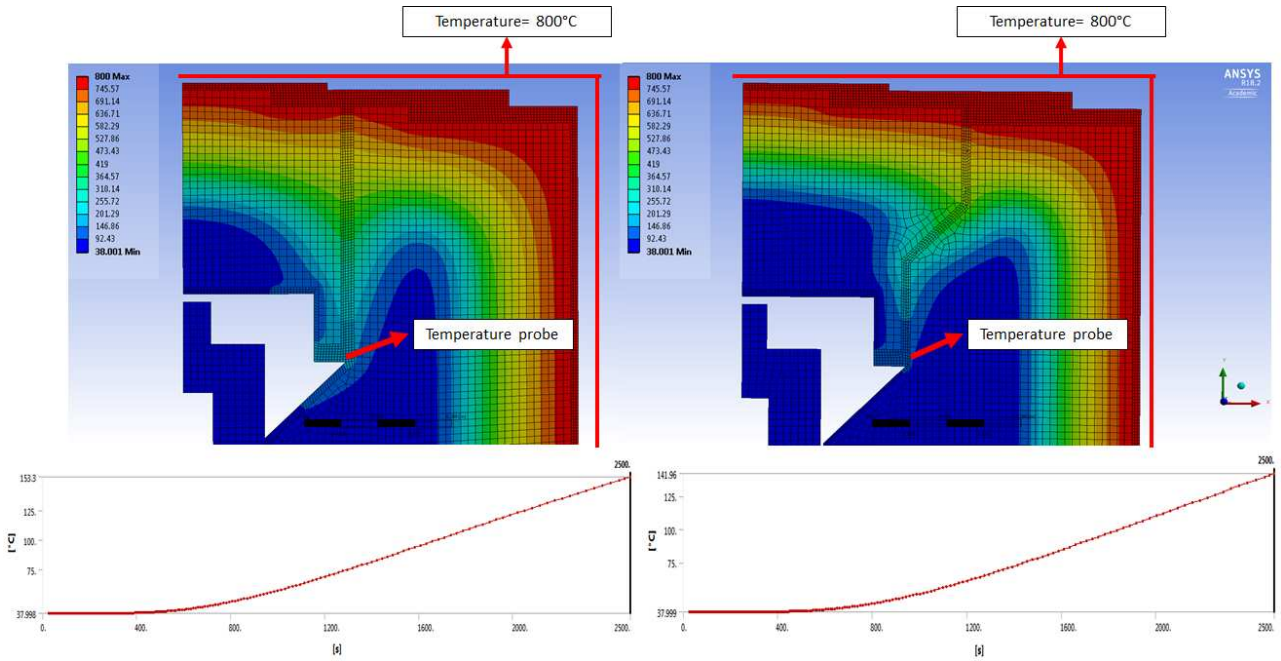

Figure 2.13: Map of the temperature after the fire test for the I (left) and the II version (right). A probe placed in the internal region of the package shows a final temperature with a difference of around 10 degrees: 153,3°C in the design I and 142°C in the design II.

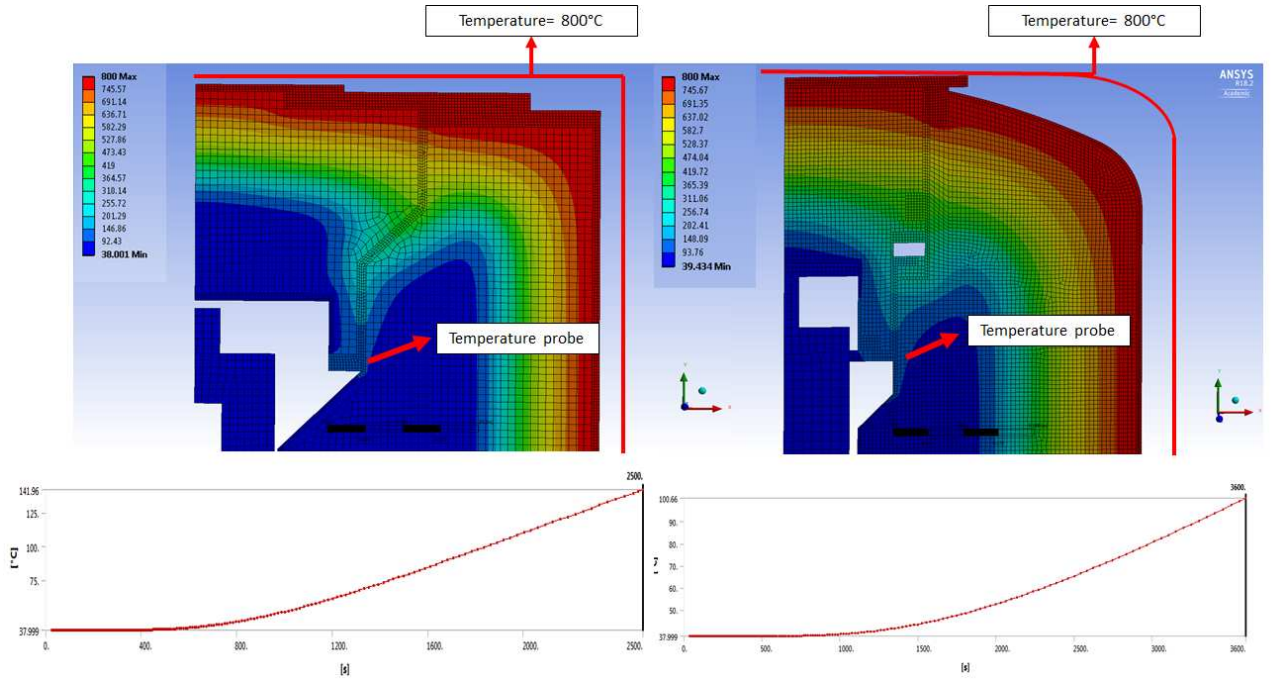

Figure 2.14: Map of the temperature after the fire test for the II (left) and the III design version (right). A probe placed in the internal region of the package shows a final temperature with a difference of around 40 degrees: 142°C in the design II and 101°C in the design III.

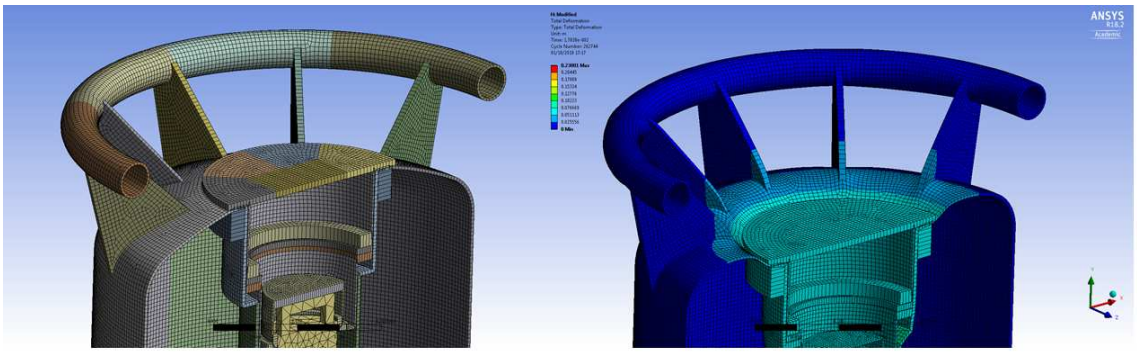

Figure 2.15: Results of the total deformation on the package with the design III after a 9m drop test in vertical configuration.

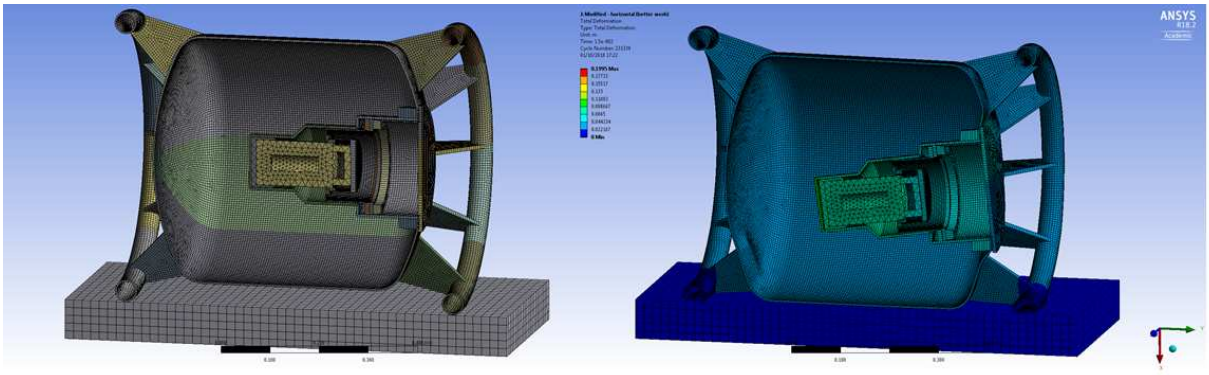

Figure 2.16: Results of the total deformation on the package after a 9m drop test in horizontal configuration for the design III.

to the main cylindrical body.

2.5.3 Technical description of the package

The ColiBRI-30 is composed by two main elements: the **overpack** and the **shielded containment system** (The official mechanical drawing is reported in the Fig.2.62 at the end of this chapter).
The total weight of the package (overpack + shield container) is 113 kg.

Overpack:
The external package is made of stainless steel 304L (Fig.2.17). It has a cylindrical shape with the lower and upper faces composed by two rounded plates. It presents a lid closed by 8 screws M16 in stainless steel Nitronic 60. The weight of the lid, 11 kg, allows the manipulation by hand.
The internal metallic surface of the overpack presents a double cone shape with an upper wide diameter that favors the allocation of tools for the manipulations and the placement of the shielded container. The thermal protection is ensured by the presence of ceramic wool that fills totally the overpack and the inner volume of the lid. Moreover ,a crown in PEEK, placed on the lid, delays the heat transmission from the outer metallic surface to the internal ones, closer to the tungsten region. This element is connected to the stainless steel body through 6 screws M6 in stainless steel.
A base in PEEK is also inserted below the shielded container and a silicone disk is placed on the lid

to absorb the shock (and partially the heat) limiting the deformation the tungsten will cause on it during the mechanical tests.
The protection against shocks is ensured by two rings in stainless steel 304L connected to the main cylindrical body through ten reinforcement plates (8mm thick).The correct positioning of the lid is possible thanks to a centering pin placed on the upper surface of the container.
The maximum overall dimensions of the overpack are 600 mm for the diameter and 700 mm for the height.
A steel plate on the body clearly identifies the type of package and reports its name and serial number. All the sticks the users must add for the transport and the address for the delivery can be allocated on the free lateral surface of the overpack in dedicated designed spaces.



Figure 2.17: On the left side, a 3D drawing of the Overpack. The names of the principal elements are highlighted. On the right, a cut view of the package.

Shielded container:
The radioprotection is insured by a removable shielded container in tungsten with a thickness of 30 mm (Fig.2.18). The internal dimensions of the shielded container are compatible with the ones defined previously:

- Maximum diameter: 33 mm;
- Height: 75 mm.

A sponge placed on the bottom of the internal volume prevents the spread of the liquid source in case a vial breaks. The shielded container presents a magnetic cup made in tungsten that can be open thanks to an additional dedicated tool. The magnet on the tool will attract the steel components on the lid causing the compression of a spring and the release of the cup.
A safety lid cover guarantees the best closure and facilitates the handling and the transport of the shielded container.
The weight of the shielded container is 16.5 kg.



Figure 2.18: 3D drawing of the shielded container. The names of the principal elements are highlighted on the left image. The right image reports the closed configuration.

2.5.4 The contents and the calculation of the activities to transport

The maximum activity that it is possible to transport with a type B package is limited by radiation protection and thermal issues.

Radiation protection constraints:
They are connected to two radiosafety factors listed in the IAEA Regulation:

- The maximum radiation level at any point on the external surface of a package or overpack must not exceed 2 mSv/h (par. 527, Chap.V of [39]) or 10 mSv/h in case of exclusive use (par. 528, Chap.V of [39] - see definition point 1 par.2.2);
- In case of accident sufficient shielding shall remain to ensure that the radiation level at 1 m from the surface of the package would not exceed 10 mSv/h with the maximum radioactive contents that the package is designed to contain (par. 659, Chap. VI of [39]).
- A Type B package is allowed to transport a limiting value of Activity equal to 3000 times the $A_{1,2}$ established for each radionuclides if the previous parameters are fulfilled.

Thermal constraints:
Another phenomena which impacts on the calculation of the maximal activity to transport is related to the heat generated by the sources during the decay.
An increase of the temperature inside the shielded container system can alter the material properties causing, for example, an expansion of the mechanical or plastic parts of the confinement system. Deformations, cracking or melting of the materials may yield to radioactive leaks and compromise the efficiency of the package or of the containment system.

- The par. 653 of [39] is regulating this effect. It states that a package shall be designed so that the heat generated in it by the radioactive contents shall not, under normal conditions of transport, affect the requirements for the containment and shielding if left unattended for a period of one week. This implies also that the dose rate at contact with the package (due not only to the radionuclides but also to its daughter nuclei through its decay chain) and the generated heat stay below the operational thresholds (2 or 10 mSv/h) for this entire periods.

In the case of the ColiBRI-30 the tightness is guaranteed by the presence of a joint placed on the lid of the internal tungsten container. The heat generated by the source shall not exceed the maximum

temperature the O-ring can sustain, both in normal and accidental conditions of transport. In case of liquid, in order to keep the integrity of the source, in normal conditions it must be insured that the temperature inside the shielded container won't exceed the evaporation temperature (100°C, treating the source as water). These two conditions, together with the limit of 3000 A_2, impose the upper limits for the activity.

It must be noticed that fissility is not of concern in this study due to the considered list of isotopes.

The next two paragraphs describe in more details the study aiming at the definition of the activity to transport and linked to the radiosafety protection and to the thermal stability of the package's components.
A summary of the requirement for the calculation of the maximum value of activity to transport is reported in the Tab.B.3.

Radioprotection limitations	**Heat generation limitations**
• Dose rate at contact with the overpack must be ≤2 mSv/h or ≤10 mSv/h for exclusive use; • The calculation of the dose rate shall take into account the contribution of all the radionuclides in the decay chain.	• The heat generated by the decay shall stay below the max resistance temperature of the O-ring: 200°C (both for solid and liquid sources); • For liquid sources the heat generated by the decay shall avoid the evaporation.
These requirements must be respected: • In normal and accidental conditions of transport; • For a period of 7 days	

Table 2.8: Summary of the specifications to calculate the maximum activity to transport.

2.5.4.1 The Radioprotection study

Radioprotection studies are necessary to ensure a good protection from radiation during the transport. They are used in the design phase for the dimensioning of two parameters: the shielding thickness of the tungsten container and the distance between the containment system and the external surface of the overpack.
As said previously, the activity to transport shall ensure a dose rate at contact with the package of 2mSv/h or 10mSv/h. Moreover this limit shall be kept for all the duration of the transport as well as during eventual stops along the way (for a total of 7 days).
Two methods have been used to evaluate the activity of the radionuclides to transport respecting the regulation limits. The first makes use of an online platform commonly used in research field, Nucleonica [29] and second method imply a 3D Monte Carlo software used in the industrial environment, RayXpert [32].
The reasons for this choice is due to the fact that Nucleonica only includes the effect of gamma and X-ray for dose calculations, while with RayXpert it is possible also to add the effect of electrons.

Method 1: Nucleonica

The software Nucleonica [29] is a web portal developed for the nuclear science community by the European commission's Joint Research Center. This resource replaces the traditional paper-based Karlsruhe Nuclide Chart. It offers online interactive nuclide charts, as well as reference data and searchable databases for internationally evaluated nuclear data.
It includes several interactive modules used for decay calculation, fission yields, range or stopping power, reactor irradiation, transport and packaging, etc.
"Dosimetry and Shielding H*(10)" is the application used for the calculation of the dose rate and integrated dose from a point source of nuclides or nuclide mixture and it is the one used in this study. The operative window (Fig.2.19) allow the insertion of the type of nuclide, the initial activity of the source, the shielding material and the source-detector distance. It is also possible to decide to include or not in the calculation all the daughters of the decay chain. The "cooling time" defines the time at which the dose must be evaluated or it gives the period of integration. The calculations are based on point like source assumption.
The nuclear data for these simulations, or better the information regarding the energy of the emitted particles during the decay and the relative branching ratio, are coming from the Joint Evaluated Fission and Fusion (JEFF 3.1) radioactive decay datafile [45] which contains decay data on 3852 nuclides in ground and isomeric states. Moreover the Nucleonica database contains supplementary information on approximately 93 additional nuclides and their half-lives which are not listed in JEFF 3.1 but are present in NUBASE'03 [46], extending the total number of nuclides (ground and isomeric states) to 3947.
The photon mass attenuation coefficients and the mass energy-absorption coefficients from the National Institute of Standards and Technology [47] while the dose coefficients from the publications ICRP 68 and 72 [48] [49].
The threshold energy can be set by the user to investigate the effect of low energy photons on the dose calculations, by default set to 15 keV. This setting has been used also in this work.

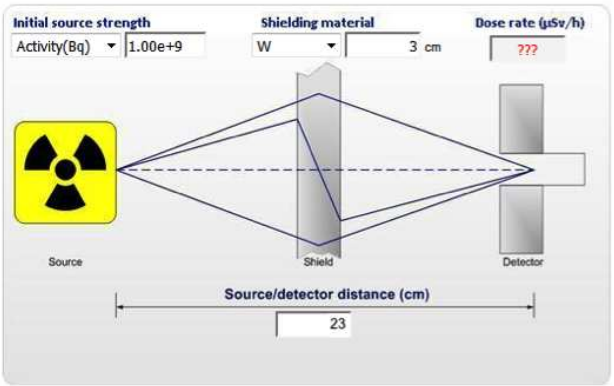

Figure 2.19: Example of the Nucleonica operative windows used to define the geometry and the source type and activity for dose rate calculations [29].

For this study an isotropic and unitary source (1 GBq) has been considered. The radionuclides are the ones listed in the Tab.2.5.
A shield of 3 cm of tungsten is used to simulate the walls of the shielded container and the detector is placed at 23 cm from the source (20 cm of shielding-detector distance). This choice is linked to the geometrical dimensions of the package under study.

The material between the tungsten shield and the detector is air. It must be noticed that with this configuration the effect of the shielding coming from the presence of a stainless steel layer (5 mm for the external shell of the overpack and 3 mm for the internal surfaces) which constitutes the overpack as well as the ceramic wool coat are neglected. This may results in a conservative method with an overestimation of the dose (but in accordance with the radioprotection principles).
A cooling time of 1h is set to evaluate the dose after the operation of loading of the package and positioning of the package for the shipment.

Once the geometry and all the parameters are set, the software is able to calculate several operational quantities used in radiation protection. The one of interest for this study is the ambient dose rate equivalent H*(10) (defined at the par.1.3).
From the value of dose rate coming from the unitary sources $H^*(10)_{1GBq}$, it is possible to calculate the maximum activity that is possible to transport in this configuration leading to 2 mSv/h, or 10 mSv/h for exclusive use, at contact with the package:

$$A_{max}[GBq] = \frac{2mSv/h}{H * (10)_{1GBq}}$$

A_{max} shall be such that the dose rate at contact with the package remains lower than 2 mSv/h also after a cooling time of 7 days, a range of time in which the effect of the daughter nuclei must be included. The same method may be applied to obtain a limit of 10 mSv/h in case of exclusive use.
Nucleonica has been then also used to check that this is valid for the chosen activity. The software is able to solve the Bateman equation for a decay chain of the chosen radionuclide and evaluate the dose rate at a specified time including their contributions.
Sometimes a rescaling of the initial activity has been necessary to obtain the regulatory suited value of dose rate. In particular, this has been the case of three isotopes among the ones in the list:

- Th-228 has an half-life of 1.91 y. It presents in its decay chain radionuclides with shorter half life and high energy gamma ray emitters as Tl-208 (h.l. 3.05 m) and Bi-212 (h.l. 60.55 m). They have respectively the main gamma emission at 2,6 MeV (99.754 %) and 727 keV (6.67%) and will be in secular equilibrium with the Th-228 after one week. After one hour of cooling the activity giving 2 mSv/h at contact with the package is 1.4E+14 Bq. The same will lead to a dose rate of 3.6E+4 mSv/h after 7 days. For this reason it has been necessary to reduce the initial activity by four orders of magnitude.
- The same thing happened for the Th-229 (h.l. 7.34 ky). Its decay chain includes Tl-209 that has an half-life of 2,2 m with main gamma emission at 1,56 MeV (99.7 %). The initial 2.5E+17 Bq after one hour of cooling, leading to 2mSv/h, would give a value of 1.6E+05 mSv/h at contact with the package after one week. In this case, then, the activity was reduced of 5 orders of magnitude.
- Ra-226 (h.l. 1.6 ky) will be in secular equilibrium with the daughters of its decay chain after one week. Among them Bi-214 (h.l. 19.9 m) is mostly contributing to the dose rate due to the high energy gamma emission. The chosen activity of 7.50E+09 leads to 1,9 mSv/h at contact with the package after one week and only to 4 μSv/h after one hour.

Method 2: RayXpert

Nucleonica is a tool able to give a rapid answer to the problem but it implies some hypothesis and simplification in the geometrical structure. For example it is not possible to customize the materials involved in the calculations or add more than one layer of shielding.
The values of ambient dose rate obtained with Nucleonica for the unitary sources ($H^*(10)_{1GBq}$) have

been checked with RayXpert [32], a Software used for the 3D modelization and calculation of dose rate with Monte Carlo techniques. The software is developed by Tests and RADiations (TRAD, France). It uses Monte Carlo method implemented in GEANT 4 V10.0 to simulate photon and electron transport for energies between 1 keV and 100 MeV. It is implemented on PC Windows and has the advantage of having a user-friendly interface that allows easy and rapid building of complex 3D geometries (Computer-Aided Design) as compared to MCNP or Geant 4.
With this tool the management of the scenario, i.e. geometries and sources, is facilitated by the possibility to give in input the step file of the geometry involved in the study (i.e. the generic output of all mechanical design software). Thanks to the graphic interface, it is possible to associate a specific material to each element. A database of reference materials is already present in the software and created with CAD programs like Catia or SolidWorks. The user can also define new compounds or modify the preexisting ones.
The nuclear database containing the informations on the decay energies of the radionuclides is by default coming from the EAF-2010 decay data library (EASY- 2010) package [50], but the JEFF 3.3 [51] may also be selected (it has been used for this work). The conversion coefficients from fluence to ambient dose equivalent, H*(10), are automatically applied by the software and are extracted from the publication 74 of ICRP [52].
RayXpert proposes a database of materials, whose compositions correspond to the one given in the report of the Pacific Northwest National Laboratory [53]. The choice of a given material for a given volume automatically attributes that composition to the volume, but it is also possible to customize it.

- In this specific study, the geometry includes both the overpack (5 mm of stainless steel in the external shell and 3 mm of the same in the internal metallic surfaces) and the shielded container (Fig.2.20). All the elements not significantly contributing to the effect of shielding have been not taken into account (like the insulation wool, small steel and plastic elements).
- Specific materials have been assigned to the elements composing the geometry. In this case only stainless steel 304 L and tungsten have been used. The first one has been selected among the materials already present in the database, while the tungsten density has been modified (from 19 g/cm^3 to 17.3 g/cm^3).
- The isotropic source is simulated by a small sphere (radius = 0,5 cm) placed inside the tungsten shield. The radionuclide type is defined and all the daughters in its decay chain are included in the simulations. The daughters are consider to be in secular equilibrium with the parent and their contributions to the dose take into account their branching ratio.
- Four detectors, reproduced with spheres and placed at contact with the external surface of the overpack, are used to obtain the ambient equivalent dose rate. Two of them are localized at the sides of the overpack, one on the lid and the other at contact with the bottom surface of the stainless steel body.

RayXpert allows to get a "cartography" of the dose rate using a graphic instrument to visualize the level of dose rate or particle flux from a coloured 3D image.
The Fig.2.21 show an example of this tools in the case of ambient dose simulations from a point-like source of 11.8 GBq of Tb-149. This corresponds to the maximum activity that it is possible to transport with the ColiBRI-30. On the top picture a legend associates the colour to the dose rate value is displayed. It is possible to see that the maximum value of the dose rate is in the center of the package (in red), where the source is placed and there is no effect of the shielding. The dose rate rapidly decreases thanks to the presence of the tungsten shield and it is below the 2 mSv/h limit outside the overpack (light green). In the bottom picture, only the regions with dose rate higher than

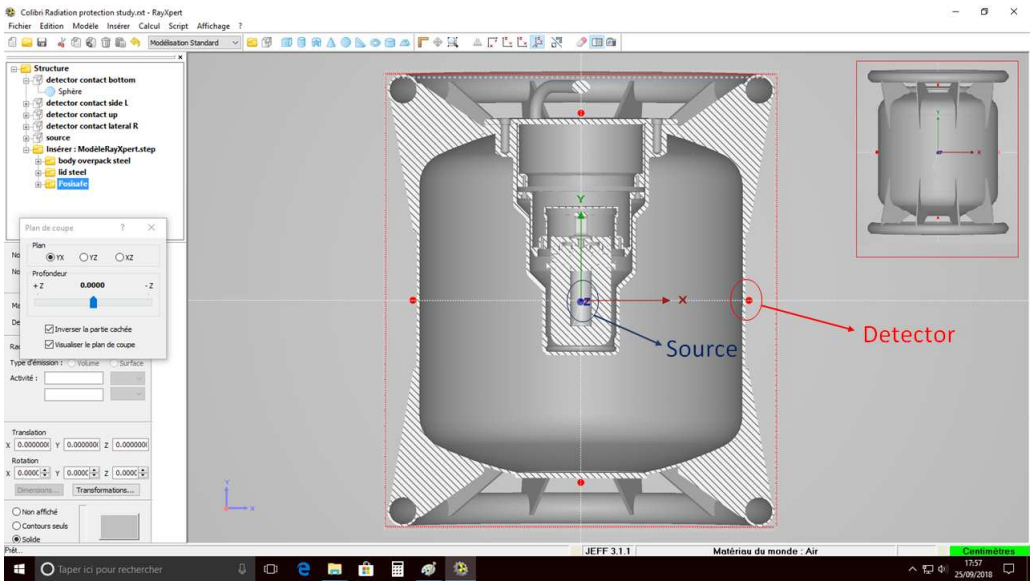

Figure 2.20: Example of the RayXpert operative windows. The step file of the ColiBRI-30 is used as reference geometry, here presented in a cut view. The four detectors (in red) and sources (in blue) are simulated with small spheres.

2 mSv/h have been plotted.

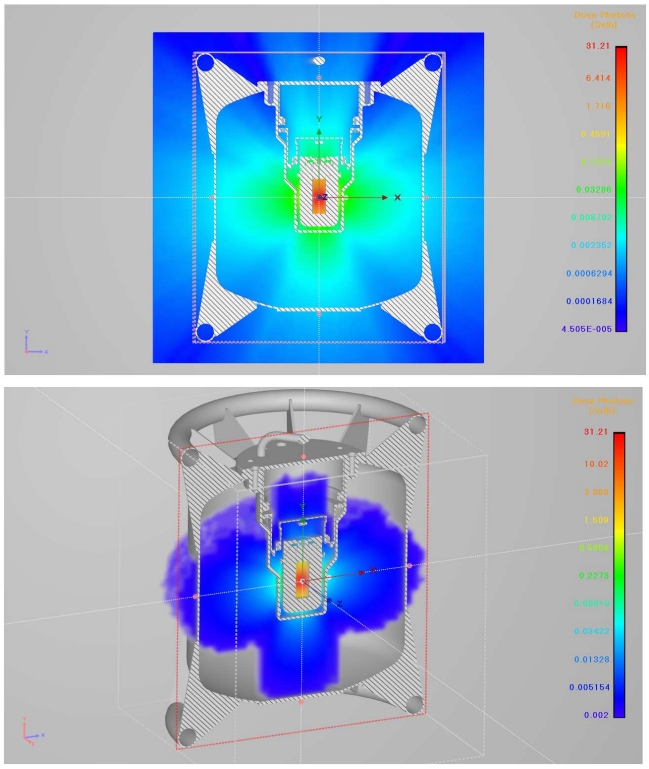

Figure 2.21: Results of the cartography for the simulation of a 11.8 GBq source of Tb-149 (top). The minimum values of the dose rate is 2 mSv/h (bottom).

The results of both methods are reported in the Tab.2.9 for non exclusive use.
The values of ambient dose rate for the unitary sources obtained with Nucleonica are compatible with the ones evaluated with RayXpert, within the statistical errors, in most cases. Nucleonica considers just the seven days for the daugther production. This is the reason for the gap observed in the cases of Yb-166, At-211, Ac-227 and Th-229. The secular equilibrium assumption used in RayXprt is, then, a conservative approach.

	Nucleonica	**RayXpert**		
Isotope	**H*(10)$_{1GBq}$** [μSv/h]	**H*(10)$_{1GBq}$** [μSv/h]	**Rel. error** [%]	**Max activity** [TBq]
C-11	4.13E-07	4.58E-07	3.5	4.84E+00
Sc-47	2.95E-38	-	-	6.78E+31
Cu-61	1.41E-05	1.25E-05	7.0	1.42E-01
Cu-67	5.93E-11	7.15E-11	3.9	3.38E+04
As-71	1.70E-05	1.15E-05	6.1	1.18E-01
As-77	1.07E-08	1.87E-08	8.6	1.87E+02
Sr-89	9.49E-09	1.05E-08	4.2	2.11E+02
Y-90	1.14E-11	1.24E-11	7.8	1.76E+05
Nd-140	4.44E-06	4.89E-06	0.0	4.47E-01
Tb-149	1.70E-04	2.20E-04	5.5	1.18E-02
Sm-153	8.40E-09	5.94E-09	7.5	2.38E+02
Tb-155	1.61E-08	1.93E-08	6.6	1.24E+02
Tb-161	1.36E-09	1.60E-09	7.6	1.47E+03
Yb-166	6.37E-05	4.52E-04	5.7	3.20E-02
Er-169	2.35E-78	-	-	8.53E+71
Yb-175	4.15E-09	6.23E-09	7.3	4.82E+02
Lu-177	2.67E-13	-	-	7.80E+06
Re-186	1.52E-08	1.78E-08	6.9	1.32E+02
Re-188	2.86E-06	8.59E-06	6.1	7.00E-01
At-211	3.23E-07	4.93E-05	5.6	6.19E+00
Ac-225	7.24E-06	1.74E-05	6.0	2.75E-01
Ra-226	2.56E-04	2.31E-04	4.6	7.20E-03
Ac-227	1.85E-07	1.23E-06	5.0	1.10E+01
Th-228	2.58E-04	2.24E-04	5.8	7.80E-03
Th-229	7.00E-07	6.83E-05	7.4	2.80E+00

Table 2.9: List of radionuclides and activities to transport as results of the radiosafety analysis with the Nucleonica and Rayexpert method. In the cases of Sc-47, Er-169 and Lu-177 Rayexpert gives results with high variance due to the low statistics and the Nucleonica results have been used.

2.5.4.2 The Thermal study

During the transport the package must be able to withstand different thermal condition, established by the IAEA Regulation. In temporal order they are:

1. **Heat generation equilibrium:**
   A Type B package must be designed such that, in absence of insolation, the temperature of the accessible surfaces of a package shall not exceed 50°C for a package transported by air and 85°C for the other way of transport (par. 619 and 654 of the [39]). To guarantee this, it must be taken into account the heat generated by the source itself at its maximum rate. This step reproduces the condition of loading and closing of the package in a laboratory or reactors sites.
2. **Insolation:**
   The specimen is placed in thermal equilibrium with an ambient temperature of 38°C, subject to the insolation conditions specified in Table 12 of the IAEA Regulation [39] (Tab.2.10) and subject to the maximum internal heat generation within the package coming from the radioactive contents (par 728 [39]). This scenario precedes the realization of the accidental conditions and simulates the (normal) thermal conditions during a shipment.
   In the case of medical radionucide's transport the duration of the shipment must be compatible with the smallest value between the half-life and the expiry date of the material in the package to allow a proper final usage. It has been defined that the maximum travel time must be equal to 3 days. In this range of time, the source's characteristics must remain the same. In particular, the temperature of a liquid source should not rise above the evaporation point (in normal transport pressure).

Form and location of the surface	**Insolation for 12h per day** [W/m^2]
Flat surfaces transported horizontally - downward facing	0
Flat surfaces transported horizontally - upward facing	800
Surfaces transported vertically	200
Other downward facing (not horizontal) surfaces	200
All other surfaces	400

Table 2.10: Insolation Data (Table 12 pag 99 of the IAEA Regulation [39].)

3. **Fire immersion:**
   This step consists in one of the tests to be performed on a type B package to obtain the approval of the competent authorities. The specimen must be exposed for a period of 30 min to a thermal environment that provides a heat flux at least equivalent to that of a hydrocarbon fuel-air fire with a minimum average flame emissivity coefficient of 0.9 and an average temperature of at least 800°C. The fire must fully engulf the specimen (par 728 a [39]).
4. **Cooling after the test:**
   The specimen must be exposed to an ambient temperature of 38°C, subject to the solar insolation conditions specified in Tab.2.10. It must also be subjected to the maximum rate of internal heat generation by the radioactive contents for a sufficient period to ensure that temperatures in the specimen decreases and/or are approaches to the initial steady state conditions (par 728 b [39]).

In the design phase it has been decided to reproduce the thermal path described before using the

software ANSYS 18.2 [54]. In particular , each phase has been performed using a *Transient Thermal* workbench since it involves temperatures and other thermal quantities that vary over time. To study the overall performance of the package it is necessary to connect the results of the four scenarios seen before: the map of temperature resulting from the application of the boundary conditions of one step has been used as input load for the following simulated step.
A summary of the scenarios with the main boundary conditions to impose in the ANSYS simulations is reported in the Fig.2.22.
The purpose of the simulations is to:

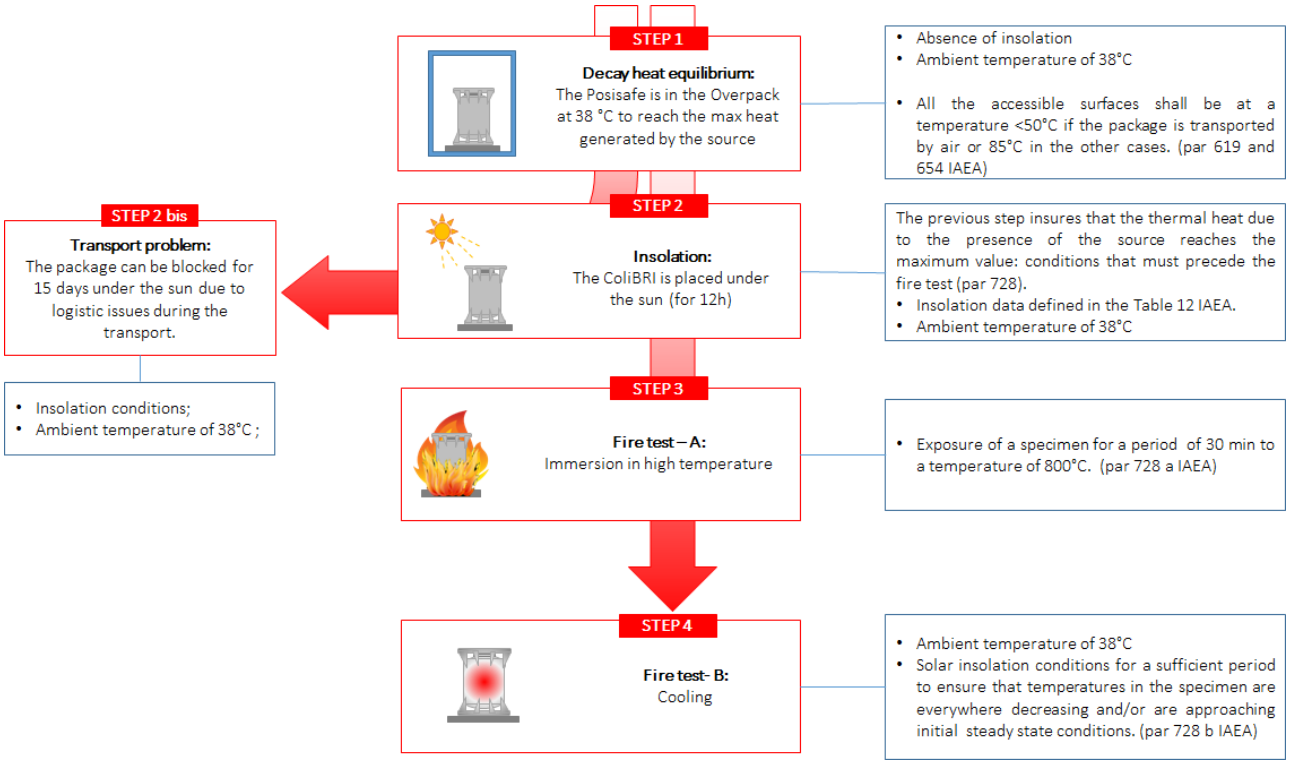

Figure 2.22: The four thermal phases the package will go through during the transport and the relative boundary conditions.

A) Ensure the good performance of the overpack's insulation layer made of ceramic wool. The heat, especially in the case of the fire test, will flow in the inner regions of the package due to the presence of metallic surfaces connecting the external environment to the area at contact with the tungsten container. The choice of the internal surfaces' shapes with a "double cone" contributes to enlarge the thermal path and consequently to slow the heat transmission.
B) Chose the maximum generated heat, P, developed by the solid source to have in all the scenarios a temperature for the O-ring (on the shielded container) lower than 200°C;
C) Chose the maximum generated heating power (volumetric heat power), P, developed by the source to avoid the evaporation of the transported radioactive contents in liquid form in all scenarios.

The definition of P satisfying the conditions at the points B and C, consequently defines the maximum activity to transport. The generated power heat (W/m^3) is directly linked to the activity of the source

to transport:

$$P = \sum_{i=1}^{n} 1.602 * 10^{-13} * A_i * Q_i \tag{2.1}$$

where A_i is the source activity (Bq), $1.602*10^{-13}$ is the conversion coefficient from MeV to Joule. Q_i is the Q-value of the decay reaction (MeV) specific for each radionuclide, giving the amount of energy released per decay. The sum in the equation is extended for a single nuclide to the n isotopes in its decay chain, considered in secular equilibrium with the father nuclide. Moreover it is supposed that all the energy released during the decay is converted in heat. This method, then, overestimates the value of P and the final value of activity will be then conservative, in line with the radioprotection principles.

2.5.4.3 The simulation model

The cylindrical symmetry of the package (both of the overpack and the inner shielded container) and of the boundary conditions with respect to a vertical cutting plane of the geometry, lead to a simplification of the problem. It is possible to use an axisymmetric configuration and pass from a 3D to a 2D study.
This simplification allows to speed up the simulation, reduce the calculation time and simplifies the meshing operations.
Actually this concept is valid if two simplifications are done: the effect of the screws are eliminated, the reinforcements and the metallic rings are not included in the simulations. In a real situation we should take into account that the ring and the steel reinforcement may hold the heat after having been exposed to the fire and that the screws connecting the metallic surface act like a bridge for the heat transmission. For this reason a safety margin will be taken into account.
Other boundary conditions include:

- No convection imposed in the inner regions of the package due to the presence of the wool, set up only for the external shell (10 W/m^2 K);
- The ambient temperature set to 38 °C;
- The high temperature environment is simulated imposing the temperature around the overpack external shell to 800 °C.

The geometry used for this study is reported in the Fig.2.23. The mechanical and thermal characteristics of the materials involved in the calculations are listed in Appendix B.

- For the simulation purposes and for the case of solid source, it is supposed that all the energy of the decay is deposited in the tungsten (in other words the heat generation is imposed only in the tungsten body). This is again a conservative hypothesis since in reality part of the gamma radiation escapes the shield and can be detected at contact with the overpack.

- Liquid sources are placed inside a glass ampoules and sometime included in plastic container used to keep the source in place during the transport. Different dimensions and specific characteristics of the ampoules and plastic elements are difficult to identify since subjected to the users decisions. For simulation purposes, the liquid sources are reproduced with a volume of water corresponding to the half of the internal volume of the tungsten container and no glass or plastic is taken into account. Moreover the dimensions and the type of source protection may be difficult to identify and subjected to the user's choice. This modelization imposes a perfect heat transfer from the liquid to the tungsten wall.

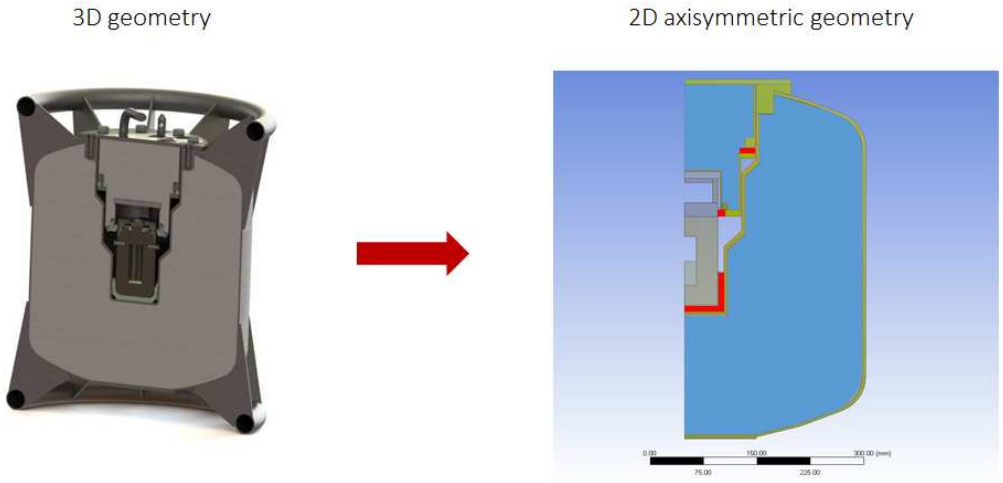

Figure 2.23: The 3D structure of the container is reduced to a 2D axisymmetric geometry. On the right the geometry used for the ANSYS calculations. In blue the ceramic wool, in red the part in PEEK and in green the stainless steel. The inner shielded container is simplified by a tungsten body with a stainless steel lid.

The chain composed by the four connected simulations have been repeated several times to evaluate the correct internal heat generation to impose in order to satisfy the conditions 2 and 3.
The P values obtained by the simulations are reported in the Tab.2.11 for solid and liquid sources:

P ($\mathbf{W/m^3}$)	
Solid sources	**Liquid Sources**
1.7E+04	1.4E+04

Table 2.11: Maximum values of volumetric heat power for solid and liquid source to transport.

2.5.4.4 Results of the simulations

For **liquid sources providing P:**
The Fig.2.24 and Fig.2.25 represent the map of temperature in the entire package at the end of each step.

The mean temperature behavior of the water can be observed from the graph in the Fig.2.26:

- When the package is in preparation for the shipment, and then not subjected to the insolation conditions, the only source of heat is coming from the radioactive decay. The maximum temperature of the liquid reached in this phase is equal to 39.8°C. In this phase, the temperature on the external surfaces must be below 50°C to allow the manipulation. With the conditions set up in this study, at the end of the first thermal scenario, the temperature on the external shell is 42.2°C.
- Subsequently, the package is placed under the sun. Since the highest heat flux coefficient must be imposed on the flat surfaces of the package, corresponding here to the overpack's lid, this will be also the point with the maximum temperature after 12h (corresponding to the hours of sun

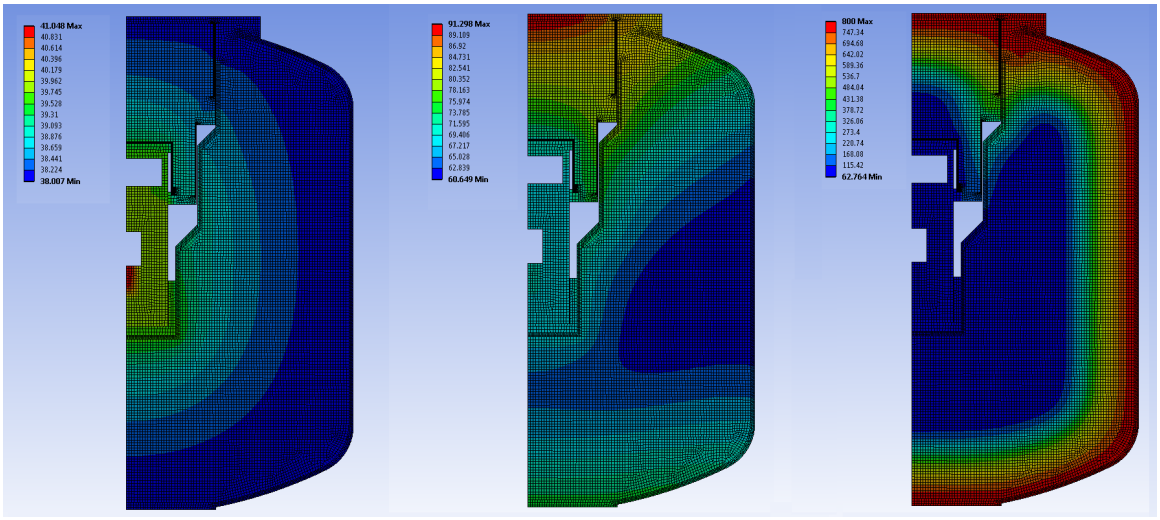

Figure 2.24: Liquid sources: Temperature map of the first three step of the thermal chain.

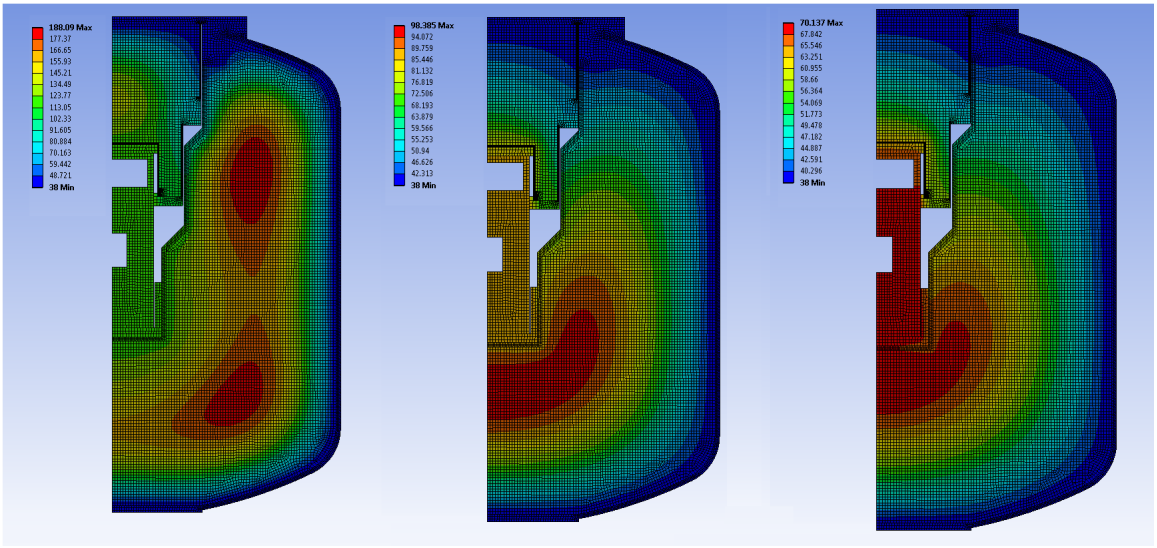

Figure 2.25: Liquid sources: Temperature maps of the forth scenario at 1000s, 3000s and 4000s after the fire immersion phase.

during the day). Due to the presence of a constant heat generation inside the shielded container, the temperature of the inner regions of the overpack will also increase. The same thing is valid for the temperature of the water, reaching in this range of time a maximum of 70°C, a value lower than the evaporation temperature.

- When the container is subjected to the fire test, the temperature of 800°C is set around it. The metallic surfaces composing the lid and the cone holding the container allow a fast heat transfer and temperature rise around them. The temperature in the shielded container, and then in the liquid, increase. The temperature of the water is 117°C, higher then the evaporation temperature, but the temperature in the tungsten is 124°C. In this situation the O-ring on the containment system keeps his characteristics.

- If on one side the presence of the wool isolate the internal regions from the fire, on the other side, when the fire test is over and the room temperature decrease to 38°C, the wool retains the heat accumulated. It is necessary to wait for 42h hours to come back to the initial conditions (end of the phase 1), if the overpack is kept closed.

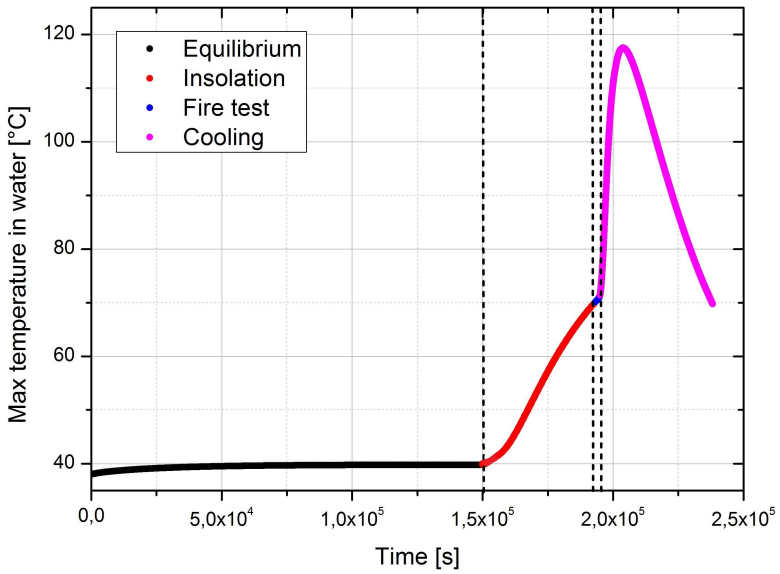

Figure 2.26: Liquid sources: variation of the water temperature in the four thermal scenarios. The dataset are separated by dashed lines.

In order to check that the water-like source does not evaporate during the transport, a simulation of the water temperature variation during three days has been carried on. The cycle consists in 12h of insolation conditions and 12h of night simulated only with room temperature of 38°C and convection coefficient on the overpack surface of 10 W/m^2C.

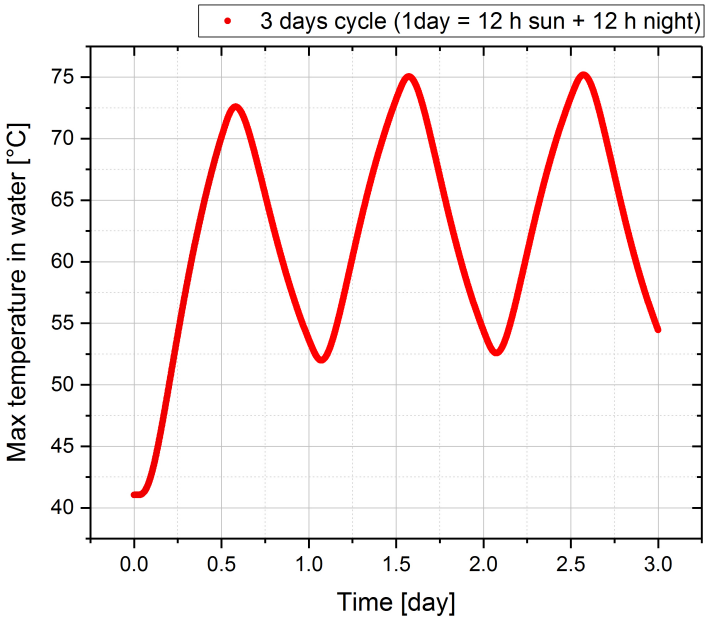

Figure 2.27: Liquid sources: water temperature behavior during 3 days.

As it is possible to observe from the results in the Fig.2.27, the temperature increase in the first 12h and reaches the maximum of 73°C when the boundary conditions are already switched to simulate the night environment. This effect is again connected to the wool capacity to retain the heat even after the temperature on the external part of the overpack rapidly decreases.
The second day, the maximum temperature reaches a peak slightly higher than the first one, 75.2°C.

For **solid sources providing P:**
The Fig.2.28 and Fig.2.29 represent the map of temperature in the entire package at the end of each step.

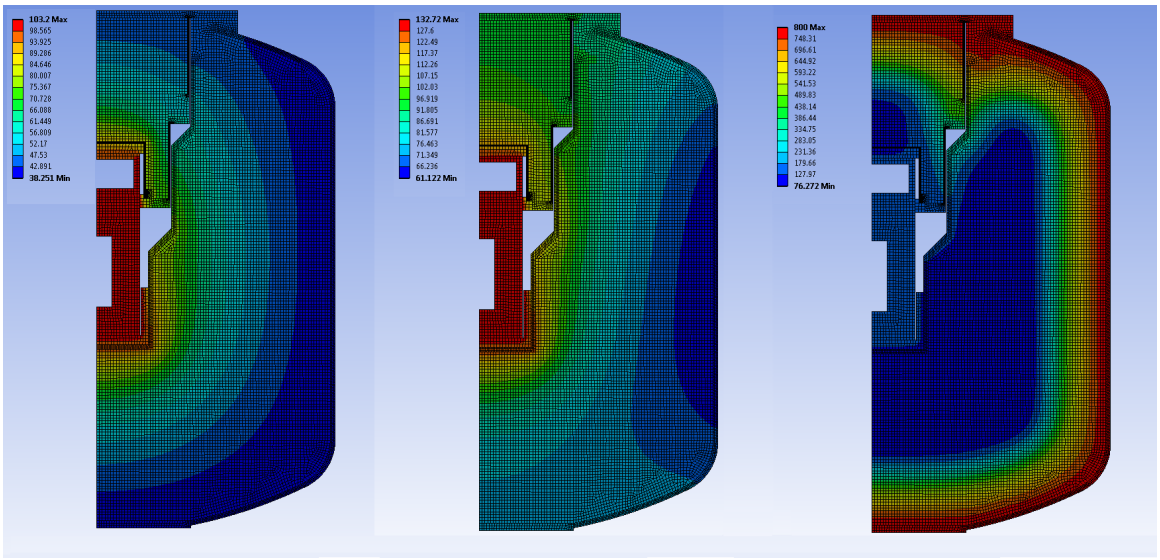

Figure 2.28: Solid sources: Temperature map of the first three step of the thermal chain.

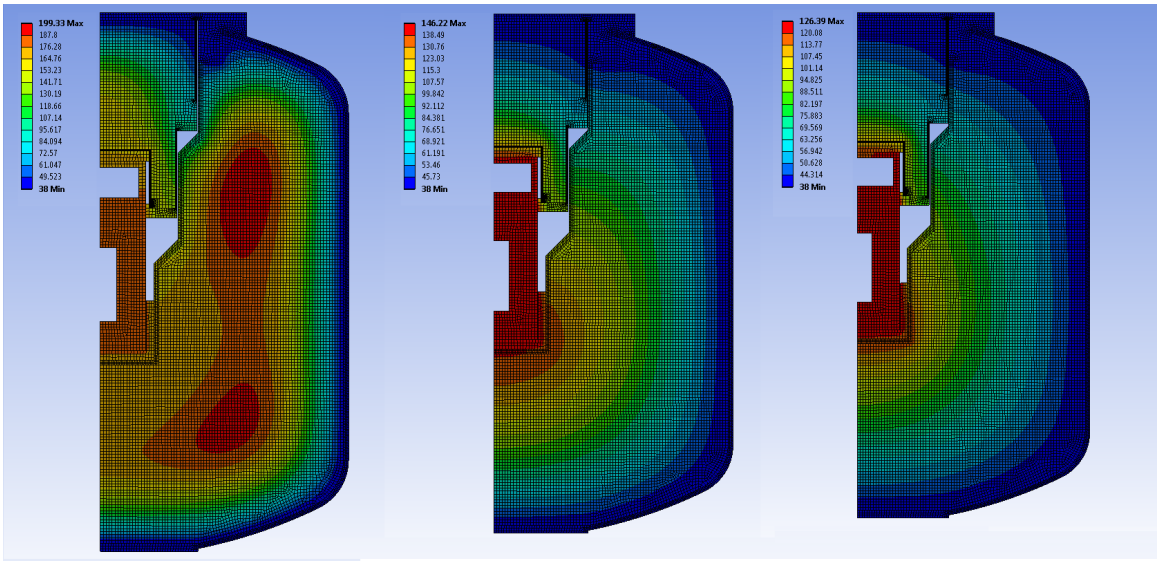

Figure 2.29: Solid sources: Temperature maps of the forth scenario at 1000s, 3000s and 4000s after the fire immersion phase.

The mean temperature behavior of the tungsten shield can be observed from the graph in the

Fig.2.30.
In this case the temperature limit is imposed by the maximum temperature the sealing/O-ring on the tungsten container can sustain (200 °C).

- In the first phase the source is placed inside the tungsten shield and the maximum heat is reached after 1.75 days, corresponding to a temperature in the tungsten of 103 °C. It must be observed that in real conditions the operations of package filling are very fast and lasts only some minutes/hours.
- The second phase previews the insolation conditions. The temperature of the tungsten container starts to rise to reach 132.5 °C after 12h.
- The fire test is divided in two parts. During the step in which the container is placed in an environment of 800°C, the metallic surfaces heats off very fast due to their high heat transport coefficient. After the 30 minutes of test, however, the temperature in the tungsten is below the imposed limit (134.4°C).
- As before, the presence of the wool will retain the heat allowing the temperature in the tungsten to rise in the second step, the one of the cooling. In other words, while the temperature of the external region of the overpack cool down, the inner part and the tungsten still rise in temperature. The maximum value reached is 178.6°C.

It has been prefered to leave a safety margin for these calculations due to the simplifications on the shape and the hypothesis done on the heat generation by the source. It is also necessary to notice that those calculations shall be compared with the experiments to be validated and that they are used in the design phase to outline the performance.

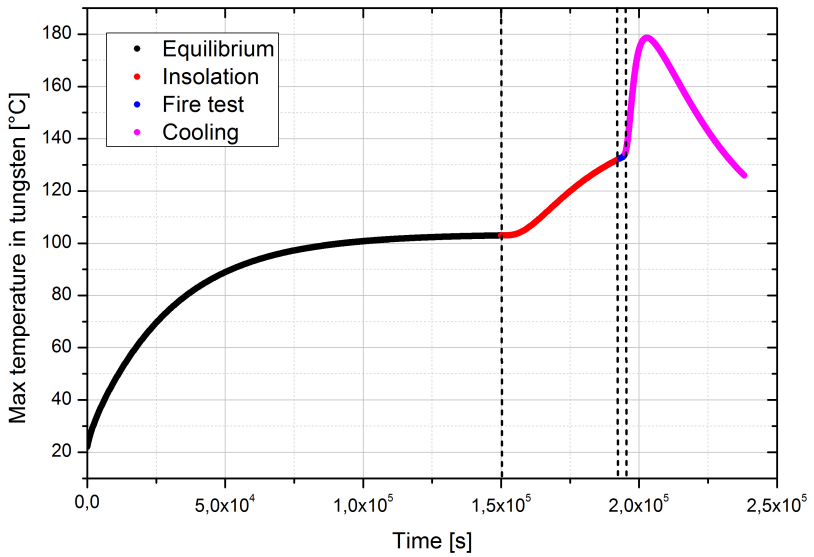

Figure 2.30: Solid sources: variation of the tungsten temperature in the four thermal scenarios. The dataset are separated by dashed lines.

As done for the liquid sources, the behavior of the tungsten temperature has been studied during three days. The results are shown in the Fig.2.31.
Considering the maximum heat generated by the source, the temperature reaches a peak of 137°C, lower than the limit of 200°C.

Using the values of generated maximum heat satisfying the requirements (reported in the Tab.2.11),

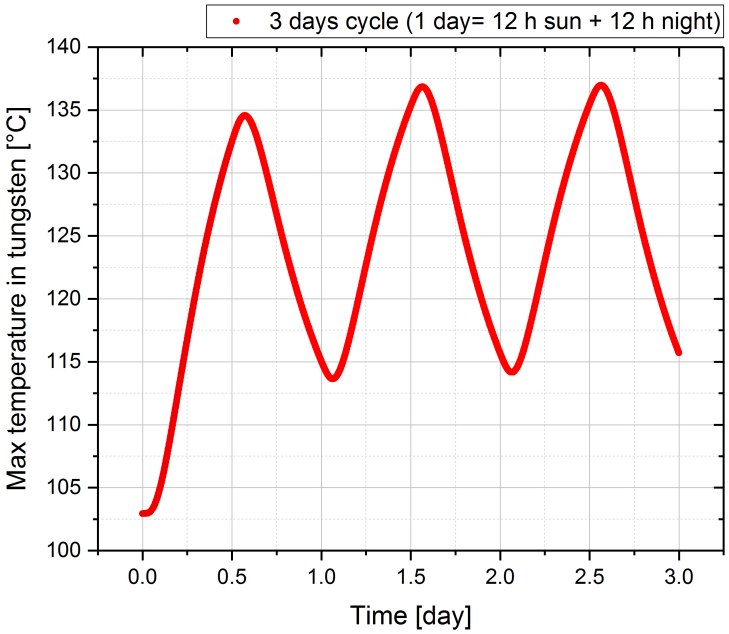

Figure 2.31: Solid sources: tungsten temperature behavior during 3 days.

it is possible to evaluate the maximum value of activity to transport (from the Eq.2.1) both for solid and liquid sources for each radionuclide listed in the Tab.2.5. The results are presented in the Tab.2.12.

	Liquid form	**Solid form**
Isotope	**Activity to tansport [TBq]**	
C-11	1.20E+00	4.66E+01
Sc-47	3.96E+00	1.54E+02
Cu-61	1.06E+00	4.13E+01
Cu-67	4.23E+00	1.65E+02
As-71	1.30E+00	5.04E+01
As-77	3.48E+00	1.35E+02
Sr-89	1.58E+00	6.16E+01
Y-90	2.55E+00	9.90E+01
Nd-140	6.20E-01	2.41E+01
Tb-149	3.76E-01	1.46E+01
Sm-153	2.94E+00	1.14E+02
Tb-155	2.89E+00	1.12E+02
Tb-161	4.01E+00	1.56E+02
Yb-166	7.10E-01	2.76E+01
Er-169	6.76E+00	2.63E+02
Yb-175	5.05E+00	1.97E+02
Lu-177	4.77E+00	1.85E+02

Re-186	2.30E+00	8.94E+01
Re-188	1.12E+00	4.36E+01
W-188	4.23E-01	1.64E+01
At-211	1.42E-01	5.51E+00
Ac-225	6.35E-02	2.47E+00
Ra-226	7.92E-02	3.08E+00
Ac-227	6.36E-02	2.47E+00
Th-228	5.55E-02	2.16E+00
Th-229	5.53E-02	2.15E+00

Table 2.12: List of Radionuclides and Activities to transport as results of the thermal study for a package in non-exclusive use.

2.5.4.5 The list of isotopes to transport

The combination of the radioprotection and the heat generation factors and in particular the lower value of activity identified by the two criteria leads to the following list of activities to transport for the radionuclides listed in the Tab.2.5. The values in the light blue cells are the ones for which the maximum activity to transport is determined by the radioprotection study. The white cells list the values for which the activity is limited by the heat generated by the source.
It must be noticed that the value equal to 3000 A_2 established by the Regulation has been set as upper limit for the activity to transport.

	Liquid form	**Solid form**
Isotope	**Activity to tansport (TBq)**	
C-11	1.20E+00	4.84E+00
Sc-47	3.96E+00	1.54E+02
Cu-61	1.42E-01	1.42E-01
Cu-67	4.23E+00	1.65E+02
As-71	1.18E-01	1.18E-01
As-77	3.48E+00	1.35E+02
Sr-89	1.58E+00	6.16E+01
Y-90	2.55E+00	9.90E+01
Nd-140	4.47E-01	4.47E-01
Tb-149	1.18E-02	1.18E-02
Sm-153	2.94E+00	1.14E+02
Tb-155	2.89E+00	6.00E+01
Tb-161	4.01E+00	6.00E+01
Yb-166	3.20E-02	3.20E-02

Er-169	6.76E+00	2.63E+02
Yb-175	5.05E+00	1.97E+02
Lu-177	4.77E+00	1.85E+02
Re-186	2.30E+00	8.94E+01
W-188	4.23E-01	7.20E-01
At-211	1.42E-01	5.51E+00
Ac-225	6.35E-02	2.75E-01
Ra-226	7.20E-03	7.20E-03
Ac-227	2.70E-01	2.70E-01
Th-228	7.80E-03	7.80E-03
Th-229	5.53E-02	1.50E+00

Table 2.13: List of Radionuclides and activities to transport with the ColiBRI-30 in non-exclusive use.

2.5.5 The Finite Element Analysis for the design's validation of the Overpack

As stated in the previous introductory paragraphs, good performance and a structural integrity of the chosen design in normal and accidental conditions must be proved in case of a Type B container (tests listed in the Tab.2.3). In the drawing phase, calculations and simulations describing the damaging of the package in the exact test conditions have been integrated to reduce the incidence of mechanical failures in the real tests.
The software used for this scope is ANSYS 18.0 [54]. The finite element method (FEA) of structural analysis helped us to detect stress and deformations during the design process and to evaluate design changes before the final version of the prototype. More information and basic details on the FEA method can be found in Appendix B.
The entire design phase has been characterized by an iterative process: once the first shape is fixed, the ANSYS simulations were carried out; adjustments of the structure coming from the stress and strain observations and from the necessity to reduce them led to new mechanical and thermal calculations. This process ended when the established compromises are reached and acceptance criteria are valid. In particular, the package is designed so that at the end of the test foreseen by the IAEA Regulation:

1. The source is kept confined inside the tungsten core placed inside the overpack: the overpack should remain closed after the tests;
2. The mechanical stress damages only the cushioning elements (or shock limiters): if the main stainless steel body is damaged, the deformation must not pierce/drill it to not expose the insulation wool in contact with fire during the last test (par. 658 of [39]).

It has been decided to perform with the Finite Element technique the most critical among the mechanical tests listed in the Tab.2.3:

- the stacking test and the 9m drop test, for the normal condition of transport;
- the 9m drop test, the drop on a rigid bar and the drop of 500kg on the container, for the accidental conditions of transport.

The following paragraphs present in details the boundary conditions and the results of the simulations performed on the final design of the ColiBRI-30.
In order to understand the meaning of the quantities and the principles used to evaluate the performance of the package when subjected to external forces and simulated with ANSYS, a small step back in the theory is needed.

2.5.5.1 Basic principles of mechanics

When a body at an initial state of equilibrium (undeformed state) is subjected to a force, it will deform correspondingly until it reaches a new state of mechanical equilibrium, or deformed state. The inner body forces are the result of a force field, such as gravity, and the surface forces are forces applied on the body through contact with other bodies.
The relations between external forces, called the *stress* (σ), and the deformation of the body, which characterizes the *strain* (ε), are called stress-strain relations. These represent properties characteristic of the material composing the body and are also known as constitutive equations.
The stress and strain relationship can be evaluated throught the tensile tests, in which one end of a rod or wire specimen is clamped in a loading frame and the other subjected to a controlled displacement (Fig.2.32). The engineering measures of stress and strain are determined from the measured load (P)

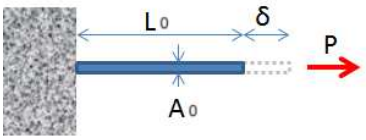

Figure 2.32: Scheme of a simple tension test.

and deflection (δ) using the original specimen cross-sectional area A_0 and length L_0 as:

$$\varepsilon = \frac{P}{A_0} \quad \text{and} \quad \sigma = \frac{\delta}{L_0}$$

The plot of the stress ε against the strain σ is presented by an engineering stress-strain curve (Fig.2.33), commonly used to predict safe loading conditions, failure point, fracture point etc. It is possible to identify different regions on this curve corresponding to a different material behavior:

- In the first (low strain) portion of the curve, many materials obey Hooke's law with reasonable approximation, so that stress is proportional to strain with the constant of proportionality given by the modulus of elasticity or Young's modulus, denoted E:

  $$\sigma = E\varepsilon$$

  In this first region the material undergo a complete and immediate recovery from an imposed displacement on release of the load. The elastic limit is the value of stress at which the material experiences a permanent residual strain that is not lost on unloading.
- As strain is increased, many materials eventually deviate from this linear proportionality. This nonlinearity is associated with stress-induced "plastic" flow in the specimen. Here the material is undergoing a rearrangement of its internal molecular or microscopic structure, in which atoms are being moved to new equilibrium positions. A closely related term is the *yield stress*, denoted

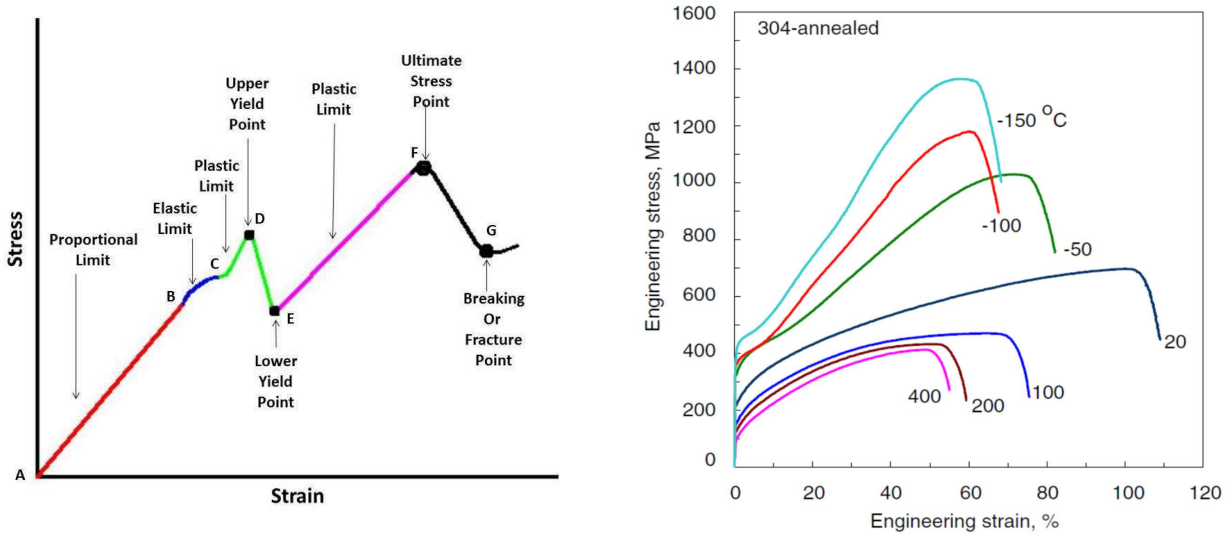

Figure 2.33: Scheme of a stress-strain diagram (left). Stress-strain curve for the stainless steel 304L [55] (right).

generally with σ_Y; this is the stress needed to induce plastic deformation in the specimen. Since it is often difficult to pinpoint the exact stress at which plastic deformation begins, the yield stress is often taken to be the stress needed to induce a specified amount of permanent strain, typically 0.2%.

- At this point, the stress-strain curve changes its slope and starts to move in negative direction. The upper point at which it reaches without changing its slope is known as *upper yield point*. Beyond the upper yield point the object continuously and rapidly changes its dimension without changing the loading condition or decreasing the loading condition or stress up to the *lower yield point*.
- After a continuous loading, it is possible to reach a point after which it is impossible to get back the object without fracture or failure. This point, corresponding to the peak point on the stress-strain graph, is known as *ultimate stress point* and represents the maximum strength that material have to bear stress before breaking.
- Breaking point or breaking stress is the point where strength of material breaks. The stress associates with this point is known as breaking strength or rupture strength.

The limits in the stress-strain curves discussed before are based on simple tension or uniaxial stress experiments. It must be observed that materials (especially ductile materials) behave differently when a non-simple tension or non-uniaxial stress experiment is conducted, exhibiting resistance values that are much larger than the ones observed during simple tension experiments. A theory involving the full stress tensor has been therefore developed.
The *Von Mises stress* (VM stress) is a theoretical value that allows the comparison between the general threedimensional stress with the uniaxial stress yield limit. It is defined as follow:

$$\sigma_{VM} = \sqrt{\frac{1}{2}[(\sigma_1 - \sigma_2)^2 + (\sigma_2 - \sigma_3)^2 + (\sigma_3 - \sigma_1)^2 + 6(\tau_{23}^2 + \tau_{31}^2 + \tau_{12}^2)]}$$

where the σ are the component of the normal stress values along the principal axis while the τ are the components of the shear stress. Shear stress arises from the force vector component parallel to the cross section of the material. Normal stress, arises from the force vector component perpendicular to

the material cross section on which it acts.
The mathematical explanation of this tensor theory is not a scope of this study, but a simple criterion has been applied to analyze the results of the different scenarios simulated with the finite element analysis. The general idea is the following:

- If the Von Mises stress (σ_{VM}) is greater than the simple tension yield limit stress (σ_Y), then the material is expected to yield and plastic (irreversible) deformations are foreseen.

A note for the observations of the results:
In the particular case of this work, the performance of the stainless steel shell composing overpack is observed after the simulation of each test. Typical stress-strain curves are reported in Fig.2.33 for different temperature. The following criterias will drive the observations of the results:

- If the VM stress is $<$ than the yield stress of the stainless steel (220 MPa [56]), elastic deformations are foreseen.
- If the VM stress is $\geq$ than the yield stress of the stainless steel (220 MPa [56]), plastic deformations are expected.
- If the VM stress » than the yield stress of the stainless steel and close to the ultimate tensile strength of the material (550 MPa [56]), fractures or perforations are foreseen.

In the model used in this study, the welding are not simulated. Their resistance to the shock is lower than the one of the stainless steel and in general a safety factor must be considered to take this into account:

- The yield stress of the welding is 80% of the stainless steel yield, ∼175 MPa.

It must be noticed that the values of stress given shall be used only as indication. Due to the hypothesis and approximations done in the geometrical model, the choices of the elements size (mesh) and the real thickness and material composition of the shells (that may vary from the theoretical ones), the values of pressure will not be the same than the one found in reality.

The accuracy of the solution greatly depends on the number of elements used to represent the geometry, the mesh. Redefining the mesh, the solution improves converging towards a specific result. If there is an analytical solution for the given problem, the mesh refinement procedure will converge towards the exact solution.
However, there are situations where the solution does not converge even with mesh refinement. In these points, with refining the mesh, the stress keeps increasing and increasing, theoretically tending to infinite. Stress singularities are one of these situations and are very common in FEA.
Typical situations where stress singularities occur are at the points where the load is applied, sharp corners or corners of connection of a body with another.
In our particular case, this may happen in the point of contact of the overpack with the target of the drop tests, in the sharp corner of the reinforcement wings or in the connections with the rings.
Although stress at these singularities is infinite, this does not mean that the model results are incorrect overall. The St. Venant's principle [57] may help to solve this problem. It states that:
"If the forces acting on a small portion of the surface of an elastic body are replaced by another statically equivalent system of forces acting on the same portion of the surface, this redistribution of loading produces substantial changes in the stresses locally, but has a negligible effect on the stresses at distances which are large in comparison with the linear dimensions of the surface on which the forces are changed."

In other words the effect of local disturbances to a uniform stress field remains local. At distances of the size of the disturbance, the results will not be perturbed.
For these reasons, in the analysis of the test done on the prototype we will observe and use as indicative values, not the stress on the singularity points but the ones "far" from them.
Moreover, as stated also previously, the scope of the test is to insure that the deformations on the cylindric body after the drops will not cause drillings. These regions are "far" from the singularities and the stress values will be reliable.

2.5.5.2 FEA Modelization

The geometry of the ColiBRI package has been reproduced in the ANSYS Mechanical Workbench.
It has the dimensions defined in the technical drawing (Fig.2.62 at the end of this chapter). The ANSYS workbench used to reproduce the mechanical tests are the Explicit Dynamics (for all the drop tests) and the Static Structural (for the stacking tests). The choice depends on the type of boundaries conditions and physics involved:

- A *Static Structural* analysis determines the displacements, stresses, strains, and forces in structures or components caused by loads that do not induce significant inertia and damping effects. This is the case of the simulation of a mass placed on the container to reproduce the stacking condition. Here the loads and the structure's response are assumed to vary slowly with respect to time.
- The *Explicit Dynamics* workbench is used instead in case of short-duration high-pressure loading as the cases involved in the drop test. It enables us to capture the physics of short-duration events with highly nonlinear, transient dynamic stresses.

Some expedients are used to increase the computational efficiency:

- Using the characteristics of symmetry of the body, only half of the structure has been reproduced with a symmetry corresponding to the vertical cutting plane (Fig.2.34). Some elements, like the hooks, the handle lids and the centering pin, not critically involved in the deformations are not considered in the simulations (the handle lid is introduced only in the drop tests on the lid side).
- Moreover, since the thickness of the elements in the structure is small compared to the other dimensions, only the mid surfaces have been reproduced. The thickness and the type of material is assigned to each surface in the solver workbench.
- In the analysis of the drop tests the stainless steel shell of the overpack and the tungsten container have been simulated. The insulation wool, indeed, contributes only in a minimal part to the deformations induced by the drops. However the weight of the wool has been included in the calculations adjusting the density of the stainless steel objects.
- The reproduced shape of the tungsten container is simplified and is composed by a body in tungsten and a full lid in stainless steel. Also in this case its weight is kept equal to the one defined in reality.
- The screws (of the overpack's lid and the ones connecting the PEEK ring) have been reproduced as beams connecting surfaces of the inox body (Fig.2.35). With this approximation we cannot evaluate the stress in the bolt. A cross section of 16mm, for the simulation of the overpack screws, or 6mm, for the simulation of the ones supporting the PEEK ring on the lid, has been assigned to them.
- Some elements like the target of the drops, the mass that will fall on the body and the bars involved in the penetration tests are considered to be rigid since the stress distributions and the wave propagation in such parts are not critical during the impacts. The targets of the simulations

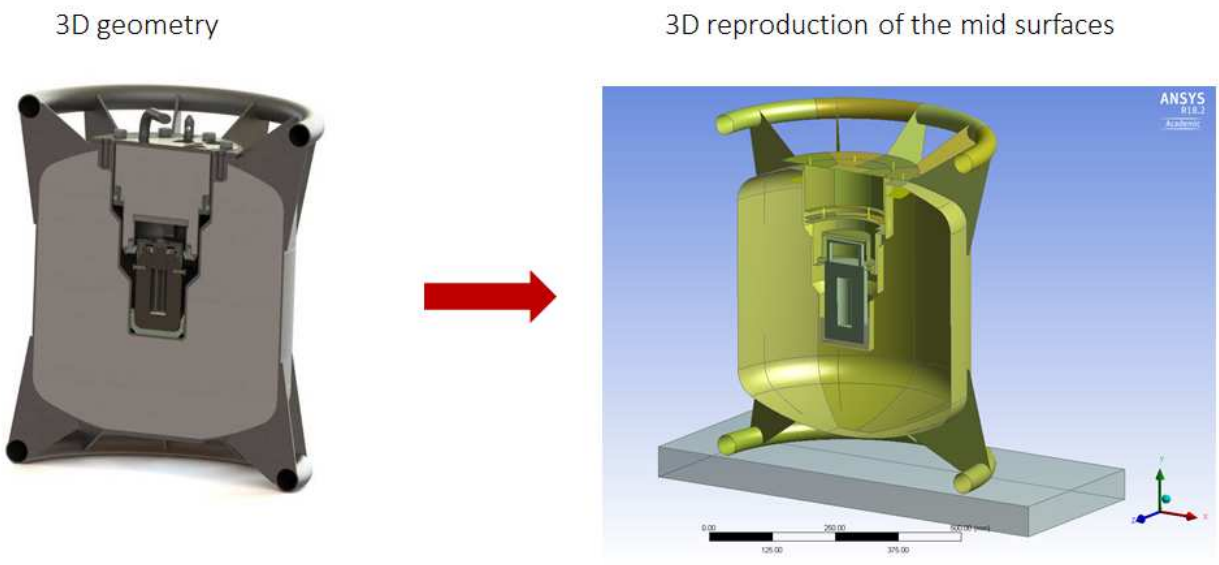

Figure 2.34: The 3D structure of the container is studied reproducing only the mid surfaces of the elements and only the half of the geometry, considering the package's characteristics of symmetry.

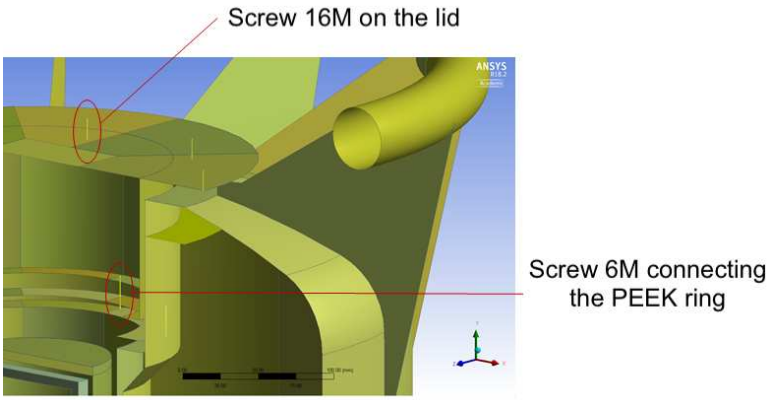

Figure 2.35: Detail of the geometry used for the FEA simulations: the screws are reproduced as beams connecting the surfaces.

(a steel plate and a rigid bar) are set up also as "Fix support" since they won't move during the tests.

The information on the materials mechanical and thermal characteristics are reported in Annex B as well as an explanation of all the basic steps to take to set up a simulation in the ANSYS workbench.

2.5.6 Results of the Finite element Analysis

2.5.6.1 Stacking test

The stacking test is used to simulate the condition in which packages are piled-up during the transport and must sustain, for a defined time, the weight of other materials or other packages.

As stated in the par. 723 of the IAEA Regulation [39], the package shall be subjected, for a period of 24 h, to a compressive load equal to the maximum between:

a) Five times the maximum weight of the package:

$$F_1 = 5 * 113kg * 9.81m/s^2 = 5,5 * 10^3 N \tag{2.2}$$

b) The equivalent of 13kPa multiplied by the vertically projected area of the package:

$$F_2 = 13kPa * 0.28m^2 = 3.64 * 10^3 N \tag{2.3}$$

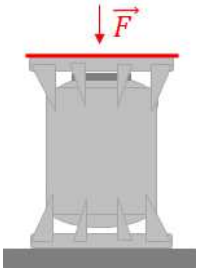

Figure 2.36: Scheme of the stacking test.

In our circumstances the case a) induces an higher stress and has been considered as boundary condition in the simulation. A uniform force (of 5,5*10^3 N) is applied on the upper ring of the overpack, laying on a fix support.

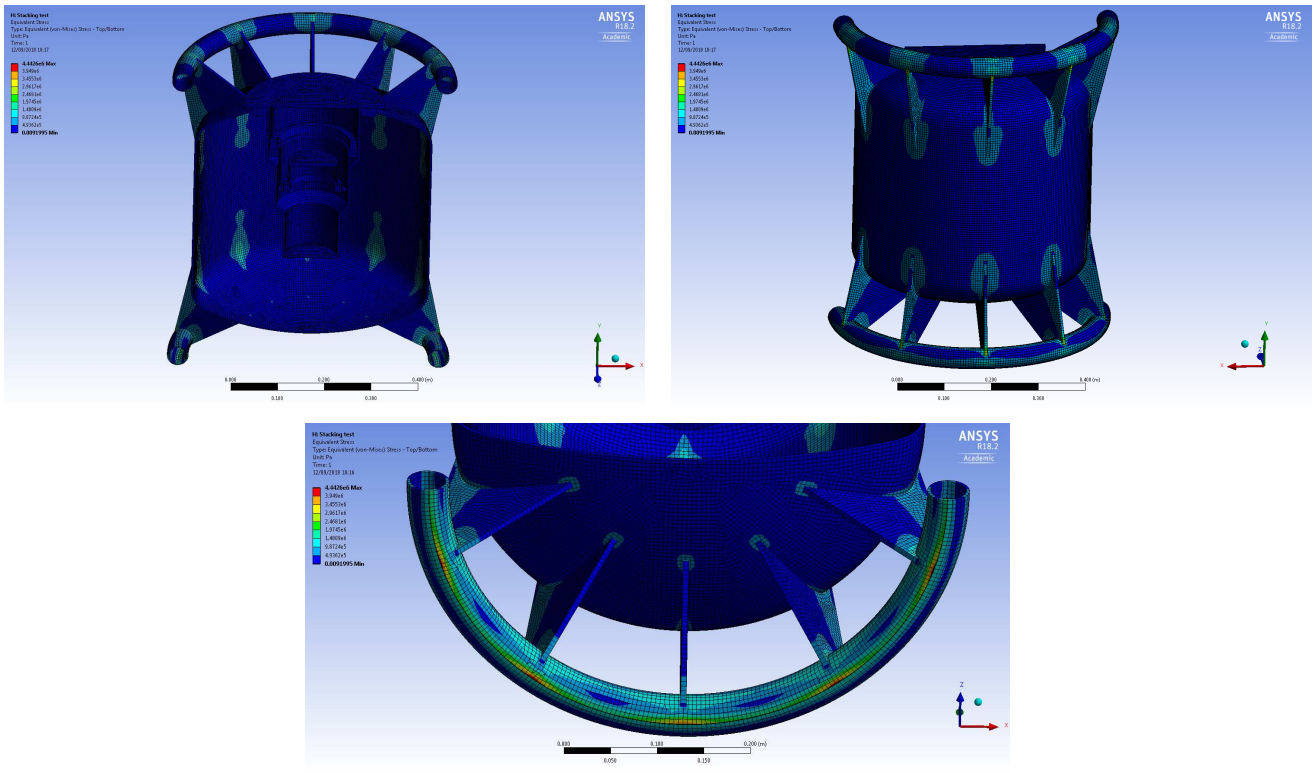

Figure 2.37: Results of the stacking test: map of the VM stress.

As it is possible to observe from the Fig.2.37, the package won't be affected by this test and no macroscopic deformations are observed. The maximum stress regions correspond to the areas of the wing connections where the reaction forces are higher. The resulting maximum value of Von Mises stress (∼4 MPa) is lower than the Yield limit for the stainless steel 304L (220 MPa). The behavior of the stainless steel container is in the elastic region and after the load removal the structure is intact.

2.5.6.2 9m drop tests

As stated in the par. 725 (normal condition of transport) and 727 a (accidental condition of transport in case of liquid sources) of the IAEA Regulation [39], the distance from the upper surface of the target to the lower one of the package is fixed to 9m. Considering the package as a rigid body and neglecting the air resistance, the final velocity of the body has then modulus equal to 13.3 m/s.
Three orientations of the package's vertical axis with respect to the target plane have been studied: perpendicular, horizontal and 45° tilted axis (Fig2.38). This has been used to investigate the conditions (as the IAEA Regulation cites, par.. 727) "that will lead to the maximum damage" on the container. The orientation leading to the maximum damage and deformations is the one to be reproduced during the experimental test.
The range of time simulated has been long enough to be able to simulate the impact on the target and the first rebounding moments.
The deformations are set to be nonlinear: large permanent deformations can happen, so the material model takes into account the nonlinear relationships between stress and strain. The subsequential comparison with the material characteristics is necessary to deduce eventual failures in the structure and design ameliorations.

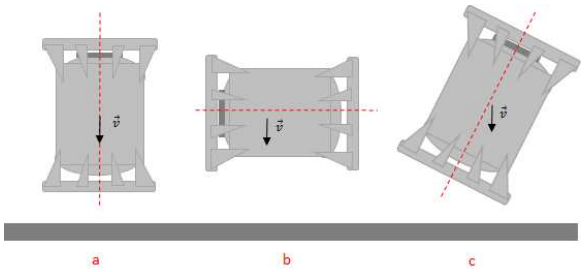

Figure 2.38: Scheme of the 9m drop test.

Case a: Vertical/perpendicular orientation
The drops on the two sides of the package have been studied:

Case a.1: normal drop with lid facing up
The value of the equivalent VM stress is higher then the ultimate tensile strength of the stainless steel 304L (550 MPa) in points located at the contact regions between the lower ring and the reinforcement wings. These are the regions impacting the target and singularity points, so no precise forecast can be done on them.
It is possible to deduce that the shock limiters, and in particular the weldings, will most probably break in those points in the real situation.
This will lead to the loss of the stability/equilibrium for the container. The main cylindrical body won't be largely affected by the impact. The deformation of the rounded bottom part of the container is due to the thrust of the reinforcement wings. In these regions the maximum equivalent stress value

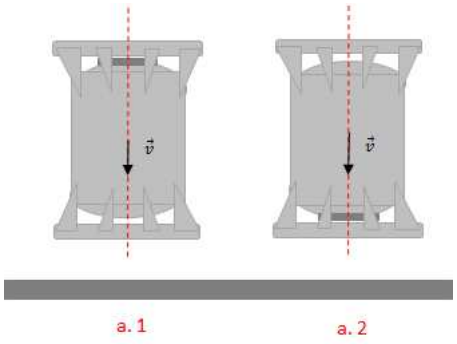

Figure 2.39: Scheme of the 9m drop test with vertical orientation: the overpack's lid can be up-facing or down-facing.

is 360 MPa (Fig. 2.40) higher than the Yield stress value of the stainless steel (220 MPa) and will involve here plastic deformations.

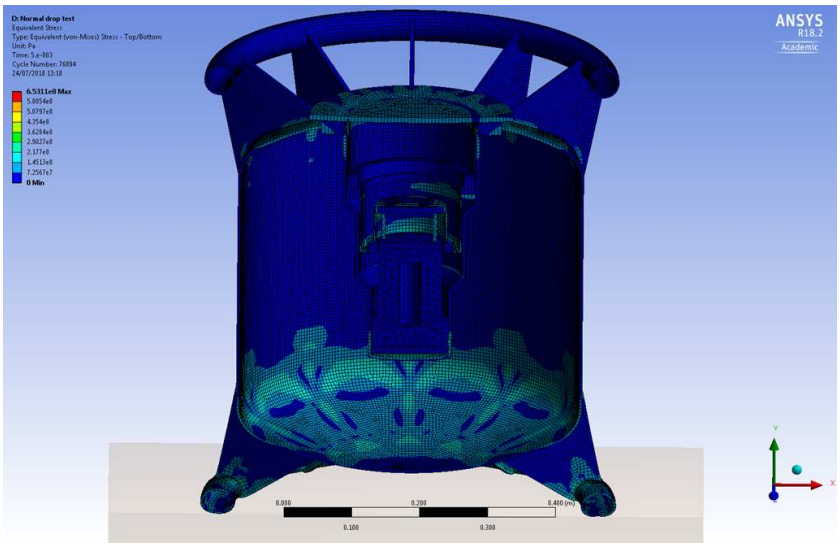

Figure 2.40: Equivalent stress results of the 9m drop test with normal direction of the package.

Case a.2: normal drop with lid facing down

This test is done reversing the package in order to observe the effect of the drop on the internal surfaces of the lid and in particular the damage to the handle lid (Fig.2.42). It must be noticed that one of the goals of the simulations is to prove that the damages on the lid won't cause its opening at the end of the tests.

The stress caused by the movement of the shielded package implies the deformation of the external metallic surface of the overpack's lid. The presence of a silicone disc aims to reduce them absorbing partially the shock.The upper ring and the wings will undergo the same deformations and stresses as observed in the case a.1.

Also in this case the main body of the container is involved in plastic deformations and no perforation are foreseen.

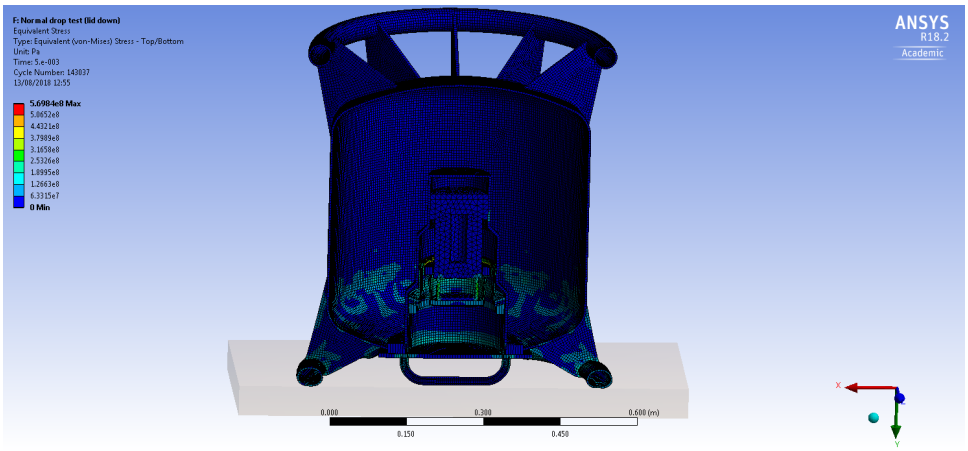

Figure 2.41: Equivalent stress results of the 9m drop test with normal direction of the package and lid in the target direction.

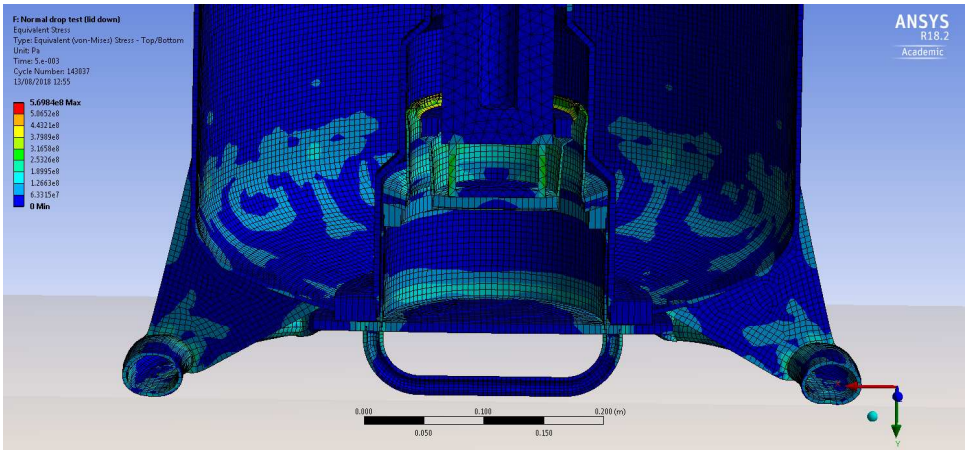

Figure 2.42: Particular of the lid region deformation after the test.

Case b: Horizontal orientation

Referring to the Fig.2.43, the points in which we observe maximum pressure are located on the upper and lower rings, in the regions impacting the target. Here the maximum equivalent VM stress has values right below the ultimate tensile strength limit of the stainless steel (500 MPa). Since they are located in singularity point, it can be assumed, to be conservative, that the weldings connecting the rings with the reinforcement wings may brake in those areas.
The weight of the tungsten container will slightly tilt the internal metallic structure during the impact. It is also possible to observe that one of the reinforcement wing pushes on the rounded bottom due to the target force reaction to the drop and a plastic deformation appears on it.

Case c: 45 degrees orientation

As we can observe from the figure (Fig.2.44), the rounded bottom is deformed due to the reinforcement wings impacting on the target. The values of the VM stress suggest that the deformation will be plastic. The wings also absorb the largest part of the impact energy and will fold causing the breaking of the welding point connecting the reinforcement ring (the max stress here is around 800 MPa but it is again

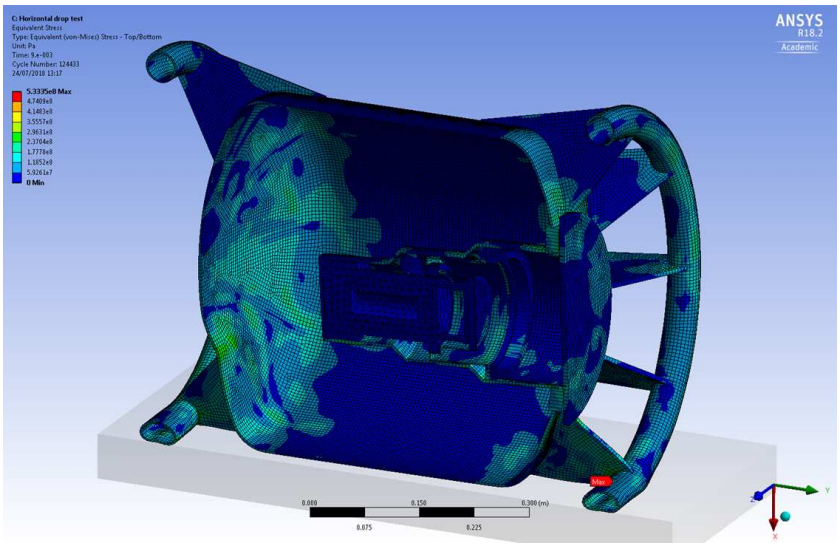

Figure 2.43: Equivalent stress results of the 9m drop test with horizontal orientation of the package

a singularity point).
This test has also been repeated with the inverted package (Fig.2.45) to observe the effect of this drop on the lid due, in particular, to the possible displacement of the shielded container. The tungsten shield remains confined in the overpack after the test and plastic deformation of the inner metallic shells arises from its movement. The force due to the weight of the container is balanced by the reaction forces of the conic surface, connected directly to the reinforcement wings. For this reason there is no tilting of those region. The stress values on the external shell are the same than the previous orientation.

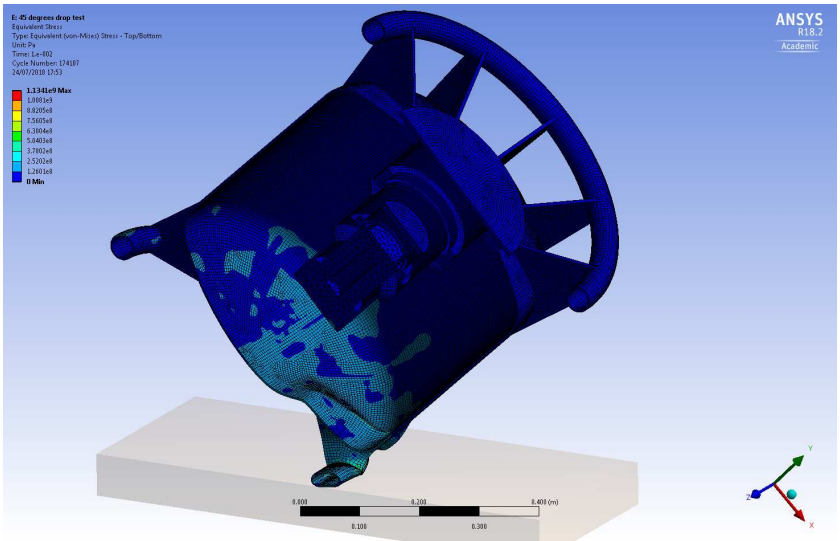

Figure 2.44: Equivalent stress results of the 9m drop test with vertical axis sloped of 45 degrees.

Conclusions on the 9m drop tests

As observed in the results showed in the previous Figures (2.40 to 2.45), the failures and the plastic

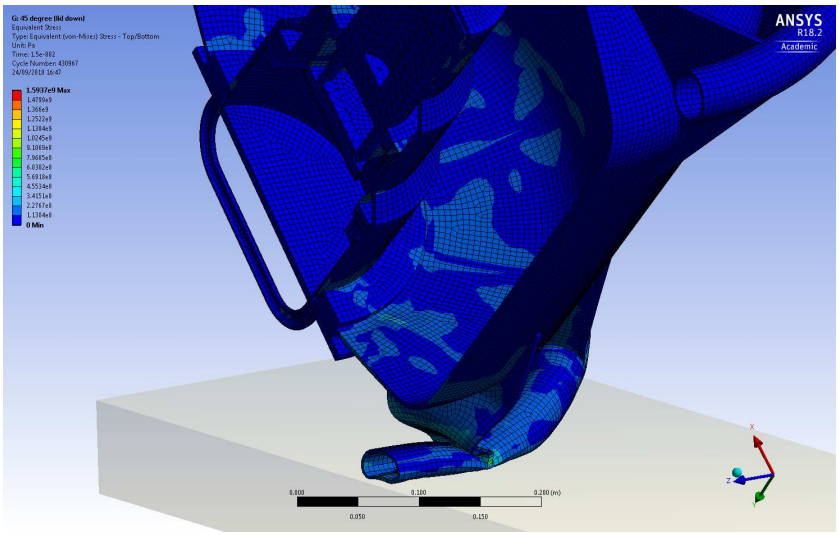

Figure 2.45: Equivalent stress results of the 9m drop test with vertical axis sloped of 45 degrees and with lid facing the target.

deformations are evident and limited to the impact regions. The maximum Von Mises stress value is, in those regions, higher than the ultimate tensile strength of the stainless steel 500 MPa. This will lead to a break in the welds with consequent loss of the package stability. At the same time, the stress won't affect drastically the main cylindric body of the container in which the plastic deformations do not imply perforations.
The maximum value of the pressures in the screws during the impact is reported in the Fig.2.46 for all the tests involving a drop from 9m. Those values are below the elastic nominal limit of 700 MPa (see Tab. in Annex B) for the M16 stainless steel screws. We can assume that the lid of the ColiBRI's overpack will remain closed after the impacts. The two acceptance criteria discussed at the paragraph 2.5.5 are, then, satisfied by this design after the 9m drop tests in all configurations.
The parallel analysis of the 9m drop test on the package and in different orientations helped in the definition of the one leading to the maximum damage. Tilting the axis of the package of 45 degrees the reinforcement wings will undergo the highest deformation among the studied cases, causing also a visible bending of the bottom plate of the package. The 45 degree orientation will be then chosen as condition for the experimental test on the prototype.

2.5.6.3 Drop onto a bar

As stated in the paragraph 727 b) of the IAEA Regulation [39], the package must drop on a bar (15.0±0.5 cm of diameter, 20cm height) rigidly mounted perpendicularly on a metallic plane target and with upper end flat and horizontal. The height from the point of impact on the package and the upper surface of the bar must be 1m. The final velocity of the entire package is then set to 4.43 m/s in modulus, again calculated considering the package as a rigid body and neglecting the air resistance.
Four orientations have been investigated (Fig.2.47) to establish the condition leading to higher deformations. Besides the ones with the vertical package's axis parallel and perpendicular to the bar, a configuration coming from a slight rotation of the package (10 degree) have been simulated. This is done to observe effect due to the drop on the edge instead than on a flat surface.

Case a

The impact is on the lateral area of the package (Fig.2.48).

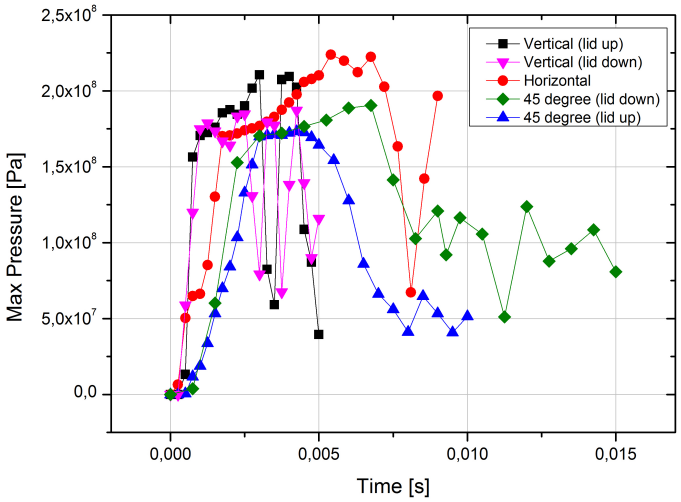

Figure 2.46: Maximum pressure values in the beams simulating the screws of the overpack's lid during the 9m drop test.

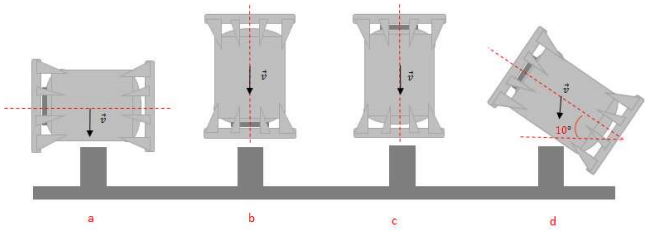

Figure 2.47: Scheme of the drop test or a rigid bar.

In this case the maximum stress region (240 MPa) is located in the contact zone with the bar and it is slightly higher than the yield stress value of the stainless steel composing the overpack (200 MPa). Plastic deformations are expected only in this area and no perforation are foreseen.

Case b

In this configuration the biggest deformation will concern the handle lid (Fig.2.49 and Fig. 2.50). It will appear bent inwards after the test, but no deformations will affect the base of the lid and the rounded metallic surface it is part of.
Plastic deformations are linked to a maximum equivalent stress value of about 430 MPa, higher than the yield stainless steel stress in the region of the handle lid. The tungsten container will slightly move downwards to touch the silicone disk causing the appearance of reaction forces on the bottom metallic surfaces of the lid.

Case c

The impact is on the bottom surface of the package in this case (Fig.2.51). The values of equivalent stress (with max of about 200 MPa) denotes that a plastic deformation will happen with no drilling/ perforation of the bottom surface.

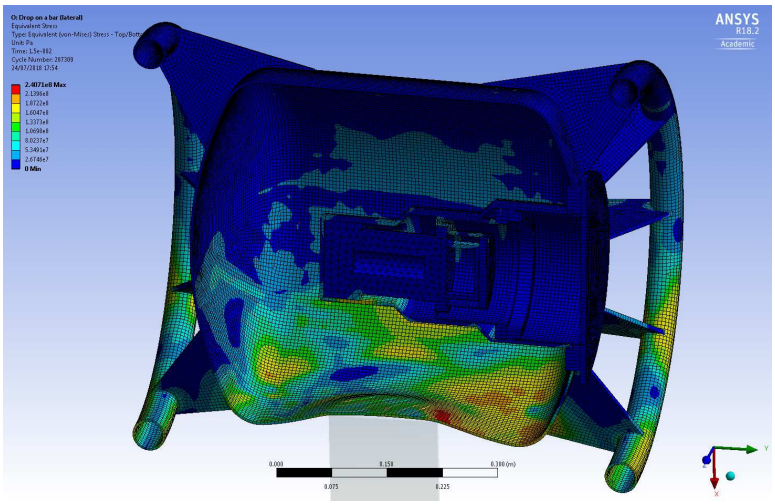

Figure 2.48: Equivalent stress results of the drop on the bar on the lateral side of the package

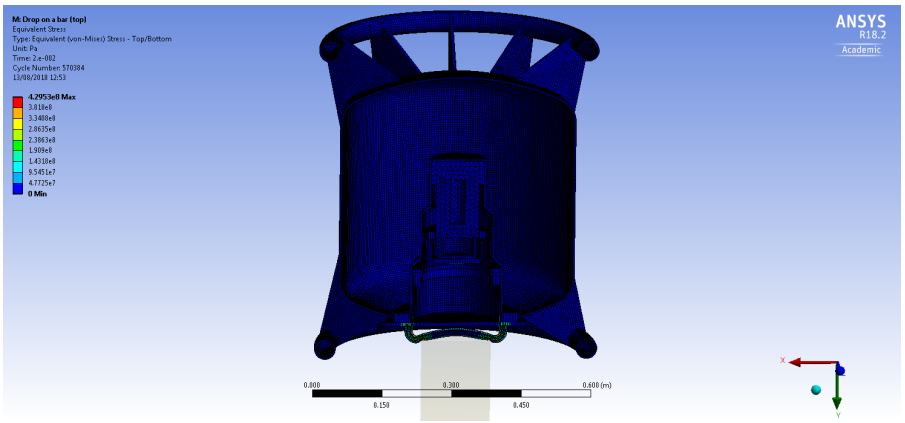

Figure 2.49: Equivalent stress results of the drop on the bar on the lid side of the package.

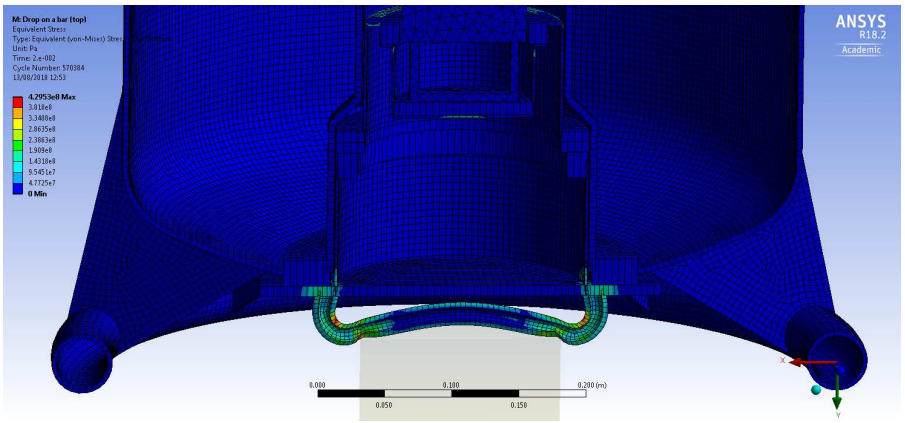

Figure 2.50: Particular of the Equivalent stress map of the overpack's lid after the drop test.

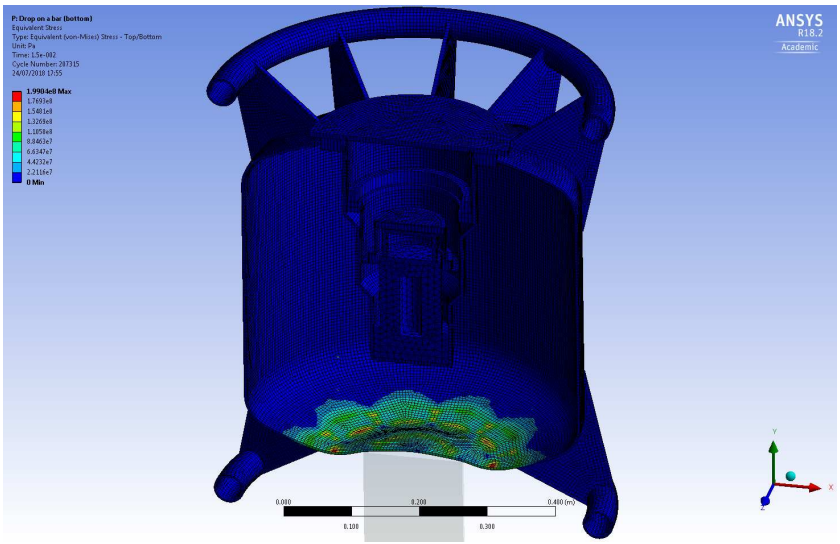

Figure 2.51: Equivalent stress results of the drop on the bar on bottom side of the package

Case d

The vertical axis of the package has been tilted by 10 degrees before letting it drop on the bar. In this scenario the deformation is given by the impact of the lateral surface of the overpack on the edge of the bar rather than from the impact on a flat surface. The maximum value of the equivalent VM stress simulated in this situation is not different from the one observed in the case a but the resulting area expressing this value is more extended in the case d, revealing an higher hazard.

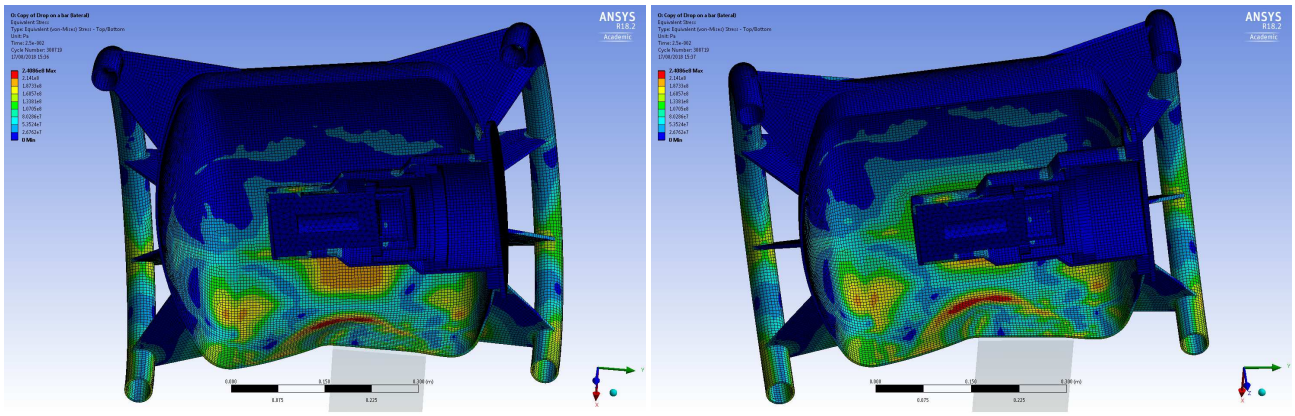

Figure 2.52: Equivalent stress results of the package drop on the bar in the 10° tilted configuration.

Conclusions on drop tests onto a rigid bar

In all the analyzed cases, the deformations will affect the main cylindrical body due to the smaller area of the target (the bar). Nevertheless the deformations will not imply perforations of the structure since the simulated stresses are lower than the rupture limit of the stainless steel.
The configuration leading to the maximum damages is the one represented in the case d and it will be the one to perform during the experimental test.
Observing the values of the pressure in the beam simulating the M16 screws of the overpack's lid, it

is possible to notice that also in these cases they are lower than the elastic nominal limit. We can deduce that the lid remains closed after the drops and that the tungsten container remains stored in the overpack.

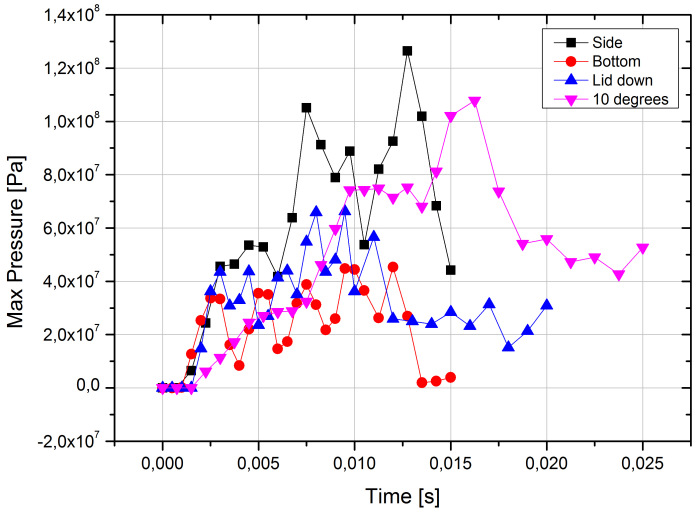

Figure 2.53: Maximum pressure values in the beams simulating the screws of the overpack's lid during the drop test on the rigid bar.

2.5.6.4 Drop of the 500 kg mass

The third drop test described in the IAEA Regulation in par. 727 c) [39] foresees the drop on the container of a solid mild steel plate of a mass equal to 500 kg and dimensions 1x1 m (thickness 6.5 cm, density 7.8 g/cm^3) . It must fall on the package horizontally from 9 m. In order to take into account all the possible scenarios, three cases have been analyzed (Fig. 2.54).

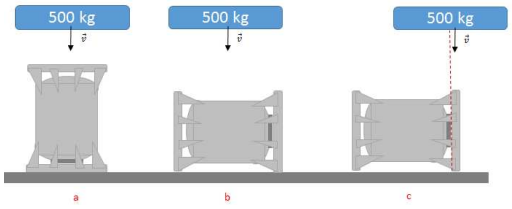

Figure 2.54: Scheme of the dynamic drop test, drop of 500 kg on the package.

Case a

In this configuration the vertical axis of the package is perpendicular to the target (Fig.2.55).
This test shows the folding of the reinforcement metallic wings and a flattening of both the upper and lower ring. The bottom rounded surface of the overpack appears corrugated due to the wings thrust inward and it will not impact the target during the drop. The values of the VM stress are in the region of the plastic deformation for the spheric base plate, but they are close to the maximum yield stress value of the stainless steel in the region of impact. This lead to the conclusion that the reinforcement wings and the welded connection with the lower ring may fail in this scenario.
The displacement of the tungsten container during the impact will cause the deformation of the

thin metallic surfaces composing the base of the overpack's lid causing also the reaction on the screws/beams. The upper surface of the lid, instead, will not be affected by the impact and no evident deformation will appear on it.

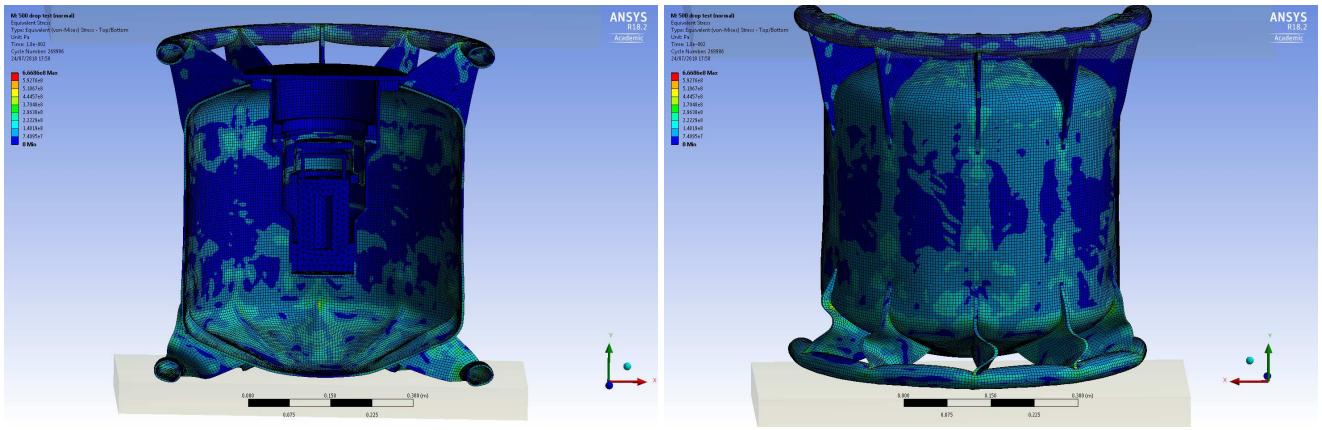

Figure 2.55: Equivalent stress results of the 500kg drop on the inverted package. Front and back view.

Case b

The horizontal case induces deformations of all the package's elements, including the cylindrical main body (Fig.2.57). The fall of the mass will cause a recess of the metallic wings through the rounded bottom area and a folding of the regions at contact with the target. The internal surfaces sustaining the shielded container appears evidently tilted. The maximum value of the VM stress is localized at the connection point between the reinforcement wings and the two rings. We can then expect a break of the welding in those regions since the stress is higher then the maximum yield stress of the stainless steel (500 MPa) also in the elements far from the singularity.

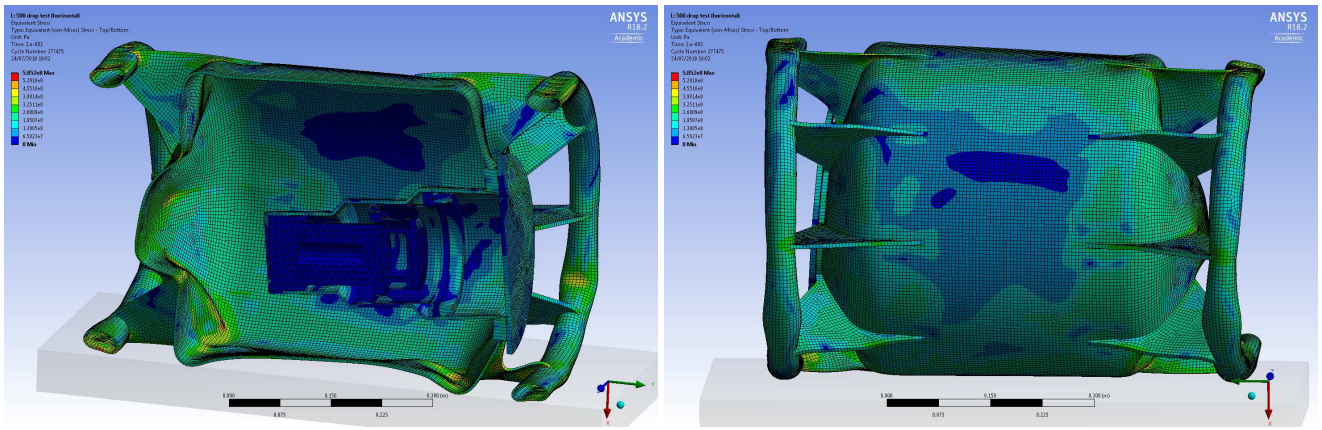

Figure 2.56: Equivalent stress results of the 500kg drop on the lateral side of the package. Front and back view.

Case c

With the scope to look for the configuration leading to the maximum deformation, the center of the steel slab has been moved to be on top of the opening of the package. The region where the screws are placed is actually the most critical.
In this case, the higher deformations are focused on the lid region of the overpack with the bending of

the wings at contact with the target and the slab. It is also possible to see a tilt of the inner metallic region. the cylindrical body will be affected only by plastic deformations since the VM stress reaches values lower than the ultimate tensile strength of the stainless steel.

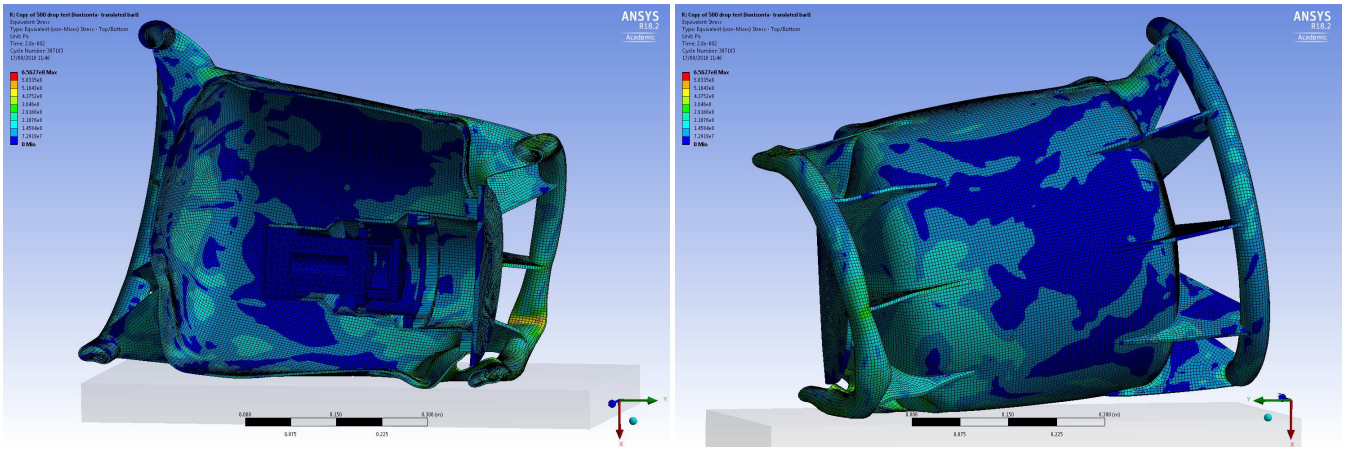

Figure 2.57: Equivalent stress results of the 500kg drop on the lateral side of the package in the translated configuration. Front and back view.

Conclusions on the 500 kg drop tests

At the end of these set of tests the container appears folded and compacted but no drill or perforations will appear on the cylindrical body. The stresses and the relative deformations are higher compared to the other sets of tests and configurations.

Among the three drop tests involving the fall of the 500 kg slab on the package the most critical one appears to be the case c. So it will be the one to be performed in the real tests.

As the previous cases, the behavior of maximum pressure in the screws composing the lid has been analyzed during the tests. These set of values will not exceed the elastic nominal limit of the M16 stainless steel screws and we can assume that the shielded container is keep confined in the overpack during the test.

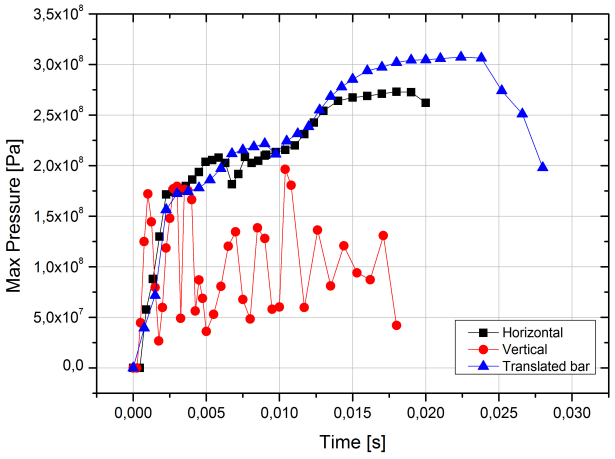

Figure 2.58: Maximum pressure values in the beams simulating the screws of the overpack's lid during the drop test of the 500kg bar on the package

2.5.7 The regulatory tests planning

The tests to perform on the type B package are reported in the Fig.2.59. They must follow a precise order established in the Chap 7 of the IAEA regulation [39] where it is also specified the possibility or not to change the prototype between two tests. In particular it is not possible to change the package between the three mechanical drop tests for the accidental conditions and the same shall be used for the fire test.

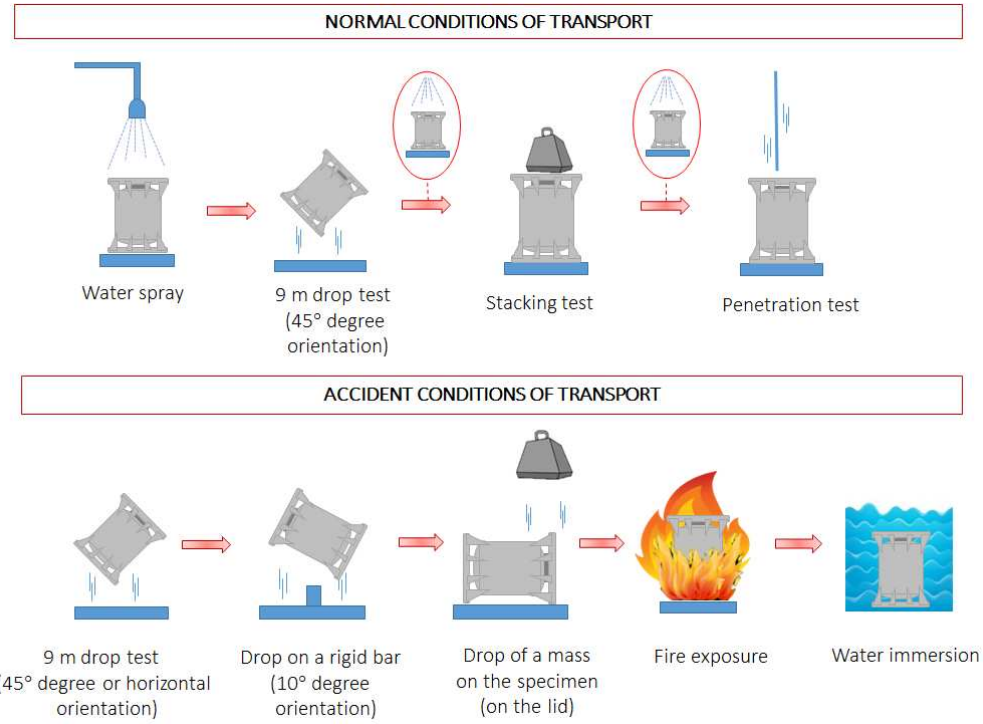

Figure 2.59: Schematic representation of the test to perform on the ColiBRI-30.

It must be noticed that the drop test in case of normal conditions is from an height of 1.2 m for packages transporting only solid sources, increased to 9 m in case of liquid or gaseous sources. This test appears both in normal and accidental conditions but in the experimental test it may be performed once if all the tests are done with only one prototype.
In the present study, it has been decided to realize two prototypes for the testing phase: one will undergo all the normal condition test and the water immersion test, while the other one the accidental chain of test.
The ColiBRI-30 is expected to be tested at the Laboratory "G. Guerrini" (ex Laboratorio Scalbatraio) of the Nuclear Engineering Department of the University of Pisa, Italy. This facility was established in the 1970 and obtained in 1983 the attestation of conformity to the IAEA norms from the Italian Authority of the nuclear energy and research, the ENEA (Agenzia nazionale per le nuove tecnologie, l'energia e lo sviluppo economico responsabile).
The facility is equipped with several platforms of testing, in compliance with the International specifications:

- A platform for the mechanical drop tests or in alternative a crane with an external rigid target,
- An oven reaching 800°C with high volume capacity for the fire test.

The comparison with the FEA simulations will be possible firstly by a visual inspections and a

photographic set of images to compare the final deformations, secondly using devices to quantify observables:

- Specific strain gauges and accelerometers will be placed on the prototypes in order to evaluate the stress and the velocity of impact during mechanical drop test.
- For the thermal test it will be intended to measure the temperature inside the package (at contact with the Posisafe) and outside (at contact with the overpack) thanks to two thermocouples.

2.5.8 Administrative steps for the approval

The final step of the process consists in the compilation of all the administrative and technical reports to submit to the competent authorities.
The development of a new package requires that applicants provide in-depth technical justifications to receive the approval. Actually this phase it is not completely disconnected from the rest. In particular, once the mechanical specifications are ready and all the methods (theoretical or computer-aided calculations) to prove the good performance are established, the meeting with the authorities can start.
A first contact preceding the realization of the tests is necessary and recommended to be sure that all the regulatory constraints have been well taken into account.
In particular in France there are three main stages linked to three different documents to prepare and send to the French Nuclear Safety Authority (ASN), distributed along the design chain. They are in the order:

1. Emission of a **Draft of Safety report** (Dossier d'opinion de sureté - DOS) to ASN: the objective is to present and justify the technical solutions selected to ensure the different safety functions relative to the requirements. A description of the hypothesis and the methodology of the calculations used for the analysis of the package's performance shall be presented.
2. **Planning of the Tests** (Programme d'essais): the test shall be performed in a recognized facility and the presence of the authority may be foreseen. The planning shall report all the information on the chosen set up of measure and configuration (i.e. package's orientation) and sequence of the tests, the number of prototypes and the instruments used. Some tests may be omitted (or also added) if it is possible to show evidences using numerical calculations, always if in agreement with the authorities.
3. Emission of the **Final Safety Report** (Dossier de Sureté): The results of the numerical and practical tests on the prototype must be included in this final document.

The previous procedure is valid in particular for Type B and C. For the other type of packages the only emission of the Safety Report containing a technical specifications and the results of the tests (that can be made in house without a previous agreement and the presence of the authorities) is sufficient.
For the present study the preliminary report containing the technical specifications of the ColiBRI-30 (ensemble of overpack and shielded container) has been already submitted to ASN. A first meeting with representatives of ASN and IRSN helped to pinpoint additional elements to prepare for the final document and for the regulatory tests.
The planning of the test is ready and has been discussed with the authorities: the orientations, the type of devices to use for the measurements and the number of prototypes have been set. It has been also discussed with the authorities.
After all the documentations are sent to the authorities a period of 12 months is generally necessary to obtain the validation of the Safety files and the certification.

2.6 Conclusions

The transport of radioactive material as well as the design of a shipping package, must follow a very strict Regulation defined by the International Atomic Energy Agency (IAEA) and reported in the SSR-6 Guide [39].
The scope of this study has been the development of a new transport container of type B for medical isotopes. The three main characteristics of the source are the small size, the high activity and short half-life. The package, whose commercial name is ColiBRI-30, is then a "compact" type B(U) container, easy to manipulate and with a removable shielded core to ease the handling and the loading/unloading operations. It differs from the usual type B package since the isotopes of interest are not fissile and with short-half lives.
The design has been a process involving different techniques and expertise:

- The radioprotecton study is necessary to ensure that the exposure during the transport is as low as reasonably possible and respects the specific values defined in the Regulation. They have been carried out with analytical and Monte Carlo techniques with the scope to evaluate the maximum value of activity to transport. Consideration on the heat generated by the sources have been also necessary to ensure that the tightness of the container is not compromised.

- The Finite Element Analysis method has been used during the mechanical design, the drawing phase and the optimization phase of the package. It is an excellent tool helping to reproduce on a virtual prototype all the regulatory tests that the container must sustain to obtain the certification. It avoids the expensive realization of the prototype (sometimes more than one is necessary) and allows to rapidly observe the effect of the modifications on the final performances. Several designs have been tested before the one presented in this work (par.2.5.2). Adjustments on the shape and the thickness of the package components, in particular for the overpack, have been necessary to reach higher efficiency.
  The results of the tests performed on the Colibri-30 show that at the end of all the tests the damages will concern only the external metallic shell of the overpack, the lid stay closed and the removable shielded container is kept confined in it.
  The method chosen has only one limitation: it is not possible with the mid-surface reproduction technique to carry on a sequential analysis. In other words it is not possible to use the results of one simulation as the input (or boundary conditions) of the following one. It must be remembered, indeed, that the mechanical drop tests for the type B in accidental conditions shall be performed all with one package. The same prototype, with the maximum damages, shall be subjected to the fire test.

Two prototypes of the ColiBRI-30 and one Posisafe KL-30 have been realized and completed with all the details, like engraved plates with names and serial numbers and adhesives (Fig.2.60 and Fig.2.61). They are ready to be tested and the administrative process, including contacts with the authorities, have been already started.



Figure 2.60: Photos of the two prototypes of the Colibri-30.



Figure 2.61: Particular of the Colibri-30 lid.

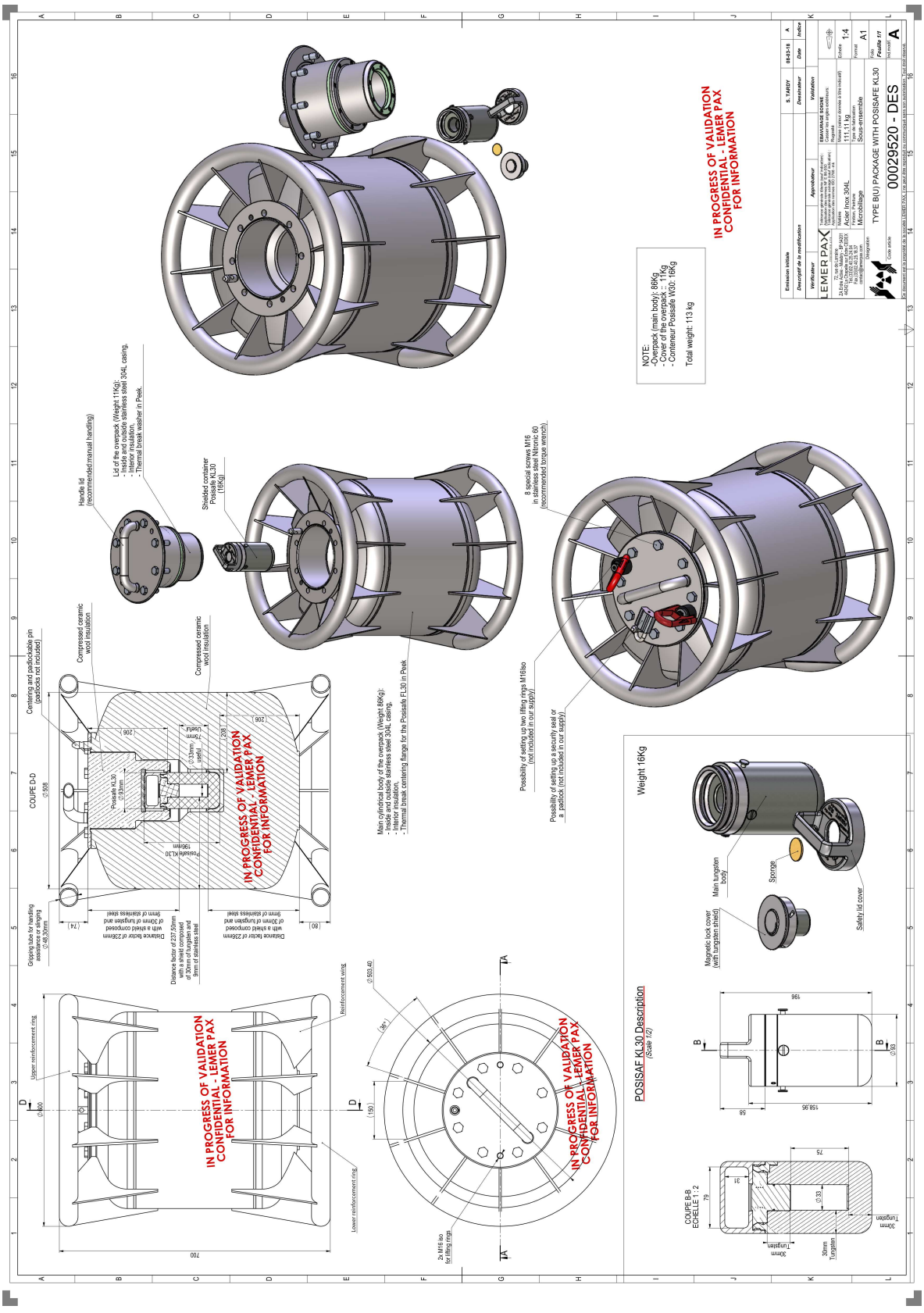

Figure 2.62: ColiBRI-30 technical drawing.

3

The Radioprotection after the collection: the waste management

Contents

3.1 Radioactive waste: definition and classification . . . 106
3.1.1 The situation in France . . . 108
3.2 The basic principles of Activation . . . 110
3.3 The ARRONAX Cyclotron . . . 112
3.4 The study of the materials' activation in the ARRONAX bunker . . . 114
3.4.1 The irradiation device . . . 115
3.4.2 The software ActiWiz . . . 116
3.4.3 The fluence simulation with MCNPX . . . 119
3.4.3.1 Particle field calculation . . . 119
3.4.3.2 Directional emission during irradiation: the different behavior of the particles . . . 123
3.4.3.3 Effect of concrete . . . 126
3.5 Examples of application . . . 128
3.5.1 The analysis of the rabbit . . . 131
3.5.1.1 The vacuum couplers . . . 137
3.5.1.2 Piston rod cylinder . . . 141
3.6 Conclusions and future perspectives . . . 145

As consequence of the irradiation process, all the tools, the devices and parts placed in proximity of the source shall be considered radioactive and treated as nuclear waste. Although elements such as target, collimators, Faraday cups or beam dumps are built to withstand radiation, they become radioactive as results of a process called *induced activation*.
Depending on the level of activity and the chemical form of the objects, their storage and disposal may follow different paths and contribute in different ways to the dose delivered to the personnel.
A proper definition and prediction of the level of hazard is of primary importance in the management of the waste for a radionuclide production facility, not only for the safety and the operational benefit of the workers but also for the optimization of the financial resources. Smaller and less critical radioactive waste corresponds, indeed, to less capital spent for disposals and end of life-cycle treatments.
The choice of the waste treatment and disposal site strongly depends on the radionuclides and the activity level present in it. A good (quantitative) knowledge of those characteristics is requested from

the regulatory Authorities.
The software ActiWiz, recently developed at CERN, is a useful tool for these purposes in the high energies physics environment. It can be used to predict the hazard, the dose rate and the inventory of the species produced during the irradiation.
The study that follows aims to add knowledge on the physical behavior (in terms of activation) of different materials when subjected to the external radiation fields typical of a target irradiation in one of the GIP ARRONAX Cyclotron bunker. This will be done using the above-mentioned software modified to be tailored to the ARRONAX applications and conditions.
The scope is to define a procedure to monitor the waste production in this facility and to clearly identify the radionuclides and the relative hazard coming from the irradiation cycles on parts present in the bunker.

3.1 Radioactive waste: definition and classification

Radioactive waste is the term used to describe radioactive substances or objects for which no further use is planned or considered [58]. It is a general term to identify different types and forms of elements that have been in contact, irradiated and/or activated by particle beams or radioactive substances and that cannot be used or reprocessed. It may take many different forms: rubble, metal, gloves, filters, resins, pipettes, bottles in chemical labs, or even everyday objects like clocks, fountains or furniture.
The origin of the radioactive waste can be found in operations like decommissioning, reprocessing of spent fuel from nuclear power plants, cleaning up of historic sites, research activities, industrial processes, medical examinations or healthcare, etc.
The situation varies from country to country, not only in terms of produced waste volume but also in the national policies and strategies for carrying out the practical management of the radioactive wastes. A general and internationally valid classification of the waste has been established by the IAEA [59]. It includes six waste categories (Fig.3.1), classified according to their disposal solution which depends on:

- the **radioactivity level**, determining the degree of protection to be provided,
- and the **half-life** of the species involved, determining the logistic disposal time of decay.

- **Exempt waste (EW):**
  Exempt waste contains such small concentration of radionuclides that it does not require provisions for radiation protection. Once the material is cleared by the regulatory authority it is no longer considered as radioactive waste and it can be handled as regular waste.
  The primary radiological basis for establishing values of activity concentration for the exemption of bulk amounts of material and for clearance is that the effective dose to individuals should be of the order of 10 μSv or less in a year.
- **Very short lived waste (VSLW):**
  It can be stored for decay over a limited period of up to a few years and subsequently cleared from regulatory control according to arrangements approved by the regulatory body, for uncontrolled disposal, use or discharge. This class includes waste containing primarily radionuclides with very short half-lives (in the order of 100 days or less) often used for research and medical purposes.
  The classification of waste as VSLW obviously depends on the point in time at which the waste is classified. Through radioactive decay, indeed, the VSLW will move into the class of exempt waste. Thus the classification scheme is not fixed and reflects the flexibility that radioactive decay provides for the management of radioactive waste.

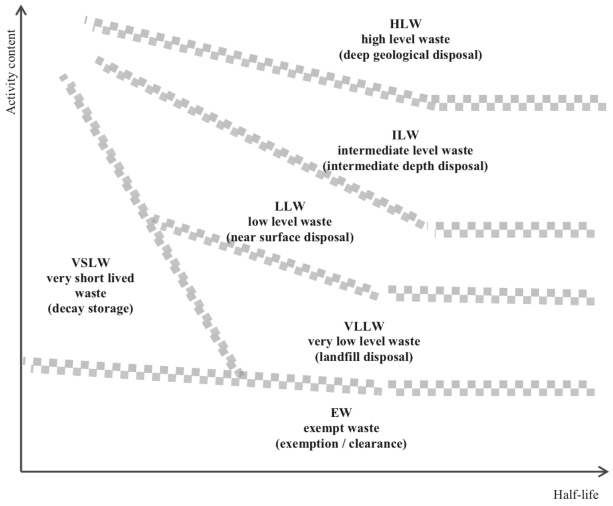

Figure 3.1: Conceptual illustration of waste classification, par. 2.5 of [59]. The vertical axis represents the activity content of the waste and the horizontal axis represents the half-lives of the radionuclides contained in the waste.

- **Very low level waste (VLLW):**
  This type of waste does not necessarily meet the criteria of EW, but does not need a high level of containment and isolation and, therefore, is suitable for disposal in near surface landfill type facilities with limited regulatory control. Such landfill type facilities may also contain other hazardous waste. Typical waste in this class includes soil and rubble with low levels of activity concentration.
  Concentrations of longer lived radionuclides in VLLW are generally very limited. They come mainly from the operation and decommissioning of nuclear facilities or from industrial sectors using naturally radioactive materials (chemistry, metallurgy, power production etc.). A big part of this waste is also coming from medical applications of radioactivity (diagnostic and therapy). In order to determine whether a particular type of waste can be considered to fall into the class of VLLW, acceptance criteria for engineered surface landfill type facilities have to be derived and may change case by case.
- **Low level waste (LLW):**
  Waste that is above clearance levels, but with limited amounts of long lived radionuclides. Such waste requires robust isolation and containment for periods of up to a few hundred years and is suitable for disposal in engineered near surface facilities. This class covers a very broad range of waste. LLW may include short lived radionuclides at higher levels of activity concentration, and also long lived radionuclides, but only at relatively low levels of activity concentration.
- **Intermediate level waste (ILW):**
  Waste that, because of its content, particularly of long lived radionuclides, requires a greater degree of containment and isolation than that provided by near surface disposal. However, ILW needs no provision, or only limited provision, for heat dissipation during its storage and disposal. ILW may contain long lived radionuclides, in particular, alpha emitting radionuclides that will not decay to a level of activity concentration acceptable for near surface disposal during the time for which institutional controls can be relied upon. Therefore, waste in this class requires

disposal at greater depths, of the order of tens of meters to a few hundred meters.

- **High level waste (HLW):**
  High level waste is defined to be waste that contains such large concentrations of both short and long lived radionuclides that, compared to ILW, a greater degree of containment and isolation is needed to ensure long term safety. Disposal in deep, stable geological formations usually several hundred metres or more below the surface is the generally recognized option for disposal of HLW. This type of waste typically has levels of activity concentration in the range of 10^4-10^6 TBq/m^3. It includes conditioned waste arising from the reprocessing of spent fuel or any other waste requiring a comparable degree of containment and isolation (few decades of cooling time).

Quantitative values of allowable activity content for each significant radionuclide will be specified on the basis of safety assessments for individual disposal sites.

3.1.1 The situation in France

In France the Institution responsible of the radioactive waste management and disposal is ANDRA, standing for Agence Nationale pour la gestion des D*x́*chets RadioActifs. It is a publicly owned industrial and commercial body, set up in 1991 [60].
ANDRA has the responsibility for the long-term management of radioactive waste produced in France (but excluding foreign waste or waste originating from foreign spent fuel processing). This agency operates waste repositories, defines the acceptance criteria for waste packages in these repositories and controls the quality of their production. The agency is also in charge of designing, siting, and constructing new disposal facilities [61].
In France the radioactive waste classification follows the same (qualitative) scheme seen in the previous paragraph. It depends always on the two factors listed before, radiation level and half-life and it is connected to the management solutions [62].
In particular in terms of half-life is possible to distinguish:

- waste in which the radionuclides have a very short half-life (less than 100 days);
- waste in which the main radionuclides have a short half life (less than or equal to 31 years);
- waste in which the main radionuclides have a long half life (higher than 31 years).

In terms of radioactive level the categories differentiate by the value of massic activity (A):

- Very low level waste (VLLW): with A $<$ 100 Bq/g;
- Low activity waste (LLW) : with A between 100 Bq/g and 1MBq/g;
- Intermediate activity (ILW): with A between 1 MBq/g and 1 GBq/g;
- High activity waste (HLW): for A $>$ 1 GBq/g.

The radionuclides commonly used in nuclear medicine fall in the first categories. Independently from the initial value, the activities generally drop in a short range of time (equivalent to a few half-lives). The management solutions adopted in France are summarized in the table at the Fig.3.2.

Radioactive waste can vary a lot in terms of physical and chemical forms. A specific storage and process is adopted for each category of waste. It includes activities of sorting, treatment, conditioning and storage.
In the phase of **sorting** the waste is separated according to the chemical properties, dimensions and the half-life of the composing radionuclides.
The **treatment** consists in transforming the initial form of waste in one better suited for long-term management. This is done for example through incineration, compaction, vitrification or melting the

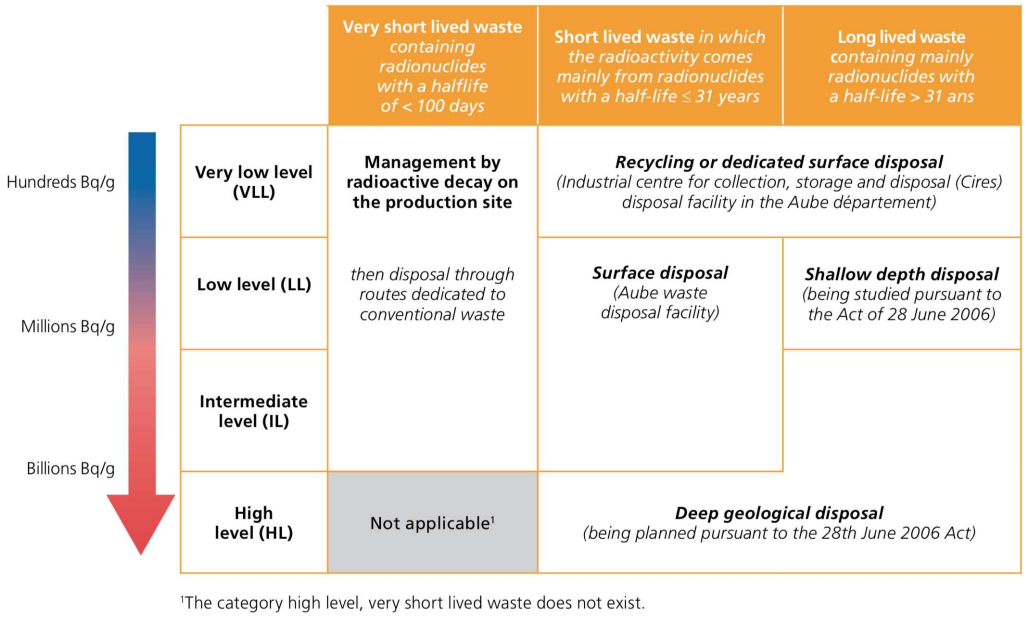

Figure 3.2: Classification of the waste associated with one or more management solutions in France [62].

materials. Due to the presence of hazards for the human health, the treated objects are also conditioned to guarantee the confinement of the radioactivity over the time. The **conditioning** consists in the incorporation of the waste in a material called "matrix". This mix is placed in suitable containers to shield the radioelements, generally done in concrete, ordinary steel or stainless steel.
The VLLW is generally stored in the place of production until their activity level reaches value not corresponding to hazards for the public and the environment. At that point they can be disposed as normal waste.
For the other types of waste, ANDRA define several ways of storages [62]:

- Surface storage: whose purpose is to isolate the radioactive products from the environment until reaching a negligible level. Two centers in France are dedicated to this: the CSM (Centre de stockage de la Manche) and the CSMFA (Aube) disposal facilities.
- Storage at mid depth: actually under study and for ILW with long half-life. Once prepared (compacted and solidified if liquid) these waste are put in packages, labelled and stacked in vaults dug out of the clay layer, a few metres below the surface. Once the vault is full, it is roofed over with a covering containing sand, a waterproof membrane and clay [62]. This is done for example at the Collection, Storage and Disposal Facility (Centre Industriel de Regroupement, d'Entreposage et de Stockage) in Cires.
- Deep geological disposal: for HLW, with high activities and long half lives. In 2006 the French Parliament opted for deep reversible disposal as the solution for the long-term management of HLW and ILW-LL radioactive wastes. The law made Andra responsible for studying the design and location on the border between the Meuse and Haute-Marne districts. Before the commissioning of the disposal facility, existing wastes are in dry storage in the buildings on the site where they are produced, mainly at La Hague, Marcoule and Cadarache.

The most restrictive waste present in facility producing radionuclides for medical purposes, like the ARRONAX Cyclotron, belongs to the category of the low activity level. They are suitable to be

sent to the center of Cires, in operation since the 2003.
The declaration to ANDRA and the evaluation of the low level activity waste shall include:

- the type of radionuclides and an evaluation of their activity;
- the declaration of the activity of the packages used for the shipment.

These information may be obtained using different methods:

1. Using of software simulating the process of activation of the materials;
2. Acquiring the gamma spectra on the whole objects;
3. Measuring the samples with other detection techniques (as gamma and alpha spectrometry or liquid scintillation);

The methods 2 and 3 may present some problematics. Among them the presence of radionuclides difficult to detect (i.e. I-129 or Th-232 that have low energy gamma emission) or pure beta emitters (like H-3, C-14, P-32, Ni-63, Tc-99), the choice of the samples that well characterize the waste, the costs of those activities and the needs to reduce to the minimum the dose to the personnel.
The method 1 is very useful to solve problems of detection and make forecasts on the activities of the waste. On the other side, for an optimal use it is necessary to know the exact composition of the material, the irradiation schedule and the cooling time as well as the radiation field. Those parameters may be difficult to identify for all the type of irradiated objects. It may happen for example in old facilities where do not exist a follow up of the installed elements or in case of manufactured parts for which no precise information of the chemical composition exists.

Recently a dialogue has been started in between ANDRA and the centers producing radioactive waste with intermediate and low activity. The objective is to share the expertise and experiences in the field of waste characterization in order to fulfill ANDRA needs with optimized resources and methodologies. Moreover a common method to use for the radionuclide identification shall be defined as well as a guide/procedure to follow for the declarations.

3.2 The basic principles of Activation

Induced radioactivity is a phenomenon present in all accelerators capable of producing particles above the reaction threshold of the activation process of interest. When the accelerated beam particle strikes a nucleus, the resultant nuclear reactions can create different nuclides that may or may not be radioactive [63].
Nuclear reactions are quantitatively characterized by their cross section, representing the probability that the nuclear reaction can happen under specific conditions. This quantity also depends on the projectile's type and energy.
If $\sigma_{T,P}$ is the known cross section of a particular reaction that converts the target nucleus T in the isotope P. The number of radioactive nuclei of the isotope P per gram of the target material produced per unit time is:

$$n_P = \Phi(E)\,\frac{N_0}{A_T}\sigma_{T,P}(E)$$

where:

- Φ(E) is the fluence rate of the projectile, defined as the number of particles striking a sample per unit surface and unit time;
- N_0 is the Avogadro's number (6.02 x 10^{23} atoms/mol);
- A_T is the mass number of the target material;

– $\sigma_{T,P}$(E) is the cross section integrated on the total spectra of fluence.

The previous formula is valid for $N_0\sigma/A \ll 1$ (for many situations the case, but not for all, for example: thermal neutrons impacting 1 g of He-3 or Li-6).
If the produced nuclide is radioactive, it will undergo a decay in time characterized by a mean-life (units of time), τ, and its reciprocal (units of inverse time), the decay constant λ.
Considering both the production rate n_P and the decay rate, the total number of nuclei produced is:

$$\frac{dN_P}{dt}(t) = n_P - \lambda_P N_P$$

If the irradiation time t_{irr} is known, it is possible to evaluate the number of total nuclei of an isotope P being present after t_{irr} from the following formula:

$$N_P(E, t_{irr}) = \Phi(E)\frac{N_0}{A_T}\sigma_{T,P}(E)\,(1 - exp[-\lambda_P t_{irr}])$$

For storage management of the target and radioprotection purposes the activated material is safely stored to let the activity decay.
It appears, then, necessary to determine the number of nuclei still in the sample after a certain cooling time t_{cool}.

$$N_P(E, t_{irr}, t_{cool}) = \Phi(E)\frac{N_0}{A_T}\sigma_{T,P}(E)\,[1 - exp(-\lambda_P t_{irr})]\,exp(-\lambda_P t_{cool}) \tag{3.1}$$

This particle dependent equation is known as activation formula. It allows to calculate the disintegration rate of a particular isotope P in one gram of the target material T when it is irradiated for a time t_{irr} and left to decay for a time t_{cool}. The fluence and the cross section depend on the energy and the type of the projectile. The activity of a radionuclide is given by the sum over the various particle types and the energy distributions of the projectiles. The specific activity of the target is given also by the sum of the specific activities of all the radionuclides produced.

In case of proton accelerators, if a proper shield is put in place against prompt radiation and a proper access control is designed to avoid direct beam-on exposure, the induced radioactivity will be the dominant source of occupational radiation exposure.

The concept of the Q-value, Qv, is useful to determine the energy threshold for a nuclear reaction. Qv is the energy released by the reaction and is defined in terms of the rest masses m_i of the particles participating in the nuclear reaction m1+m2 $\rightarrow$ m3+m4 as:

$$Qv = [(m_1 + m_2) - (m_3 + m_4)]c^2$$

A Qv>0 implies an exothermic reaction while endothermic reactions (Qv<0) are characterized by a threshold energy E_t related to the absolute value of Qv;

$$E_t = \frac{m_1 + m_2}{m_2}\,|Qv|$$

At intermediate energies (from a few MeV up to about 50 MeV) various types of nuclear reactions are involved. The particles entering the nucleus are capable of knocking out one or more nucleons, or even a part or fragment of the target nucleus.
In particular, when the projectile is a proton, it is possible to find reaction like (p,n), (p,np), (p,2n), (p,α) requiring increasing threshold energy and causing the expulsion of a neutron, a proton and neutron, two neutrons or an alpha particle.

At higher energies (> 100 MeV), the possible phenomena are more complex. The secondary particles produced (including nucleons struck) by the incident particle in the target atom obtain enough energy to travel through the nucleus and to hit other nucleons of the same atom.

There is not a common formula able to collect and summarize this set of phenomena, so predictions in the field of induced activity are complex and difficult.
The large variety of radionuclides can be produced bombarding a target with high energy particle beam. The isotopes produced from this interaction can have an atomic weight that goes up to the one of the target nucleus (or even higher in the case of a capture reaction). The probability of producing a particular isotope in a given target material, or the isotope production cross section, depends on the energy of the incident particle. The relative importance of a particular isotope, from the point of view of its contribution to the dose rate, depends on its half-life and on the radiation emitted during its decay.

During accelerator operations, radiation is produced when the beam interacts with targets, with the isotopes collection devices and other accelerator materials, like Faraday cups or collimators. Secondary radiation, as neutrons, protons and pions (for high energy), generates additional radiation that may also incude nuclear reactions and participate to the generation of wastes.
Neutrons dominate activation in low-energy domain. Since they have no charge they are not affected by the Coulomb barrier of nuclei, so they will not be repelled by the electrostatic charge of the target nucleus and can react at any energy, producing radioactive nuclides.
High-energy neutrons cause spallation reactions that can produce any nuclide lighter than the target nucleus. On the other side, thermal neutrons may cause significant induced radioactivity due to the high capture cross section of some materials for these energies.

3.3 The ARRONAX Cyclotron

ARRONAX is an acronym for Accelerateur pour la Recherche en Radiochimie et en Oncologie à Nantes Atlantique X (Accelerator for Research in Radiochemistry and Oncology in Nantes Atlantique) [64]. The letter X has been added to connect the name of a Jules Verne's character, the professeur Aronnax in the novel *Twenty thousand leagues under the seas*. This accelerator has been inaugurated in 2008 and fully operational since 2011.

This cyclotron accelerates both positive ions (H_2^+, He^{2+}) and negative ions (H^-, D^-) up to 70 MeV for protons and He2+. It has been designed to deliver up to 750 μA of protons (in case of dual beam mode) and 70 μA of alpha particles. The ARRONAX beam characteristics are summarised in the Tab.3.1.

Ion	**Extracted** particles	**Available energies** [MeV]	**Max Intensity** [μA]	**Dual beam**
H^-	proton	30 to 70	375	yes
HH^+	proton	17.5	50	no
D^-	deuteron	15 to 34	50	yes
He^{2+}	alpha	67.4	70	no

Table 3.1: Characteristics of ARRONAX beams.



Figure 3.3: IBA ARRONAX Cyclotron in the principal bunker.

The particle beams can be delivered in six experimental vaults (Fig.3.4).

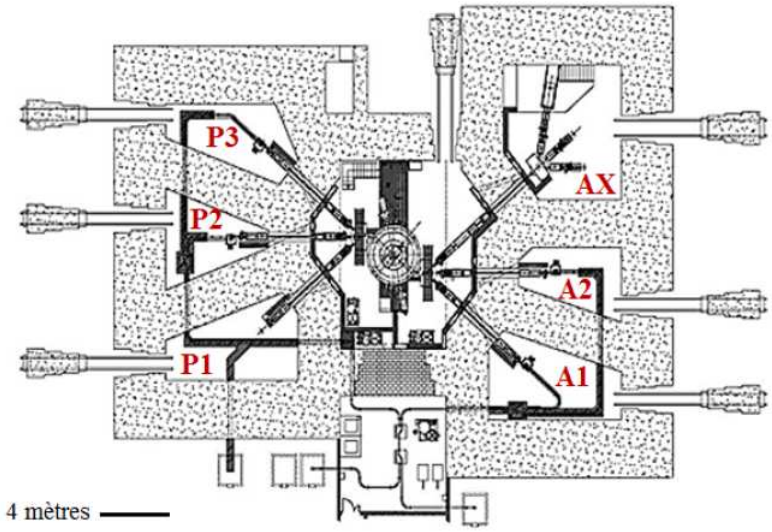

Figure 3.4: Beamlines scheme of the ARRONAX cyclotron and its bunkers.

Vaults A1, A2, P2 and P3 are devoted to radionuclide production. The beamlines are equipped with a target system that allow the perfect alignment with respect to the beam. A pneumatic transfer system connects the irradiation point directly to the hot cells. In this way after the irradiation, due to the high level of activities produced, the samples are transferred in remote without the human intervention in the bunker.
Vault P1 is used to perform research and development on high-intensity current beams and used to accomodate a neutronic activator (production of secondary neutrons from a proton beam interacting with a target).
The largest vault, AX, is devoted to experiments on radiolysis, radiobiology and physics and for high-grade student training. It is characterized by three beamlines called AX1, AX2 and AX3 for irradiation at low intensity.

3.4 The study of the materials' activation in the ARRONAX bunker

The ARRONAX facility produces different types of waste, both in solid and liquid form. Among them it is possible to find:

- Mechanic and activated pieces of the cyclotron substituted for maintenance and characterized by radionuclides with half-lives (h.l.) $>$ 100 days (like Na-22, Mn-54, Co-60). This is the case for example of collimators, rabbits, screws, vacuum pumps or connection tubes.
- The cooling water of the cyclotron, containing H-3, Be-7 and other impurities with h.l.$>$ 100 days.
- Radioactive liquids coming from the radiochemistry activities, as mix of resines and other waste solutions containing radionuclides with h.l. both lower and higher then 100 days (as Rb-83/84/86, Sr-82/85/83 and Ge-68 coming from the contaminants of the productions).
- Other type of waste is represented by single use objects as soiled papers, gloves, plastic seals, paper suits or masks that workers use to protect themselves or the lab tools.



Figure 3.5: Examples of waste from the ARRONAX facility: electrical components, metallic activated pieces, vacuum pumps cables, liquids.

All these activated pieces are stocked inside drums or placed on shelves in cooling rooms and separated depending on the waste category.
ANDRA is responsible for the collection and the treatment of the waste. It established a series of rules and limits on surface contamination, dose rates at contact and at 1m, for the packages to use for the shipment. Moreover a limit of activity per kg of material is defined. It varies depending on the size and the chemical form of the object.
For example, metallic objects with total mass (of the drum) lower than 30 kg, where the mass of each element is $<$ 1kg, belong to the class of "Compactable Solid" (in French Solide Compactable - SC). It can also contain cellulosic waste, rubber or polystyrene.
In this case the total massic activity shall be:

- $<$ 0,1 MBq/kg if the content has beta and/or gamma emitters with h.l. $<$ 31 years,
- while in case it contains only H-3 and C-14, the massic activity shall be $<$ 1 MBq/kg.

These limits are important for this study since the biggest majority of the ARRONAX's waste fall in the SC category.

The first step to take in the definition and the classification of the waste consists in the identification of the type of nuclides produced and their activity. To do so, it is important to define the field associated to all secondary particles in the bunker.
The scope of this study is to determine the particle fluence characterizing the radiation field in the ARRONAX bunker during the irradiation of a rubidium/gallium target with a 70 MeV proton beam. This corresponds to the main cause of activation (due to high intensity, high energy and long irradiation time). The knowledge of cross sections data will put the particle fluence in relation with the number of radioactive radionuclides produced (cifr. eq.3.1).

3.4.1 The irradiation device

The study described in the following sections concerns the bunker A1 (Fig.3.6) but it could be applied also to the other vaults in future (with specific geometrical modifications).
The system used for the irradiation is called "rabbit" or "navette" in French. The Fig.3.7 shows the station with the pneumatic system used to transfer the rabbit directly in the hot cells for the dismantling, the extraction and the purification of the samples.
The rabbit considered in this study contains a target used for the joint production of Sr-82 and Ge-68, both used for the manufacturing of generators (^{68}Ge/^{68}Ga, ^{82}Sr/^{82}Rb). To this end the rabbit accommodates a so-called dual target, composed of two layers of materials placed one after another in the beam direction and cooled with water.

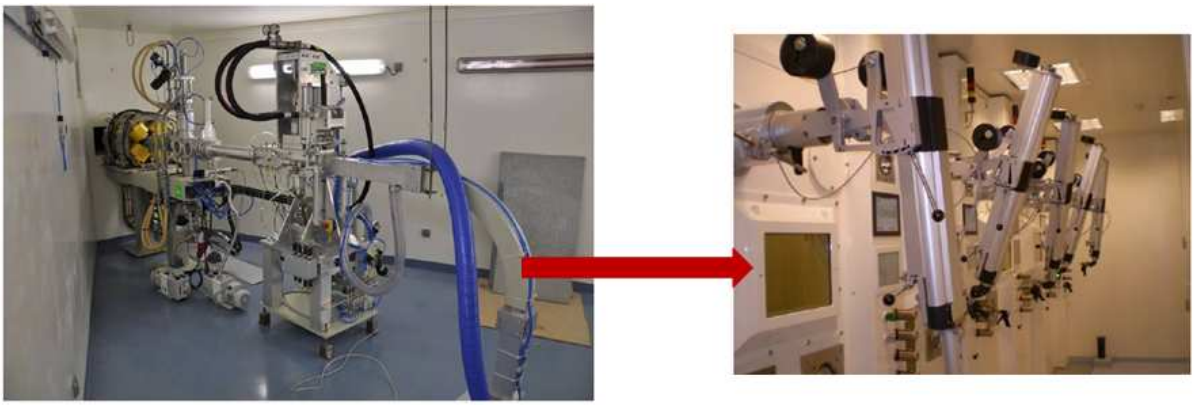

Figure 3.6: Photo of the Irradiation bunker A1 (left) and of the connected hot cells (right) for the target dismounting.

The rabbit can be considered as a box composed by several elements and materials. It has an aluminum body with parallelepiped shape and with two bases/end protections in PEEK. The sample to irradiate is placed inside the protection in aluminum, where holes for the cooling water flow are made.
The target, whose position in the rabbit is shown in the Fig.3.7, is itself a stack of different layers that it is possible to schematize as in Fig.3.8.
The first layer is made in aluminium and corresponds to the external surface of the rabbit, the beam window. It allows the separation between the vacuum in the beamline and the water circuit used to cool down targets and other elements around them during the irradiation. The rubidium target is placed inside a stainless steel container. The nickel/Gallium target is placed on a Ni support and and encapsulated in a niobium container to limit the impact in case the target melts. The niobium,

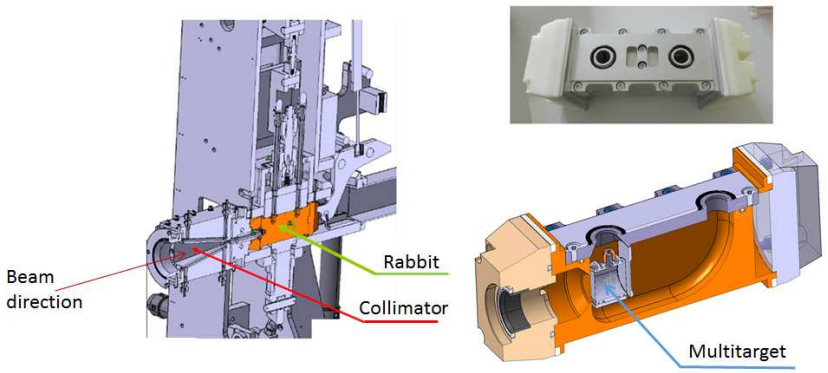

Figure 3.7: On the left side a cross section of the irradiation system. The rabbit is the element in orange. A photo and the internal details of the rabbit are reported on the right side of the picture.

indeed, has an high melting temperature (2477 °C) and it is chemically resistant to liquid Ga. Another aluminium layer is used behind the targets to guide the cooling water and get an appropriate cooling of both targets.
The information on the materials composing the different layers and their thickness are listed in the Tab.3.2.

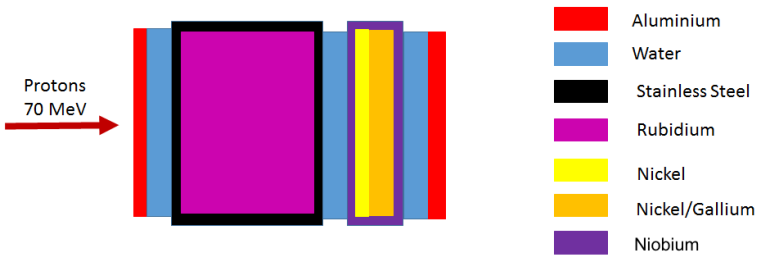

Figure 3.8: Scheme of the target placed inside the rabbit. The layers shall be considered in order of the beam direction. The total dimension of the target is about 4.6 cm.

3.4.2 The software ActiWiz

In order to provide a tool to select materials for particle accelerators and define the radiological hazards, the software ActiWiz has been recently developed at CERN [65] (Fig.3.11).
It allows the simulation in several irradiation scenarios of the radionuclides inventory it is possible to find for material exposed to particles fluence.
The code is based on a large number of FLUKA [30] simulations of the radionuclides inventory coming from the activation of basic chemical elements (n.82 and few radionuclides) or compounds. The JEFF 3.1 cross section library for neutrons below 20 MeV. The method of calculation consist in a double step process.

- The **first step** consisted in the simulation of the particle fluence spectra (neutrons, protons and charged pions) at selected locations in the accelerator and for different energies of the primary proton beam. The irradiation conditions are the one typical of the high-energy proton accelerators of CERN [66]: the Large Hadron Collider (LHC - with protons of 7 TeV), the Super Proton Synchrotron (SPS - with 400 GeV/c) , the Proton Synchrotron (PS - with 14 GeV/c),

Material	Density [g/cm^3]	Composition	Thickness [mm]
Rubidium	1.475	natural	20
Nickel	8.9	natural	0.05
Niobium	8.57	natural	0.1
Ni/Ga	7.1		0.8
Stainless steel 316L	8		0.1
Aluminium	2.7		0.8 (I layer) 1 (II layer)
Water	1		1.7 (I layer) 10.05 (II layer) 5.8 (III layer)

Table 3.2: Characteristics of the target materials.

the Booster (with 1.4 GeV), and the Linear Accelerator 4 (Linac4 - with 160 MeV).
In order to properly characterize the activation level, the irradiation scenarios shall take into account different locations of the materials in the radiation environment. For this purpose the accelerator is reproduced on FLUKA as a tunnel, having the shape of an hollow cylinder, with wall made of concrete (2 m thickness) and iron, representing the magnets (Fig.3.9). The dimensions of this last element may vary depending on the characteristics of the accelerator; for example for the LHC it is a bulky cylinder of 30 cm of radius. An iron cylinder simulates a target at the center of the tunnel structure. Alternatively to the beam impact on bulky objects, a beam on target situation can be chosen as the radiation field production center.
The fluence has been simulated for seven predefined locations scenarios (Fig.3.10).

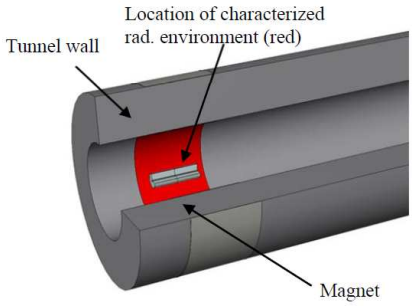

Figure 3.9: Geometry implemented in FLUKA to simplify the accelerator structure.

- In a **second step** the fluence spectra was used as input of other FLUKA simulations to determine the nuclide production inventory. this has been done exposing a thin disk to the radiation environments mentioned above.
  The subsequent convolution of the results with legal limits and activity-to-dose conversion factors made possible to assess and quantify the hazard, for example in terms of operational radiation protection quantities like the ambient equivalent dose rate (H*(10), H*(0.07)).

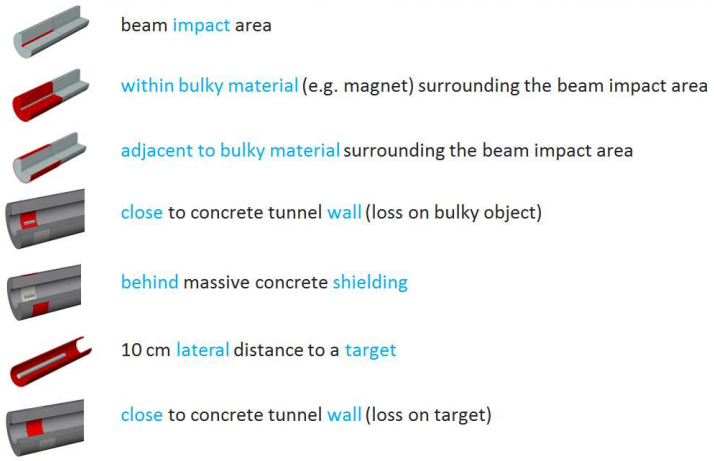

Figure 3.10: Schematic representation of the seven possible scenarios of irradiation implemented in ActiWiz [66].

The users can define the irradiation time and conditions (beam energy and intensity) and an eventual cooling period. The material composition can be user-defined chosing among the 85 differet constituents (82 elements 3 isotopes) to build specific materials.
If complex, the irradiation-cooling pattern may be defined in an external file.
ActiWiz also gives in output the list of the nuclides produced with the relative massic activities at the specified time. Another useful tool implemented in ActiWiz is the shielding module. It allows the calculation of the shielding thickness to implement to obtain a defined relative attenuation for several materials (concrete, iron, lead, tungsten, aluminium, tin, uranium and water).

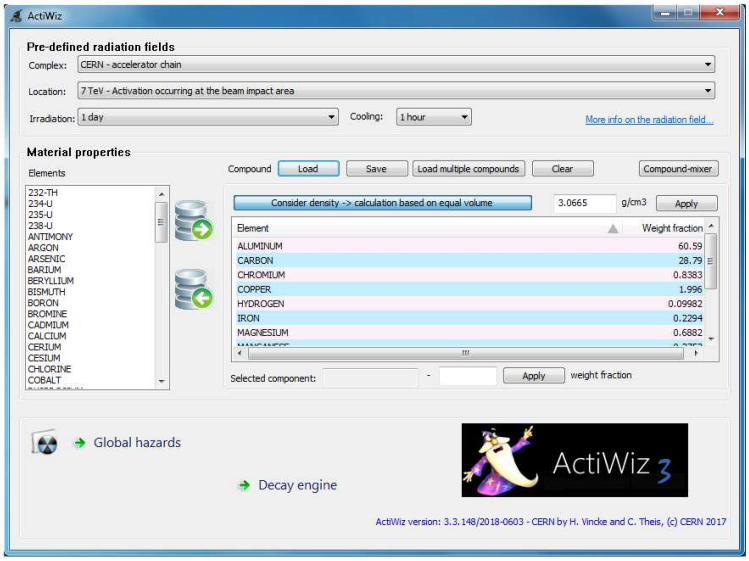

Figure 3.11: Screenshot of the Actiwiz operative windows. TOP: Definition of the radiation field (the accelerator and the position of the material to study) and the irradiation conditions (irradiation time and cooling). CENTER: Specification of the material's composition or load customized materials. BOTTOM: Calculation of hazard, radioprotection quantities and nuclide inventory [66].

3.4.3 The fluence simulation with MCNPX

The software Actiwiz is equipped with predefined irradiation fields typical of the big CERN accelerators. The energies, particles and the geometrical structures are, then, very far from the values and the irradiation conditions it is possible to find in the ARRONAX bunkers.
For this reason the authors of the software agreed to add new scenarios of irradiation to reproduce the situations in ARRONAX.
To associate an hazard and to evaluate the species created during the irradiation and their activities after a period of cooling, it is necessary as first step to evaluate the fluence values for the secondary particles particles in different locations of the bunker where equipment is commonly installed.

3.4.3.1 Particle field calculation

The software MCNPX 5.0 [31] has been used for this purpose. This Monte Carlo N-Particle (MCNP) radiation transport code is well suited for the simulation of different types of particle and their interactions with matter in a broad range of energies.
In order to increase the statistic and reduce the variance of the simulated quantities it has been decided to use some expedients in the geometry reproduction to ameliorate the simulation's performance.
The principle is shown in Fig.3.12:

- Two detectors with the same dimensions and characteristics are placed at two different distances from the target (left side of the picture). The fluence of the particles they will detect depends on the solid angle that the opening cone will intercept at that place (the hypothesis is that the matter around and the detector itself have no effect on the particles behavior).
- The behavior of the two detectors at a fixed distance d can be simulated varying the opening of the visual cones.
  The geometry reproduced with MCNPX is schematized in the Fig.3.12 (right side of the picture).

A tally F4 is used to evaluate the fluence in the cell defined as the intersection of the cones with opening angles θ_i (i=1-7) and the spheres S1 and S2. The distance between the spheres is set to 1 mm.
The behavior of three types of particles has been simulated: neutrons, protons and photons. At our beam energy they are the only significantly contributing to the matter activation.

Using the described method, avoids the modelization of the real dimensions of the room. All the elements composing the beamline (sustainment structure, Faraday cups, transport tube, etc,) are not included in the simulations as most of the beam is stopped in the target.

Seven different positions have been chosen in the bunker A1: considering the origin of the axis coincident with the mean point of the target structure, four detector have been placed in the forward direction (x positive direction), two in the backward direction and one on the lateral side of the target (Fig.3.13). With the chosen method, different distances correspond to different solid angles.
The position of the detection points have been chosen in correspondence of devices on the beamline or structural elements of the bunker in which activation shall be studied:

- The detector d1 placed at 10 cm from the impact point is used to reproduce the activation of the materials in close proximity to the target. This include for example the rabbit system and the collimators.

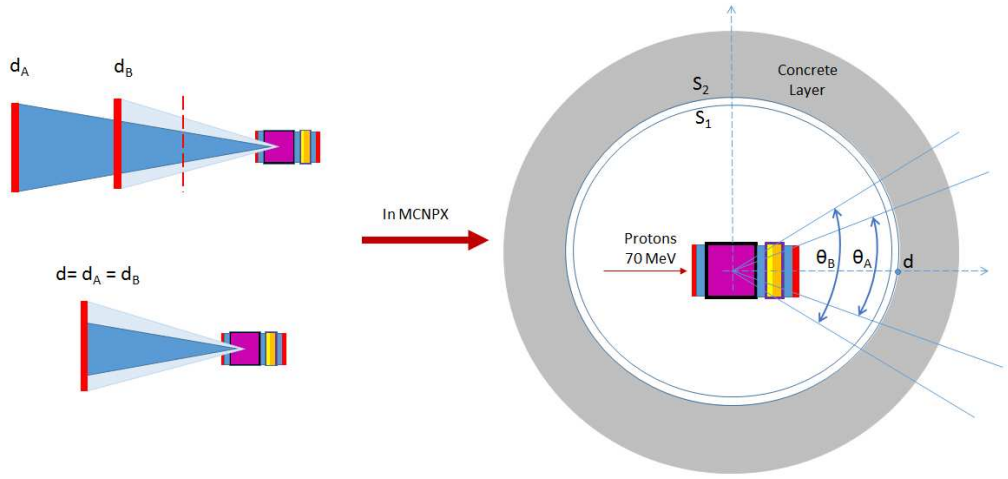

Figure 3.12: The principle (left) and the scheme (right) of the geometry reproduced with MCNPX (drawing not to scale).

- The detectors d4, d5 and d7 are placed close to the walls respectively in the forward, lateral and backward direction with respect to the proton beam direction. They can be used to reproduce the effect of the particle fluence on objects like neon lights, panels or metallic grids connected to the walls.
- The detector d6 is placed at 80 cm from the target and it corresponds to the region in which beam monitoring devices (as Faraday's cup) are installed. Finally the detectors d3 and d4 are placed in the area of the pneumatic transfer system.

A proton beam of 70 MeV impact the target structure (same than the one reported in Fig.3.8) used to simulate the irradiation during a production run.

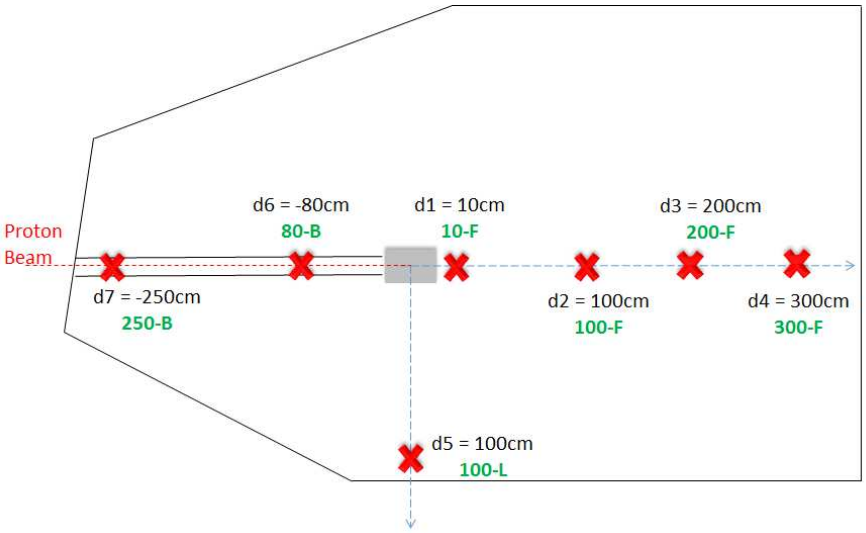

Figure 3.13: Scheme of the chosen positions of the fluence detectors. The names in green are the ones used to identify the detectors in the following graphs.

A layer of concrete (50 cm thickness), simulating the walls of the bunker, is placed around the

detector. More details on the effect of the concrete on the particle's fluence will be discussed later in the Par.3.4.3.3.
The results of the MCNPX simulations are reported below for three types of particles: protons, neutrons and gamma.

Protons:
Only the detector placed at 10 cm from the target (d1) will measure a high proton fluence. The energy of the particles coming out the target are lower than the initial 70 MeV due to the interaction of the projectiles with the target materials. The detector placed on the lateral side (at 1m distance) receives some protons with a maximum energy of 45 MeV.

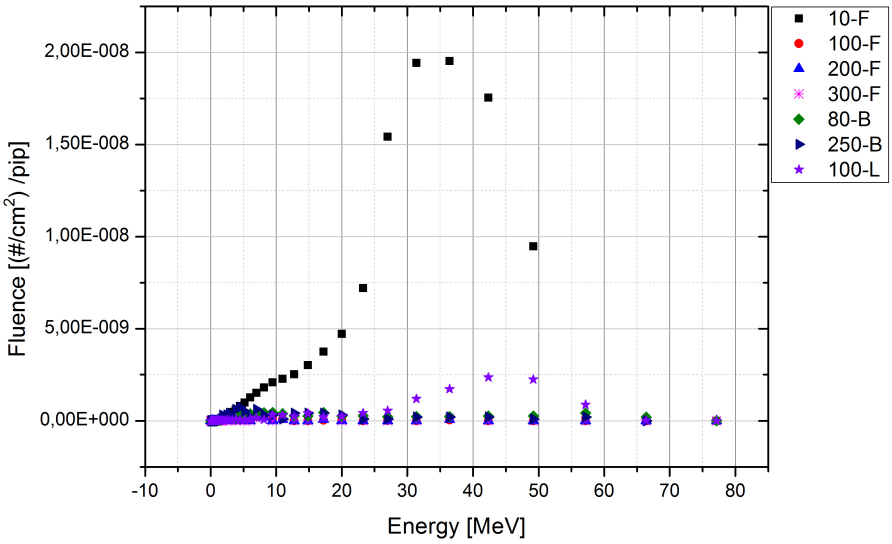

Figure 3.14: Results of the MCNPX simulation of the protons fluence at different positions in the A1 bunker .

Neutrons:
The results of the MCNPX simulations for the neutron fluence is shown in Fig.3.15 for the seven chosen detectors.

It reproduces the typical energy spectrum of a nuclear reaction with incident energy of several tens of MeV (Fig.3.16). Indeed it is possible to observe and divide the graph in three zones.

1. The **Compound process** involves long reaction time ($\sim 10^{-18}$ s) and are predominant at low energies (below 10MeV) and/or when the energy of the system decreases after the secondary particles emissions. In this phase the incident particle is captured by the target nucleus to form a compound nucleus. Subsequently, the incident energy is shared among the other nucleons and only after a certain time of thermalization of energy, the nucleons can escape the target. The excited nucleus can emit secondary particles by evaporation or break-up.
   Apart from the conservation of the total energy and the total momentum, the outgoing and the incident channel are completely uncorrelated (effect sometimes called Bohr's amnesia hypothesis). It results in an isotropic angular and energetic distribution: independently from the position of the fluence detector for low energy. This effect is evident from the Fig.3.15.
2. The **Direct process** is characterized by high energies and short reaction times ($\sim 10^{-22}$ s) since they are generally carried out in one step. The projectile's energy allows the excitation of the

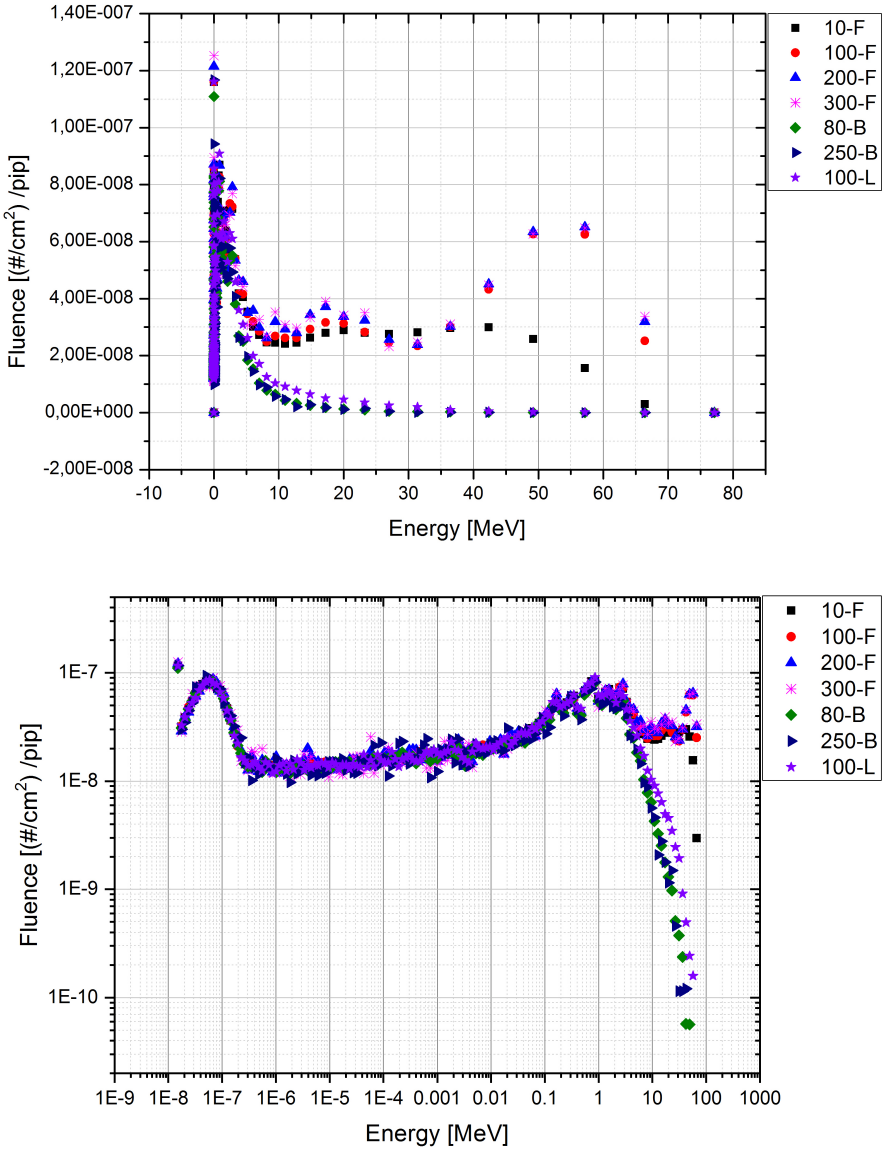

Figure 3.15: Results of the MCNPX simulation of the neutrons fluence at different positions in the A1 bunker (top: liner scale, bottom: log-log scale).

first discrete states close to the fundamental level through precise mechanisms of interaction, like inelastic diffusion, knock-out, charge changing reactions, pick-up, etc..
Here there is a strong correlation between the initial and the final channel of the reaction: the secondary particles in this case are emitted with a direction that is close to the one of the projectile.
This reflects also in the situation analyzed in this study. As it is possible to observe from the Fig.3.15, for high energies the fluence of the neutrons is higher for the detectors placed in the forward direction.

3. As intermediate stage between the aforementioned two extremes, it exists a reaction type zone that embodies both direct- and compound-like features, called **Pre-equilibrium**. These reactions are characterized by a multistep process. They correspond to the emission of the particles after the first stage of the reaction but long before statistical equilibrium of the compound nucleus is

reached. In this range of time the nucleus undergoes to intermediate states and gradually loses the memory of the initial projectile and direction. The secondary particles emitted are shared on the energy spectra and retain a certain onward components. For this reason the detector placed in the negative direction of the x axis observe a neutron fluence lower than the detector set forward.

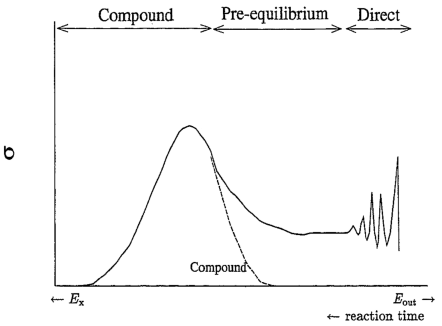

Figure 3.16: Typical cross section as a function of energy for a reaction A(a,b)B with incident energy in the order of tens of MeV.

Photons:
The results of the simulated fluence for the gamma particles are shown in Fig.3.17.

Contrary to the two previous cases, the interaction of the protons with the target give rise to an isotropic gamma emission. Those particles are consequences of the radioactive decay of the nuclides created during the interaction with the target materials and also excited states.
As it is possible to observe from the graph, the photons have energies lower than 10 MeV. The phenomena that it is possible to find in this range are mainly photoelectric effect, Compton effect and pair production (above 1.02 MeV). They determine secondary gamma or electron emission with scattering angles and energies depending on the characteristics of the incident particles.

3.4.3.2 Directional emission during irradiation: the different behavior of the particles

In the phase of the fluence model validation, an MCNPX simulation has been used to study the main direction of the particles (n, p, and γ) emitted during an irradiation of a rubidium/gallium target with 70 MeV proton beam. They have been also useful to validate the choice of the detectors positions and the results presented before.
For this study the geometry reproduced in MCNPX is presented in Fig.3.18. A series of F4 fluence tallies have been placed in the blue highlighted spherical areas around the target. Their center placed on a straight line through the origin and forming different angles with respect to the x-axis. These detectors are also placed at the same distances from the center of the target.

The results of the simulations are shown in the Fig.3.19, Fig.3.20, Fig.3.21.

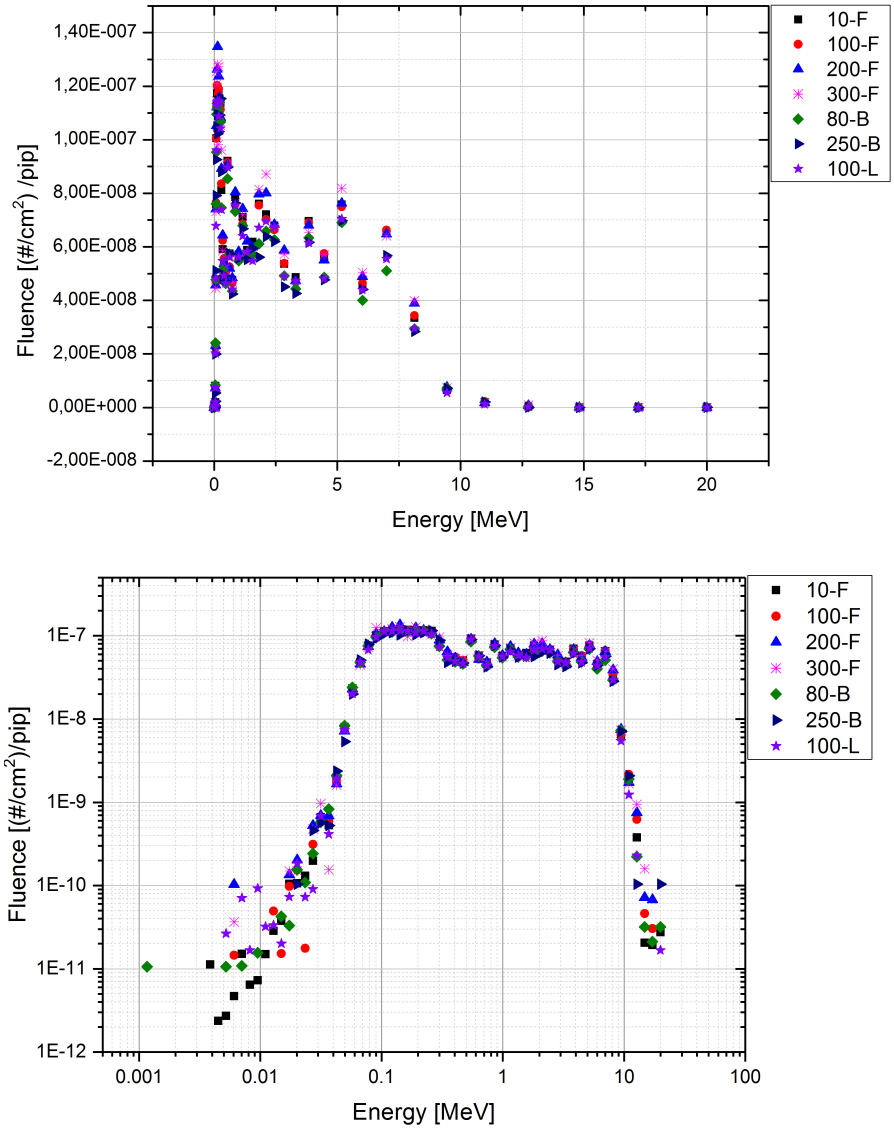

Figure 3.17: Results of the MCNPX simulation of the photons fluence at different positions in the A1 bunker (top: liner scale, bottom: log-log scale).

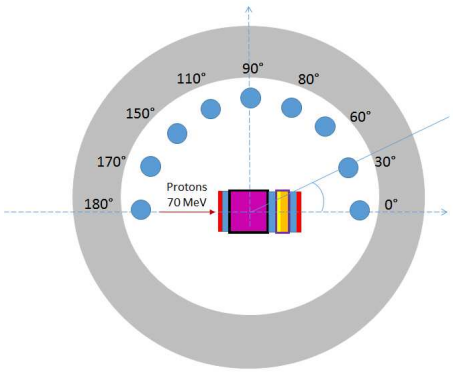

Figure 3.18: Scheme of the geometry used in MCNPX for the directional study of the emitted particles.

Neutrons:

The curves presents the same behavior as the one seen in the Fig.3.15.

Low energy range the neutrons (< 10 MeV) have no preferential direction of emission. The isotropic angular and energetic distribution is a consequence of the compound reaction process.

In the range of the intermediate energies (10 MeV< E< 30 MeV) it can be observed a decrease of the fluence values with the increase of the angles. High energy neutrons (> 30 MeV) are mostly emitted in the forward direction (0-10 degrees), or mostly in the same direction of the primary proton beam, with maximum around 50 MeV. It is a consequence of direct processes discussed above.

For angles higher than 90° the fluence of neutrons reaches the minimum values.

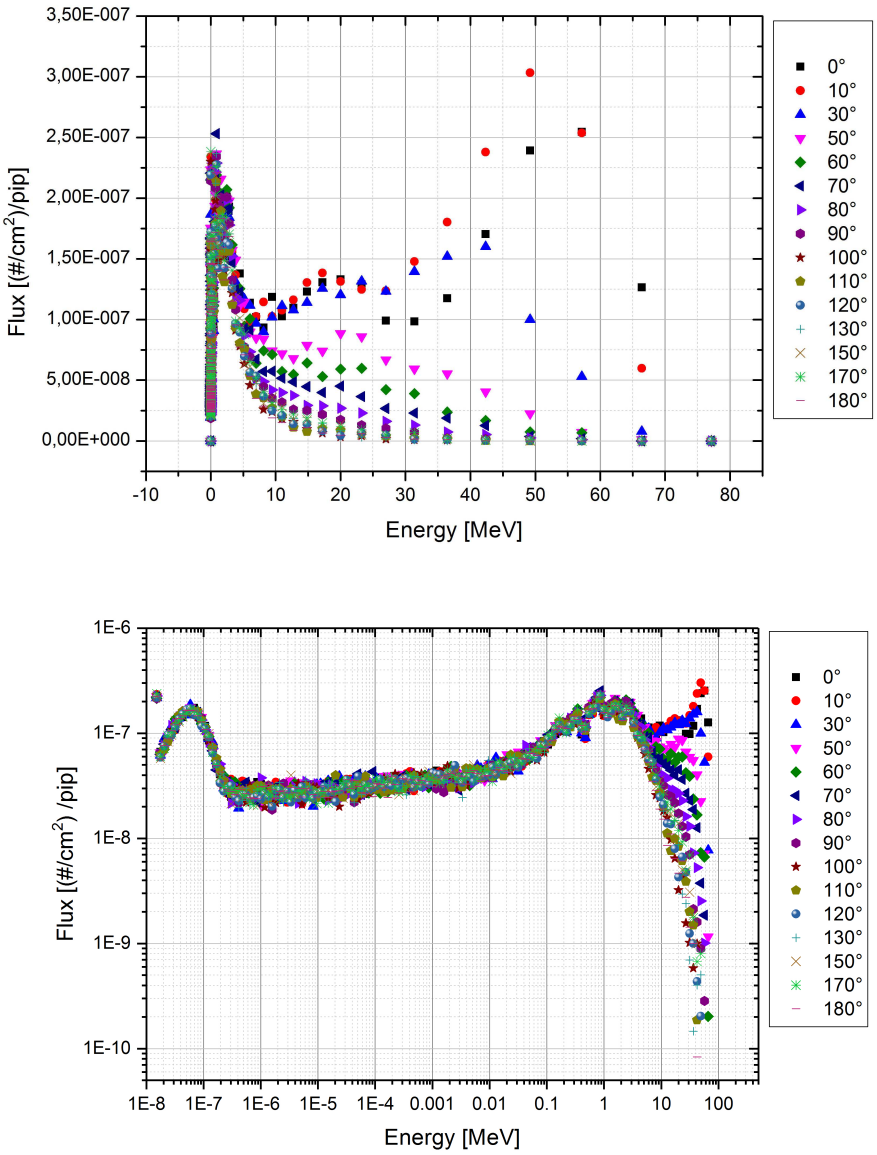

Figure 3.19: Results of the MCNPX simulation for neutrons (top: liner scale, bottom: log-log scale).

Protons:

Protons are mostly emitted in the forward direction. The highest fluence is observed for the detector placed at an angle of 30°, revealing a scattering effect due to the interaction with the target materials. The maximum value of fluence is obtained for the energy range from 35 to 40 MeV. There is also a

non-zero component of the fluence in case of detectors placed in between 60° and 90°. This is the reason why it is possible to observe (Fig.3.14) a non-zero fluence component for the detector placed on the lateral side of the target.

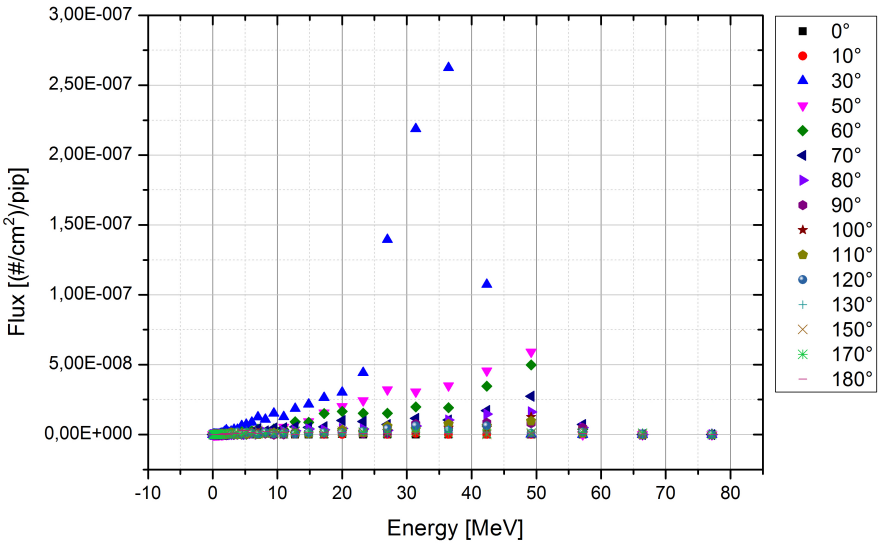

Figure 3.20: Results of the MCNPX simulation for protons.

Photons:
These type of particles are the results of the decays of radioactive nuclei as excited states produced in the interaction of the proton beam with the materials composing the target. Their emission has not a preferential direction. The consequence of this isotropic behavior is that the detectors placed around the target will observe a similar fluence at different angles (Fig.3.21).

3.4.3.3 Effect of concrete

In the preparation of the model used for the fluence calculation with MCNPX, a layer of 50 cm of concrete has been considered. In this paragraph the reason of this choice is explained.
The ARRONAX irradiation bunkers are separated by thick concrete walls (2 m in between bunkers and 3,8 m to separate them from the corridors), used to shield the radiations coming from the irradiation processes during operations.
If on one hand the presence of these walls aims to protect the users limiting the external dose rate, inside the bunker scattering phenomenae will slow down neutrons and change the fluence distribution as a function of the particle energy.
The biggest consequence of this effect is the increase of the level of activation for the tools and devices in the irradiation bunker.
This study has the scope to understand if it is possible to reduce the concrete thickness used on the previous model (for the fluence calculation) to reduce the simulation time while taking into account all possible effects on the neutron spectra. A simple MCNPX analysis has been carried out using two parallel simulations: one without the concrete (substituted by air) and one with a variable thickness of concrete.
The concrete composition used here is coming from the CEA compendium of materials [41].
An isotropic source of 70 MeV neutron is placed in the origin of the axis. This energy has been chosen to be conservative since a larger interaction length is expected as compared to lower energy neutrons. It is surrounded by a spherical crown (r=350 cm) of variable thickness and composed of concrete.

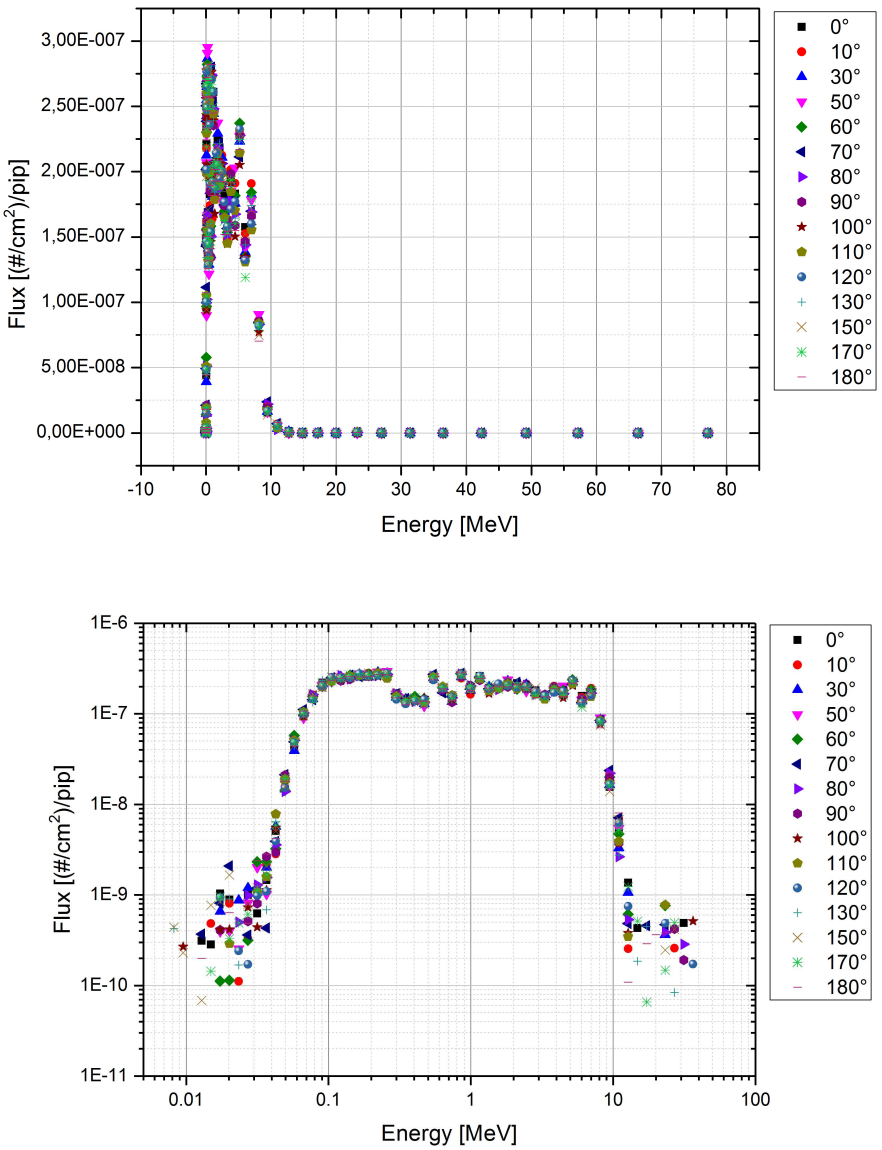

Figure 3.21: Results of the MCNPX simulation for gamma (top: liner scale, bottom: log-log scale).

The neutron fluence is checked at two different distances from the source (origin): d_1= 80 cm and d_2= 250 cm.

From the obtained simulations it is possible to make several observations (Fig.3.23 and Fig.3.24):

1. The dataset obtained without the concrete layer occupies a range of values that is about two orders of magnitudes lower than the range encountered in the cases with the concrete layer. The absence of data at low energies is due to the absence of the scattering phenomena due to the wall. Concrete is then a necessary element to introduce in the simulation to encounter real situation.
2. When the concrete thickness increase, more and more neutrons are created (the integral of the curve is higher) and low energy neutrons appear.
3. Above 12.5 cm, which is close to the expected value of the mean free path of 70 MeV neutrons in concrete, the neutron spectra evolve slightly. For a thickness higher then 50 cm there is no effect on the neutron flux.
4. Varying the distance from the wall the effect at the point 2 is less evident since the flux of

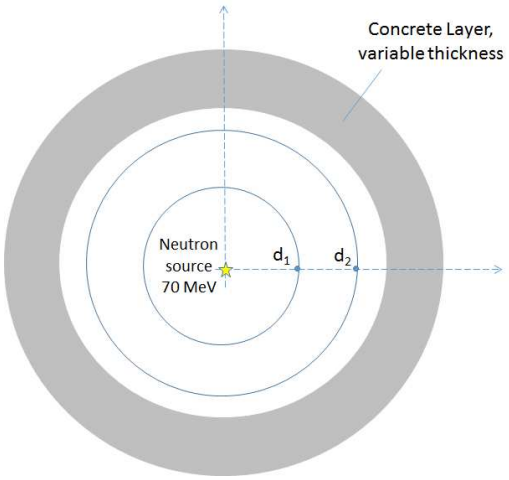

Figure 3.22: Scheme of the geometry used for the MCNPX simulations of the effect of concrete thickness.

particles with lower energy is higher close to the scattering zone than in the middle of the room.

It is possible to conclude that the use of 50 cm thickness for the concrete wall is sufficient to well describe the effect of scattering inside the bunker.

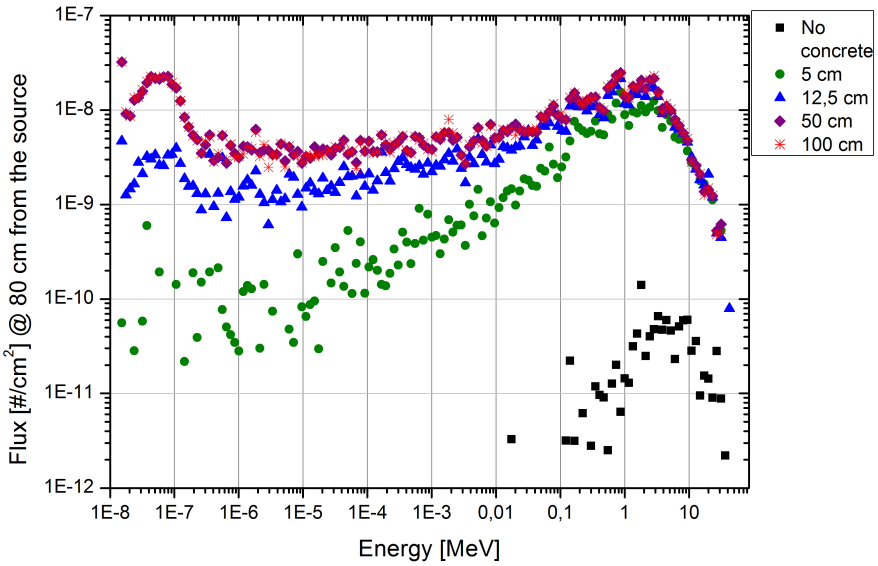

Figure 3.23: Results of the MCNPX simulation for a detector placed in the room, at 80 cm from the source.

3.5 Examples of application

The simulated fluence for the seven chosen positions in the irradiation bunker have been used to define new scenarios in the software ActiWiz.
In order to benchmark and test the simulated activities and dose rate with some of these new conditions,

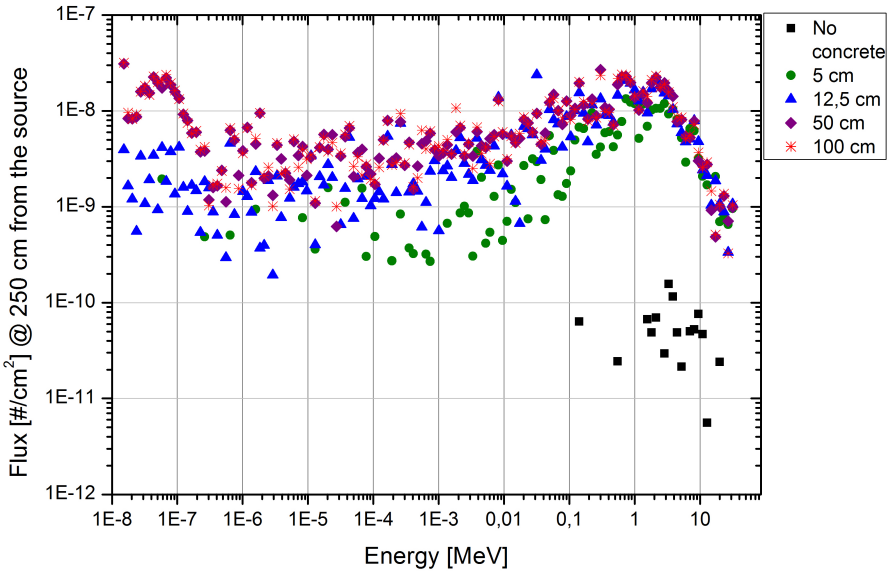

Figure 3.24: Results of the MCNPX simulation for a detector placed close to the wall, at 250 cm from the source.

it has been decided to study the activation of three samples that have been installed on the beamline of the A1 bunker:

1. A rabbit used for a Rb/Ga production;
2. A bunch of vacuum connectors;
3. Piston rod cylinders.

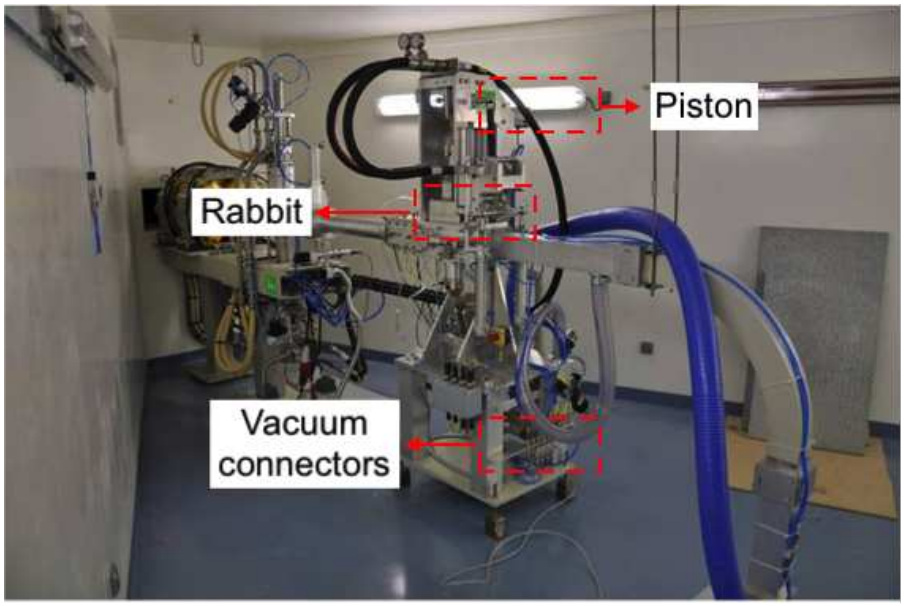

Figure 3.25: Position of the analyzed objects.

The data acquired experimentally are:

1. The **ambient equivalent dose rate H*(10)** at different distances form the objects.
   This quantity has been measured with four different detectors. They are generally used in

ARRONAX for radiological control and in particular to measure photon radiation (gamma and X-ray). The main characteristics are reported in the Tab.3.3.

Commercial name	Measuring range	Detectable energy range
MiniTrace γ	0,5μSv/h -10 mSv/h	45 keV - 3 MeV
6150 AD5	0,1μSv/h -10 mSv/h	45 keV - 3 MeV
Teletector 6150 AD5	2μSv/h -10 mSv/h	45 keV - 3 MeV
Sonde LB 1236-H10	50 nSv/h -10 mSv/h	30 keV- 1,3 MeV

Table 3.3: Characteristics of the gamma dose rate measurement tools.

2. The **gamma spectrum** of the source.
   The spectra have been obtained with the Micro-Detective HX (ORTEC), a Germanium detector cooled at low temperature using an electric cooling system. The detector has been energy calibrated with a Ce-137 source of known activity and corrected for the ambient noise.
   To note:
   - The information it is possible to deduce from the spectra are only qualitative, i.e. the ratio of the radionuclides contribution and not the specific activities.
   - The annihilation peak at 511 keV is in common to all the positron emitters and cannot be used to identify a radionuclide.

The measured ambient dose rate and the gamma spectra detected are compared with the results given by the software ActiWiz. The main parameters determining the radionuclides production, and at the same time the inputs of the software, are the following:

1. The **irradiation condition:** the duration of the irradiation, the period of cooling and the beam current (in particle/s);
2. The **position of the element with respect to the beam impact area**: given by the choice of one of the new seven locations;
3. The **chemical composition of the activated elements**: if an object is composed by more than one piece, several calculations are necessary and the results are given by the sum of the single contributions.

The item 1 is well defined for the rabbits, for which it is possible to retrieve the time of start and stop of the irradiation and the value of the beam current. Moreover it is an object used for only one production cycle. For the other elements of the beamline it can be sometimes difficult to reconstruct these information since they are present on the beamline for more than one irradiation cycle. In this case some hypothesis must be done to reproduce this situation.
The position of the objects under study, the item 2, may be different from the ones identified by the new seven detectors. The hypothesis done is that the scenarios are used to identify real zones of the bunker and not single points of the radiation fields.
The item 3 may strongly vary the results. Detailed informations are sometimes not accessible on the producer's data sheets and hypothesis are necessary also for this parameter.

ActiWiz is used to simulate the ambient equivalent dose rate H*(10) at 1 meter of distance from the source and the H*(0,07) at 10 cm.
The second value takes into account also the dose rate coming from beta particles. Since the instruments

used for the measures detect only gamma radiation, the comparison of experimental and simulated dose rate is possible only using the first value.

3.5.1 The analysis of the rabbit

As explained in the previous sections, the rabbit used in ARRONAX for the target irradiation is a system composed by two main elements: a body in aluminium and two bases in PEEK. The aluminum plates are connected through steel screws and plastic joints are used for the tight connection of the rabbit to the water cooling system.
The Tab.3.4 summarizes the properties of the different materials composing the rabbit.

Material	**Density** [g/cm^3]	**Composition** [%]	**Mass** [g]	**Volume** [cm^3]
Aluminium 2024	2.77	Al: 92.2 Cr: 0.1 Cu: 4.35 Fe: 0.5 Mg: 1.5 Mn: 0.6 Si: 0.5 Zn: 0.25	1142.7	322.2
PEEK	1.31	C: 78.25 H: 4.38 O: 17.37	718.6	544.4
Steel	8	C: 5 Cr: 0.5 Cu:1 Fe: 91 Mo: 0,5 Ni: 2	345.9	43.8
EPDM	1.22	C: 86.67 H: 13.33	42.6	35

Table 3.4: Characteristics of the rabbit materials ([67] [68] [69]). For the screws, general information from the manufacturer have been used. The details on the volumes have been retrieved from the 3D CAD files.

The particular rabbit analyzed in this study has been irradiated for about 2,5 days and kept in a shielded area for cooling, after the removal of the target, for about 2 years. The summary of the irradiation parameters are reported in the Tab.3.5.

The activation of the rabbit is not homogenous. The beam window, the thin layer of aluminum that separates the target from the vacuum of the beamline, corresponds to the most active region. Indeed it is the first element interacting with the proton beam.

Total irradiation time	2d 10h
Beam intensity	8.81E+14 pps (141 μA)
Cooling period	2y 2m 9d

Table 3.5: Irradiation and cooling parameters for the rabbit.

For this reason, two set of dose rate measurements have been taken (Fig3.26): one with the window facing the detectors (Set 1) and another set with the window placed in the opposite direction (Set 2). The distance from the detector has been varied and measured from the external face of the PEEK base facing the instruments.

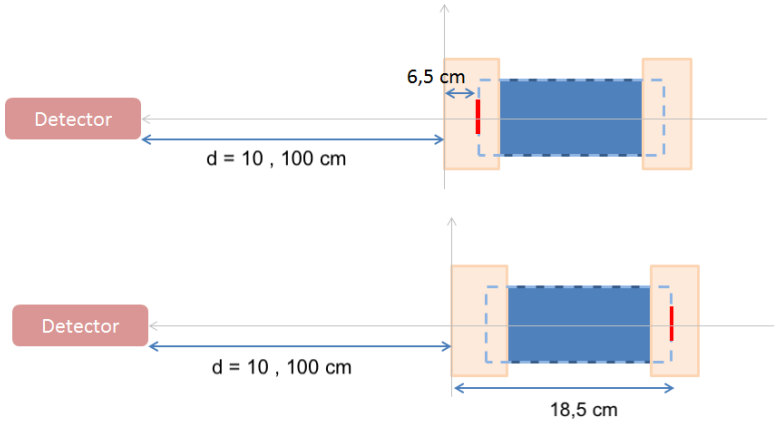

Figure 3.26: Scheme of the two set up used for the ambient equivalent dose rate measurements. The position of the beam window is in red.

In the Tab.3.6 are listed the results of the two sets of measures.

	H*(10) at 10 cm	**H*(10) at 1m**
	[μSv/h]	
Set 1	1.14E+03	3.52E+02
Set 2	2.32E+02	1.81E+02

Table 3.6: Ambient dose rate measured at two distances from the rabbit and for two set up. Each value corresponds to the mean of the five measurements done with different detectors. The error on the single measures is 0.01 μSv/h.

Using the information on the materials and the parameters of irradiation specified before, the software ActiWiz has been used to simulate the ambient equivalent dose rate at 1m of distance from the rabbit (H*(10)) and the one at 10 cm (H*(0.07)).

The scenario chosen for the ActiWiz simulations is the one defined by the detector placed at 10 cm from the impact point (10-F), the closest among the seven new points (Fig.3.13). A simulation has

been done for each material composing the rabbit and then the results have been summed fo obtain the dose rate of the entire object. The results are listed in the Tab.3.7.

Material	**H*(10)** [μSv/h]	Rel error [%]	**H*(0.07)** [μSv/h]	Rel error [%]
Aluminium 2024	2.28E-02	2.10E-01	1.26E+02	1.60E-01
PEEK	4.41E-07	2.40E-01	3.78E-02	1.60E-01
Steel	1.53E-03	1.20E-01	1.60E+01	1.10E-01
EPDM	2.80E-08	2.50E-01	2.22E-03	1.70E-01
Sum	**2.44E-02**	2.45E-01	**1.28E+02**	1.70E-01

Table 3.7: Results of the ActiWiz simulations on the different elements of the rabbit.

The biggest contribution to the dose rate is coming from the activation of the aluminum body, representing almost the 99% of the total dose rate.
With the software ActiWiz it has been also possible to obtain the inventory of all the species produced and present in the object after the defined cooling period. The Tab.3.8 lists the radionuclides that mostly contribute to the dose rate for the aluminum body.

Material	**Radionuclide**	**Contribution to H*(10) at 1m [%]**
Aluminium 2024	Na-22	90
	Mn-54	5
	Zn-65	3
	Co-60	2

Table 3.8: ActiWiz simulations of the inventory produced on the Al body of the rabbit.

The top contributors is the Na-22 (90 %), due to his long half-life (2.6 y) and high energy emitted gamma rays (511.0 keV -180.76% and 1.27 MeV - 99.940 %).
The results coming from the Actiwiz simulations are lower than the measured dose rate values. The reason of this underestimation is the following:

- The scenario linked to the detector 1 (10-F) placed at 10 cm from the target reproduces only the activation hazard due to the secondary particles emitted from the Rb/Ga target. The direct interaction of the beam with the aluminum window is not taken into account.

In order to evaluate the dose rate coming from the beam window activation, a separate calculation has been done with the Radionuclide Yields Calculator (RYC) [70], a software has been elaborated in Nantes by M. Sitarz as part of his PhD.
It is a free tool able to evaluate the yield of a reaction and the activity at the end of beam (EOB) of the radionuclide created based on inputs like cross sections and irradiation parameters (defined by the user). RYC may be used for different primary particles as protons, deuterons and alpha particles.
From the ActiWiz results it is possible to deduce that the aluminium is the material mostly contributing to the dose rate due in particular to the Na-22 produced. For this reason, the cross section information of the reaction Al-27(p,x)Na-22 is used for this study. They are coming from the charged-particle cross

section database for medical radioisotope production of the IAEA web portal [71].
Introducing in the software the irradiation conditions (defined in the Tab.3.5), it is possible to obtain the total Na-22 activity EOB:

$$A(\text{Na-22})_{EOB} = 106\ MBq$$

After a cooling period of 2 y: 2m : 9d , the activity decreased exponentially to the value:

$$A(\text{Na-22})_{cool} = A(\text{Na-22})_{EOB}\ exp(-\lambda_{\text{Na-22}}\ t) = 59.2\ MBq$$

where λ_{Na-22} is the Na-22 decay constant (0,27 y^{-1}).
With the software Nucleonica [29] it is then possible to evaluate the ambient equivalent dose rate H*(10) for a rabbit-detector distances equal to 10 cm and 1 m. The actual distance from the source shall take into account the two set-up of measures shown in the Fig.3.26 and an additional distance factor depending on the position of the beam window on the rabbit.
The simulation results are reported in Tab.3.9.

	H*(10) at 10 cm	**H*(10) at 1m**
	[μSv/h]	
Set 1	7.23E+02	1.72E+01
Set 2	2.43E+02	1.39E+01

Table 3.9: Dose rate results from Nucleonica due to the contribution of the Al beam window for the set up shown in Fig.3.26.

Adding these values to the contribution given from Actiwiz, it is possible to obtain the following final (simulated) dose rates results to compare with the measurements:

		H*(10) at 10 cm	**H*(10) at 1m**
		[μSv/h]	
Set 1	Simulated	8.51E+02	1.72E+01
	Experimental	1.14E+03	3.52E+01
Set 2	Simulated	3.70E+02	1.39E+01
	Experimental	2.32E+02	1.81E+01

Table 3.10: Dose rate values at two distances from the rabbit. The simulated values are the sum of the ActiWiz (body contribution) and Nucleonica results (beam window contribution). The measurements have been added for the comparison.

The results of this double method (Actiwiz for secondary particle effect and Nucleonica for one of the primary beam) gives dose rate values consistent with the ones measured experimentally.
It must be noticed that the dose rate calculations with Nucleonica are very sensitive to the distance effect. On the other side, there may be also experimental errors linked to the positioning of the detectors. The sum of these two effects contributes to the numerical gap.

A gamma spectroscopy of the rabbit has been acquired using the portable HP-Ge detector (the spectra is reported in the Fig.3.27). The inventory of the radionuclides found experimentally, reported in the Tab.3.11, can be compared with the ones given by ActiWiz at the Tab.3.12.

Radionuclide	Percentage [%]
Na-22	95.6
Mn-54	3.8
Co-60	0.7

Table 3.11: Radionuclides inventory obtained by the gamma spectroscopy with an HP-Ge detector.

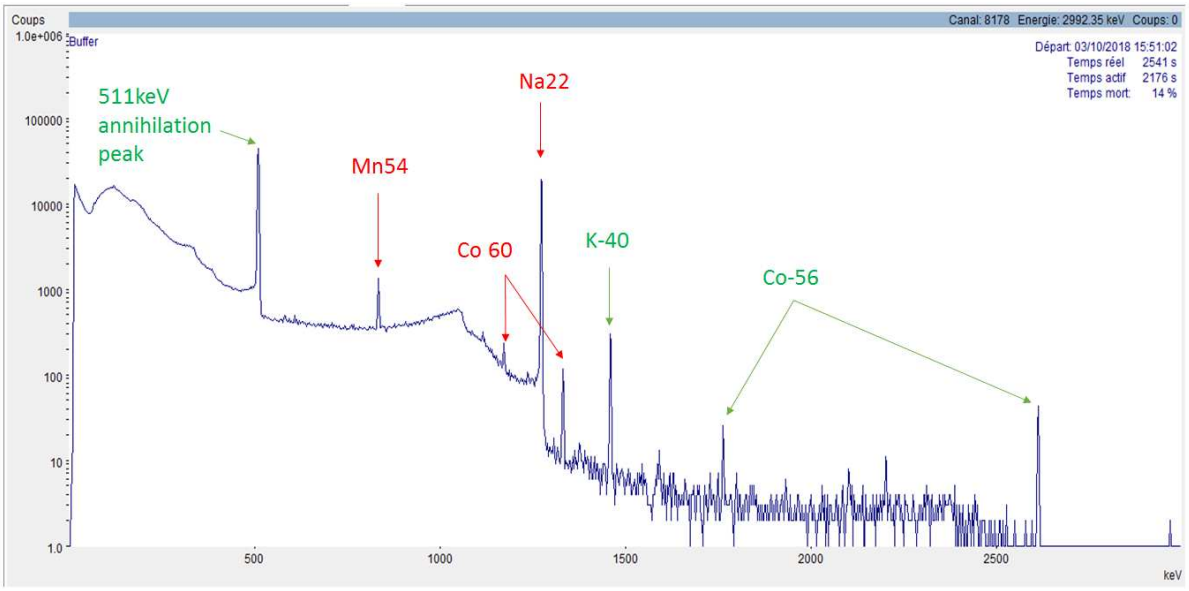

Figure 3.27: Gamma spectrum of the rabbit acquired with the portable HP-Ge detector. In red the main peaks, in green the ones coming from the background.

The radionuclides Fe-55 and H-3 are not detectable with the experimental tool. The first has gamma energies below the detection threshold ($<$ 6keV) while the second is a pure beta emitter. Rearranging the table with the only radionuclides that it is possible to observe from the sample, the contribution coming from ActiWiz can be compared with the one obtained by the gamma spectroscopy (Tab.3.13).

Conclusions of the analysis:
The scenario prepared in ActiWiz corresponding to a distance of 10 cm from the target does not reproduce the correct irradiation conditions for the rabbit. This is due to the fact that the region of the aluminum beam window is subjected not only to the fluence effect of the secondary particles flowing out the target, but mainly to the direct impact of the proton beam. The fluence spectra used in ActiWiz are not compatible with the real fluence spectra responsible for activation in the experiment. To take this effect into account, the results of two methods have been merged: on one side the ActiWiz simulation will give the value of the dose rate for the rabbit body (aluminium, peek and steel), while the RYC calculation allows the simulation of the Na-22 produced in the beam window.
In this way, the simulated values are in the same order of magnitude as the measured ones.

Material	Radionuclide	Percentage [%]	Specific activity [Bq/g]
Aluminum 2024	Na-22	61	6.95E+01
	Fe-55	11	1.21E+01
	Mn-54	10	1.11E+01
	H-3	9	9.81E+00
	Zn-65	7	7.73E+00
	Co-60	1	1.58E+00
	Co-57	1	1.34E+00
PEEK	H-3	100	5.17E+01
EPDM	H-3	100	5.03E+01
Steel	Fe-55	84	2.08E+03
	Mn-54	15	3.44E+02
Global	Na-22	25.1	2.86E+01
	Fe-55	18.4	3.57E+02
	Mn-54	6.6	6.55E+01
	H-3	46	2.53E+01
	Zn-65	2.9	3.18E+00
	Co-60	0.4	6.49E-01
	Co-57	0.4	5.5E-01

Table 3.12: Inventory produced as results from the gamma spectrum. The results for the single materials have been merged to evaluate the percentage of the radionuclides specific activity of the entire sample.

Radionuclide	Recalculated Percentage ActiWiz [%]	Percentage Exp. [%]
Na-22	78.2	95.5
Mn-54	20.6	3.8
Co-60	1.3	0.7

Table 3.13: Inventory of the species present on the sample: a comparison between the simulated and measured values for the rabbit.

ActiWiz has been also used to compare the inventory of the species produced by the irradiation and present on the sample after a fixed cooling time. Comparing the results with the information coming from the acquired spectrum, it has been possible to observe the same group of radionuclides.
The difference in the results is strictly connected to uncertainties in the chemical composition of the materials.

3.5.1.1 The vacuum couplers

These elements are placed below the target station (as shown in Fig.3.25). The connectors are composed by small pistons and are used to control the vacuum-air step during maintenance operations. The analyzed objects are 21 simple and 3 t-shape connectors, all installed and removed at the same time from the beamline (Fig.3.28).

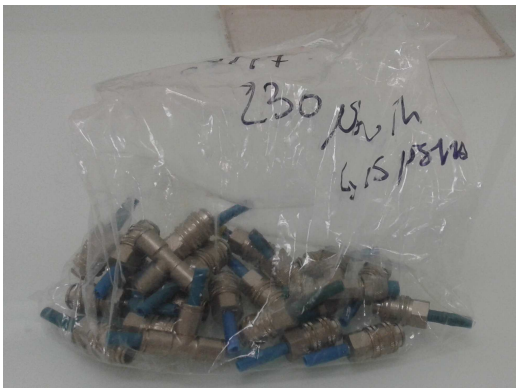

Figure 3.28: Picture of the vacuum connectors used for the study.

The irradiation conditions in this case are more complex since they don't correspond to, a simple irradiation followed by a cooling period. The couplers, indeed, were placed inside the bunker for approximately one year and withstand in total 19 irradiation runs. After the last irradiation they were disposed in the waste room for a cooling period of about 2 years.
For this study a specific file containing the irradiation/cooling pattern has been prepared and given in input to ActiWiz (Tab.3.14).

The irradiation scenario chosen is the one reproduced by the detector placed at 100 cm from the target on the lateral side (100-L).
Some hypothesis must be done on the chemical composition of the materials composing the samples since the information given on the technical description found on the producer website are not detailed. In particular, from the technical information it is possible to attribute:

- brass nickel plated to the external shell (coupler and nipple): for the simulations one of the brass material listed in the ActiWiz catalogue has been used (the "Brass_CuZn39Pb3");
- stainless steel to the inner elements (pistons, springs, balls): considered as stainless steel 304L in the simulations.

The properties and the materials chemical compositions are reported in the Tab.3.15.

The choice of these materials has been supported by the inventory of radionuclides observed on the acquired gamma spectrum (Tab.3.16 and Fig.3.29). The detection of Co-60/57 and Mn-54 reveals the presence of stainless steel while the Zn-65 shall result form the activation of a material containing a not negligible quantity of zinc.

With the chosen materials and irradiation parameters, an Actiwiz simulation of the specific activity (Bq/g) has been performed in order to compare the list of radionuclides with the ones obtained experimentally. The results of the simulations on the two materials, brass and stainless steel, have been done separately and subsequently merged to obtain the contribution of the radionuclides in the assembly (Tab.3.17).

Beam intensity	Irradiation time [day]	Cooling Time [day]
100 μA (6,2E+14 pps)	2.25	1.56
	5.42	18.9
	0.97	21.9
	0.26	1.40
	5.59	19.5
	1.18	2.70
	4.61	1.50
	2.17	13.3
	4.05	1.40
	5.63	22.4
	5.58	1.40
	1.10	36.5
	2.40	9.03
	5.74	9.83
	4.04	1.40
	2.44	13.3
	4.00	1.42
	4.15	20.42
	0.52	753.3

Table 3.14: Irradiation-Cooling profile for the vacuum connectors.

At this point, another hypothesis has been made on the ratio between the masses (and then the volumes) of the two components. No drawings with inner dimensions have been found in the technical sheet but it can be assumed that the brass represents the majority of the volume, while the stainless steel only a small part.

- It has been decided to associate the 70% of the mass to the brass and the remaining 30% to the stainless steel comparing the experimental data with the simulation.

The results of the Activiz simulation of specific activities are reported in Tab.3.17.

The list of radionuclides that mostly contribute to the specific activity corresponds to the one identified experimentally. The contribution of the radionuclides to the total specific activities (in %) is comparable with the experimental results. The inventory found with ActiWiz gives also information on the radionuclides that it is not possible to detect with the tool used in this study:

- the Fe-55, characterized by a low energy gamma emission ($<$ 6 keV);
- the Ni-63, a pure beta emitter.

Rescaling the list only for the detectable radionuclides, it is possible to obtain the values in the Tab.3.18.

Material	Density [g/cm^3]	Composition [%]	Total mass [g]
Brass	8.47	Cu: 58 Zn: 37.37 Pb: 3.5 Fe: 0.5 Ni: 0.3 Sn: 0.3 Al: 0.05	650
Stainless Steel 304-L	8	C: 0.03 Cr: 18.5 Co: 0.1 Fe:67.08 Mn: 2 Ni: 11.25 P: 0.025 Si: 1 S: 0.015	588.8

Table 3.15: Characteristics and chemical composition of the vacuum connector's materials.

Radionuclide	Percentage [%]
Zn-65	88.8
Co-60	7.6
Mn-54	2.9
Co-57	0.7

Table 3.16: Inventory of the radionuclides present in the vacuum connectors resulting from the gamma spectrum acquired using the HP-Ge detector.

The simulated value of the ambient dose rate equivalent H*(10) at 1 m is:

$$H^*(10) = (8.3 \pm 0.3)\text{E-}01\ \mu\text{Sv/h}$$

to be compared with the one obtained experimentally:

$$H^*(10) = (4.3 \pm 0.2)\text{E-}01\ \mu\text{Sv/h}$$

Conclusions:
The list of radionuclides identified from the spectrum is the same as the one simulated with ActiWiz, with the difference that the software is also able to give information on the pure beta and low gamma

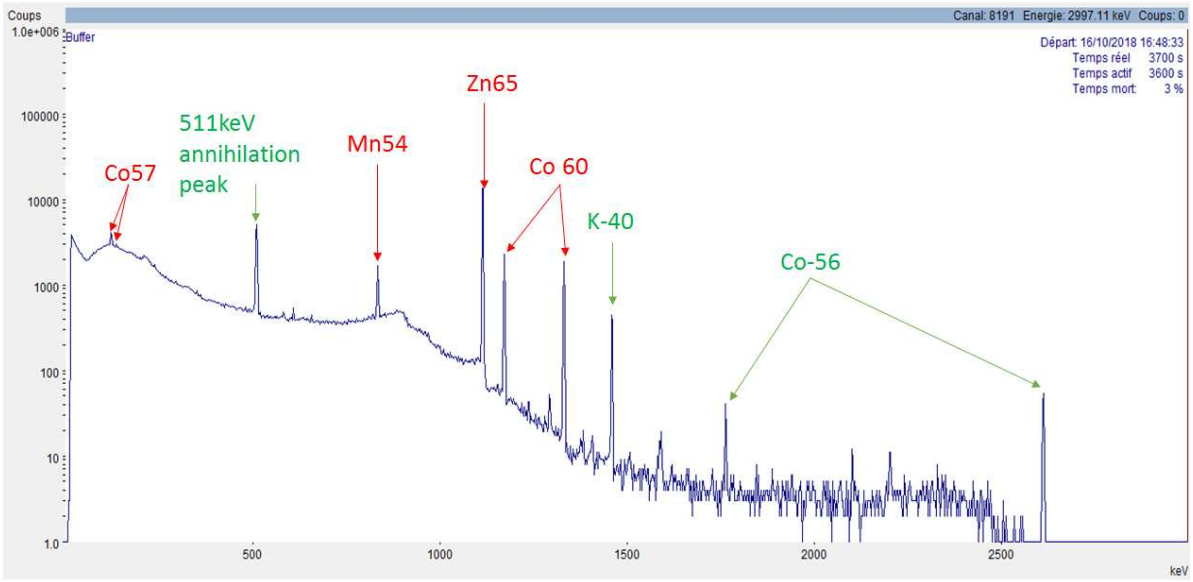

Figure 3.29: Gamma spectrum of the vacuum connectors acquired with the portable HP-Ge detector. In red the main peaks, in green the ones coming from the background.

Material	**Radionuclide**	**Percentage** [%]	**Specific activity** [Bq/g]	**Total specific activity** [Bq/g]
Brass	Zn-65	98	1.45E+04	1.48E+04
Stainless steel	Fe-55	74	1.34E+04	1.80E+04
	Mn-54	4	7.17E+02	
	Co-60	18	3.27E+03	
	Co-57	1	2.06E+02	
	Ni-63	2	3.82E+2	
Global	Fe-55	22.2	4.01E+03	1.58E+04
	Mn-54	1.2	2.15E+02	
	Co-60	5.4	9.82E+02	
	Co-57	0.3	6.19E+01	
	Ni-63	0.6	1.15E+02	
	Zn-65	68.6	1.01E+04	

Table 3.17: ActiWiz simulations of the inventory produced on the vacuum connectors. List of the top contributors ($> 1\%$) to the total specific activity.

energy emitters.
The values of the ambient dose rate simulated with Actiwiz at 1 m are higher than the ones measured (by a factor 2).
This may depend on several factors: the overestimation of the percentage of Zn-65 in the material, a probable self-absorbtion of the low energy gamma in the material composing the source, the hypothesis

Radionuclide	Recalculated percentage ActiWiz [%]	Percentage Exp. [%]
Zn-65	90.8	88.8
Mn-54	1.6	2.9
Co-60	7.2	7.6
Co-57	0.4	0.7

Table 3.18: Inventory of the species present on the sample: a comparison between the simulated and measured values.

on the chemical composition of the materials and the choice of the ratio 70-30% in between stainless steel and brass nickel volume.

3.5.1.2 Piston rod cylinder

The piston rod cylinder is a device used for the mechanical movement of metallic plates on the target station.
It is composed by three elements: a box/case in aluminum, a stainless steel piston and a connector ring in galvanized steel (Fig.3.30).

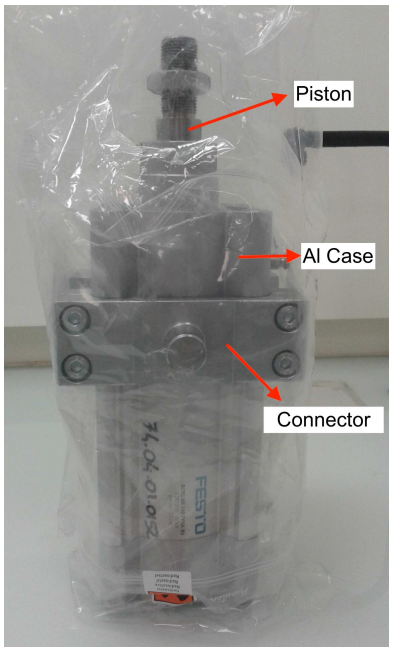

Figure 3.30: Picture of the Piston rod cylinders used for the study.

This assembly is placed above the target station as shown in the Fig.3.25.
The radiation field chosen for the ActiWiz simulation is the one defined by the detector placed at 1m from the target and on lateral side (100-L).
The cylinder has been installed and removed the same day as the vacuum connectors previously

studied. For this reason the irradiation/cooling path coincides with one defined in the previous analysis (Tab.3.14).
As in the case of the vacuum connectors, the technical description of this object given by the producer is not detailed and only the generic names of the materials are listed. It has been decided to make some assumptions and choose:

- Stainless steel 304L for the piston;
- Aluminum 6061 for the case;
- Steel with traces of zinc for the connector.

For the first two, the composition defined in the ActiWiz database has been used, while the third material has been considered as composed of iron with a small percentage of zinc.
The technical specifications report the main dimensions of the cylinder, so it has been possible to extrapolate the volume and consequently the mass of three parts (Tab.3.19).

Material	**Density** [g/cm^3]	**Composition** [%]	**Mass** [g]
Galvanized steel	8	Fe: 99 Zn: 1	1494
Aluminum 6061	2.7	Al: 97.9 Cr: 0.2 Cu: 0.3 Mg: 1 Si: 0.6	2877.3
Stainless Steel 304-L	8	C: 0.03 Cr: 18.5 Co: 0.1 Fe: 67.08 Mn: 2 Ni: 11.25 P: 0.025 Si: 1 S: 0.015	588.8

Table 3.19: Characteristics of the rod piston materials.

The choice of the materials has been again justified by the analyzed spectra of the cylinder (Fig.3.31 and Tab.3.20).

With this choice of materials, an ActiWiz simulation has been performed to compare the inventory of radionuclides with the experimental ones (Tab.3.21).
It results in a list containing the same type of identified radionuclides with the addition of low energy gamma emitters, as the Fe-55, and beta pure emitters, like H-3 and Ni-63.

The contribution to the total specific activity can be recalculated to make a comparison with the detectable radionuclides (Tab.3.22).

Radionuclide	Percentage (%)
Mn-54	79.5
Zn-65	10.4
Co-60	6.6
Na-22	3.5

Table 3.20: Inventory produced as results from the gamma spectrum.

Material	Radionuclide	Percentage [%]	Specific activity [Bq/g]	Total pecific activity [Bq/g]
Galvanized steel	Zn-65	2	5.78E+05	2.14E+04
	Fe-55	94	1.95E+04	
	Mn-54	5	9.46E+02	
Aluminium 6061	Zn-65	36	9.69E+01	2.67E+02
	Co-60	3	6.67E+00	
	H-3	2	6.23E+00	
	Fe-55	34	9.87E+01	
	Mn-54	10	2.58E+01	
	Na-22	10	2.64E+01	
	Ni-63	2	5.48E+00	
Stainless steel 304L	Co-60	18	3.27E+03	1.80E+04
	Fe-55	74	1.34E+04	
	Mn-54	4	7.71E+02	
	Ni-63	2	3.82E+02	
	Co-57	1	2.06E+02	
Global	Zn-65	0.6	1.17E+02	8.43E+03
	Co-60	2.7	3.89E+02	
	H-3	1.1	3.78E+00	
	Fe-55	37.1	7.46E+03	
	Mn-54	2	3.70E+02	
	Na-22	45.2	1.60E+01	
	Ni-63	0.8	4.56E+01	
	Co-57	0.1	2.45E+01	

Table 3.21: ActiWiz simulations of the inventory produced on the piston. List of the top contributors ($> 1\%$) to the total specific activity.

The simulated dose rate is the sum of the ones coming from the three elements (Tab.3.23).

$$H^*(10) = (10.0 \pm 0.1)\text{E-}01\ \mu\text{Sv/h}$$

Radionuclide	**Recalculated percentage ActiWiz** [%]	**Percentage Exp.** [%]
Zn-65	17.9	10.4
Mn-54	39.9	79.5
Co-60	40.7	6.6
Na-22	1.6	3.5

Table 3.22: Inventory of the species present on the sample: a comparison between the simulated and measured values.

	H*(10) at 1 m [μSv/h]	Rel. Error [%]
Connector	2.06E-01	1.24E+00
Piston	7.65E-01	2.39E+00
Cover	2.60E-02	2.40E+00
Sum	9.98E-01	1.42E+00

Table 3.23: Results of the ActiWiz simulations with the detector 100-L.

As in the previous cases, this value can be compared with the one measured at 1m from the radioactive object:

$$H^*(10) = (6.5 \pm 0.2)\text{E-}01\ \mu\text{Sv/h}$$

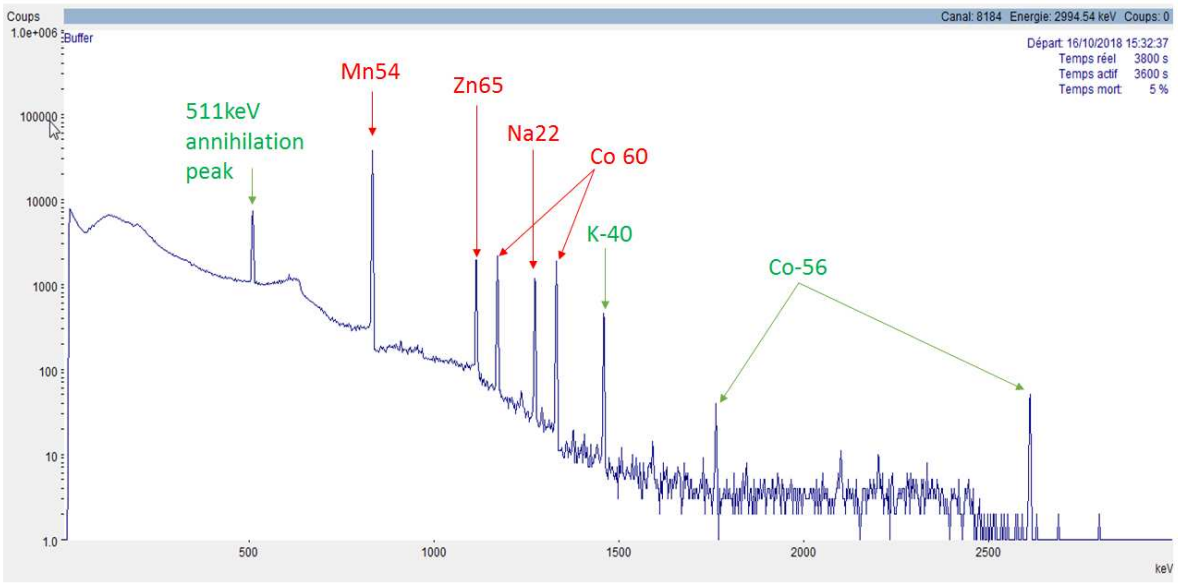

Figure 3.31: Gamma spectrum of the rabbit acquired with the portable HP-Ge detector. In red the main peaks, in green the ones coming from the background.

Conclusions:
The irradiation scenario used in this analysis has been the one for a detector based at 1m on the lateral side of the target. Also in this case the choice of the material composition plays a central role. The drawing on the technical description of the device has been used to calculate the volume of the elements and then their weight to calculate the relative contributions. It does not report all the dimensions, so hypothesis has been done due to the lack of information.
The comparison with a gamma spectrum may help to overcome this difficulty and makes possible a redefinition of the chemical composition. With the chosen volumes and composition, the simulated dose rate values are in the same order of magnitude than the experimental one and the list of radionuclides found experimentally match the one coming from ActiWiz.
The new irradiation scenario can be validated even if more statistics is needed to complete the study.

3.6 Conclusions and future perspectives

The waste management and disposal is a fundamental task in the life of a facility. Activated parts and apparatus can be stored locally for cooling and then sent to dedicated storage centers.
In France, the Institution responsible for the radioactive waste disposal is the ANDRA (Agence Nationale pour la gestion des Dechets Radioactif).
The management of activated radiological waste in ANDRA's storage centers requires a good knowledge of the radionuclides inventory (including pure beta emitters and low gamma emitters) and their activity levels. These data are essential for the definition of the management methods to ensure the safety of storage centers in operation phase. It is also mandatory to insure safety in the long run for the public and the environment.
However, methods to use for the radiological characterization of such waste can be complex, difficult to implement and/or expensive. It is generally made through sample measurements and numerical modeling. They require a good knowledge of the nature of the materials as well as of the irradiation conditions (energy, irradiation history, decay time, position of the materials, etc.). These data are usually difficult to collect due to the variability of the materials present and the history of the facility.
Recently a discussion is started between different users and producers of activated waste (low level of waste) from accelerators in France, in particular in between the ones producing medical isotopes. The scope is to define a methodology agreed by ANDRA for the radiological characterization of the waste.
The process of waste disposal (or the process of study) in facilities like ARRONAX can be considered as consisting in different phases:

1. The first step is the definition of the radionuclides inventory (radionuclides and quantities) produced as consequence of the activities done in the facility. This phase is also characterized by a study and a forecasting of their activities.
2. Parallely the chemical and physical form of the waste is defined. This is needed for the identification of the treatment the waste must undergo before being stored;
3. Definition of the size and the identification of packages that will be suitable to transport the waste to ANDRA storage centers.

This project is connected to the first item of the list. It aimed to define a method useful for the study of the species produced during the operation cycles in ARRONAX.
The software ActiWiz, developed at CERN for scenarios typical of high energy particle accelerators, has been customized to simulate the hazard coming from material activations in the ARRONAX bunkers. Here a 70 MeV proton beam is impacting a double target material made of rubidium and gallium. Seven scenarios, corresponding to seven positions in the bunker have been set. They are

characteristics of irradiation conditions encountered by the material in the bunker.
Two scenarios have been tested comparing the results of the simulations with dose rate measurements on irradiated object: a rabbit, a set of vacuum connectors and a piston.
The software and in particular the new irradiation scenarios prepared offers a good method to evaluate the species produced, both gamma and beta emitters (the latter are of difficult detection). It may be also used to foresee the cooling time or the shielding to impose for the single elements to get values coherent with the ANDRA limits of shipment.
The scenarios prepared with MCNPX do not reproduce the effect of the direct beam interaction with the material, but only the effect of the secondary particles produced by the beam-target interaction. This makes the tool not efficient for the identification of the hazard of those elements directly interacting with the proton beam, like collimators, Faraday cups or beam window. The complement use of other techniques (RYC and Nucleonica) is necessary to evaluate the activity and the relative dose rate of the species produced from the direct interaction.
In the future it would be necessary to test also the irradiation conditions defined by the detector placed far from the target.
An idea can be also the proper installation of samples, maybe composed of different and well known materials, in different points of the bunkers. Their irradiation history can be followed. Finally the measure of their activity and radioactive components can be used as reference for the other objects. A comparison with the ActiWiz calculation is eased by the good knowledge of the irradiation parameters and of the materials.
This study may also help in the definition of new scenarios to reproduce with software like ActiWiz.

4

Calculation of Transport limits with the Q-System

Contents

4.1 Introduction and background 147
4.2 Methodology for calculating A_1 and A_2 defined by IAEA 150
4.2.1 The basis of the Q-System 150
4.2.2 Calculation of Q_A: External dose due to photons 151
4.2.3 Calculation of Q_B: External dose due to beta emitters 152
4.2.3.1 Considerations on the Shielding Factor (SF) calculation 153
4.2.4 Calculation of Q_C : Internal dose via inhalation 153
4.2.5 Calculation of Q_D: Skin contamination and ingestion dose 154
4.2.6 Calculation of Q_E: External exposure in air 155
4.2.7 Special considerations 155
4.3 Calculation of A_1 and A_2 with Monte Carlo method 156
4.3.1 Calculation of Q_A with the MC 158
4.3.2 Calculation of Q_B with the MC 160
4.3.3 Calculation of Q_D with the MC 162
4.3.4 Example of application: Calculation of the Q-values for Y-90 163
4.3.4.1 Q_A calculation 164
4.3.4.2 Q_B calculation 164
4.3.4.3 Q_C value 166
4.3.4.4 Q_D calculation 166
4.3.4.5 Conclusions on the Y-90 example 168
4.3.5 Results of the A_1 and A_2 limit with the Monte Carlo technique 169
4.4 Conclusions and Future perspectives 175

4.1 Introduction and background

As seen in the Chap.3, the International Atomic Energy Agency (IAEA) Regulation for the Safe Transport of Radioactive material [39] describes different types of packages for the transport of radioactive material in relationship to the associated risk arising from the activity and the physical

form of the radioactive material contained in the package. For each radionuclide the regulation defines two values, called A_1 and A_2 that are used to determine the activity limit for the transportation with each type of container. In particular A_1 means the activity value for *special form radioactive material* (indispersible solid or sealed capsule), while A_2 is the activity limit for radioactive material *other than special form*. Type A containers allows the transport of radioisotopes with Activity below A_1 or A_2. type B packages are required for the transport of highly radioactive material. More precisely, when the activities to transport are higher than the value A_1 or A_2 and lower than 3000 $A_{1,2}$ (for shipment by plane).

The definition of those activity limits for each radionuclide is made through the so-called *Q-System* model. It consists in a methodology in which a series of exposure scenarios are used to quantify the exposure to the different type of radiations present in the source in case of accident.
The development of the method was performed by H.F. Macdonald and E.P. Goldfinch (1973), members of the United Kingdom Central Electricity Generating Board through a Research Agreement with the International Atomic Energy Agency (IAEA) [72]. The method has been reviewed several times in the past years. The last version is dated back to 1996 by L. Bologna (ANPA, Italy), K. Eckerman (ORLN, USA) and S.Hughes (NRPB, UK). They incorporated new intake dose coefficients in the calculations coming from the Recomandations of the International Commission on Radiological Protection (ICRP) of 1991. Moreover they re-examinated the dosimetric models used in the derivation of the type A package content limits and added a broader range of specific exposure pathways.
The actual Regulation, and the literature in general, still suffer of a lack of knowledge concerning those limits.
For some radionuclides, indeed, there are no available/tabulated A_1 and A_2 and in these cases a very conservative set of values is used (Tab.4.1). They are based on the type of the radiation emitted in the nuclide decay and on the qualitative hazard that the exposition implies; their estimation is not based on specific calculations. Moreover, in some cases they are drastically below the quantity of activity that is useful for research purposes and applications.
Low limits often imply the use complex (and expensive) type of packages, like type B, whose design and homologation need competent authority approval.

Radioactive Content	$\mathbf{A}_1$ [TBq]	$\mathbf{A}_2$ [TBq]
Only beta or gamma emitting nuclides	0.1	0.02
Alpha emitting nuclides (no neutrons)	0.2	9×10^{-5}
Neutron emitting nuclides or no relevant data available	0.001	9×10^{-5}

Table 4.1: Activity limits for unknown radionuclides or mixture.

An impelling example of the necessity of a new calculations is the case of the terbium isotopes and in particular Tb-149 and Tb-161.
Tb-149 is a low-toxicity alpha emitter with α energy of 3,97 MeV and a branching ratio of 16,7%. The remainder decay is by EC/$\beta+$ through a mean $\beta+$ energy of 0,73 MeV and a total $\beta+$ intensity of 7,1%. This isotope is used in nuclear medicine research and in particular for radioimmunotherapy studies. Since IAEA or the ADR [73] give no specific transport limit for this isotope, the generic A_2 value of 9E-05 TBq (90 MBq) for alpha emitter nuclide must be used. For research purposes, involving for example the treatment of a series of mice, few hundred MBq would be needed (value of activity

after chemical separation, labelling yield and decay losses) [74]. The limit for the usage of a type A package is then exceeded. We will see in the next sections that the limit for the activity to transport for this isotope is not coming from the alpha but from the gamma hazards and dose rate.
Tb-161 is a low-energy beta and Auger electron emitter used for endoradiotherapeutic treatments. It has an half-life of 6.9 d and relatively low-energy β- emitted (mean energy of 0.15 MeV). Also in this case there is no tabulated values and the generic A_2=0,02 TBq (20 GBq) for unknown beta emitters is applied in case of non special form radioactive material. A single patient injection would require the use of several GBq [75]. Considering that the transport of the source from the place of production to the radiopharmaceutical lab is before the chemical separation, the quality control and the labelling, the activity to transport at the end would be enough for only for one or two patient doses. A proper recalculation of the beta dose rate based on the effective nuclide spectra characteristics will lead, as described later, to a dose hazard allowing an increase of the transport limit.
It is, then, necessary to review the generic values reported in the IAEA Transport Regulation and add more complete and accurate information on the transport limit taking into account the real hazard coming from the nuclide spread during an accident.
The non-tabulated values can be obtained following the method defined by the Q-system.
The study that follows takes back the calculation of A_1 and A_2 making use of Monte Carlo (MC) techniques in the evaluation of the dose rate coming from the defined exposition routes, giving suggestions for possible modifications of the transportation values.
It is particularly addressed to a group of isotopes of interest for the nuclear medicine research (listed in the Tab.4.2 below) but it can be applied to all the others nuclides.

Isotope	**Decay type**	A_1 [TBq]	A_2 [TBq]
Be-7	EC	2.00E+01	2.00E+01
Na-22	EC B+	2.00E+01	2.00E+01
Na-24	B-	2.00E-01	2.00E-01
Ca-47	B-	3.00E+00	3.00E-01
Co-58	EC B+	1.00E+01	1.00E+00
Co-60	B-	4.00E-01	4.00E-01
Cu-61	EC B+	1.00E-01	2.00E-02
As-71	EC B+	1.00E-01	2.00E-02
Se-72	EC	1.00E-01	2.00E-02
Sr-82	EC	2.00E-01	2.00E-01
Y-90	B-	3.00E-01	3.00E-01
Cs-137	B-	2.00E+00	6.00E-01

Isotope	**Decay type**	A_1 [TBq]	A_2 [TBq]
Nd-140	EC	1.00E-01	2.00E-02
Tb-149	EC B+ A	2.00E-01	9.00E-05
Tb-152	EC B+	1.00E-01	2.00E-02
Tb-155	EC	1.00E-01	2.00E-02
Tb-156	EC	1.00E-01	2.00E-02
Tb-161	B-	1.00E-01	2.00E-02
Tm-166	EC B+	1.00E-01	2.00E-02
Yb-166	EC	1.00E-01	2.00E-02
At-211	A EC	2.00E+01	5.00E-01
Bi-213	EC B+ A	2.00E-01	9.00E-05
Ac-225	A	8.00E-01	6.00E-03

Table 4.2: List of some radionuclides of interest for nuclear medicine and used for the A_1 and A_2 calculation with MC method in this work. The actual activity limits for the transport is reported as well as the type of decay. The isotope in bold are the ones with generic A_1 and A_2.

This chapter is structured as follow. The first part is a summary of the Q-system theoretical bases and assumptions given by the IAEA Regulation. It follows the presentation of the method used to re-calculate some of the A_1 and A_2 values for interesting isotopes in nuclear medicine research using the Monte Carlo (MC) technique. In order to give an example of the strenght of this technique and to

better explain all the steps and details of the MC calculations, the cases of the Y-90 is described. In conclusion, the obtained Q values are compared with the tabulated ones and with the results of other working groups. Some critical points of the method and propositions for future improvements will be highlighted in the last paragraph.

4.2 Methodology for calculating A_1 and A_2 defined by IAEA

In the following paragraphs the main principles/hypothesis of the Q-system method are reported as described in the Appendix 1 of the IAEA Safety guide TS-G-1.1 [76].

4.2.1 The basis of the Q-System

Under the Q-System, a serie of exposure routes are considered, each of which may lead to radiation exposure (external or internal) of a person in proximity of the damaged type A package involved in a severe transport accident causing the release of some of the content. The dosimetric routes are illustrated in the Fig.4.1 and led to five limit values, called, indeed, *Q values*:

- Q_A for external dose due to photons,
- Q_B for external dose due to beta emission,
- Q_C for internal dose due to inhalation,
- Q_D for skin contamination and ingestion dose from beta emission,
- Q_E for submersion dose due to gaseous isotopes.

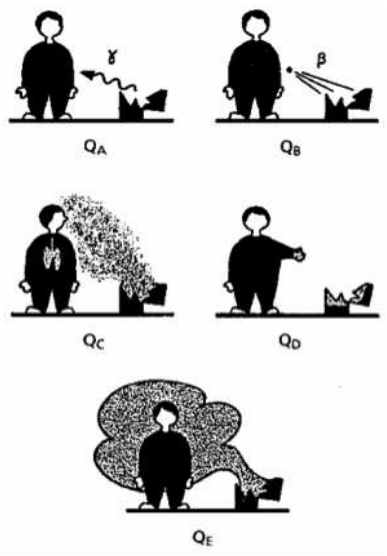

Figure 4.1: Schematic representation of the exposure pathways included in the Q system.

The derivation of the Q values is based on radiological criteria and assumptions that are in line with the main driving idea in the field of radioprotection, the ALARA principle:

1. The effective or committed effective dose received by a person in proximity of a damaged package should not exceed a reference dose of 50 mSv. In the old version of the regulation this value was linked to the annual dose limit, considered earlier no longer valid for potential exposures. In the revised one, however, this value and assumption is still retained but it is linked to the very low dose rates and exposures that historically are involved in type A packages accidents [77].

2. The effective or committed effective dose received by the individual organs (skin included) for a person involved in an accident should not exceed a reference dose of 0.5 Sv or 0.15 Sv in the special case of the eye's lens.
3. For computational purposes, the exposed person on the scene of the accident is considered to be at 1m distance from the source for 30 min. This time has been considered as the average time for the recovery operations taking place under the health physics supervisions and control. It is also more realistic than the period of exposure of 3h and at 3m distance chosen in the original method.

Special form radioactive materials are able to retain eventual gas or fragments of the source following an accident due to their characteristics of certified sealed capsule. For this reason, the scenarios defined by Q_C, Q_D and Q_E values are not relevant. Consequently, the A_1 value, for special form materials, corresponds to the minimum value between Q_A and Q_B.
For non-special form radioactive materials, instead, the source is not necessarily sealed: A_2 is the minimum among the five Q values, since all the scenarios are possible.

4.2.2 Calculation of Q_A: External dose due to photons

The Q_A value is determined by the consideration of the external radiation dose due to the gamma or the X-rays to the whole body of a person exposed near a type A package following an accident. In this scenario the source is considered placed at 1 m from the person and the shield is assumed completely lost during the accident. In the revised Q-system, the information from the gamma emission spectrum for the radionuclides are coming from the ICRP Publication 38 (1984) [78] and for the calculations the source is considered isotropic and punctual. The Q_A values are given by:

$$Q_A = \frac{D/t}{DRC_\gamma\ A} C \tag{4.1}$$

where D is the reference dose of 0.05 Sv (50 mSv), t is the exposure time of 0,5 h (30 min), DRC_γ is the effective dose rate coefficient for the radionuclide, C is the conversion factor determining the units for Q_A (10^{-12} since Q are given in TBq) and A is the activity of the source (1 Bq).
Including all these values in the previous equation we obtain:

$$Q_A(TBq) = \frac{10^{-13}}{\dot{e}_{pt}} \tag{4.2}$$

where: $\dot{e}_{pt}$ is the effective dose rate coefficient for the radionuclide at a distance of 1m in air (Sv Bq^{-1} h^{-1}). A (non exhaustive) list of dose and dose rate coefficients may be found in Table II.2 Appendix II of the IAEA Safety Guide [76].
The dose rate coefficient has been calculated from the following equation:

$$\dot{e}_p = \frac{C}{4\pi d^2} \sum_i \left(\frac{e}{X}\right)_{E_i} Y_i\ E_i \left(\frac{\mu_{en}}{\rho}\right)_{E_i} e^{-\mu_i d}\ B(E_i,\ d) \tag{4.3}$$

where:

- $(\mathrm{e/X})_{Ei}$ is the relationship between the effective dose and exposure in free air (Sv R^{-1}; R stands for Rontgen unit measure of the exposure, 1R = 2.58x10^{-4}C kg^{-1});
- Y_i is the yield of photons of energy E_i per disintegration of the radionuclide (Bq s^{-1});
- E_i is the energy of the photon (MeV);

- $(\mu_{en}/\rho)_{E_i}$ is the mass energy absorption coefficient in air for photons of energy E_i (cm^2 g^{-1});
- μ_i is the linear attenuation coefficient in air for a photon of energy E_i (cm^{-1});
- B(E_i,d) is the air Kerma buildup factor for photons of energy E_i and distance d of 1m;
- C is a constant given by the above units.

The values of $(e/X)_{E_i}$ are obtained by interpolating the data from ICRP Publication 51 [79] for photons in the range 5 keV to 10 MeV.

4.2.3 Calculation of Q_B: External dose due to beta emitters

The Q_B value is determined as the beta dose to the skin of a person exposed following an accident involving a type A package. The shielding of the transport package is not assumed to be completely lost in the accident as for the previous case, but a residual shielding factor for beta emitters (such as the source protection elements, package debris, etc.), included in the 1985 Edition of the Transport Regulations, is considered. Contrary to the gamma radiation, the electrons of the source can strongly interact with the materials around it and so the presence of a residual shielding can contribute to absorb the radiation (and to reduce part of the dose).
In the revised Q system, Q_B is calculated by using the complete beta spectra for the radionuclides of ICRP Publication 38 [78]. The spectral data for the nuclide of interest are used to evaluate skin dose rate per unit activity of a monoenergetic electron emitter [80] [81].
Q_B is given by:

$$Q_B = \frac{D/t}{DRC_\beta} C \tag{4.4}$$

where:

- D is the reference dose to a particular organ (here the skin) of 0.5 Sv;
- t is the exposure time of 0.5 h;
- DRC_β is the equivalent skin dose rate coefficient for the radionuclide;
- C is a conversion factor that determines the units for Q_B (10^{-12} since the Q are given in TBq).

Thus, including in the equation the correct factors, the Q_B can be calculated from:

$$Q_B(TBq) = \frac{1 \times 10^{-12}}{\dot{e}_\beta} \tag{4.5}$$

where $\dot{e}_\beta$ is the equivalent skin dose rate coefficient for beta emission at a distance of 1 m in air from the self-shielded material (Sv Bq^{-1} $h^{-}1$). Dose and dose rate coefficients may be found in Table II.2 of Appendix II [76].
The dose rate coefficient is defined as:

$$\dot{e}_\beta = \frac{1}{SF_{\beta_{max}}} J_{air}\ C \tag{4.6}$$

with:

- $SF_{\beta_{max}}$ is the shielding factor computed at the maximum energy of the beta spectrum (see more details below);
- J_{air} is the dose at 1 m (in air) per disintegration (MeV g^{-1} $Bq^{-1}s^{-1}$);
- C is a numerical conversion constant.

The factor J_{air} is computed as:

$$J_{air} = \frac{n}{4\pi\rho r^2} \int_0^{E_{max}} N(E) j(r/r_E)(E/r_E) dE \tag{4.7}$$

where:

- n is the number of beta particles emitted per disintegration;
- N(E) is the number of electrons emitted with energy between E and E+dE ($Bq^{-1}s^{-1}$);
- j(r/r_E, E) is the dimensionless dose distribution that represents the fraction of emitted energy deposited in a spherical shell of radius r/r_E;
- r/r_E+d(r/r_E) is as tabulated by Cross [80] [81].

Finally, a comment should be made about the treatment of positron annihilation radiation and conversion electrons in the determination of Q values. The latter are treated as monoenergetic beta particles, and weighted according to their yields. In the case of annihilation radiation this has not been included in the evaluation of the beta dose to the skin since it contributes only to an additional few per cent to the local dose to the skin basal layer. However, the 0.511 MeV gamma rays are included in the photon energy per disintegration used in the derivation of Q_A.

4.2.3.1 Considerations on the Shielding Factor (SF) calculation

The self- shielding of the package was taken to be a smooth function of the maximum energy of the beta spectrum ($E_{\beta,max}$):

$$SF = e^{\mu d} \tag{4.8}$$

Where d is the thickness of the absorber equal to 150 mg/cm^2 and μ [cm^2/mg] is the apparent absorption coefficient given by the following empirical equation:

$$\mu = 0.017(E_{\beta,max})^{-1.14} \tag{4.9}$$

The method assumes a very conservative shielding factor of 3 for beta emitters of maximum energy $\geq$2 MeV, and based on an absorber of approximately 150 mg cm^{-2} thickness.

4.2.4 Calculation of Q_C : Internal dose via inhalation

The Q_C value is connected to the inhalation risk, supposed to be negligible for special form radioactive materials. Following an accident, a portion of the material escapes from the package becoming airborne and leading to a dose for the worker via inhalation.This scenario includes accidents occurring both indoors and outdoors. Potentially the most severe type of accident for many type A packages is the combination of mechanical damage with a fire, producing relatively large sized particles that may be inhaled.
Data on the respirable aerosol fractions produced under accidental conditions are generally sparse and are only available for a limited range of materials.
In the new version of the Regulation, it is assumed that 10^{-6} of the package contents is escaped as a result of an accident and that this quantity of material is inhaled by a person on the scene. It represents a combination of releases typically in the range up to 10^{-3}-10^{-2} of the package contents as a respirable aerosol, combined with an uptake factor of up to 10^{-4}-10^{-3} of the released material.

Considering also the limiting doses, this leads to an expression for the contents limit based on inhalation of the form:

$$Q_C = \frac{D}{1 \times 10^{-6} D\, C_{inh}}\, C \tag{4.10}$$

where:

- D is the reference dose of 0.05 Sv;
- 10^{-6} is the fraction of the inhaled content of the package;
- DC_{inh} is the dose coefficient for inhalation;
- C is the conversion factor that determines the units of Q_C (10^{-12}).

Using these factors and coefficients, the Q_C value can be calculated as follow:

$$Q_C(TBq) = \frac{5 \times 10^{-8}}{\dot{e}_{inh}} \tag{4.11}$$

where $\dot{e}_{inh}$ is the effective dose coefficient for inhalation of the radionuclide (Sv/Bq). Values for $\dot{e}_{inh}$ may be found in Table II and III of the Safety Series n.115 [82], while dose and dose rate coefficients may be found in Table II.2 of Appendix II [76].

4.2.5 Calculation of Q_D: Skin contamination and ingestion dose

The Q_D value for beta emitters is determined by the beta dose to the skin of a person contaminated with radioactive material as a consequence of handling a damaged type A package. The model proposed within the Q system assumes that 1% of the package contents are spread uniformly over an area of 1 m^2; handling of the debris is assumed to result in contamination of the hands to 10% of this level [83]. It is further assumed that the exposed person is not wearing gloves but would recognize the possibility of contamination or wash the hands within a period of 5 h.
The dose rate limit for the skin is fixed to 0.1 Sv/h based on a 5 h exposure period.
The values for Q_D have been calculated using the continuum beta spectra and discrete electron emissions for the radionuclides as tabulated by the ICRP 38 and 51 [78] [79].
Q_D is given by:

$$Q_D = \frac{D}{10^{-3} \times DRC_{skin} \times t} C \tag{4.12}$$

where:

- D is the reference dose to a particular organ (skin in this case) of 0.5 Sv;
- 10^{-3} is the fraction of the package content distributed per unit area of the skin (m^{-2});
- DRC_{skin} is the equivalent skin dose rate coefficient for skin contamination;
- t is the exposure time of 1.8×10^4 s (5 h);
- C is a conversion factor that determines the units for Q_D (set to 1).

With those factors, Q_D can be evaluated as:

$$Q_D(TBq) = \frac{2.8 \times 10^{-2}}{\dot{h}_{skin}} \tag{4.13}$$

where $\dot{h}_{skin}$ is the equivalent skin dose rate per unit activity and unit area of the skin (Sv s^{-1} TBq^{-1} m^2). dose and dose rate coefficients may be found in Table II.2 of Appendix II [76].
The models used in deriving the Q_D values here may also be employed to estimate the possible uptake of radioactive material via ingestion, but since the dose per unit intake via inhalation is generally of the same order as, or greater than, the one via ingestion [48], the inhalation pathway will normally be limiting for internal contamination under the Q system.

4.2.6 Calculation of Q_E: External exposure in air

For gaseous isotopes which do not become incorporated into the body, such as noble gases, an additional Q value, Q_E, is determined from the dose from external irradiation in a cloud of gas.
Both the effective dose and skin dose must be calculated in this case, assuming that:

1. the entire package contents is released;
2. the release occurred in a room or cargo handling bay of 300 m^3 of volume, area in wich the person is exposed;
3. there are 4 air changes per hour within the room.

These assumptions led to an initial airborne concentration of $Q_E/300$ Bq m^{-3}, which decreased exponentially at a rate of 4 h^{-1}. The average activity concentration in air over the exposure time (0.5 h) was 1.44 10^{-3} Q_E (m^{-3}). Submersion dose coefficients for effective and skin dose are given in the Federal Guide n.12 [84] and are listed in IAEA TS-G-1.1 [76].
Q_E values for effective dose is calculated as follows:

$$Q_E = \frac{DL_{eff}}{TIAC\, h_{subeff}}\, C \tag{4.14}$$

While the Q_E values for the dose to the skin (TBq) is calculated as:

$$Q_E(TBq) = \frac{DL_{skin}}{TIAC\, h_{subskin}}\, C \tag{4.15}$$

where:

- DL_{eff} and DL_{skin} are the dose criteria for effective dose (0,05 Sv) and equivalent dose to the skin (0,5 Sv), respectively;
- TIAC is the time-integrated activity concentration in air per unit activity released which was set to 2.6 Bq s m^{-3} per Bq;
- C is the conversion factor that determines the units for Q_E (10^{-12});
- h_{subeff} and $h_{subskin}$ are the submersion dose coefficient for effective dose and skin equivalent dose respectively (Sv $Bq^{-1}s^{-1}m^3$), provided by IAEA TS-G-1.1 [76].

The Q_E value is the lesser of two values calculated for the effective and skin equivalent dose.

4.2.7 Special considerations

- ***Treatment of the progeny:***
  The Q system assumed a maximum transport time of 50 days, and thus radioactive decay products with half-lives lower than 10 days were assumed to be in secular equilibrium with their longer lived parents. In such cases, the Q values were calculated for the parent and its progeny, and the limiting value was used in determining A_1 and A_2 of the parent. In cases where a daughter radionuclide has a half-life either greater than 10 days or greater than the one of the parent nuclide, such progeny, with the parent, are considered to be a *mixture*. The A1 and A2 values for mixtures of n radionuclides are determined as follow [39]:

$$X_m = \frac{1}{\sum_i^n \frac{f(i)}{X(i)}} \tag{4.16}$$

where:

- X_m is the derived value of A_1 or A_2 in case of a mixture;
- f(i) is the fraction of activity or activity concentration of the radionuclide i in the mixture;
- X(i) is the A_1 or A_2 value for the radionuclide i.

- ***Rounding method:***
  The Q values are quoted to 2 significant digits whereas A_1 and A_2 values are rounded up or down to the nearest significant figure.

4.3 Calculation of A_1 and A_2 with Monte Carlo method

The methodology described in the previous sections implies the use of analytic formulae or empiric coefficients and relies in some cases on the approximation of integral equations. Moreover the information on the isotopes' spectra are based on old libraries dated 1984-94.
A good alternative is represented by the use of Monte Carlo simulations to evaluate directly the dose rate parameters to use in the formulae for the calculation of the Q values: $\dot{e}_{pt}$, $\dot{e}_b$, $\dot{h}_{skin}$, $\dot{e}_{inh}$.
This method avoids the solution of complex equations and takes into account all the phenomena involved in the interaction of the source's particles with the matter and the surrounding air, giving a realistic evaluation of the dose in the single accidental scenarios. It will include the recent nuclear physics interaction cross sections of the particles as well as effects like Bremsstrahlung that has not been fully included in the current Q-system. However the basic principles, like the geometrical factors and the radiological criteria of the current Q system, remain.
The software MCNPX [31] has been used for these calculations. The information relative to the decay spectra of the single isotopes are coming from the ICRP 107 publication [85].
Each nuclide is characterized by a typical spectrum of emission. A procedure that allows a fast calculation for each nucleide without the need to set a different MC code for each of them has been used: the dose rate values is computed for monoenergetic particles sources; then, using the typical spectra characteristics (energy distribution and branching ratio of the particles emitted in the decay), the effective dose rate is associated to each radionuclide.
The applied method is similar in all the cases/scenarios and it is composed by the following main steps (Fig.4.2):

Step 1:
- The geometry resuming as close as possible the accidental scenario described by the Regulation for the single Q value is modeled in the MCNPX code;

Step 2:
- A punctual source of beta or gamma particles of 1 Bq is set up (in the origin) and its emission considered isotropic and monoenergetic.
- The dose rate for the defined active/detection area and associated to the single energy with emission probability of 100% is evaluated using the MCNPX F8 tally;

Step 3:
- Using the spectra of each isotope, the dose rates associated to the single energies are retrieved;
- The dose rate for each i-th particle energy composing the spectra is weighted by the relative effective Branching Ratio;
- When the emitted particle energy is not present in the simulated data set, a linear interpolation is done for that particular energy bin;

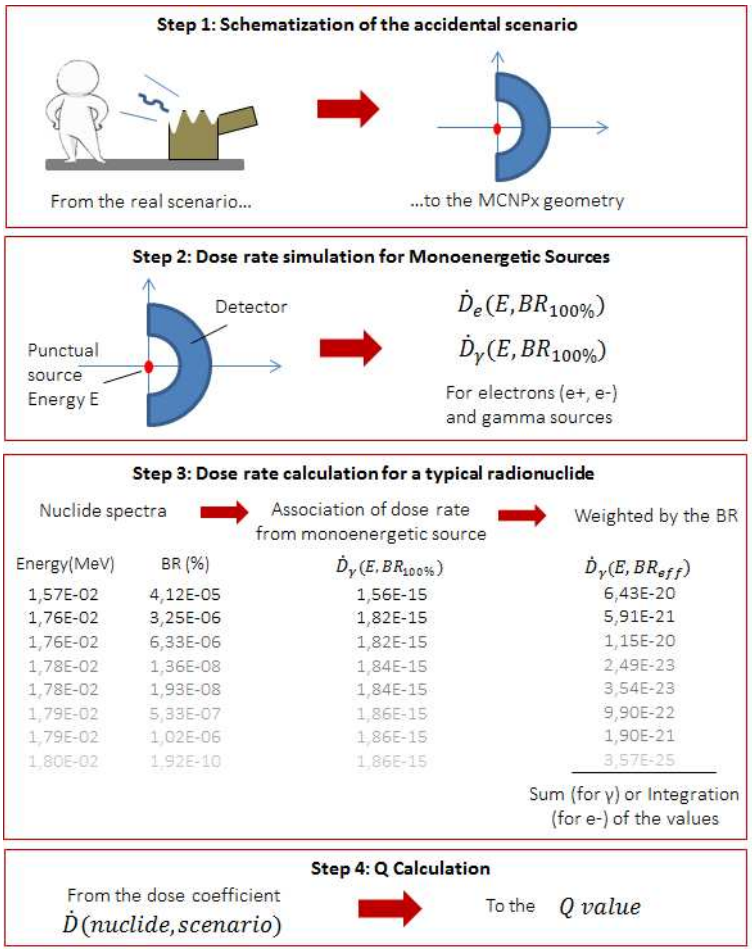

Figure 4.2: Schematic of the method used for the Q value calculation with the Monte Carlo technique.

- For monoenergetic spectra the total dose rate is given by the arithmetic sum of the single dose rates weighted by the probability of decay:
- In case of continuum spectra (i.e. beta emission) the dose rate is coming from the trapezoidal integration rule of the data set.
- If the isotope is characterized by both monoenergetic and a continuous spectra, the dose rate is the sum of the two components.

Step 4:

- The obtained dose rate coefficient is used to calculate the Q value under study using the formulae presented in the previous section.

In all calculations the dose rate is relative not only to the primary particles emitted from the source, but also to the effect of the secondary particles, coming from the elastic and inelastic scattering with the surrounding materials. Unlike the analytical calculations, these effects can be easily taken into account using the Monte Carlo method.

- The evaluation of h_{skin}, involved in the calculation of the Q_C value, is linked to the dose rate released to the organs of the respiratory tract. The complexity related to the needs to understand the fractional deposition and the chemical affinity in each sector of the respiratory organs for each radionuclide, led us to use the values of h_{skin} defined in the ICRP119 publication [86] for the calculations.

- The recalculation of the dose coefficient h_{subeff} and $h_{subskin}$, involved in the calculation of Q_E value, is not of interest (is not an objective) for this study. The main reason is that the gaseous form of radioactive medical isotopes to transport is very rare. Moreover the Q_E calculations imply the knowledge of the isotopes concentration on the air volume of the room with the time and the need to simulate the dose for the general human phantom.

This study focuses in particular on the re-calculation of the Q_A, Q_B and Q_D values, keeping the ones defined in the Regulation for Q_C and Q_E unchanged for the final comparison.
The Monte Carlo method have been initially tested for a *control group* of Isotopes for whom the dose coefficients that appear in the equations for the Q values are tabulated in the IAEA Safety Guide. A comparison between the listed coefficients and the ones simulated in this study have been done to validate the method.
The procedure have been then applied to evaluate the dose rate coefficients ($\dot{e}_{pt}$, $\dot{e}_b$, $\dot{h}_{skin}$, $\dot{e}_{inh}$) for some nuclides who present non-tabulated Q values and generic limits of transport.
In the following sections all the parameters and the modeling approach used in the Monte Carlo simulations for each accidental scenario defined by the Q-system will be described.

4.3.1 Calculation of Q_A with the MC

As defined by the IAEA method, the $\dot{e}_{pt}$ dose rate is given by the whole body exposure to gamma or the X-Rays of a person as consequence of an accident.
The scenario described by the IAEA method and modeled with MCNPX is reported in the Fig.4.3.

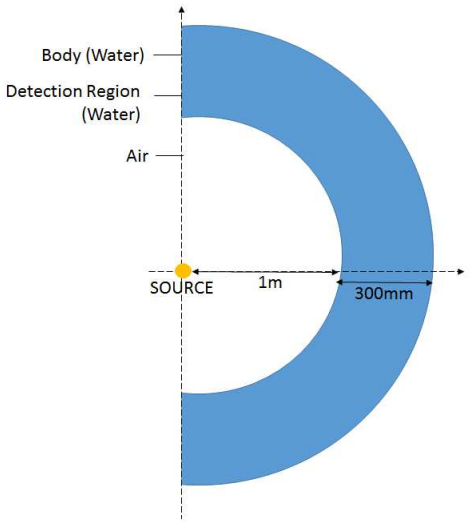

Figure 4.3: Scheme of the geometry reproduced with MNCPX representing the accidental scenario involved in the Q_A simulations.

The gamma source, isotropic and monoenergetic, is placed in the center of the axis. The person (representing our active area/detector) is placed, in air, at 1m from the source: the active area is represented by a spheric shell with inner radius of 1 m and thickness of 0,30 m composed by water. The reason of this material choice is due to the similar density and composition of water with the human body (Tab 4.3). The thickness of 30 cm has been chosen as mean thickness of the human body. The cylindrical symmetry of the simulated geometry is made to increase the number of particles reaching the detection area and reduce consequentially the variance of the results.

Material	Weight fraction [%]	Density [g cm^{-3}]
Air	Ar: 1.28 O: 23.18 C: 0.012 N: 75.53	0.001205
Water	H: 11.2 O. 88.8	1

Table 4.3: Composition of materials used for the gamma dose simulations in MCNPX.

The values of the simulated dose rates with the energy for the monoenergetic gamma sources are plotted in the Fig.4.4.

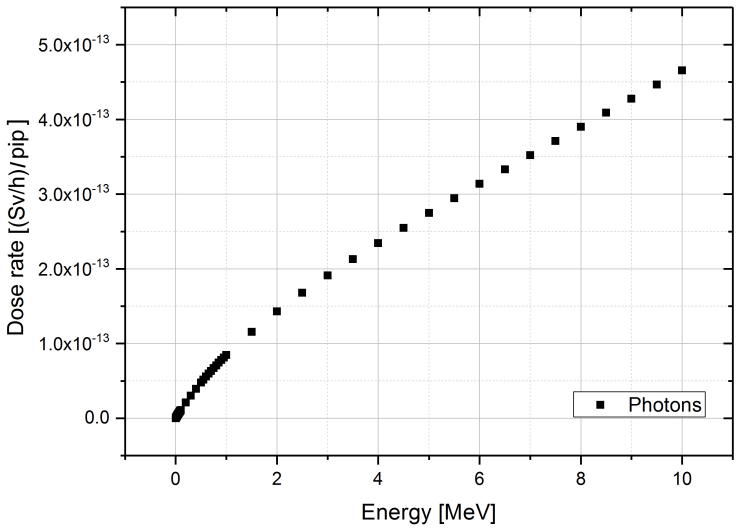

Figure 4.4: Dose rate results of MCNPX simulations for monoenergetic gamma sources. The range of simulated energies goes from 0.01 to 10 MeV.

Considering the gamma spectra for each isotope (energy and associated branching ratio), the $\dot{e}_{pt}$ dose rate factor is given by the sum of the dose rate associated to the single energies ($\dot{D}(Ei)$) weighted by their relative probability of emission (I(Ei)).

$$\dot{e}_{pt} = \sum_{i=1}^{n} I(E_i)\dot{D}(E_i) \tag{4.17}$$

Using the equation 4.2 the Q_A factor is then evaluated. The results of simulation for the dose rate coefficient $\dot{e}_{pt}$ and the relative Q_A values for the chosen control group and for the other nuclides of interest are reported in the Tab.4.14.

4.3.2 Calculation of Q_B with the MC

The Q_B value is determined by the beta dose to the skin of a person exposed during an accident involving a type A package containing special form material. A residual shielding factor (SF) for beta emitters is considered.
The geometry reproduced in MCNPX is reported in Fig.4.5. The person exposed is at 1m from the source. In this case the dose to the skin is of interest, so the active area is a spheric shell with thickness of 0,04 mm and depth of 0,07 mm. It corresponds to the position of the layer of the skin called dermis, containing blood vessels and lymph nodes.

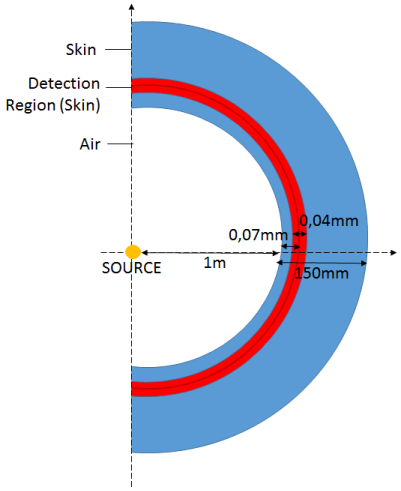

Figure 4.5: Scheme of the geometry reproduced with MNCPX representing the accidental scenario involved in the Q_B simulations.

The composition of the skin used for the calculation is reported in the Tab.4.4, while air composition is the same used in the Q_A calculation (Tab.4.3).

Material	**Weight fraction** [%]	**Density** [g cm^{-3}]
Skin	H: 10,1 % O: 76,2 % C: 11,1 % N: 2,6 %	1

Table 4.4: Skin composition used for the beta dose simulations in MCNPX [87].

The simulated dose rate to the skin for the single energy e+ and e- source is reported in the graph below (Fig.4.6). The energy of 0,36 MeV has been chosen as lower energy limit. It corresponds to the minimum energy for a e- particle to have a range comparable with the source-water layer distance, i.e. 1 m in this case.

In the range of energies 0.3-0.5 MeV we can observe that the dose rate increases up to a peak. This corresponds to the electron energy values for which the particle ranges are comparable to the source-

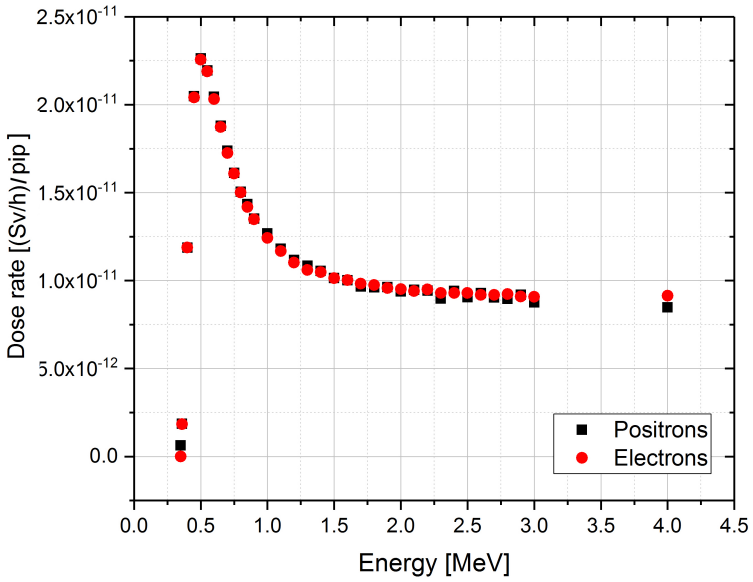

Figure 4.6: Dose rate results of the MCNPX simulations for monoenergetic e- and e+ sources. The simulated energy range goes from 0.36 to 4 MeV.

detector distance (1 m in air + 0.07 mm of water + 0.04 mm of water detector in this case). Increasing the energy, the electrons ranges become higher and they will go through the detector depositing only a fraction of their energy. Above 2 MeV the behavior can be assumed linearly decreasing.The choice of the binning reflects this behavior: small bin is used to sample the peak region and a larger one in the linear decreasing region and at the end of the curve tail.
Positrons and electrons have basically the same behavior (same deposited energy) in the skin tissue. There is a density effect correction coefficient that differentiates the collision stopping power of the two charged particles [88]. For positrons, annihilation occurs leading to the production of two 511 keV gammas which have been already taken into account in the gamma spectrum characterizing the Q_A value.
The dose rate is given by the result of the sum of two factors: the dose coming from the continuum beta specrum ($\dot{e}_b^{cont}$) and the dose given by the monoenergetic electrons emitted during the decay ($\dot{e}_b^{mono}$). A coefficient dependent to the maximum beta energy, linked to the residual shielding (SF) and defined as in the paragraph 4.2.3.1 is also included:

$$\dot{e}_b = SF\ (\dot{e}_b^{cont} + \dot{e}_b^{mono}) \tag{4.18}$$

For the evaluation of the first factor e_b^{cont}, the single dose rate values are weighted by their branching ratio and integrated using the trapezoidale rule:

$$\dot{e}_b^{cont} = \sum_{i=1}^{n} \frac{(BR_n\ \dot{D}_n + BR_{n-1}\ \dot{D}_{n-1})}{2} \Delta E_i \tag{4.19}$$

The second factor e_b^{mono} is given by the sum of the dose rate of the single energies weighted by their branching ratio:

$$e_b^{mono} = \sum_{i=1}^{n} BR_i\ \dot{D}(E_i) \tag{4.20}$$

In both equations (4.19 and 4.20) the dose rate values are weighted by the probability of emission (BR).

The calculation of the adimensional SF follows the method established in the IAEA regulation: if the isotope under study presents particles with energies higher than 2 MeV, the shielding factor is set to 3, otherwise it will depend on the maximum beta energy of the beta spectra (Eq.4.8). In case the isotope presents only monoenergetic electrons, a shielding factor of 3 is chosen a priori, independently from the spectra.

4.3.3 Calculation of Q_D with the MC

The Q_D factor is related to the accidental scenario in which the dose is transferred to the person due to the handling of the damaged Type A package.
The geometry reproduced in the code is reported in the Fig.4.7.

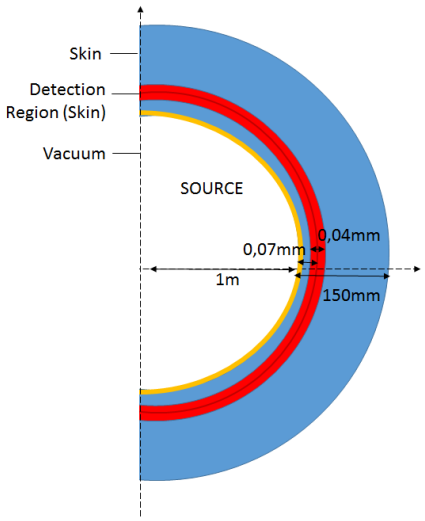

Figure 4.7: Scheme of the geometry reproduced with MCNPX representing the accidental scenario involved in Q_D simulations. The range of simulated energies goes from 0.06 to 4 MeV.

The source is now at contact with the skin and the area of detection is still represented by a spherical shell with thickness of 0.04 mm and at a depth 0.07 mm. The skin composition is the same than the one reported in the Tab4.4.
The method of the h_{skin} dose factor calculation is similar to the one used for the coefficient $\dot{e}_b$ except for the absence of the shielding factor effect.
As first step, the dose rate for the single energies (with 100% of branching ratio) is evaluated. The results of the simulations are reported in Fig.4.8.
The range of chosen energies goes from 0.06 (minimum energy to have electrons with range comparable to the skin thickness) to 4 MeV.
As for the previous $\dot{e}_b$ case, it is possible to distinguish three regions in the dose rate behavior as a function of the energy.
In the first region, the dose rate increase up to a maximum value corresponding to the energy for which the electrons range is equal to the source-skin derma distance. For higher energies, the range of the electrons increases at the expense of the deposited dose in the detection area. Then the second region is characterized by an exponential decay of the dose rate values. Starting from 1 MeV, it is possible to assume a linear decreasing behavior, corresponding to the third region. The choice of the

energy bin for the spectra reflects this trend: small bins are used to sample the first two regions, while a larger one is used for the curve tail.

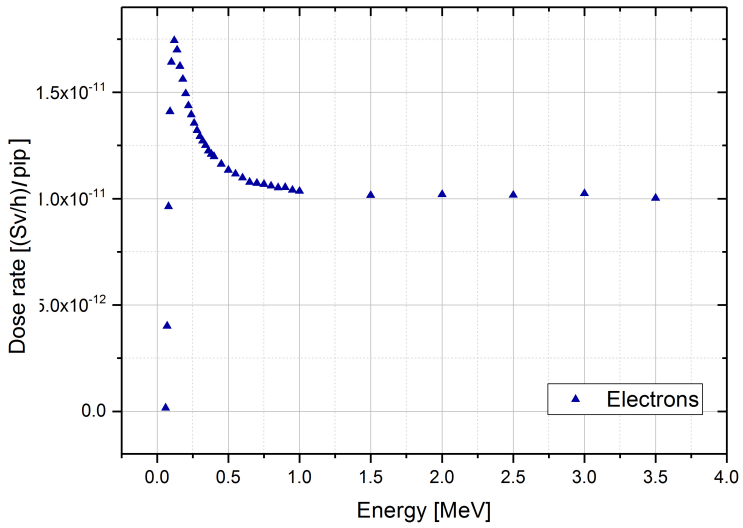

Figure 4.8: Dose rate results of the MCNPX simulations for monoenergetic e- sources. The results for the e+ source provide a dataset that differentiates from the one of the e- of a factor minor that the 1% and it has not been reported in the graph for simplicity.

Subsequently, the spectra of the isotopes under study are retrieved. Once again, the dose rate coming from the (n) monoenergetic electron of the spectra is given by the sum of the single contribution to the dose ($\dot{D}$(Ei)) weighted by the relative probability of emission (BR). The contribution to the dose coming from the continuum spectra is given by the trapezoidal integration of the single contribution always weighted by their relative probability of emission.

$$h_{skin} = h_{skin}^{cont} + h_{skin}^{mono} \tag{4.21}$$

where:

$$h_{skin}^{cont} = \sum_{i=1}^{n} \frac{(BR_n\ \dot{D}_n + BR_{n-1}\ \dot{D}_{n-1})}{2} \Delta E_i \quad \text{and} \quad h_{skin}^{mono} = \sum_{i=1}^{n} BR_i\ \dot{D}(E_i) \tag{4.22}$$

4.3.4 Example of application: Calculation of the Q-values for Y-90

To better illustrate all the steps in the dose coefficient calculations, let's take as example the case of the Y-90, nuclide widely used in medicine for the liver treatment. This isotope has an half-life of 64,05 h and decays β^- in Zr-90 (stable). The IAEA safety guide [76] lists the Q values associated to this nuclide, belonging to the control group of radionuclides for this study (Tab. 4.5):

$\mathbf{Q}_A$	$\mathbf{Q}_B$	$\mathbf{Q}_C$	$\mathbf{Q}_D$
[TBq]			
1.0E+03	3.2E-01	3.3E+01	5.9E-01

Table 4.5: Q values associated to the nuclide Y-90 in the IAEA Regulation [39].

The nuclide data used in this study are coming from the ICRP publication 107 [85].

4.3.4.1 Q_A calculation

In the Tab.4.10 are listed energies and relative probabilities of emissions of the gamma particles in the Y-90 decay (Note: a lower limit of 0.01 MeV has been chosen).
Using the dose rate results (in the Tab.C.1 in the Appendix C) coming from the single energy method, to each energy of the nuclide spectra is associated the energy bin (E_{max} and E_{min}) and the parameters of linearization to obtain the value of dose rate for that precise energy from the equation:

$$\dot{D}_{Ei,\, I=100\%} = aE(i) + b\,, \qquad \text{i=1,...,n} \tag{4.23}$$

This must be weighted for the effective branching ratio (I), obtaining the real contribution to the dose rate of each gamma emitted ($\dot{D}$). The $\dot{e}_{pt}$ dose rate coefficient is then the arithmetic sum of those values.

Energy [MeV]	**I** [part/(s MeV)]	$\mathbf{E}_{min}$ [MeV]	$\mathbf{E}_{max}$ [MeV]	**a** [Sv/(h MeV)]	**b** [Sv/h]	$\dot{D}_{I=100\%}$ [Sv/h]	$\dot{D}$ [Sv/h]
1.56E-02	2.16E-05	1.50E-02	2.00E-02	1.37E-13	-5.94E-16	1.55E-15	3.33E-20
1.57E-02	4.12E-05	1.50E-02	2.00E-02	1.37E-13	-5.94E-16	1.56E-15	6.43E-20
1.76E-02	3.25E-06	1.50E-02	2.00E-02	1.37E-13	-5.94E-16	1.82E-15	5.91E-21
1.76E-02	6.33E-06	1.50E-02	2.00E-02	1.37E-13	-5.94E-16	1.82E-15	1.15E-20
1.78E-02	1.36E-08	1.50E-02	2.00E-02	1.37E-13	-5.94E-16	1.84E-15	2.49E-23
1.78E-02	1.93E-08	1.50E-02	2.00E-02	1.37E-13	-5.94E-16	1.84E-15	3.54E-23
1.79E-02	5.33E-07	1.50E-02	2.00E-02	1.37E-13	-5.94E-16	1.86E-15	9.90E-22
1.79E-02	1.02E-06	1.50E-02	2.00E-02	1.37E-13	-5.94E-16	1.86E-15	1.90E-21
1.80E-02	1.92E-10	1.50E-02	2.00E-02	1.37E-13	-5.94E-16	1.86E-15	3.57E-25
1.80E-02	2.70E-10	1.50E-02	2.00E-02	1.37E-13	-5.94E-16	1.86E-15	5.03E-25
2.19E+00	1.40E-08	2.00E-02	3.00E-02	1.37E-13	-3.64E-16	2.74E-13	3.83E-21
						Sum	**1,22 E-19**

Table 4.6: Results of the simulations for the gamma spectra of Y-90.

$$\dot{e}_{pt} = 1.22\text{E-}19\ Sv/h \tag{4.24}$$

$$Q_A = \frac{10^{-12}}{\dot{e}_{pt}} = 8.21\text{E+}05\ TBq \tag{4.25}$$

4.3.4.2 Q_B calculation

Q_B is linked to the evaluation of the dose to the skin for an electron source placed at 1m distance in air. The Y-90 beta decay spectra is characterized by two components: a continuum spectra emission and a set of monoenergetic electrons (Auger and Internal Conversion electrons). In both cases, using the information coming from the monoenergetic source simulations (Tab.C.2 in the Appendix C), dose rate values are associated to each electron energy, both for the continuum and monoenergetic electrons (Tab.4.7 and Tab.4.8).

The Q_B scenario previews a residual shielding that will attenuate the absorbed dose rate to the skin. Since the beta decay spectra presents energy values higher than 2 MeV, the Regulation sets the

Continuum Spectra			
Energy [MeV]	**I** [pps/MeV]	$\dot{D}_{I=100\%}$ [(Sv/h)/(pps)]	$\dot{D}$ [(Sv/h)/(pps)]
3.60E-01	5.56E-01	1.85E-12	1.03E-12
4.0E-01	5.71E-01	1.19E-11	6.78E-12
4.5E-01	5.87E-01	2.04E-11	1.20E-11
5.00E-01	6.00E-01	2.26E-11	1.35E-11
5.50E-01	6.10E-01	2.19E-11	1.34E-11
6.00E-01	6.18E-01	2.03E-11	1.26E-11
6.50E-01	6.24E-01	1.87E-11	1.17E-11
7.00E-01	6.27E-01	1.73E-11	1.08E-11
7.50E-01	6.29E-01	1.61E-11	1.01E-11
8.0E-01	6.29E-01	1.50E-11	9.44E-12
8.50E-01	6.28E-01	1.42E-11	8.90E-12
9.0E-01	6.25E-01	1.35E-11	8.42E-12
1.00E+00	6.14E-01	1.24E-11	7.63E-12
1.10E+00	5.98E-01	1.17E-11	6.98E-12
1.20E+00	5.76E-01	1.10E-11	6.34E-12
1.30E+00	5.47E-01	1.06E-11	5.79E-12
1.40E+00	5.10E-01	1.05E-11	5.35E-12
1.50E+00	4.65E-01	1.01E-11	4.71E-12
1.60E+00	4.11E-01	1.00E-11	4.12E-12
1.80E+00	2.77E-01	9.74E-12	2.70E-12
2.00E+00	1.28E-01	9.52E-12	1.21E-12
2.20E+00	1.40E-02	9.50E-12	1.33E-13

Table 4.7: Results of the simulations for the continuum beta spectra of Y-90.

SF to 3.
Using the equations 4.19 and 4.20, the monoenergetic component is given by the arithmetic sum of the dose rates values, while the continuum is derived from a trapezoidal integration.
The two components of the electron dose rate coefficient $\dot{e}_b$ are:

$$\dot{e}_b^{mono} = 3.75\text{E-}16 \text{ Sv h}^{-1} \text{ Bq}^{-1} \tag{4.26}$$

$$\dot{e}_b^{cont} = 3.73\text{E-}12 \text{ Sv h}^{-1} \text{ Bq}^{-1} \tag{4.27}$$

The sum of the two factors is used for the Q_B calculation:

$$\dot{e}_b = \dot{e}_b^{mono} + \dot{e}_b^{cont} = 3.73\text{E-}12 \text{ Sv Bq}^{-1}\text{h}^{-1} \tag{4.28}$$

$$Q_B = 2.68\text{E-}01 \text{ TBq} \tag{4.29}$$

Monoenergetic Spectra							
Energy [MeV]	**I** [pps/ MeV]	$\mathbf{E}_{min}$ [MeV]	$\mathbf{E}_{max}$ [MeV]	**a** [Sv/(h MeV)]	**b** [Sv/h]	$\dot{D}_{I=100\%}$ [(Sv/h)/pps]	$\dot{D}$ [(Sv/h)/pps]
1.74E+00	1.02E-04	1.70E+00	1.80E+00	-7.60E-13	1.11E-11	9.79E-12	9.96E-16
1.76E+00	1.10E-05	1.70E+00	1.80E+00	-7.60E-13	1.11E-11	9.78E-12	1.07E-16
1.76E+00	1.94E-06	1.70E+00	1.80E+00	-7.60E-13	1.11E-11	9.77E-12	1.90E-17
1.76E+00	3.36E-07	1.70E+00	1.80E+00	-7.60E-13	1.11E-11	9.77E-12	3.29E-18
2.17E+00	1.72E-12	2.10E+00	2.20E+00	1.03E-12	7.24E-12	9.47E-12	1.63E-23
2.18E+00	1.86E-13	2.10E+00	2.20E+00	1.03E-12	7.24E-12	9.49E-12	1.77E-24
2.18E+00	2.07E-15	2.10E+00	2.20E+00	1.03E-12	7.24E-12	9.49E-12	1.96E-26
2.18E+00	2.03E-15	2.10E+00	2.20E+00	1.03E-12	7.24E-12	9.49E-12	1.93E-26
2.19E+00	3.39E-14	2.10E+00	2.20E+00	1.03E-12	7.24E-12	9.49E-12	3.22E-25
2.19E+00	5.67E-15	2.10E+00	2.20E+00	1.03E-12	7.24E-12	9.49E-12	5.38E-26

Table 4.8: Results of the simulations for the monoenergetic electrons in the of Y-90 decay spectra.

4.3.4.3 Q_C value

As stated in the previous section (Par.4.3), the value of Q_C is not a scope of this work and the dose rate coefficients $dote_{inh}$ with the relative Q value can be found in the ICRP119 publication [86].

$$\dot{e}_{inh} = 1.5\text{E-}09 \text{ Sv Bq}^{-1} \tag{4.30}$$

$$Q_C = 3.3\text{E+}01 \text{ TBq} \tag{4.31}$$

4.3.4.4 Q_D calculation

The method of calculation for the $\dot{h}_{skin}$ factor is the same that the one used for $\dot{e}_b$ with two main differences:

- The dose rate values for the single energy source are coming from a different geometry: in this case, indeed, the electron source is at contact with the skin, simulating a probability of handling or contact in accidental scenario;
- No Shielding Factor;
- the dose rates values must be normalized by the surface of the detector since the h_{skin} dimensions are $m^2 TBq^{-1} s^{-1}$.

The two components of the electron dose rate coefficient $\dot{h}_{skin}$ are:

$$h_{skin}^{mono} = 4.08\text{E-}06 \text{ Sv m}^2 \text{ TBq}^{-1} \text{ s}^{-1} \tag{4.32}$$

$$h_{skin}^{cont} = 3.769\text{E-}02 \text{ Sv m}^2 \text{ TBq}^{-1} \text{ s}^{-1} \tag{4.33}$$

The sum of the two factors is used for the Q_D calculation:

$$h_{skin} = h_{skin}^{mono} + h_{skin}^{cont} = 3.77\text{E-}02 \text{ Sv m}^2 \text{ TBq}^{-1} \text{ s}^{-1} \tag{4.34}$$

$$Q_D = 7.43\text{E-}01 \text{ TBq} \tag{4.35}$$

Monoenergetic Spectra

Energy [MeV]	**I** [part/(s MeV)]	E_{min} [MeV]	E_{max} [MeV]	**a** [Sv/(h MeV)]	**b** [Sv/h]	$\dot{D}_{I=100\%}$ [Sv/h]	$\dot{D}$ [Sv/h]
1.74E+00	1.02E-04	1.50E+00	2.00E+00	1.68E-13	2.01E-11	2.04E-11	2.07E-15
1.76E+00	1.10E-05	1.50E+00	2.00E+00	1.68E-13	2.01E-11	2.04E-11	2.24E-16
1.76E+00	1.94E-06	1.50E+00	2.00E+00	1.68E-13	2.01E-11	2.04E-11	3.95E-17
1.76E+00	3.36E-07	1.50E+00	2.00E+00	1.68E-13	2.01E-11	2.04E-11	6.85E-18
2.17E+00	1.72E-12	1.50E+00	2.00E+00	1.68E-13	2.01E-11	2.04E-11	3.51E-23
2.18E+00	1.86E-13	2.00E+00	2.50E+00	-1.21E-13	2.06E-11	2.04E-11	3.79E-24
2.18E+00	2.07E-15	2.00E+00	2.50E+00	-1.21E-13	2.06E-11	2.04E-11	4.21E-26
2.18E+00	2.03E-15	2.00E+00	2.50E+00	-1.21E-13	2.06E-11	2.04E-11	4.14E-26
2.19E+00	3.39E-14	2.00E+00	2.50E+00	-1.21E-13	2.06E-11	2.04E-11	6.91E-25
2.19E+00	5.67E-15	2.00E+00	2.50E+00	-1.21E-13	2.06E-11	2.04E-11	1.15E-25

Table 4.9: Results of the simulations for the monoenergetic electrons in the of Y-90 decay spectra due to the handling.

Continuum Spectra

Energy [MeV]	**I** [part/(s MeV)]	E_{min} [MeV]	E_{max} [MeV]	**a** [Sv/(h MeV)]	**b** [Sv/h]	$\dot{D}_{I=100\%}$ [Sv/h]	$\dot{D}$ [Sv/h]
6.00E-02	3.75E-01	6.00E-02	7.00E-02	7.70E-10	-4.59E-11	1.16E-13	3.49E-15
6.50E-02	3.79E-01	6.00E-02	7.00E-02	7.70E-10	-4.59E-11	1.58E-12	7.72E-15
7.00E-02	3.83E-01	7.00E-02	8.00E-02	1.13E-09	-7.08E-11	3.06E-12	1.93E-14
7.50E-02	3.86E-01	7.00E-02	8.00E-02	1.13E-09	-7.08E-11	5.27E-12	4.01E-14
8.00E-02	3.90E-01	8.00E-02	9.00E-02	8.93E-10	-5.22E-11	7.51E-12	7.21E-14
8.50E-02	3.94E-01	8.00E-02	9.00E-02	8.93E-10	-5.22E-11	9.34E-12	1.14E-13
9.00E-02	3.98E-01	9.00E-02	1.00E-01	4.65E-10	-1.37E-11	1.12E-11	1.66E-13
1.00E-01	4.05E-01	1.00E-01	1.20E-01	1.01E-10	2.27E-11	1.33E-11	2.88E-13
1.10E-01	4.12E-01	1.00E-01	1.20E-01	1.01E-10	2.27E-11	1.40E-11	4.24E-13
1.20E-01	4.20E-01	1.20E-01	1.40E-01	-4.42E-11	4.02E-11	1.46E-11	5.67E-13
1.30E-01	4.27E-01	1.20E-01	1.40E-01	-4.42E-11	4.02E-11	1.47E-11	7.14E-13
1.40E-01	4.34E-01	1.40E-01	1.60E-01	-7.69E-11	4.47E-11	1.47E-11	8.61E-13
1.50E-01	4.41E-01	1.40E-01	1.60E-01	-7.69E-11	4.47E-11	1.46E-11	1.01E-12
1.60E-01	4.48E-01	1.60E-01	1.80E-01	-6.11E-11	4.22E-11	1.45E-11	1.15E-12
1.80E-01	4.61E-01	1.80E-01	2.00E-01	-6.71E-11	4.33E-11	1.44E-11	1.44E-12
2.00E-01	4.74E-01	2.00E-01	2.20E-01	-5.69E-11	4.13E-11	1.42E-11	1.73E-12
2.20E-01	4.86E-01	2.20E-01	2.40E-01	-4.24E-11	3.81E-11	1.40E-11	2.01E-12

2.40E-01	4.98E-01	2.40E-01	2.60E-01	-3.99E-11	3.75E-11	1.39E-11	2.29E-12
2.60E-01	5.09E-01	2.60E-01	2.80E-01	-3.35E-11	3.58E-11	1.38E-11	2.57E-12
2.80E-01	5.19E-01	2.80E-01	3.00E-01	-2.87E-11	3.45E-11	1.37E-11	2.84E-12
3.00E-01	5.29E-01	3.00E-01	3.20E-01	-2.14E-11	3.23E-11	1.37E-11	3.11E-12
3.20E-01	5.39E-01	3.20E-01	3.40E-01	-2.08E-11	3.21E-11	1.37E-11	3.39E-12
3.60E-01	5.56E-01	3.60E-01	3.80E-01	-1.51E-11	2.99E-11	1.36E-11	3.93E-12
4.00E-01	5.71E-01	4.00E-01	4.50E-01	-1.42E-11	2.96E-11	1.37E-11	4.48E-12
4.50E-01	5.87E-01	4.50E-01	5.00E-01	-1.15E-11	2.84E-11	1.36E-11	5.16E-12
5.00E-01	6.00E-01	5.00E-01	5.50E-01	-7.11E-12	2.62E-11	1.36E-11	5.84E-12
5.50E-01	6.10E-01	5.50E-01	6.00E-01	-7.40E-12	2.64E-11	1.36E-11	6.53E-12
6.00E-01	6.18E-01	6.00E-01	6.50E-01	-7.99E-12	2.67E-11	1.36E-11	7.21E-12
6.50E-01	6.24E-01	6.50E-01	7.00E-01	-2.02E-12	2.29E-11	1.34E-11	7.88E-12
7.00E-01	6.27E-01	7.00E-01	7.50E-01	-1.92E-12	2.28E-11	1.35E-11	8.55E-12
7.50E-01	6.29E-01	7.50E-01	8.00E-01	-3.17E-12	2.37E-11	1.34E-11	9.23E-12
8.00E-01	6.29E-01	8.00E-01	8.50E-01	-3.27E-12	2.38E-11	1.33E-11	9.89E-12
8.50E-01	6.28E-01	8.50E-01	9.00E-01	5.64E-13	2.06E-11	1.32E-11	1.06E-11
9.00E-01	6.25E-01	9.00E-01	9.50E-01	-5.25E-12	2.58E-11	1.32E-11	1.12E-11
1.00E+00	6.14E-01	1.00E+00	1.50E+00	-7.72E-13	2.15E-11	1.27E-11	1.25E-11
1.10E+00	5.98E-01	1.00E+00	1.50E+00	-7.72E-13	2.15E-11	1.23E-11	1.38E-11
1.20E+00	5.76E-01	1.00E+00	1.50E+00	-7.72E-13	2.15E-11	1.18E-11	1.50E-11
1.30E+00	5.47E-01	1.00E+00	1.50E+00	-7.72E-13	2.15E-11	1.12E-11	1.61E-11
1.40E+00	5.10E-01	1.00E+00	1.50E+00	-7.72E-13	2.15E-11	1.04E-11	1.72E-11
1.50E+00	4.65E-01	1.50E+00	2.00E+00	1.68E-13	2.01E-11	9.44E-12	1.82E-11
1.60E+00	4.11E-01	1.50E+00	2.00E+00	1.68E-13	2.01E-11	8.35E-12	1.91E-11
1.80E+00	2.77E-01	1.50E+00	2.00E+00	1.68E-13	2.01E-11	5.64E-12	2.05E-11
2.00E+00	1.28E-01	2.00E+00	2.50E+00	-1.21E-13	2.06E-11	2.60E-12	2.13E-11
2.20E+00	1.40E-02	2.00E+00	2.50E+00	-1.21E-13	2.06E-11	2.86E-13	2.16E-11
2.28E+00	0.00E+00	2.00E+00	2.50E+00	-1.21E-13	2.06E-11	0.00E+00	2.16E-11

Table 4.10: Results of the simulations for the continuum beta spectra of Y-90 for the skin dose due to the handling.

4.3.4.5 Conclusions on the Y-90 example

The Tab.4.11 helps to compare the value from the Regulation with the one found applying the Monte Carlo method.

- The Q_A value resulting from the MC method is almost three orders of magnitude higher then the one found in the Regulation. The reason may be linked to a limiting factor of 1.0E+03 TBq for

	$\mathbf{Q}_A$	$\mathbf{Q}_B$	$\mathbf{Q}_C$	$\mathbf{Q}_D$	$\mathbf{A}_1$	$\mathbf{A}_2$
	[TBq]					
IAEA	1.0E+03	3.2E-01	3.3E+01	5.9E-01	3.0E-01	3.0E-01
MCNPX	8.2E+05	2.7E-01	3.3E+01	7.4E-01	2.7E-01	2.7E-01

Table 4.11: Comparison between the Q-values of the Regulation and the ones coming from the MC method. Rounded method is applied.

activity to transport for gamma emitters (not explicitly reported in the methodology described in [76] and used also for the other Q values).

- The Q_B and Q_D values are in the same order of magnitude than the tabulated ones. the gap is lower than the 30% of the IAEA values.
- The A_1 and A_2 values are defined by the Q_B, the minor among the Q values, both in the case of the IAEA and the Monte Carlo method.

4.3.5 Results of the A_1 and A_2 limit with the Monte Carlo technique

The entire set of results of the Monte Carlo method described in the previous paragraph are summarized in the Tab.4.13, Tab.4.14 and Tab.4.15 , reporting respectively the dose rate coefficients $\dot{e}_p$, $\dot{e}_b$, h_{skin}, $\dot{e}_d$, the relative Q values and the A_1 and A_2 limits compared with the ones specified in the IAEA Safety Guide. Three graphs can be useful to visually compare the Monte Carlo sets of data with the Regulatory ones and make some conclusions.

Results of the control group

The first 10 cases represent what we called the *control group*, for which the IAEA values are available and tabulated. The two graphs in Fig.4.9 report the ratio between the MC simulated values and the IAEA tabulated. As we can observe, there is a good agreement between the results of the Monte Carlo simulations and the listed factors both in the calculation for A_1 and A_2 (the ratio is almost 1 in all the cases). There are two exceptions:

1. The exception for A_1 is represented by the case of Ca-47 for which the recalculated value is smaller than the one in the Regulation. The explanation is found in the different $\dot{e}_b$ dose coefficients. A reason for this discrepancy could be the use of different nuclear data sets for the beta decay of this radionuclide and the daughter included in the calculation (Sc-47).
2. An exception for A_2 seems to be represented by the case of Be-7. As said previously, the A_2 value is given by the minor of all the Q values. In the case of the Monte Carlo method, the limiting factor for the Be-7 is imposed by the Q_D value, almost two orders of magnitude lower than the tabulated one.

Be-7	$\mathbf{h}_{skin}$ [Sv m^{-2} TBq^{-1} s^{-1}]	$\mathbf{Q}_D$ [TBq]
IAEA	2.80E-05	1.0E+03
MCNPX	9.64E-03	2.90E+00

Actually in the Regulation it is assumed that if Q_D results to be a value higher than 10^3 TBq, Q_D shall be limited to 10^3 TBq. Applying this rules, the A_2 for Be-7 becomes limited by the gamma dose rate coefficient and equal to: 2.09TBq.

The MC method is able to well reproduce the scenarios, the hypothesis and mostly the physics behind the Regulation. Moreover those results allowed us to validate the MC simulation codes and apply them to obtain a dataset of A_1 and A_2 values for those radionuclides presenting generic transport limits. The relative errors of the simulations are always lower than 1% (statistical error) and not reported in the tables and the graph.

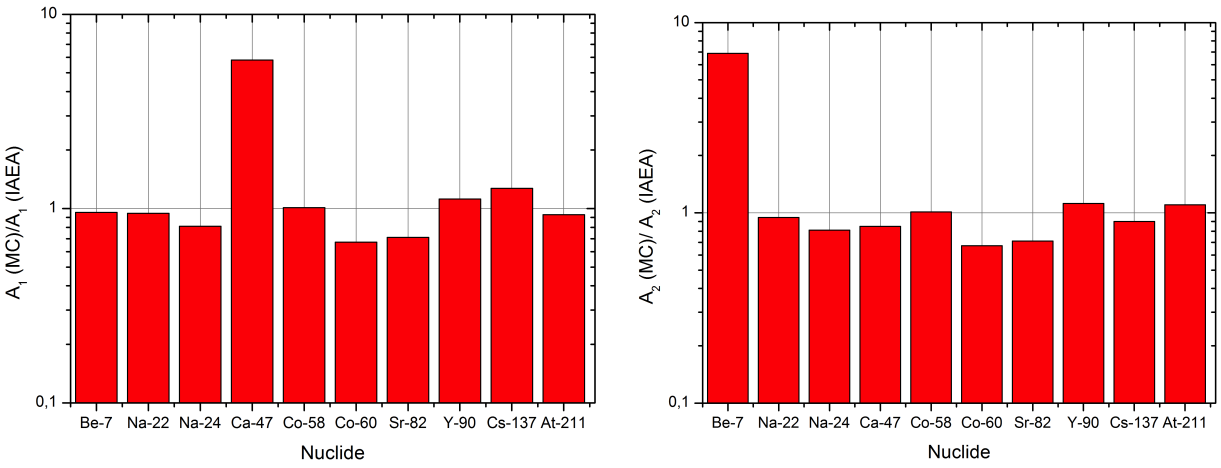

Figure 4.9: Ratio between the simulated values and the tabulated ones for A_1 (right) and A_2 (left) for the isotopes in the control group.

Results and the comparison for electrons emitters

The generic value imposed by the Regulation [39] for beta emitters is 0,1 TBq for A_1 and 0,02 TBq for A_2 (Fig.4.10).

- The case of the A1 values, we can observe that the Monte Carlo method does not involve a big increase of those limits. Among the cases examined, only for Cu-61, As-71, Tb-161 and Tb-155 an increase in the limit of one order of magnitude is observed, while in the remaining cases the increase is maximum of a factor 6.
- The gap between the regulatory values and the simulated ones is more evident in the case of the A2 data sets. In all the cases analyzed, in fact, the results of the MC method allow, an increase of the Transport limit of one or, in some cases (as for the Tb-155), two orders of magnitude.

Results and the comparison for alpha emitters

For the two alpha emitters with generic transport limits, Tb-149 and Bi-213:

	$\mathbf{A_1/A_2}$ [TBq]
Tb-149	8.56E-01
Bi-213	4.54E-01

- the A_1 limits are respectively 2 and 4 times higher than the generic one (2.0E-01 TBq);
- the recalculated A_2 values are four orders of magnitude higher than what prescribed by the Regulation (9E-05 TBq)
- in the case of Tb-149 the limiting value is coming from the Q_A, the dose from gamma source exposure.
- for Bi-213, instead, the lower of the Q values is the Q_B, due to the beta dose to the skin.

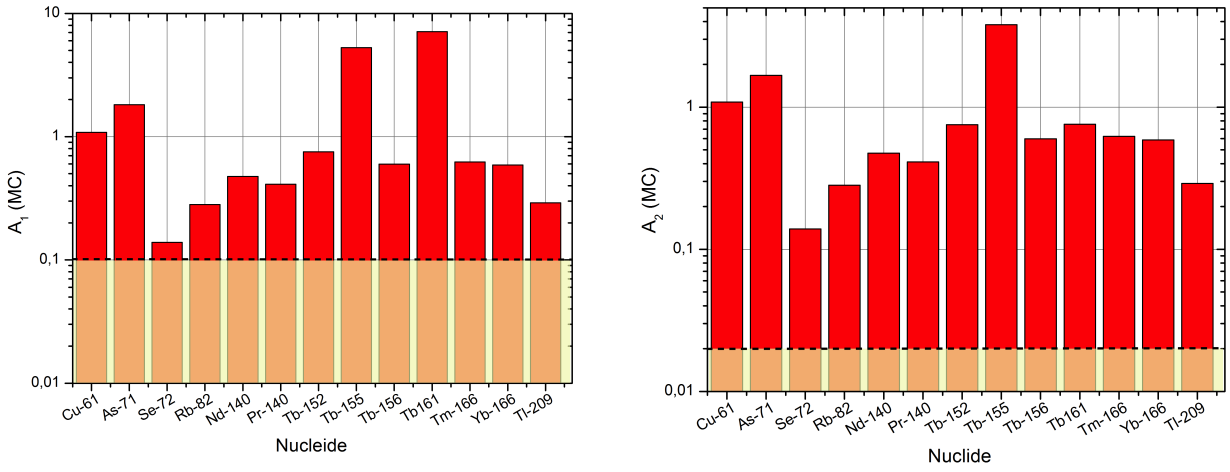

Figure 4.10: Simulated values with the Monte Carlo technique (MC) for A_1 (right) and A_2 (left) compared with the values of the Regulation (yellow rectangle) for the electron emitters.

Comparison with other dataset

The values listed in the previous tables are also in good agreement with the ones obtained, for the same group of isotopes, from a working group of the Radiation Protection group at CERN. The main differences with the present study is the use of Fluka as the Monte Carlo software used for the calculations [89] and geometrical structures without a spherical symmetry. The basic principles of calculations remain the same. Some examples are reported in the Tab.4.12. They are relative to the dose rate coefficients due to the beta particles $\dot{e}_b$ and $\dot{h}_{skin}$.

Isotope	$\dot{e}_b$ [Sv $Bq^{-1}h^{-1}$]		$\dot{h}_{skin}$ [Sv $m^{-2}TBq^{-1}s^{-1}$]	
	MCNPX	FLUKA	MCNPX	FLUKA
Co-60	3.32E-15	3.28E-15	3.03E-02	2.92E-02
Tb-149	4.17E-13	3.94E-13	1.21E-02	1.27E-02
Tm-166	8.87E-14	8.51E-14	1.65E-02	1.24E-02
Bi-213	2.2E-12	1.63E-12	8.42E-02	8.82E-02

Table 4.12: Results of the $\dot{e}_b$ and $\dot{h}_{skin}$ dose coefficients from the Monte Carlo method with MCNPX and FLUKA.

	Radionuclide	Daughter	Decay mode	$\dot{e}_{pt}$		e_b		e_{inh}		h_{skin}	
				Sv $Bq^{-1}h^{-1}$		Sv $Bq^{-1}h^{-1}$		Sv Bq^{-1}		Sv $m^{-2}TBq^{-1}s^{-1}$	
				MCNPX	IAEA	MCNPX	IAEA	MCNPX	IAEA	MCNPX	IAEA
Control Group	Be-7		EC	4.78E-15	4.80E-15	5.48E-19	1.00E-15	5.20E-11		9.64E-03	2.80E-05
	Na-22		EC B+	1.89E-13	2.00E-13	3.69E-13	2.60E-13	2.00E-09		4.02E-02	4.20E-02
	Na-24		B-	2.87E-13	3.30E-13	4.05E-12	5.00E-12	2.90E-10		3.99E-02	4.70E-02
	Ca-47	Sc-47	B-	9.61E-14	3.70E-14	1.94E-12	2.70E-14	2.83E-09		7.92E-02	8.40E-02
	Co-58		EC B+	1.01E-13	9.10E-14	1.12E-14	1.30E-15	2.00E-09		6.97E-03	7.40E-03
	Co-60		B-	1.68E-13	2.20E-13	3.32E-15	1.40E-15	2.90E-08		3.03E-02	2.90E-02
	Sr-82	Rb-82	EC	1.05E-13	1.00E-13	3.55E-12	4.20E-12	1.00E-08		6.97E-02	4.70E-02
	Y-90		B-	1.22E-19	1.00E-16	3.73E-12	3.10E-12	1.60E-09		3.77E-02	4.70E-02
	Cs-137	Ba-137m	B-	6.36E-14	5.60E-14	4.02E-13	1.20E-13	4.80E-09		4.20E-02	4.40E-02
	At-211	Po-212	A EC	4.65E-15	4.00E-15	6.42E-15	1.00E-15	1.10E-07		1.20E-04	6.30E-05
Other Radionuclides	Cu-61		EC B+	8.90E-14	-	9.21E-13	-	1.20E-10	-	2.50E-02	-
	As-71		EC B+	5.51E-14	-	9.15E-14	-	5.00E-10	-	1.67E-02	-
	Se-72	As-72	EC	1.64E-13	-	7.20E-12	-	9.20E-10	9.20E-10	6.72E-02	-
	Nd-140	Pr140	EC	3.17E-15	-	2.11E-12 -	-	-	-	1.92E-02	-
	Tb-152		EC B+	1.26E-13	-	1.33E-12	-	-	-	9.98E-03	-
	Tb-155		EC	1.90E-14	-	8.06E-16	-	2.50E-10	-	7.36E-03	-
	Tb-156		EC	1.67E-13	-	3.09E-14	-	1.40E-09	-	2.27E-02	-
	Tb161		B-	1.41E-14	-	5.37E-15	-	1.20E-09	-	3.69E-02	-
	Tm-166		EC B+	1.61E-13	-	8.87E-14	-	2.80E-10	-	1.65E-02	-
	Yb-166	Tm-166	EC	1.70E-13	-	9.77E-14	-	1.19E-09	-	1.96E-02	-
	Tb-149		EC B+ A	1.17E-13	-	4.17E-13	-	3.10E-09	-	1.21E-02	-
	Bi-213	Po-213.Tl-209	EC B+ A	1.89E-13	-	2.20E-12	-	4.10E-08	-	4.55E-02	-

Table 4.13: Results of the dose coefficients obtained with the Monte Carlo method. The IAEA values for the different radionuclides are also listed [76].

	Radionuclide	Q_A		Q_B		Q_C		Q_D	
		TBq							
		MCNPX	IAEA	MCNPX	IAEA	MCNPX	IAEA	MCNPX	IAEA
Control Group	Be-7	2.09E+01	2.10E+01	1.82E+06	1.00E+03	9.62E+02		2.90E+00	1.00E+03
	Na-22	5.29E-01	5.00E-01	2.71E+00	3.80E+00	2.50E+01	3.85E+01	6.96E-01	6.50E-01
	Na-24	3.48E-01	3.00E-01	2.47E-01	2.00E-01	1.72E+02	1.70E+02	7.02E-01	6.00E-01
	Ca-47	1.04E+00	2.70E+00	5.16E-01	3.70E+01	1.77E+01	2.00E+01	3.54E-01	3.30E-01
	Co-58	9.89E-01	1.10E+00	8.95E+01	7.80E+02	3.57E+01	2.50E+01	4.01E+00	3.80E+00
	Co-60	5.95E-01	4.50E-01	3.01E+02	7.30E+02	2.07E+00	1.70E+00	9.23E-01	9.70E-0
	Sr-82	9.53E-01	9.70E-01	2.82E-01	2.40E-01	5.00E+00		4.02E-01	5.90E-01
	Y-90	8.21E+05	1.00E+03	2.68E-01	3.20E-01	3.30E+01		7.43E-01	5.90E-01
	Cs-137	1.57E+00	1.80E+00	2.49E+00	8.20E+00	7.46E+00	1.00E+01	6.66E-01	6.30E-01
	At-211	2.15E+01	2.50E+01	1.56E+02	1.00E+03	4.55E-01	5.10E-01	2.33E+02	4.40E+02
Other Radionuclides	Cu-61	1.12E+00	-	1.09E+00	-	4.17E+02	-	1.12E+00	-
	As-71	1.82E+00	-	1.09E+01	-	1.00E+02	-	1.67E+00	-
	Se-72	6.09E-01	-	1.39E-01	-	5.43E+01	5.10E-01	4.17E-01	-
	Nd-140	3.16E+01	-	4.75E-01	-	-	-	1.46E+00	-
	Tb-152	7.94E-01	-	7.53E-01	-	-	-	2.81E+00	-
	Tb-155	5.27E+00	-	1.24E+03	-	2.00E+02	-	3.81E+00	-
	Tb-156	5.99E-01	-	3.24E+01	-	3.57E+01	-	1.23E+00	-
	Tb161	7.11E+00	-	1.86E+02	-	4.17E+01	-	7.58E-01	-
	Tm-166	6.23E-01	-	1.13E+01	-	1.79E+02	-	1.70E+00	-
	Yb-166	5.88E-01	-	1.02E+01	-	4.20E+01	-	1.43E+00	-
	Tb-149	8.56E-01	-	2.40E+00	-	1.61E+01	-	2.31E+00	-
	Bi-213	5.29E-01	-	4.54E-01	-	1.22E+00	-	6.15E-01	-

Table 4.14: Results of the Q values obtained using the simulated dose rate coefficients and the ones listed in the IAEA Safety guide [76].

	Radionuclide	A_1		A_2	
		TBq			
		MCNPX	**IAEA**	**MCNPX**	**IAEA**
Control Group	Be-7	2.09E+01	2.00E+01	2.90E+00	2.00E+01
	Na-22	5.29E-01	5.00E-01	5.29E-01	5.00E-01
	Na-24	2.47E-01	2.00E-01	2.47E-01	2.00E-01
	Ca-47	5.16E-01	3.00E+00	3.54E-01	3.00E-01
	Co-58	9.89E-01	1.00E+00	9.89E-01	1.00E+00
	Co-60	5.95E-01	4.00E-01	5.95E-01	4.00E-01
	Sr-82	2.82E-01	2.00E-01	2.82E-01	2.00E-01
	Y-90	2.68E-01	3.00E-01	2.68E-01	3.00E-01
	Cs-137	1.57E+00	2.00E+00	6.66E-01	6.00E-01
	At-211	2.15E+01	2.00E+01	4.55E-01	5.00E-01
Other Radionuclides	Cu-61	1.09E+00	1.00E-01	1.09E+00	2.00E-02
	As-71	1.82E+00		1.67E+00	
	Se-72	1.39E-01		1.39E-01	
	Nd-140	4.75E-01		4.75E-01	
	Tb-152	7.53E-01		7.53E-01	
	Tb-155	5.27E+00		3.81E+00	
	Tb-156	5.99E-01		5.99E-01	
	Tb161	7.11E+00		7.58E-01	
	Tm-166	6.23E-01		6.23E-01	
	Yb-166	5.88E-01		5.88E-01	
	Tb-149	8.56E-01	2.00E-01	8.56E-01	9.00E-05
	Bi-213	4.54E-01		4.54E-01	

Table 4.15: Results of the A1 and A2 values obtained with the MC method compared with the ones listed in the IAEA Safety guide [76].

4.4 Conclusions and Future perspectives

The value of activity to transport, different for each radionuclide, is the quantity defining the type of package to use for transport.
The International Atomic Energy Agency established a method, the so-called Q-system, based on different kind of expositions during an accident involving the damage of a transport container.
Those values are most of the time general and not based on specific calculations. Moreover the nuclear data refers to not updated database and references to the used ones are difficult to identify.
The use of the Monte Carlo method for the evaluation of the transport limit A_1 and A_2 based on the *Q-system* as set by IAEA have been described in this chapter. It has been used as a basis of an alternative method of calculation making use of Monte Carlo techniques and in particular of the software MCNPX to evaluate dose rate parameters in specific scenarios.
The strength of this method relies on the possibility to include in the calculations, all the phenomena and the effects linked to the particle interaction with matter. Moreover the recent nuclear data sets are used for the calculations.
This method has been validated with a control group of nuclides with known/tabulated Q values. The results of the simulations, also in agreement with the ones obtained by other working groups, would allow an increase of the generic tabulated values.
The increase of such limits would affect the choice of the type of transport package, allowing the use of more compact and cheaper containers, like type A. On the other hand it adds knowledge on the effective dose rate values, and then the hazard, associated to a single radionuclide, avoiding the use of generic common limits.

A future development and improvement of these calculations must include Monte Carlo simulations to quantify the alpha emitter's hazard (for the Q_C evaluation) and a study of the dose due to the submersion accidental scenario (for the calculation of Q_E) in case of gaseous sources. This may be done including in the simulations the information on the ICRP human phantom.
Additional study is needed also to better determine the Shielding Factor included in the Q_B calculations and in particular the geometry and the material composing the shield associated to this calculation.

Conclusions

Nuclear medicine has been developed over the past years through a unique partnership among the national laboratories, academia, and industry. The innovations goes parallely to the collaboration and the development of particle accelerators and techniques of radionuclides production, chemical processes to synthesize radiopharmaceuticals and instruments that can detect the radiation emitted from the radionuclides accumulated in the human body.
The progress has to be followed also by the identification of new techniques and devices that allow the protection of the public and the workers during the activities of radionuclides production.

For example a fast, but especially safe, connection between the different places of production and usage of the radionuclides shall be put in place. This is even more important when high activity (and than high hazard) has to be manipulated.
This is the case of the packages used for the transport, whose design is highly regulated.
One of the objective of this PhD thesis has been the design of a new container for the transport of medical radionuclides following the prescription of the International Atomic Energy Agency (IAEA).
The new package has been named ColiBRI-30 (Colis type B pour RadioIsotopes). It is a type B(U) package, suitable for the transport of activities higher then the limits imposed by the regulation for type A.
It differentiates from the other type B containers by its reduced dimensions and weight.Those characteristics make it suitable for the manipulation in environments like radiopharmacies or production laboratories.
It is composed by a shielded core (3 cm tungsten) and an overpack with overall dimensions 600 mm diameter and 700 mm height and its total weight is 113 kg. The removable core insures a good protection for high activity sources while the overpack has the scope to protect them from the effect of high temperature and mechanical shocks.
The design, presented in the Chapter 3, has been the result of a well defined path. It started with the identifications of all the specifications and the requirements the container must comply with. Some of them are coming from the regulation, while others, like the limit in weight and dimensions have been chosen by us to facilitate the user's activities.
Then an iterative process making use of finite element analysis techniques has been used to define the right compromise in between the materials and the chosen shape of the package and its performances in order to make sure it will pass the regulatory test.
It is an excellent technique that allows the parallel study and benchmarking of different design, avoiding the waste of budget for the realization of prototypes and tests.
The test in silico performed on the ColiBri30 shows that the source remains protected inside the shielded core in all the tested conditions. Moreover the FEA has been used to define the limit of the activity it is possible to transport considering the heat generated by the decay. In this way both the package and the source keep their integrity for all the duration of the travel.
Two prototypes have been realized and are ready to be tested. In particular, the configuration leading to the virtual maximum damages will be reproduced experimentally.
The process of homologation started with the preparation of the safety reports and the technical description of the test to submit to the Autorité de Sûreté Nucléaire (ASN).

As said, the process of the transport of radioactive material is highly regulated and limits of activity to transport with specific types of packages for each radionuclides have been set. Those values are called A_1 and A_2 and are calculated through the co-called "Q-system". It is a method that associates to five values, the Qs, the hazard of the different types of radiation and in different accidental scenarios.

The limit of transport is given by the lower of those calculated Qs.
For some radionuclides the A_1/A_2 limits are not tabulated and generic ones (low values) are used, not reflecting their real hazard.
In this PhD work, Monte Carlo calculations have been done to evaluate the dose rate coefficients to insert in the Q system formulae.
The method has been applied to a list of radionuclides of interest for nuclear medicine, but it is of wider application.
It reveals the possibility to increase the limits from a factor two to several orders of magnitudes, depending on the radionuclide under study.
This will have consequences on the choice of the package to use for the transport. Increase the A_1/A_2 limits can result in the use of type A packages for the transport instead of type B, more complex and expensive.

The work with radioactivity leads to additional safety constraints not only during the activities of collection, shipment and chemical treatment, but also at the end of the cycle. This is due to the activation of the materials exposed in irradiation bunkers or used for the manipulation and the treatment of irradiated targets. They must be treated as radioactive waste when not reusable.
The management and the storage follow the rules identified by each specific country. In France the ANDRA Institution is in charge of the identification of the methodology and to set up storage facilities.
The first step to do in the field of the waste management is the identification of the radionuclides present in the waste and the definition of their activities. These two factors will characterize the type of waste and then the decision to sort it in specific centers.
The software ActiWiz, developped at CERN, has been used in this work to study the activation of mechanical parts present in one of the ARRONAX bunkers. It has been customized with seven new irradiation scenarios simulating the radiation field in different position with respect to the irradiated target.
The parameter to give in input to the software are: irradiation and cooling time, beam intensity and chemical composition of the materials. Their identification may not be an easy task. Indeed, except for the objects (as rabbits) used for only one irradiation, it is then necessary to retrieve the history of the object from logbook or maintenance reports.
Moreover the sample can be composed by several parts with different materials, contributing in different ways to the dose rate.
To overcome these difficulties, hypothesis must be made both on the shape and on the material composing the samples to study with the help of gamma spectra.
Two of the new radiation fields have been tested:

- the one for an object placed at 10 cm from the target: benchmarked with the experimental analysis of a rabbit;
- the one at 1 m aside the target: tested with the comparison of a batch of vacuum connectors and a rod piston.

With some hypothesis on the volume and the materials of the samples, it has been possible to obtain with ActiWiz a list of radionuclides that reflects the results of the gamma spectra acquired experimentally. Moreover the software provides in the list also pure beta emitters, not easily detectable.
The software has been used to make predictions on the dose rate and the radionuclides produced after an irradiation/cooling cycle. For the three analyzed objects the experimental ambient dose rate values are of the same order of magnitude as the simulated ones. In the case of study of the rabbit, the device

used for the target irradiation, the additional contribution from the direct interaction of the beam is necessary to simulate the activation of the beam window from the proton interaction. In this case the general fluence calculation result does not fit with real fluence seen by experiment. The new scenarios, indeed, reproduce only the radiation field coming from the secondary particles produced in the target. In this context possible improvements have been identified. Among them the possibility to introduce well known material in several positions of the bunker and study their activation with the software. This will help to obtain more statistics for the validation of the new scenarios without the problematic associated to the material (and volume) identification.
Moreover the other irradiation scenarios shall also be tested with new experimental analysis. This will help in setting a list of possible beam configurations, materials and geometries that well fit the real values.
Once the method is validated, it can be presented to ANDRA and used as tool for the ARRONAX waste management.

Appendices

A

The Isotope's collection: a study on the MEDICIS collection point

Contents

A.1 The CERN-MEDICIS facility 184
A.2 The Isotope collection in MEDICIS 185
A.2.1 The main principles/ ideas 185
A.3 The original project 188
A.3.1 The layout 188
A.4 The actual system 192
A.5 Conclusions 194

The first step involved in a radiopharmaceutical production is the collection of the specific radioisotope. Depending on the reaction producing it and the primary particles energy and type, the site of the production may vary.
In the first months of this PhD project, the joint research group of the Lemer Pax Company and Arronax has been involved in the realization of the CERN-MEDICIS collection point in collaboration with the Engineering department at CERN.

Besides proper engineering set-up to assure the good physical conditions for the experiments, the design of dedicated collection stations shall take into account radioprotection principles. This can be done in two ways:

1. By including tools and devices that limit the (direct) manipulations or that increase the distance between the operator and the source;
2. By reducing the ambient dose rate using proper shielding depending on the type of radiation involved.

A specification document containing the details and the basic steps of the collection procedures has been produced [90]. It contains also details on the vacuum, the electrical connections, beam instrumentation and ideas on the connection/interfaces with the other devices.
The project, presented in the following paragraphs, has been later replaced by a "simpler" device manually driven due to budgetary issues and to the needs to speed up the manufacturing procedures. The basic conceptual design remained the same.
This chapter will give an overview of the MEDICIS facility followed by the fundamental characteristics and original specifications of the collection system. The behavior of the actual device is also presented.

A.1 The CERN-MEDICIS facility

The MEDICIS facility is a brand new (2014) off-line separator built at CERN in the area behind the older ISOLDE facility (in operation since the 1991) [91].
The name is an acronym revealing its scopes and its connection with ISOLDE: MEDical Isotopes Collected from ISOLDE. Both facilities are integrated into the CERN accelerator complex as shown in Fig.A.1.

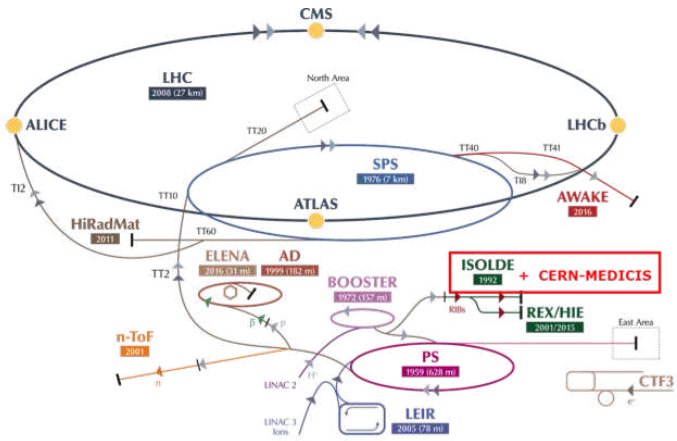

Figure A.1: The CERN accelerator complex with the MEDICIS position.

ISOLDE (Isotope Separator Online DEvice) uses the bunched, 1.4 GeV proton beam provided by the CERN Proton Synchrotron Booster (PSB) as a driver beam to produce radioactive nuclides by spallation, fragmentation and fission reactions [92]. The proton beam is sent towards two identical target front-ends.They are coupled to two magnetic mass separators, the so-called General Purpose Separator (GPS, composed by one magnet) and the High Resolution Separator (HRS, with two subsequential magnets), arranged such that the beam from either machine can be fed into a common beam distribution system to which almost all of the experiments (in the experimental hall) are connected.

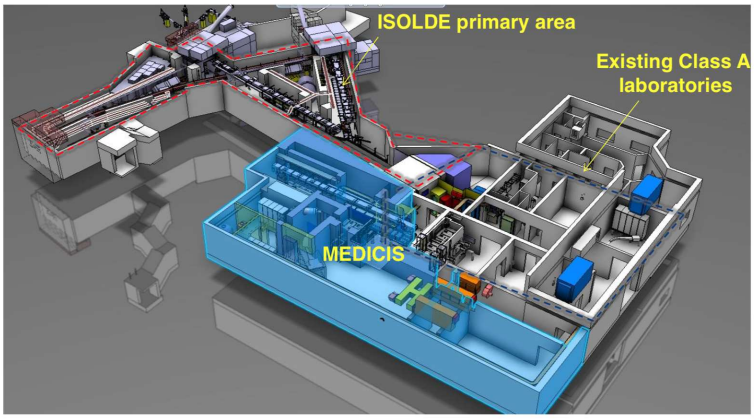

Figure A.2: Layout of the MEDICIS building connected to the pre-existing Isolde facility [93].

ISOLDE receives about 50% of all CERN protons, and from these, about 85% traverse the ISOLDE

target without any interaction. The idea originating the project of a new facility relies on the possibility to use this lost beam taking advantage of the fact that a large part of its characteristics remain intact. To achieve this, an irradiation point dedicated to CERN-MEDICIS has been installed in the ISOLDE target area, between the HRS Front-End and the beam dump.
Nowadays the MEDICIS target station is receiving less than $1.5x10^{20}$ protons per year at 1.4 GeV. In the upgraded beam version (2.0 GeV, 6 μA) each CERN-Each MEDICIS target sample is expected to receive about $6x10^{20}$ protons per year, increasing production rates by at least a factor of three compared to the facility at start-up.
After irradiation, the CERN-MEDICIS target is transported into the extension area by a rail conveyor system (in 10 min). The target is placed in a shielded decay and monitoring area, for a suitable time, depending on the type of target and isotope to be extracted. It is then either directly coupled to the CERN-MEDICIS mass separator in the bunker or first transferred in a dedicated hot cell for a fast chmical preparation before starting the batch extraction. A remotely controlled robotic arm helps to move or manipulate the target.
The secondary beam can be extracted heating up the target, separated through the magnetic mass separator and finally collected (Fig.A.3).

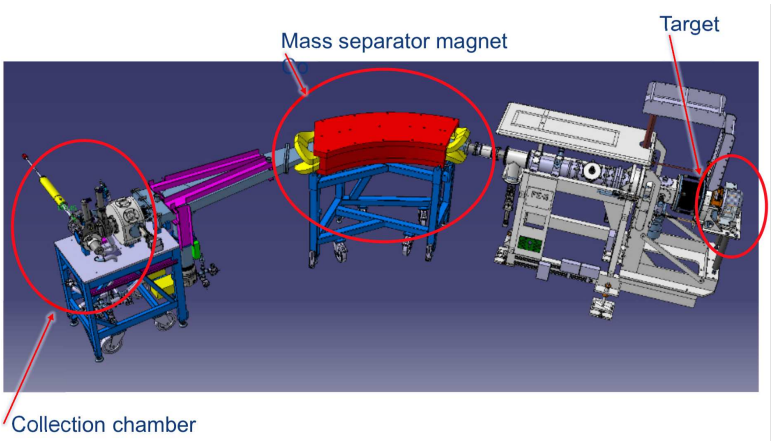

Figure A.3: Drawing of the principal elements of the MEDICIS beamline: the frontend assembly with the target, the separator magnet and the collection point [93].

The composition and characteristics of the secondary beam will depend on the material of the target, the ion source, the aging of the unit and the characteristics of the primary beam with which it was irradiated.
The Table A.1 gives some examples of isotopes that could be produced at CERN-MEDICIS with the current target design [91]. This list is not exhaustive and could evolve following the requests of the CERN-MEDICIS collaboration and endorsement by CERN.

A.2 The Isotope collection in MEDICIS

A.2.1 The main principles/ ideas

After the magnetic mass separation, the isotopes are implanted in solid samples in form of metallic or polymeric thin foils. In most of the cases they are gold foils coated with zinc (Fig.A.4).

The reason of this choice is connected to the subsequential chemical treatment of the irradiated samples: the zinc coated foils are washed with acid that will dissolve only the coating, leaving the gold

Medical Application	Isotope	Half-life	Parent isotope	In-target Activity [Bq]	Extracted Activity [Bq]
α, β- therapy, SPECT, dosimetry	Bi-213	45.6m	Ac -225	2.8E+08	2.8E+07
α, β therapy	Bi-212	60.6m	Ac-224	1.7E+09	1.7E+08
β therapy	Lu-177	6.7d	Lu -177	6.4E+08	6.4E+06
Auger therapy	Yb-166	56.7h	Yb-166	4.1E+010	2.1E+09
β therapy	Ho-166	25.8h	Ho-166	9.6E+06	4.8E+05
β-, Auger therapy	Tb -161	6.9d	Tb-161	1.9E+07	9.5E+05
β -, therapy	Tb-156	5.35d	Tb-156	5.5E+07	5.5E+05
SPECT	Tb-155	5.33d	Dy/Tb-155	5.3E+09	5.3E+07
β therapy	Sm-153	46.8h	Sm-153	2.8E+09	1.4E+08
PET,CT	Tb-152	17.5h	Dy/Tb-152	3.7E+10	3.7E+08
α therapy	Tb-149	4.1h	Tb-149	3.8E+10	3.8E+08
PET,Auger therapy	Nd-140	3.4d	Nd-140	1.2E+10	6.0E+08
β- therapy	Sr -89	50.5d	Sr-89	2.0E+09	1.0E+08
PET	Sr-82	25.5d	Sr-82	1.7E+09	8.5E+07
β- therapy	As-77	38.8h	As-77	5.8E+09	2.9E+08
PET	As -74	17.8d	As-74	3.8E+08	1.9E+07
PET	As-72	26.0d	As-72	9.1E+09	4.6E+08
PET	As-71	65.3h	As-71	5.9E+09	3.0E+08
β therapy	Cu-67	61.9h	Cu-67	1.5E+09	1.1E+08
PET, dosimetry, therapy	Cu-64	12.7h	Cu-64	7.1E+09	3.6E+08
PET	Cu-61	3.3h	Cu-61	5.1E+09	2.6E+08
β therapy	Sc-47	3.4d	Sc-47	4.2E+10	2.1E+09
PET	Sc-44	4.0h	Sc-44	5.7E+10	2.9E+09

Table A.1: Examples of the radionuclides that will be produced and collected at the CERN-MEDICIS facility [91].

intact. The latter can then be re-used for other collections. The liquid solution, instead, shall undergo a chromatographic process to clean all the contaminants.
The irradiated samples can be transferred to the CERN-MEDICIS laboratory for the chemical separation process (the lab is placed next to the experimental hall) or they can be directly shipped to the partners laboratories. To ease this process, the isotope collection system is a device equipped with a shielded transfer box to move the radioactive samples from the irradiation area to the glovebox.

The samples to irradiate in MEDICIS are three: one to be used for the beam tuning and two for



Figure A.4: Gold foils used for the collection in MEDICIS [photo: R. Formento].

the collection of specific radionuclides. They have identical size (about 1x1 cm) and they are placed on one sample holder, a thin stainless steel plate.
The main working principle of the collection system is the following. A mechanical arm is used to move (sliding) the samples in the correct position for the irradiation. After the collection, the samples are inserted in a transportation box that can be disconnected to the beamline and brought to the glovebox. This last step is done using a customized shielded cart.
The samples are not the only elements to use for a proper collection, but the objects to place inside the collection chamber are (in order, along the beam direction):

1. A Collimator: used to narrow the radionuclides beam. It is the first element along the line of the beam and it will receive around the 10% of the total primary particles;
2. Electron deflector plate (EDP),

The collimator and the EDP have three holes, one for each sample, that can vary in dimensions depending on the experiment and the type of collection to carry on.
The three elements are connected through electrical feedthroughs for polarization and current measurements. Moreover they are connected to a common base (in polyether ether ketone - PEEK - for the electrical isolation) to be moved together/simultaneously by the sample moving system.
After the collection, as previously said, the ensemble of the three plates will be recovered in a collection box.
In other words, the displacement of the mechanical arm connected to the base along a linear axis has two main functions:

1. places the three samples in the irradiation positions and move them through the different chambers
2. to lock the sample holder in the transport container.

The closure of the transport container is managed thanks to the shape of the sample holder base. The top part of the sample holder takes the function of the cap of the transport container. The design of the transport container must ensure that the closure is air tight. Since the container is closed under vacuum, a venting valve is necessary to vent it before recovering samples inside the glovebox.
A transfer trolley moved manually equipped with a shielded transfer box is used to move the sample from the isotope collection system to the glovebox placed in the MEDICIS lab.
A peripheral shielding lead wall surrounds the entire collection area to ensure an optimal protection of the workers and limit their exposure to radiation and contamination.

A.3 The original project

A project of collection chamber for the CERN-MEDICIS experimental hall have been developed in collaboration between CERN, the GIP Arronax and the Lemer Pax Company [90]. It differentiates from the actual system from the fact that all the operations of the samples movements are remotely controlled. It ensures more protection for the operators and precise alignment along the beam axis. This project is actually antecedent to present design, in which the main principles and operational phases are still valid. A combination of factors like timing and budget has led to a simplified design and it can be considered as a future upgrades for the MEDICIS collection point.

A.3.1 The layout

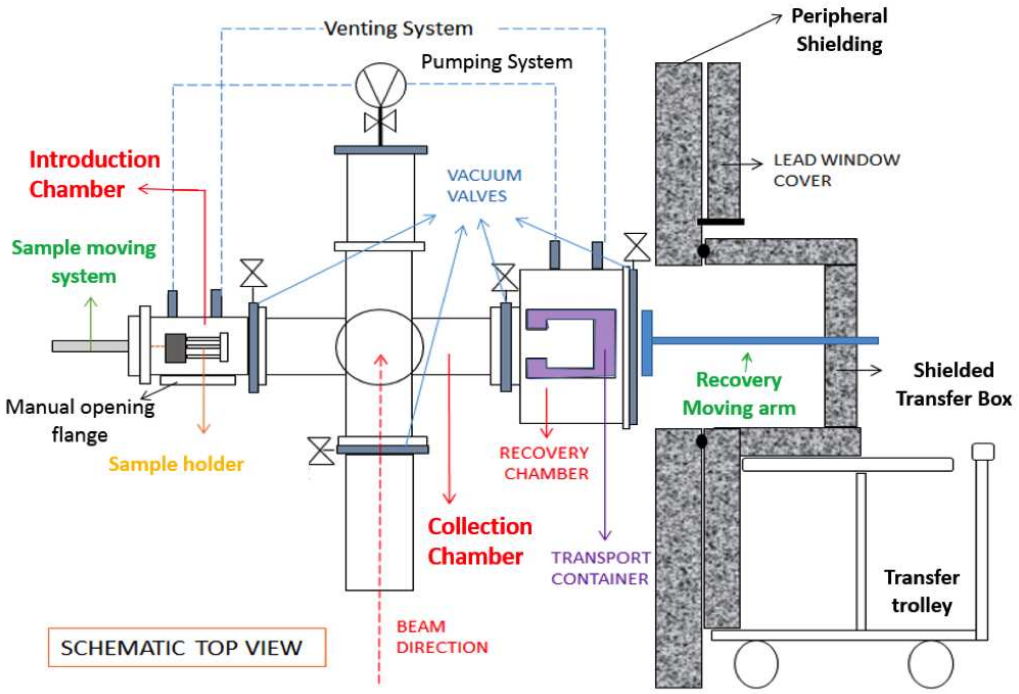

Figure A.5: Isotope collection system conceptual layout top view and the transfer trolley in side view.

Referring to the Figure A.5, it is possible to identify four different areas in the assembly of the isotope collection system:

1. An **Introduction chamber**: it is a vacuum chamber in which the clean sample holder can be connected to a sample moving system. This operation can be done manually after opening a manual opening flange which gives access to the inner part of the chamber. This chamber is equipped with a window to provide a visual check before opening. It is also equipped with connection to pumping and venting system.

2. A **collection chamber**: it is a 6-way cross vacuum chamber. This is the area where the collection on the three samples takes place. This area is kept under vacuum all the time (but during maintenance) and closed by several remotely controlled valves. A vacuum valve separates the collection chamber from the beamline. It will be open only during isotope collection.

3. A recovery chamber: it is a vacuum chamber housing a stainless steel transport container used for the transfer of the irradiated samples.

4. The shielded **Transfer box**: it is installed on a transfer trolley and used to transport the irradiated samples from the isotope collection system to the glovebox. It is possible to access to this area thanks to the window in a peripheral shielding that encloses the entire collection area. This shielded box is equipped with a lead glass window to check the operation with the recovery moving arm or is equipped with a feedback control system to be sure that the transport container is in.

The chosen configuration, and therefore the movement, is horizontal to reduce radioactive dust accumulation on the recovery chamber.
The proposed layout guarantees the airtight closure of the transport container used from the isotope collection system to the glovebox and aims to keep the collection chamber under vacuum for the entire collection process. In this way the probability to spread radioactive gasses or dusts is very low as well as risks of contamination during the transfer phase.
In Table A.2, the different operational steps during the collection are illustrated and described.

Step	Description
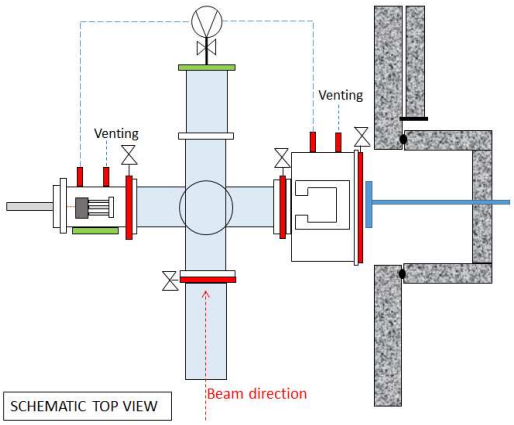	STEP 1: • Vacuum is done into the collection chamber with the dedicated pumping system. • The valve through the beamline is open only during collection. • The sample holder (Collimator+ EDP + Sample plate) is inserted through the introduction chamber and fixed to sample moving system. • The transport container to recover the samples after the collection must be also put in place. NOTE: In the actual system the sample holder with the new sample to irradiate is inserted on the same side used for the recovery. The collection box is open with the magnetic arm traversing all the collection box and putting the plates in the irradiation.

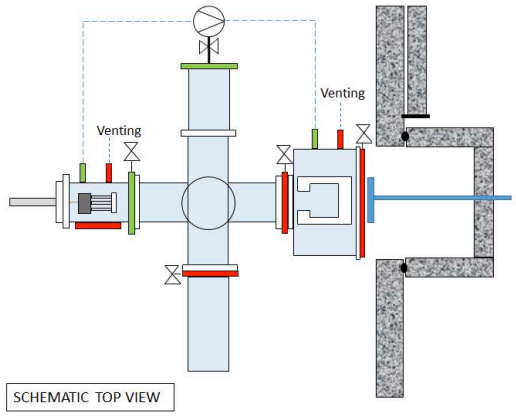	STEP 2: • The manual opening flange is closed and vacuum is made in the introduction chamber in order to open the valve through the collection chamber. • In this phase the recovery chamber is pumped.
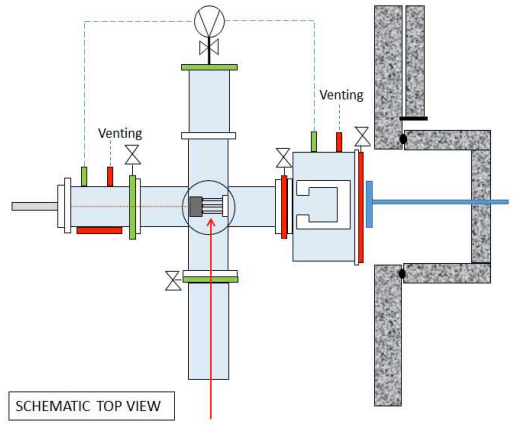	STEP 3: • The sample holder is moved in the first position for the beam tuning. • Then it is moved for the irradiation of the two next samples. • During the irradiation process the pumping system is always active and the valves connecting the collection chamber to the beamline and the introduction chamber are open.
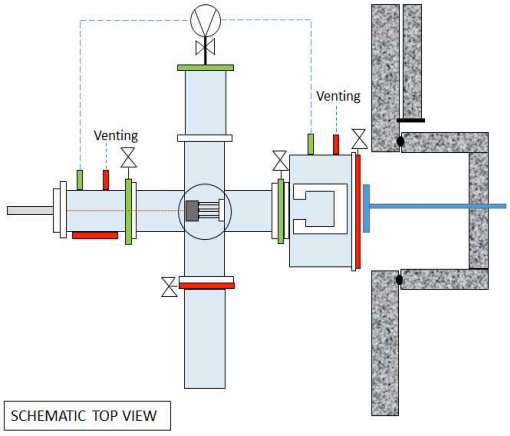	STEP 4: • After the collection the valve through the beamline is closed. • The valve connecting the collection chamber to the recovery chamber is open to allow the sample holder transfer.

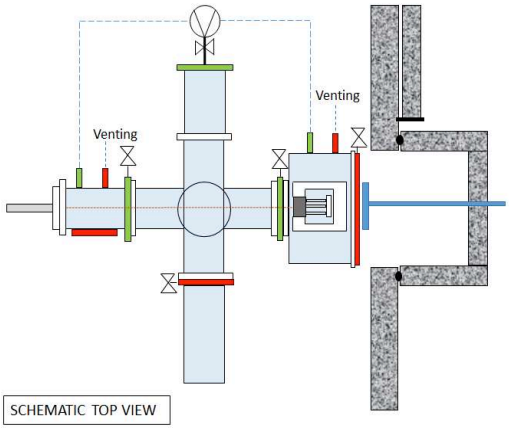	STEP 5: • The sample holder is transferred into the transport container and it is locked hermetically.
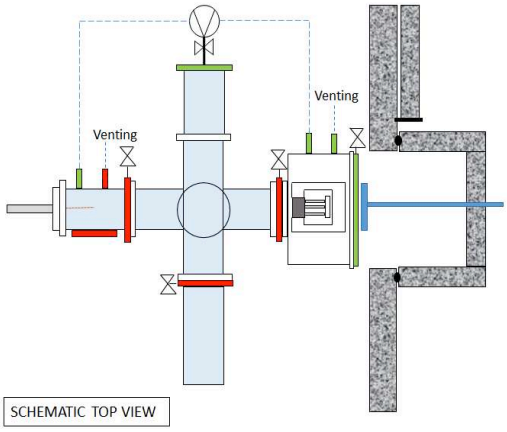	STEP 6: • The sample moving system is pulled back and the vacuum valves of the collection chamber are closed. • The recovery chamber is vented in order to open the lateral valve and allow the exit of the transport container.
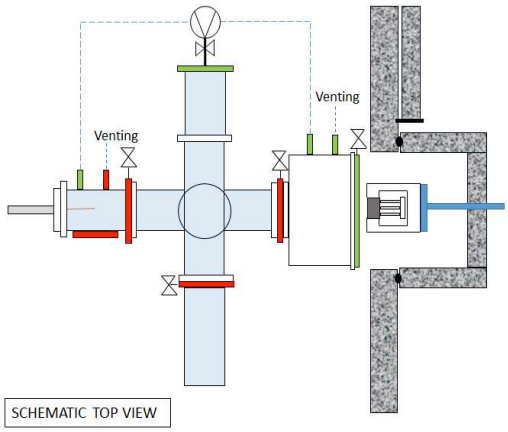	STEP 7: • A recovery moving arm pulls the transport container to the shielded transfer box, placed on the transfer trolley. • This intervention is done behind the protection of the peripheral shielding, the operator will not enter the collection area.

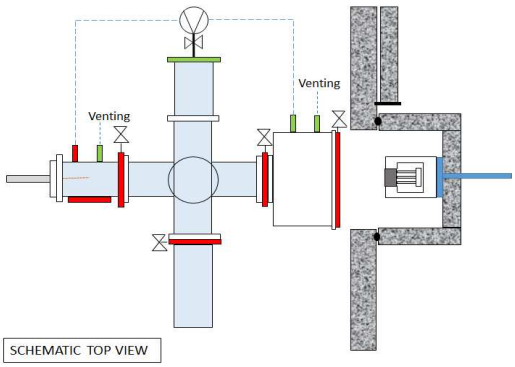	STEP 8: • The transport container is placed into the shielded transfer box and the valve trough the recovery chamber is closed.
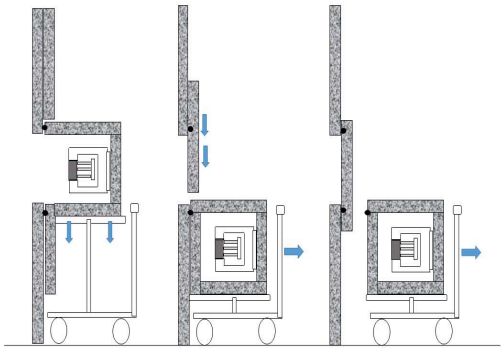	STEP 9: • Once the transport container is inside the shielded transfer box, this one is moved down to be closed. • The window in the peripheral shielding is then locked with a lead window cover, (open during the previous operations). • The closure of this lead window cover must be done at the same time as the shielded transfer box disconnection. A small chicane on the top of the trolley will make sure that the protection is always fine. • The transfer trolley is moved to the glovebox.

Table A.2: Operational steps before, during and after the collection and the transfer of the irradiated samples. The red color indicates a closed valve, the green is used for open valves.

The glovebox in the MEDICIS laboratory is equipped with the same coupling configuration present on the peripheral shielding to connect the shielded transfer box on it. Then, the recovery moving arm can be used to move the transport container into the glovebox.

A.4 The actual system

The actual collection system is shown in Fig.A.6.

This assembly is composed by the following areas:

- the collection chamber where samples are irradiated;
- the transfer container : It consists in a stainless steel cylinder used to transport the samples after irradiation and also to insert new samples in the collection zone.
- the coupling lock system: used to interface the transfer container with the collection chamber taking into account the presence of the vacuum valve;

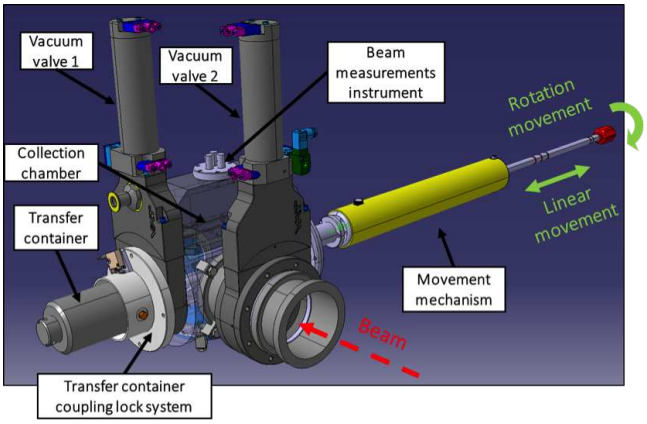

Figure A.6: 3D drawing of the actual Isotope collection system in MEDICIS [drawing: S.Marzari, CERN].

- the movement mechanism: used to change the position of the samples and manually-driven;
- two vacuum valves: to separate the different vacuum sectors. In particular the valve 1 is used to separate/isolate the transfer box, while the valve 2 connects the collection chamber to the rest of the machine;
- the beam measurements instrumentation: to measure the current on the samples and the voltage on the other plates;

The elements to move inside the collection chamber with the manual arm are the same than the ones described in the par.A.3.1. The electrical connection of the samples is done through an optimized copper base.

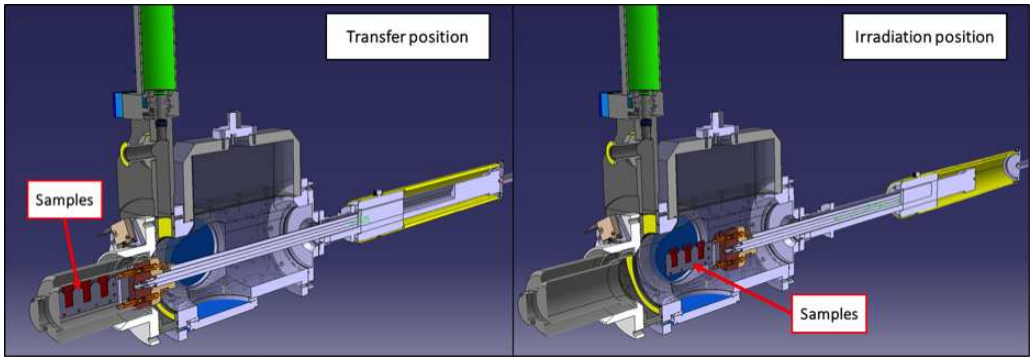

Figure A.7: 3D drawing of the phases of the radionuclides collection with the actual system in MEDICIS [drawing: S.Marzari, CERN].

The steps of the irradiation procedure are the following:

1. The transfer container with the non-irradiated samples is coupled to the collection chamber and locked in position.
2. The transfer container is put under vacuum.The vacuum valve 1 is opened while the valve 2 is kept closed to preserve the vacuum in the rest of the machine. The volume in between the valve

and the container is pumped thanks to the presence of a small piston on the cup of the recovery box.

3. The movement mechanism is pushed inside the collection chamber to reach the transfer container (linear movement) and to connect the samples base (rotation movement).
4. The non-irradiated samples are transferred inside the collection chamber using the moving mechanism (linear movement).
5. Vacuum valve 1 is closed and vacuum valve 2 is opened.
6. The samples can be irradiated. The position of the samples and then the three distances to be covered with the mechanical arm have been appropriately calibrated.

In order to retrieve the irradiated samples from the collection chamber steps 1-5 are carried out in the inverse order.
Once the plates are in the box they can be removed using an external shielded cart (Fig.A.8).
The cart is connected to the wall, the door of the shielding/wall is open and the manual rod is used to grab the box and disconnect it from the collection chamber (with a rotational move).
The box with the irradiated samples is then transferred to the glovebox inside the shielded cart and the door of the shield is closed.
The gloveboxes or the fume hoods are equipped with the same connection system present on the wall. With this technique it is insured a continuity of the shield and a protection of the workers during the transfer.

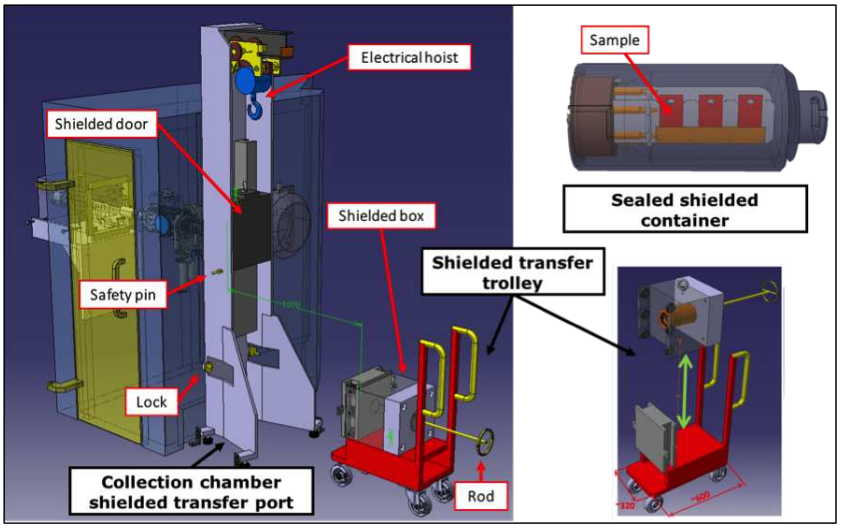

Figure A.8: 3D drawing of the shielded wall around the collection chamber assembly [drawing: S.Marzari, CERN].

A.5 Conclusions

The first layout of the collection point has been presented. On those bases a new and compact collection chamber has been drawn, built and tested.
The new project differentiates from the original one for the following elements:

- The zone of insertion of non-irradiated samples is the same then the one of recovery of the irradiated foils. The recovery box is integral part of the beamline and connected. This eliminates

the need of an external chamber around it.

- The system to move the sample to the irradiation position is totally manual. An upgrade of the collection point could consist in the substitution of the mechanical arm with a remotely controlled system. This will results in two main advantages: the reduction of the dose to the personnel, especially when the machine will run with the total power, and a better and systematic alignment method.

An additional update consists in the installation of three identical chambers with three collection foils. In this way it will be possible to collect at the same time different isotopes playing on the deflection of different masses.

The activities in MEDICIS officially started last year. The first collection of Tb-155 has been done on December 2017 to test the machine and the separator. A proper implantation of Er-169 has been done later in May 2018 when the collection chamber and the peripheral shield have been terminated. The schedule of the run foresees also collection of Tb-149, Tb-152 and C-11 to be sent to the partners Institutions.

B

Contents

B.1 Dictionary of RAM transport 197
B.2 The basic principles of the Finite element analysis (FEA) 199
B.2.1 The ANSYS simulation: a description of the basic steps 200
B.3 Tables of physical characteristics of the materials involved in the FEA of the ColiBRI-30 204
B.3.1 Mechanical data of the ColiBRI's screws 204
B.3.2 Engineering data for Thermal calculations 205
B.3.3 Engineering data for Mechanical calculations 206

B.1 Dictionary of RAM transport

Here below the definition of some of the common words used in th Chapter 3 and coming from the Section II of the IAEA Safty Transport Regulation [39].

A1 and A2

201. A1 shall mean the activity value of special form radioactive material that is listed in Table 2 or derived in Section IV and is used to determine the activity limits for the requirements of these Regulations. A2 shall mean the activity value of radioactive material, other than special form radioactive material, that is listed in Table 2 or derived in Section IV and is used to determine the activity limits for the requirements of these Regulations.

Competent authority

207. Competent authority shall mean any body or authority designated or otherwise recognized as such for any purpose in connection with these Regulations.

Confinement system

209. Confinement system shall mean the assembly of fissile material and packaging components specified by the designer and agreed to by the competent authority as intended to preserve criticality safety.

Containment system

213. Containment system shall mean the assembly of components of the packaging specified by the designer as intended to retain the radioactive material during transport.

Contamination

214. Contamination shall mean the presence of a radioactive substance on a surface in quantities in excess of 0.4 Bq/cm^2 for beta and gamma emitters and low toxicity alpha emitters, or 0.04 Bq/cm^2 for all other alpha emitters.

Exclusive use

221. Exclusive use shall mean the sole use, by a single consignor, of a conveyance or of a large freight container, in respect of which all initial, intermediate and final loading and unloading and shipment are carried out in accordance with the directions of the consignor or consignee, where so required by these Regulations.

Low specific activity material

226. Low specific activity (LSA) material shall mean radioactive material that by its nature has a limited specific activity, or radioactive material for which limits of estimated average specific activity apply. External shielding materials surrounding the LSA material shall not be considered in determining the estimated average specific activity.

Low toxicity alpha emitters

227. Low toxicity alpha emitters are: natural uranium, depleted uranium, natural thorium, uranium-235, uranium-238, thorium-232, thorium-228 and thorium-230 when contained in ores or physical and chemical concentrates; or alpha emitters with a half-life of less than 10 days.

Overpack

230. Overpack shall mean an enclosure used by a single consignor to contain one or more packages and to form one unit for convenience of handling and stowage during transport.

Package

231. Package shall mean the complete product of the packing operation, consisting of the packaging and its contents prepared for transport.

Radioactive contents

235. Radioactive contents shall mean the radioactive material together with any contaminated or activated solids, liquids and gases within the packaging.

Radioactive material

236. Radioactive material shall mean any material containing radionuclides where both the activity concentration and the total activity in the consignment exceed the values specified in paras 402-407.

Shipment

237. Shipment shall mean the specific movement of a consignment from origin to destination.

Special form radioactive material

239. Special form radioactive material shall mean either an indispersible solid radioactive material or a sealed capsule containing radioactive material.

Specific activity

240. Specific activity of a radionuclide shall mean the activity per unit mass of that nuclide. The

specific activity of a material shall mean the activity per unit mass of the material in which the radionuclides are essentially uniformly distributed.

Vessel

249. Vessel shall mean any seagoing vessel or inland waterway craft used for carrying cargo.

B.2 The basic principles of the Finite element analysis (FEA)

The description of the physics' laws for space and time dependent problems is usually expressed in terms of partial differential equations and boundary conditions. For the vast majority of geometries and problems, these cannot be solved with analytical methods. Instead, an approximation of the equations can be constructed. It is typically based upon different types of discretization that approximate the differential equations with numerical model equations, which can be solved using numerical methods [94].

In contrast to analytical solutions, which shows the exact behavior of a system at any point within the system, numerical solution approximate exact solution at discrete points, called "nodes".
The basic philosophy of this technique is the following. The structure is modelled using small interconnected elements, the so-called "finite elements". A displacement function is associated to each of them. Each interconnected element is linked, directly or indirectly, to every other element through common (or shared) interfaces, including nodes and/or boundary lines and/or surfaces. By using known stress/strain properties for the material composing the structure, it is possible to determine the behavior of a given node in terms of the properties of every other element in the structure. The total set of equations describing the behavior of each node results in a series of algebraic equations expressed in matrix notation.
The basic steps involved in any finite element analysis (and then the path also followed in the software ANSYS 18.0 [54] ,used in this PhD work) are listed below.

Step 1: Discretization and Selection of the Element Types

The discretization of the domain is the first and probably the most important step in any finite element analysis.Tthe manner in which the domain is discretized will affect the computer storage requirements, the computation time, and the accuracy of the results.
This phase consists in dividing the body into an equivalent system of finite elements with associated nodes and choosing the most appropriate element type to model most closely the actual physical behavior [95]. The total number of elements used and their variation in size and type within a given body are primarily matters of engineering judgment. The elements must be made small enough to give good results and yet large enough to reduce computational effort. Small elements are generally desirable where the results are changing rapidly, such as where changes in geometry occur; large elements can be used where results are relatively constant. Moreover, the choice of the most appropriate element for a particular problem is one of the major tasks that must be carried out by the designer/analyst.
For a 1D, domain which is actually a straight of curved line, the elements are often short line segments interconnected to form the original line. For a 2D domain, the elements are usually small triangles and rectangles. The firsts are best suited for discretizing rectangular regions, while the seconds can be used for irregular regions. In a 3D solution, the domain may be subdivided into tetrahedral elements, triangular prisms, or rectangular bricks, among which the tetrahedra are the simplest and best suited for arbitrary-volume domains.
A problem in which the geometry, loadings, boundary conditions and materials are symmetric with

respect to an axis can be solved as an axisymmetric problem instead of as a three dimensional problem. In this case the study of a 3D geometry can be reduced to the one of a 2D structure. The use of this expedient is investigated for our studies.
Another expedient that can help in the reduction of the number of elements to simulate, and then the time of calculation, is the simulation of only a segment (clove) of the geometry if it presents a symmetry by rotation around one axis (Fig.B.1).

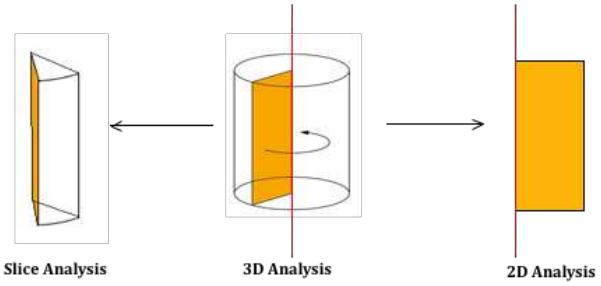

Figure B.1: The 3D analysis can be simplified to a 2D study or to the analysis of a slice element if the object presents a symmetry for the rotation around one axis.

Step 2: Preprocessing phase
After the creation and the discretization of the solution's domain into finite elements, boundary conditions, initial conditions and loadings must be applied on specific nodes, phases or body. Moreover the material's definition and the specification of all the relative properties involved in the analysis are necessary. This phase involves also the definition of the physical quantities to simulate, their initial conditions and eventually specific nodes where to obtain and observe the final values.

Step 3: Solution Phase
This phase consists in the solving a set of linear or nonlinear algebraic equations simultaneously to obtain nodal results, such as displacement values at different nodes or temperature values in heat transfer problems.

Step 4: Post processing Phase
The final phase consists in obtaining the values of the principal stresses, heat fluxes, etc.
First the secondary variables of the problem are calculated from the solution. Then, the nodal values of the primary and secondary variables are used to construct their graphical variation over the domain either in the form of graphs (for 1-D problems) or table or 2D/3D contours.

B.2.1 The ANSYS simulation: a description of the basic steps

The workbench used in our work to simulate the response of structures to loads and in particular for the simulations of the mechanical tests is the ANSYS Explicit Dynamic.
This workbench is normally used in case of problems involving short-duration severe loading, large material deformation and material failure. The explicit solution method can handle geometries with complex nonlinear contact that may cause difficulty with the implicit solver in ANSYS Mechanical. Indeed in nonlinear implicit analysis, solution of each step requires a series of trial solutions (iterations) to establish equilibrium within a certain tolerance. In explicit analysis, no iteration is required as the

nodal accelerations are solved directly.
To ensure stability and accuracy of the solution, the size of the time step used in explicit time integration is limited by the Courant-Friedrichs-Levy (CFL) condition. This condition implies that the time step be limited such that a disturbance (stress wave) cannot travel further than the smallest characteristic element dimension in the mesh, in a single time step. The time steps used for explicit time integration will generally be much smaller than those used for implicit time integration.
The Explicit Dynamic component is composed by several modules (Fig.B.2). They outline the steps that are required to complete a finite element analysis:

- Engineering Data module is used to define the materials involved and the relative properties;
- Geometry module opens the Design Modeler application, which can be used to import CAD models from other software like SolidWorks or to sketch a new 2D or 3D geometry;
- Model, Setup, Solution, and Results modules opens the Mechanical application, which can be used to set up and solve the simulation (includes meshing, loads and boundary condition applications, solving, and results).

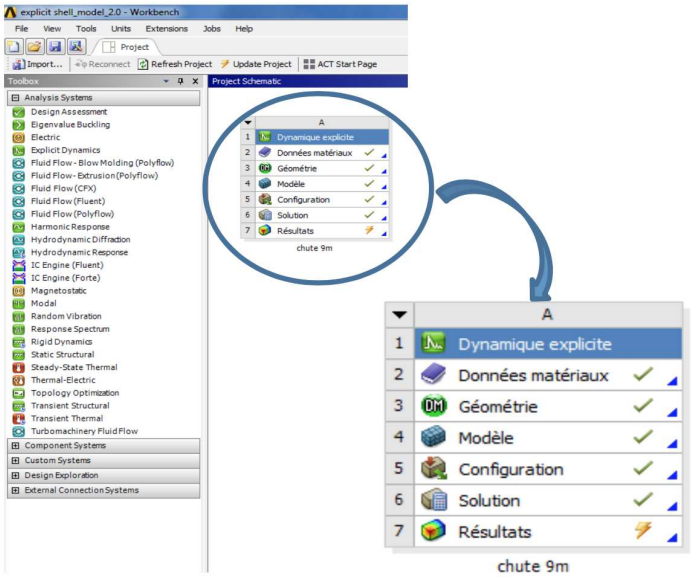

Figure B.2: Example of ANSYS 18.0 Explicit Dynamic module.

Engineering Data

This step consists in the definition of the main mechanical characteristics of the materials involved, like density, isotropic elasticity (Young modulus, Poisson's Ratio), yield strength, tangent modulus (Fig.B.3). It is possible to insert manually the mechanical properties (also in tabular form in case of non-constant values), modify the existing one or simply accept the ones given by default. Moreover, new materials with user defined characteristics can be created.

Geometry module

By default, ANSYS Workbench will analyze the problem in 3D. In some cases we can study a plane stress scenario, which allows us to reduce the analysis down to a 2D problem. This decision must be done at the very start.
The geometry to analyze can be reproduced with external CAD software (as SolidWorks or Catia) and

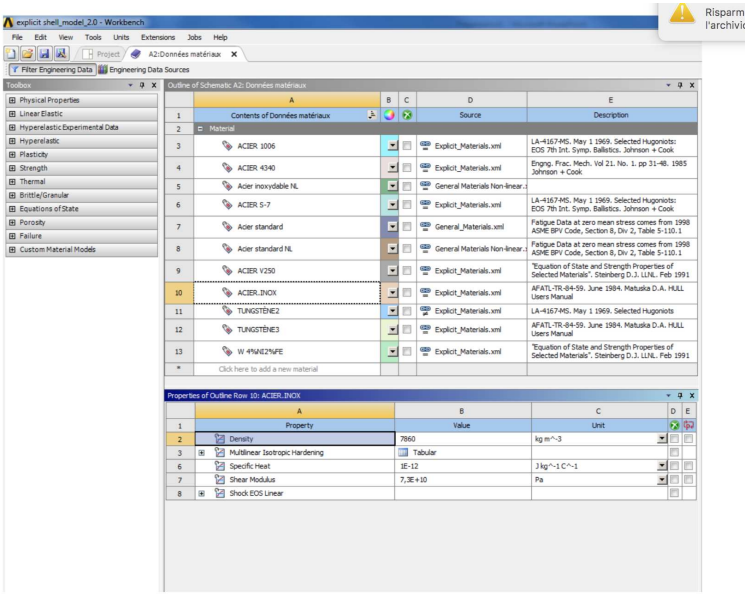

Figure B.3: Example of the Engineering Data module in Ansys 18.0.

uploaded in ANSYS or it can be drawn directly in the ANSYS workbench.
As previously stated, in case the geometry is symmetric for a rotation around an axis, we can choose to simulate only the 2D projection or even one quarter of the 3D structure. It is also possible to reproduce only the mid-planes of the surfaces and attribute them the thickness in the Model section (Fig.B.4). The latter method gives accurate stress results when it is used to model structures whose thickness is small relative to the other dimensions.

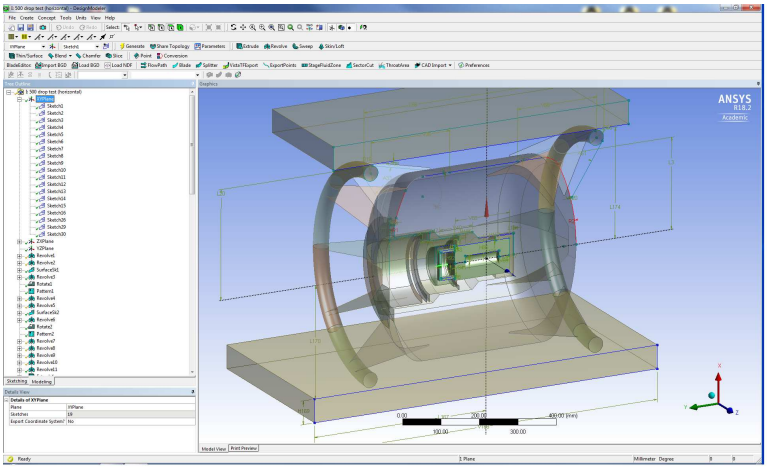

Figure B.4: Example of the Geometry module in Ansys 18.0.

Model

This part of the preprocessing phase is related to the choice of the boundary conditions. It consists in the following sub-steps:

1. Geometry
   Definition of some properties of the body and surfaces:

   - In case of surfaces structure, the definition of the thickness is necessary.
   - Some elements can be defined as rigid while others will be characterized by flexible stiffness. More in particular, in a finite-element model, certain relatively stiff parts can be represented by rigid bodies when stress distributions and wave propagation in such parts are not critical. An advantage of using rigid bodies rather than deformable finite elements is computational efficiency. Elements that belong to the rigid bodies have no associated internal forces or stiffness.
     In our particular case, the target of the drop and the mass falling on the container will be defined as rigid since their deformations can be considered negligible compared to the one induced in the container.
   - To each surfaces or solid is associated a material previously defined in the Engineering module.
   - The case of axisymmetric analysis must be chosen when the geometry under study present a symmetry respect an axis;

2. Mesh
   This stage consists in the discretization of the geometry and the determination of the mesh eventually defining the elements' size. The choice of the 2D analysis simplifies the meshing tasks. The mesh influences the accuracy, convergence and speed of the solution. Furthermore, the time it takes to create and mesh a model is often a significant portion of the time it takes to get the results. Therefore, the better and more automated the meshing tools, the better the solution. It is always recommended to have a look to statistical methods to evaluate the mesh quality.
   The value of the element size property can be automatically computed or user-defined. It is also possible to redefine the mesh using the Methods option.

3. Symmetry
   In case of the existence of plane of symmetry in the geometry, the presence in the tree of the "symmetry zones" must be verified.

4. Connection

   - Body interaction: There are four options for the Type of Body Interaction: Bonded (joined), Frictionless (sliding contact), Frictional (sliding contact), Reinforcement (for embedded beams).
   - Contact: By default, if the faces of any two bodies are touching, or within a certain tolerance, a bonded contact region will be defined and scoped automatically to the two faces. In the case of the drop test analysis the simulation starts from the moment right before the impact in which the body does not touch the target so the contact between the target and the body is eliminated.

5. Analysis setting

   - Initial conditions: by default, all bodies in an Explicit Dynamics system are at rest, unconstrained, and stress free. At least one initial condition, constraint, or load must be applied to the model. Two forms of velocity are available as initial conditions for explicit dynamics: velocity (translational) or angular velocity (rotational). This condition can be applied to one or more than one body in the local or global system of coordinates. In the case of our mechanical analysis we deal with drop of elements, so the values of initial velocity and end time of simulation must be defined. The body (or the bodies) that are the object of the dynamics must be highlighted.
   - Others: In the case of the drop tests this stage is linked to the choice of a "Fix support": the solid in steel is chosen as rigid since not deformable during the impact;

6. Solution
   At this stage the physical quantity to calculate and eventually the interested nodes must be defined: i.e. Total displacement, Plastic deformation, Equivalent stress. The variation of the kinetic and internal energy can be also obtained as well as a complete report of the simulation's parameters.

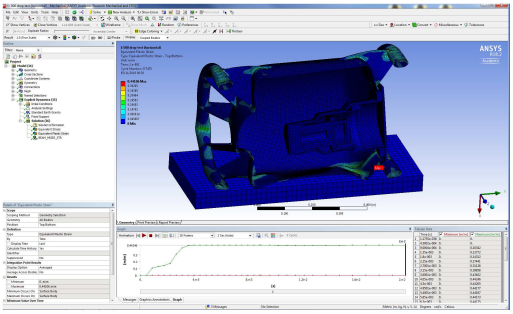

Figure B.5: Example of the Model module in Ansys 18.0

B.3 Tables of physical characteristics of the materials involved in the FEA of the ColiBRI-30

B.3.1 Mechanical data of the ColiBRI's screws

Type	Breaking limit [kN]	Elastic limit [kN]	Resistance Section [mm^2]
A70 - M16	109.9	70.6	157
A70 - M6	14	9	20.1

Table B.1: Summary of the engineering data for mechanical calculations.

B.3.2 Engineering data for Thermal calculations

Material	Density [kg/m^3]	Thermal Conductivity [W/m C]		Specific heat [J /kg K]	
Steinless steel 304L	17850	14.92	@ 60.5°C	510,03	@26.85°C
		15.27	@ 80°C	523,42	@126.85°C
		15.62	@ 107°C	536,81	@226.85°C
		16.16	@ 130°C	550.2	@326.85°C
		17.04	@ 180°C	564	@426.85°C
		17.40	@ 200°C	577.39	@526.85°C
		18.99	@ 300°C	590.78	@626.85°C
		20.46	@ 400°C	604.17	@726.85°C
		24.33	@ 700°C	631.37	@926.85°C
				658.14	@1126.85°C
				685.34	@1326.85°C
Tungsten	17500	174	@ 26.85°C	132	@300°C
		167	@ 76.85°C	137	@400°C
		159	@ 126.85°C	142	@600°C
		137	@ 326.85°C	145	@800°C
		125	@ 526.85°C	148	@1000°C
		118	@ 726.85°C	152	@1200°C
		112	@ 926.85°C	157	@1500°C
		108	@ 1126.9°C	167	@2000°C
		104	@ 1326.9°C		
		95	@ 2226.9°C		
Ceramic wool	128	0.04	@ 200°C	1200	@1090°C
		0.08	@ 400°C		
		0.14	@ 600°C		
		0.23	@ 800°C		
		0.34	@ 000°C		
		0.48	@ 1200°C		
Peek (4)	1300	0.25		100	

Table B.2: Summary of the engineering data for the thermal calculations.

B.3.3 Engineering data for Mechanical calculations

Material	**Density** [kg/m^3]	**Young's Modulus** [Pa]	**Poisson's ratio**
Stainless Steel	7850	2.00E+11	0.3
Tungsten	16290	4.10E+11	0.27
Peek	1.3	3.75E+09	0.378

Table B.3: Summary of the engineering data for mechanical calculations.

C

Contents

C.1 Tables with MCNPX results for monoenergetic source particles 207
C.1.1 For Q_A calculations 207
C.1.2 For Q_B calculations 209
C.1.3 For Q_D calculations 210
C.2 Example of MCNPX code for beta dose calculation 212

C.1 Tables with MCNPX results for monoenergetic source particles

C.1.1 For Q_A calculations

Energy [MeV]	**Transfer function** [MeV/(g part s)]	**Error** [%]	**Dose rate** [Sv/h]	**Error** [Sv/h]
4.00E-03	3.64E-07	3.32E-02	4.18E-20	1.39E-21
5.00E-03	4.08E-05	3.50E-03	4.69E-18	1.64E-20
1.00E-02	5.58E-03	3.00E-04	6.41E-16	1.92E-19
1.50E-02	1.27E-02	1.00E-04	1.46E-15	1.46E-19
2.00E-02	1.86E-02	1.00E-04	2.14E-15	2.14E-19
2.50E-02	2.41E-02	1.00E-04	2.77E-15	2.77E-19
3.00E-02	2.93E-02	0.00E+00	3.37E-15	0.00E+00
3.50E-02	3.44E-02	0.00E+00	3.96E-15	0.00E+00
4.00E-02	3.94E-02	0.00E+00	4.53E-15	0.00E+00
4.50E-02	4.44E-02	0.00E+00	5.10E-15	0.00E+00
5.00E-02	4.92E-02	0.00E+00	5.66E-15	0.00E+00
5.50E-02	5.40E-02	0.00E+00	6.20E-15	0.00E+00
6.00E-02	5.87E-02	0.00E+00	6.74E-15	0.00E+00
6.50E-02	6.33E-02	0.00E+00	7.28E-15	0.00E+00
7.00E-02	6.80E-02	0.00E+00	7.81E-15	0.00E+00

7.50E-02	7.25E-02	0.00E+00	8.34E-15	0.00E+00
8.00E-02	7.71E-02	1.00E-04	8.86E-15	8.86E-19
8.50E-02	8.16E-02	1.00E-04	9.38E-15	9.38E-19
9.00E-02	8.61E-02	1.00E-04	9.90E-15	9.90E-19
9.50E-02	9.06E-02	1.00E-04	1.04E-14	1.04E-18
1.00E-01	9.51E-02	1.00E-04	1.09E-14	1.09E-18
2.00E-01	1.82E-01	1.00E-04	2.09E-14	2.09E-18
3.00E-01	2.64E-01	1.00E-04	3.03E-14	3.03E-18
4.00E-01	3.41E-01	1.00E-04	3.92E-14	3.92E-18
5.00E-01	4.14E-01	1.00E-04	4.76E-14	4.76E-18
5.50E-01	4.50E-01	1.00E-04	5.17E-14	5.17E-18
6.00E-01	4.84E-01	1.00E-04	5.57E-14	5.57E-18
6.50E-01	5.18E-01	1.00E-04	5.96E-14	5.96E-18
7.00E-01	5.51E-01	1.00E-04	6.34E-14	6.34E-18
7.50E-01	5.84E-01	1.00E-04	6.71E-14	6.71E-18
8.00E-01	6.16E-01	1.00E-04	7.07E-14	7.07E-18
8.50E-01	6.47E-01	1.00E-04	7.43E-14	7.43E-18
9.00E-01	6.77E-01	2.00E-04	7.78E-14	1.56E-17
9.50E-01	7.07E-01	2.00E-04	8.13E-14	1.63E-17
1.00E+00	7.37E-01	2.00E-04	8.47E-14	1.69E-17
1.50E+00	1.01E+00	2.00E-04	1.16E-13	2.31E-17
2.00E+00	1.24E+00	2.00E-04	1.43E-13	2.86E-17
2.50E+00	1.46E+00	2.00E-04	1.68E-13	3.36E-17
3.00E+00	1.66E+00	2.00E-04	1.91E-13	3.82E-17
3.50E+00	1.85E+00	3.00E-04	2.13E-13	6.39E-17
4.00E+00	2.04E+00	3.00E-04	2.34E-13	7.03E-17
4.50E+00	2.22E+00	3.00E-04	2.55E-13	7.64E-17
5.00E+00	2.39E+00	3.00E-04	2.75E-13	8.25E-17
5.50E+00	2.56E+00	3.00E-04	2.94E-13	8.83E-17
6.00E+00	2.73E+00	3.00E-04	3.14E-13	9.42E-17
6.50E+00	2.90E+00	3.00E-04	3.33E-13	9.99E-17
7.00E+00	3.06E+00	3.00E-04	3.52E-13	1.06E-16
7.50E+00	3.23E+00	3.00E-04	3.71E-13	1.11E-16
8.00E+00	3.39E+00	3.00E-04	3.90E-13	1.17E-16

8.50E+00	3.56E+00	2.00E-04	4.09E-13	8.18E-17
9.00E+00	3.72E+00	3.00E-04	4.28E-13	1.28E-16
9.50E+00	3.89E+00	4.00E-04	4.47E-13	1.79E-16

Table C.1: Results of the simulations for the gamma dose rate in the Q_A scenario.

C.1.2 For Q_B calculations

Energy [MeV]	**Transfer function** [MeV/(g part s)]	**Error** [%]	**Dose rate** [Sv/h]	**Error** [Sv/h]
3.50E-01	0.00E+00	0.00E+00	0.00E+00	0.00E+00
3.60E-01	1.61E-03	3.70E-03	1.85E-12	6.83E-15
4.00E-01	1.04E-02	2.50E-03	1.19E-11	2.97E-14
4.50E-01	1.78E-02	1.30E-03	2.04E-11	2.65E-14
5.00E-01	1.97E-02	8.00E-04	2.26E-11	1.81E-14
5.50E-01	1.91E-02	8.00E-04	2.19E-11	1.75E-14
6.00E-01	1.77E-02	1.00E-03	2.03E-11	2.03E-14
6.50E-01	1.63E-02	1.10E-03	1.87E-11	2.06E-14
7.00E-01	1.50E-02	1.30E-03	1.73E-11	2.24E-14
7.50E-01	1.40E-02	1.50E-03	1.61E-11	2.41E-14
8.00E-01	1.31E-02	1.60E-03	1.50E-11	2.40E-14
8.50E-01	1.24E-02	1.80E-03	1.42E-11	2.55E-14
9.00E-01	1.18E-02	1.90E-03	1.35E-11	2.56E-14
1.00E+00	1.08E-02	2.20E-03	1.24E-11	2.73E-14
1.10E+00	1.02E-02	2.40E-03	1.17E-11	2.80E-14
1.20E+00	9.61E-03	2.50E-03	1.10E-11	2.75E-14
1.30E+00	9.25E-03	2.70E-03	1.06E-11	2.86E-14
1.40E+00	9.15E-03	2.80E-03	1.05E-11	2.94E-14
1.50E+00	8.85E-03	2.90E-03	1.01E-11	2.94E-14
1.60E+00	8.75E-03	3.00E-03	1.00E-11	3.01E-14
1.70E+00	8.57E-03	3.00E-03	9.82E-12	2.95E-14
1.80E+00	8.50E-03	3.10E-03	9.74E-12	3.02E-14
1.90E+00	8.35E-03	3.30E-03	9.58E-12	3.16E-14
2.00E+00	8.30E-03	2.90E-03	9.52E-12	2.76E-14
2.10E+00	8.20E-03	3.70E-03	9.40E-12	3.48E-14
2.20E+00	8.29E-03	3.40E-03	9.50E-12	3.23E-14

2.30E+00	8.11E-03	3.80E-03	9.29E-12	3.53E-14
2.40E+00	8.10E-03	3.50E-03	9.29E-12	3.25E-14
2.50E+00	8.11E-03	3.50E-03	9.30E-12	3.26E-14
2.60E+00	8.02E-03	3.80E-03	9.19E-12	3.49E-14
2.70E+00	8.01E-03	4.00E-03	9.18E-12	3.67E-14
2.80E+00	8.05E-03	3.20E-03	9.23E-12	2.95E-14
2.90E+00	7.93E-03	3.90E-03	9.09E-12	3.55E-14
3.00E+00	7.91E-03	3.80E-03	9.07E-12	3.45E-14
4.00E+00	7.98E-03	3.80E-03	9.15E-12	3.48E-14

Table C.2: Results of the simulations for the beta dose rate in the Q_B scenario.

C.1.3 For Q_D calculations

Energy [MeV]	**Transfer function** [MeV/(g part s)]	**Error** [%]	**Dose rate** [Sv/h]	**Error** [Sv/h]
6.00E-02	2.71E-04	1.40E-03	3.10E-13	4.34E-16
7.00E-02	6.99E-03	6.00E-04	8.01E-12	4.80E-15
8.00E-02	1.68E-02	5.00E-04	1.93E-11	9.63E-15
9.00E-02	2.46E-02	4.00E-04	2.82E-11	1.13E-14
1.00E-01	2.86E-02	4.00E-04	3.28E-11	1.31E-14
1.20E-01	3.04E-02	4.00E-04	3.49E-11	1.39E-14
1.40E-01	2.96E-02	5.00E-04	3.40E-11	1.70E-14
1.60E-01	2.83E-02	5.00E-04	3.24E-11	1.62E-14
1.80E-01	2.72E-02	5.00E-04	3.12E-11	1.56E-14
2.00E-01	2.61E-02	6.00E-04	2.99E-11	1.79E-14
2.20E-01	2.51E-02	6.00E-04	2.87E-11	1.72E-14
2.40E-01	2.43E-02	7.00E-04	2.79E-11	1.95E-14
2.60E-01	2.36E-02	7.00E-04	2.71E-11	1.90E-14
2.80E-01	2.30E-02	8.00E-04	2.64E-11	2.11E-14
3.00E-01	2.25E-02	9.00E-04	2.58E-11	2.33E-14
3.20E-01	2.22E-02	1.00E-03	2.54E-11	2.54E-14
3.40E-01	2.18E-02	1.10E-03	2.50E-11	2.75E-14
3.60E-01	2.14E-02	1.20E-03	2.45E-11	2.94E-14
3.80E-01	2.11E-02	1.20E-03	2.42E-11	2.90E-14
4.00E-01	2.09E-02	1.30E-03	2.40E-11	3.11E-14

4.50E-01	2.03E-02	1.60E-03	2.32E-11	3.72E-14
5.00E-01	1.98E-02	1.40E-03	2.27E-11	3.17E-14
5.50E-01	1.95E-02	2.10E-03	2.23E-11	4.69E-14
6.00E-01	1.91E-02	2.50E-03	2.20E-11	5.49E-14
6.50E-01	1.88E-02	2.70E-03	2.16E-11	5.82E-14
7.00E-01	1.87E-02	2.90E-03	2.15E-11	6.22E-14
7.50E-01	1.86E-02	3.20E-03	2.14E-11	6.83E-14
8.00E-01	1.85E-02	3.40E-03	2.12E-11	7.21E-14
8.50E-01	1.83E-02	3.70E-03	2.10E-11	7.78E-14
9.00E-01	1.84E-02	3.90E-03	2.11E-11	8.21E-14
9.50E-01	1.81E-02	4.20E-03	2.08E-11	8.74E-14
1.00E+00	1.81E-02	4.50E-03	2.07E-11	9.31E-14
1.50E+00	1.77E-02	6.60E-03	2.03E-11	1.34E-13
2.00E+00	1.78E-02	8.60E-03	2.04E-11	1.75E-13
2.50E+00	1.77E-02	9.90E-03	2.03E-11	2.01E-13
3.00E+00	1.79E-02	1.27E-02	2.05E-11	2.60E-13
3.50E+00	1.75E-02	1.47E-02	2.00E-11	2.95E-13

Table C.3: Results of the simulations for the beta dose rate in the Q_D scenario.

C.2 Example of MCNPX code for beta dose calculation

```
Simulation of e- dose in water for E= 0.1 MeV
C ——————————————————————————————————————————————
C CELLS CARDS: Definition of the zones of interest
C ——————————————————————————————————————————————
001 0 -1
002 2 -1 +1 -2
003 2 -1 +2 -3
004 2 -1 +3 -4
005 0 +4 -5
006 0 +5
C END OF CELLS CARDS

    C ——————————————————————————————————————————————
C SURFACE CARD: Definition of the geometry; SO= sphere with center in the origin
C ——————————————————————————————————————————————
1 SO +100
2 SO +100.005
3 SO +100.009
4 SO +150
5 SO +200
C END OF SURFACES CARDS

    C ——————————————————————————————————————————————
C MATERIAL CARD: Definition of the chemical composition of the materials
C ——————————————————————————————————————————————
M1          6000 -0.000124 $C Air composition
7014 -0.755268 $N
8016 -0.231781 $O
18000 -0.012827 $Ar
M2 1001 -0.101 $Skin composition
8016 -0.762
7014 -0.026
6000 -0.111
C ——————————————————————————————————————————————
C DATA CARD: Definition of the physics phenomena to include and source characteristics
C ——————————————————————————————————————————————
lca 2 1 1 23 1 1 0 1 0
lea 1 4 1 0 1 0 0 1
mode p e
phys:p 100 0 0 0 1 0
phys:e 100 1 1 0 0 0 0 0 0 0
imp:e 0 1 2m 2m 2m 0
imp:p 0 1 2m 2m 2m 0
sdef SUR=1 par=3 erg=0.1
nps 10000000
```

```
ctme 10
C ——————————————————————————————————————————————————————————————
C TALLIES: Definition of the physicsl quantities in output
C ——————————————————————————————————————————————————————————————
*F18: e,p 3
F26: e 3
F31: p 1
```

Bibliography

[1] Royal Society of Chemistry, Radiochemical Methods Group, *Discovery of Radioactivity*, Royal Society of Chemistry website (2012).

[2] G. de Hevesy, *Radioelements as tracers in physics and chemistry*, Chem News **108:166** (1913).

[3] G. de Hevesy, *The absorption and translocation of lead by plants: A contribution to the application of the method of radioactive indicators in the investigation of the change of substance in plants*, Biochem J **17, 39:445** (1923).

[4] H.L. Blumgart, S.Weiss, *Studies on the velocity of blood flow*, J Clin Invest **4, 5:31** (1927).

[5] E.O. Lawrence, M-S. Livingston, *The production of high-speed light ions without the use of high voltages*, Phys Rev **40, 19:30** (1932).

[6] B. Cassen, L. Curtis, C. Reed, R. Libby, *Instrumentation for I-131 use in medical studies*, Nucleonics **9, 46:50** (1951).

[7] H.O. Anger, *Scintillation camera*, Rev Sci Instr **29, 27:33** (1958).

[8] F.R. Wrenn, M.L. Good, P. Handler, *The use of positron- emitting radioisotopes for the localization of brain tumors*, Science **113, 525:527** (1951).

[9] P.V. Harper, R. Beck, D Charleston, K.A. Lathrop, *Optimization of a scanning method using technetium- 99m*, Nucleonics **122, 50:54** (1964).

[10] EURATOM supply Agency, *Supply of medical radioisotopes*, EURATOM website (2018).

[11] W.G. Myers, *Nuclear medicine: How it began*, Hosp Pract **9, 103:113** (1974).

[12] W.G. Myers, *The Anger scintillation camera becomes of age*, E J Nucl Med **20, 565:567** (1979).

[13] S.R. Cherry et al, *Physics in nuclear medicine*, Elsevier editor (2012).

[14] M.E Phelps, E.J. Hoffman, N.A Mullani, M.M. Ter Pogossian, *Application of annihilation coincidence detection of transaxial reconstruction tomography*, J Nucl Med **16, 210:215** (1975).

[15] M.E Phelps, E.J. Hoffman, N.A Mullani, M.M. Ter Pogossian, *Labeled 2-deoxy-D-glucose analogs: 18F labeled 2-deoxy-2-fluoro-D-glucose, 2-deoxy-2-fluoro-D-mannose and 14C-2-deoxy-2-fluoro-D-glucose*, J of Labelled Compounds and Radiopharmaceuticals **14(2), 175:183** (1978).

[16] S.S. Kelkar, T.M. Reineke, *Theranostics: combining imaging and therapy*, Bioconjug Chem **122, 879:903** (2011).

[17] S. Hertz, A. Roberts, *Radioactive iodine in the study of thyroid physiology: VII. The use of radioactive iodine therapy in hyperthyroidism*, JAMA **131(2), 81:86** (1946).

[18] A.S Esteban et al, *Comparison of sequential planar Lu-177-DOTA-TATE dosimetry scans with Ga-68-DOTA-TATE PET/CT images in patients with metastasized neuroendocrine tumors undergoing peptide receptor radionuclide therapy*, E J Nucl Med **39(3), 501:511** (2011).

[19] E.B. Podgorsak, *Review of Radiation Oncology Physics: A Handbook for Teachers and Students*, IAEA publication (ISBN 92-0-107304-6) (2012).

[20] J.E. Martin, *Physics for Radiation Protection*, Wiley-VCH Editor (2013).

[21] H. Bateman, *Solution of a system of differential equations occurring in the theory of radioactive transformations*, Proc Cambridge Philos Soc **15, 423:427** (1910).

[22] J. Cetnar, *General solution of Bateman equations for nuclear transmutations*, Annals of Nuclear Energy 33 (2006) 640-645 **33, 640:645** (2006).

[23] H. Nikijoo, S. Uehara, D. Emfietzoglou, *Interaction of radiation with matter*, CRC Press (2012).

[24] F.H. Attix, *Introduction to radiological physics and radiation dosimetry*, Wiley-VCH Editor (2004).

[25] International Atomic Energy Agency (IAEA), *Calibration of radiation protection monitoring instruments*, Safety Reports Series No.16. (2000).

[26] International Commission on Radiological Protection (ICRP) - Publication 103, *Recommendations of the International Commission on Radiological Protection*, Ann ICRP **37** (2007).

[27] International Commission on Radiation Unit and measurements (ICRU) - Report 85, *Fundamental quantities and units for ionizing radiation (Revised)*, **11** (2011).

[28] Grove Software, *MicroShield 7.01. User's Manual.*, (2006).

[29] Nucleonica GmbH, *Nucleonica Nuclear Science Portal (www.nucleonica.com), Karlsruhe, Germany*, Nucleonica website (2017).

[30] A. Ferrari, P.R. Sala et al, *FLUKA: a multi-particle transport code*, CERN-2005-10, INFN/TC-05/11, SLAC-R-773 (2005).

[31] D.B. Pelowitz , *MCNPX Users Manual Version 2.7.0*, **LA-CP-11-00438** (2011).

[32] TRAD Company, *RayXpert website*, RayXpert website (2014).

[33] Mirion Company, *Apha, Beta, Gamma, X-Ray, and neutron radiation*, Mirion Company website (2018).

[34] C. Suresh, L. Srivastava, F. Mausner, *Therapeutic Radionuclides: Production, Physical Characteristics, and Applications*, R. P. Baum (ed.), Therapeutic Nuclear Medicine **DOI: 10.1007/174-2012-782** (2013).

[35] IAEA Human Health Campus, *Radionuclide Purity*, IAEA website (2018).

[36] HyperPhysics, , website .

[37] P. Van Duppen, *Isotope separation on line and post acceleration*, Lect. Notes Phys **700, 37:77** (2006).

[38] G. Vieru, *Qualification tests for a Type B(U) package*, Proceeding of 14th International Symposium on the Packaging and Transportation of Radioactive Materials (PATRAM) (2004).

[39] International Atomic Energy Agency (IAEA), *Regulations for the safe transport of radioactive material*, No. SSR-6 (2012).

[40] D.L. Logan, *A First Course in the Finite Element Method*, CENGAGE Learning Editor (2016).

[41] Institut de protection et de sûreté nucléaire (CEA), *Catalogue des materiels et équipements normalise: écrans de protection contre le rayonnements ionisants*, CEA report **863 Tome I, Vol.1-2** (1987).

[42] J. Vu, *Modelling of Convective Heat Transfer in Porous Media*, PhD Thesis at the University of Western Ontario, online link **4852** (2017).

[43] Coalition represents the North American High Temperature Insulation Wool (HTIW) industry, , HITW website (2018).

[44] France Joint Company, *Online Catalogue: Les joint toriques, Les bagues anti-extrusion*, Company website (2018).

[45] M.A. Kellet et al., *The JEFF-3.1/-3.1.1 radioactive decay data and fission yields sub-libraries, JEFF Report 20*, Data bank of Nuclear Energy Agency **6287** (2009).

[46] G. Audi et al., *The NUBASE evaluation of nuclear and decay properties*, Nuclear Physics **A 729, 3:128** (2003).

[47] J.H. Hubbell, S.M. Seltzer, *X-Ray Mass Attenuation Coefficients*, NIST Standard Reference Database **126** (2004).

[48] International Commission on Radiological Protection (ICRP) - Publication 68, *Dose Coefficients for Intakes of Radionuclides by Workers*, Ann ICRP (1995).

[49] International Commission on Radiological Protection (ICRP) - Publication 72, *Age-dependent Doses to the Members of the Public from Intake of Radionuclides - Part 5 Compilation of Ingestion and Inhalation Coefficients*, Ann ICRP **26** (1996).

[50] Data bank of Nuclear Energy Agency, *NEA website*, (2010).

[51] Data bank of Nuclear Energy Agency, *NEA website*, (2017).

[52] International Commission on Radiological Protection (ICRP) - Publication 103, *Conversion Coefficients for use in Radiological Protection against External Radiation*, Ann ICRP **26** (1996).

[53] R.G. Williams et al. for the U.S. Department of Energy, *Compendium of Material Composition Data for Radiation Transport Modeling*, **PNNL-15870** (2006).

[54] ANSYS, Inc., *ANSYS 18.0 User Guide*, (2017).

[55] T. Byun, N. Hashimoto, K. Farrell, *Temperature dependence of strain hardening and plastic instability behaviors in austenitic stainless steels*, Acta Mater **52, 3889:3899** (2004).

[56] Euro Inox, European stainless steel development association, *Stainless Steel: Tables of Technical Properties*, Materials and Applications Series **5** (2007).

[57] L. Pope, J. Edward, *Rules of thumb for mechanical engineers: a manual of quick, accurate solutions to everyday problems*, Gulf Publishing Company (1996).

[58] Institut de radioprotection et de surete nucleaire (IRSN), *Radioactive waste management*, Thematic series document on the IRSN website: https://www.irsn.fr/en/publications (2013).

[59] International Atomic Energy Agency (IAEA), *Classification of radioactive waste*, General Safety Guide GSG-01 (2009).

[60] Agence nationale pour la gestion des déchets radioactifs (ANDRA), , ANDRA website .

[61] Nuclear Energy Agency (NEA), *Radioactive Waste Management Programmes in NEA Member Countries*, NEA website (2015).

[62] Autorit de Suret Nucleaire (ASN), *French National Plan for the management of radioactive materials and waste 2013-2015*, NEA website (2015).

[63] J. Donald Cossairt, *Induced Radioactivity at Accelerators*, Proceedings of the Health Physics Society 2008 Professional Development School - Topics in Accelerator Health Physics **FERMILAB-PUB-07-201-ESH** (2008).

[64] F. Haddad et al, *ARRONAX, a high-energy and high-intensity cyclotron for nuclear medicine*, Eur. J. Nucl. Med. Mol. Imaging **35, 1377:1387** (2008).

[65] C. Theis, H. Vinke, *The use of ActiWiz in operational radiation protection*, Workshop Proceedings Shielding Aspects of Accelerators, Targets and Irradiation Facilities (SATIF 12) **NEA/NSC/R 3, 88:98** (2015).

[66] C. Theis, H. Vinke, *ActiWiz optimizing your nuclide inventory at proton accelerators with a computer code*, Proceedings of the ICRS12 conference, 2012, Nara, Japan, Progress in Nuclear Science and Technology **4, 228:232** (2014).

[67] United Aluminum Company, *Chemical Composition and Properties of Aluminum Alloys*, Company website .

[68] Polyfluor Company, *General properties of Peek*, Company website .

[69] R-A. Shanks, I. Kong, *General Purpose Elastomers: Structure, Chemistry, Physics and Performance*, Advances in Elastomers I, Blends and Interpenetrating Networks (2013).

[70] M. Sitarz, *Radionuclide Yield Calculator*, link to RYC Software (2017).

[71] IAEA Coordinated Research Project 2012-2017 (F41029), *Charged-particle cross section database for medical radioisotope production: diagnostic radioisotopes and monitor reactions* , IAEA website (2017).

[72] S. Benassai, L. Bologna, *Re-evaluation of QA and QB values on the basis of complete spectra for gamma, X and beta emissions*, ANPA, Rome, ANPA-DIR/NOR-RT **2 (94)** (1994).

[73] Commission Économique pour L'Europe - Comité des transports intérieurs, *Accord européen relatif au transport international des marchandises dangereuses par route (ADR)*, ECE/TRANS/242 **Vol.1** (NATIONS UNIES New York et Genève, 2014).

[74] C. Mûller et al., *A unique matched quadruplet of terbium radioisotopes for PET and SPECT and for α and β- radionuclide therapy: an in vivo proof-of-concept study with a new receptor-targeted folate derivative*, J Nucl Med **53 (12), 1951:1959** (2012).

[75] C. Mûller et al., *Direct in vitro and in vivo comparison of (161)Tb and (177)Lu using a tumour-targeting folate conjugate.*, Eur J Nucl Med Mol Imaging **41(3), 476:85** (2014).

[76] International Atomic Energy Agency (IAEA), *Advisory material for the IAEA regulations for the safe transport of radioactive material*, Safety Series TS-G-1.1 **Rev 1** (Vienna, 2008).

[77] International Commission on Radiological Protection (ICRP) - Publication 60, *Recommendations of the International Commission on Radiological Protection*, Ann ICRP (1991).

[78] International Commission on Radiological Protection (ICRP) - Publication 38, *Radionuclide transformations: energy and intensity of emissions*, Ann ICRP (1983).

[79] International Commission on Radiological Protection (ICRP) - Publication 51, *Data for use in protection against external radiation*, Ann ICRP **17** (1987).

[80] W.G. Cross , H. Ing et al, *Table of beta-ray dose distributions in an infinite water medium*, Health Physics Journal 63 **2** (1992).

[81] W.G. Cross , H. Ing et al, *Tables of beta-ray dose distributions in water, air, and other media*, Rep. AECL-7617, Atomic Energy of Canada Ltd. (1982).

[82] International Atomic Energy Agency (IAEA), *International Basic Safety Standards for Protection against Ionizing Radiation and for the Safety of Radiation Sources - Safety Series N.115*, (1996).

[83] H.J. Dunster , *Maximum Permissible Levels of Skin Contamination*, Rep. AHSB (RP) R78, UKAEA, Harwell (1967).

[84] United States Environmental Protection Agency, *External Exposure to Radionuclides in Air, Water and Soil, Federal Guidance Report No. 12*, Rep. AHSB (RP) R78, UKAEA, Harwell (Washington, DC, 1993).

[85] International Commission on Radiological Protection (ICRP) - Publication 107, *Nuclear Decay Data for Dosimetric Calculations*, Ann ICRP **38** (2008).

[86] International Commission on Radiological Protection (ICRP) - Publication 119, *Compendium of Dose Coefficients based on ICRP Publication 60*, Ann ICRP 41(s) **3** (2012).

[87] International Commission on Radiation Unit and measurements (ICRU) - Report 39, *Determination of dose equivalent resulting from external radiation sources*, (1991).

[88] M. Seltzer et al., *Evaluation of the collision stopping power of Elements and Compounds for electrons and positrons*, Int J Appl Radiat Isot **33** (2011).

[89] T. Frosio, P. Bertreix et al, *Spectrum-and-yield-to-dose conversion coefficients for beta skin doses linked to the Q-System*, Health Physics Journal (2018 - to be published).

[90] T.Stora, M.Maietta et al, *Technical specification of the CERN-MEDICIS collection chamber*, CERN internal note **EDMS n. 1734239** (2017).

[91] R.M. dos Santos Augusto et al., *CERN-MEDICIS (Medical Isotopes Collected from ISOLDE): A New Facility*, Appl. Sci. **4, 265:281; doi:10.3390/app4020265** (2014).

[92] E. Kugler, *The ISOLDE facility*, Hyperfine Interactions **129, 23:42** (2000).

[93] Y. Amador, B. Conde Fernandez, *Safety file for CERN-MEDICIS (descriptive part)*, CERN internal note **EDMS n. 1541088** (2017).

[94] S. Moaveni, *Finite Element Analysis : Theory and Application with ANSYS*, Minnesota State University (1999).

[95] D. Van Doan, A. Szeleziski, L. Murawski, A. Muc, *Finite Element Method in modelling of ship structures, part I: theoretical background*, Scientific Journal of Gdynia Maritime University **100, 51:62** (2017).

Acknowledgements

And finally comes the sweetest part. The page that will be more read in the next years and probably the hardest to be written.
If you find your name in it, this means you wrote part of my history.
I think I have a big list of people that I would like to thank, that have been a fundamental piece for the success of this project.
So, let's start!

Special thanks go to Ferid. With your tenacity and equilibrium you've always been an inspiration for me. Thank you for always gave me a broad view, for teaching me the real sense of team spirit and leadership, for having always found a minute to discuss with me even when you were superbusy or you simply come back from a long travel. Thank you for always trusted me and have treated me as more than a simple student. Your confidence made me feel stronger. The way you teached me to be indipendent made me more confident in myself.
Who said superhumans doesn't exist?

Thank you Sebastien, for that email at the end of August 2015. You gave me the chance to live a wonderfull experience and to learn and grow up professionally and personally. Thank you also for having allowed me to make mistakes even if you knew you were right and thank you also for the support in finding the right way to solve them. You have been for me a great guide in the unknown world of industry. Thanks for teaching me that "there is no fun if you don't take the risks". Thank you for the jokes and the smiles in the rainy days. If I'm more confident on my possibility and dreams is also because of you.

I have also tho thank Arnaud. From the day I met you I knew that everyday it would have been a surprise with you. You helped me to discover a world I never approached, where the word "stress" has a total different and psychedelic meaning. You did it always giving me new food for thoughts and ideas for possible scenarios to explore. Thanks for having fun working to this project.

Thanks to this PhD committee, Daniel Coussol, Helmut Vincke, Ulli Koester, Nino Burgio and again Thierry Stora, for the comments, the interesting discussions and the support during the redaction and the revision of this thesis work.
Un grand merci va à l'Université de Nantes et aux laboratoires Subatech pour les outils et les ments mis à disposition pour ce travail.

Merci Sebastien Tardy, pour ta curiosité, ton immense aide dans la phase de conception et realization du conteneur, avec ton professionnalisme, ta créativité et ta aimable disponibilité. Merci pour avoir supporté tous les changements, les longues explications des points réglementaires et sourtout... mon accent italian.

Un grande merci à Mr Lemer, Mme Chevreul et à toute la Lemer Pax pour avoir décidé de croire et d'investir en moi. Merci de m'avoir acceilli dans votre grande famille.

Thanks to all the people in Arronax, especially to Laurent, Ilyes and Nathalie, for the interesting and lightening chats, for your availability to answer to all my questions, but also for the gossip, the laughs, the rides to the bus stop and the your truly friendly smile.

Thanks to the MEDICIS-Promed team, and in particular to Thierry, Thomas and Cristina to have put all their professional soul in this project. I'm very proud to have been part of this amazing Network. It formed my personality and gave me the chance to acquire new skills and to be more confident about the possibility and the dreams of young minds. All the trainings, the events and the walks on the snow or the bike runs will remain as photos printed in my mind.
Thanks to all the ESRs for the complicity. I found in you not only smart and professional people but also great friends. I wish you all the best for your carrer. If one day you will conquer the world, and I know you will do it, ...please remember about me.

Thanks to my special friends, Roberto and Estelle. Thanks for having allowed my daily 5 minutes of complainng on French administration, weather or food. You made my days lighter and you tried to smouth all the tricky situations with positive toughts. Thanks for having been by my side in hard times and have shared with me flights, caffé, jokes. Love u guys.

Mattia, Matheusz, Etienne, Alex, thanks for your kind souls. You are the best collegues I could imagine. My "left side of the brain" is also hugging you. :-)

Let me switch in Italian to thank some other very important people.
Grazie alla mia meravigliosa famiglia, per avermi sostenuta sempre nonostante la distanza. Grazie per il coraggio e la forza che mi avete sempre donato, per aver viaggiato anche solo per portarmi un sorriso (e/o pezzi di pizza), per le coccole a casa, per i proverbi e le canzoncine inventate.

Grazie Mirko per essere stato il mio primo cheerleader, la mia spalla, il mio carburante, il mio segretario, il mio zucchero, per aver lasciato andare un pezzettino del tuo cuore tre anni fa e aver deciso di volerlo custodire per sempre.
Un ultimo grazie devo dirlo con gli occhi al Cielo, all'Angelo presente ogni sera.

If you are reading this pages this means that in one way or another, you have been part of this wonderul journey. Someone keep reminding me that "everithing in life is an experience" and this, my friends, has been a full and unforgettable one.

E come vuole la tradizione...
IO SPERIAMO CHE ME LA CAVO!

UNIVERSITE MATIERE BRETAGNE MOLECULES LOIRE ET MATERIAUX

UNIVERSITÉ DE NANTES

Titre : Aspects de radioprotection associés aux radionucléides pour applications médicales.

Mots clés : Radionucléides médicaux, radioprotection, emballages de transport, gestion des déchets

Résumé : La protection des travailleurs et du public est de primordiale importance dans toutes les phases de la chaîne de production des radionucléides, de la collecte à l'expédition, en passant par la gestion et l'élimination des déchets. Ce travail de thèse explore différents aspects de ces étapes. Les phases de la collecte dans l'installation CERN-Medicis ont été étudiées et la première idée de la chambre de collecte a été décrite.
Dans le secteur des transports, l'Agence internationale de l'énergie atomique (AIEA) établit des règles strictes en matière de respect de la conception de nouveaux emballages. De plus, lorsque les activités produites dépassent certaines limites imposées par la réglementation, des emballages spécifiques doivent être utilisés pour le transport. Ils doivent assurer une protection optimale dans des conditions de transport normales et accidentelles et sont appelés type B. Le cœur de cette étude est la conception d'un nouveau conteneur pour déplacer les échantillons irradiés du site de production aux radiopharmacies.
La conception utilise la technique des calculs de Monte Carlo pour l'analyse de la radioprotection et la technique par éléments finis pour prévoir les performances de l'emballage dans les conditions d'essai. Un prototype a été réalisé et la procédure d'homologation a commencé.
Pour certains radionucléides, les limites de transport ne sont pas tabulées et des valeurs générales sont utilisées. Une méthode utilisant des calculs de Monte Carlo a été mise en place pour recalculer ces quantités en fonction de leur risque réel. La méthode montre la possibilité d'augmenter la limite de transport pour une liste d'isotopes utilisés dans le domaine de la médicine nucléaire.
Le processus de collecte des radionucléides a comme principale conséquence la production de matériaux hautement activés à traiter et à éliminer en tant que déchets. Un outil permettant de définir correctement le niveau de dangerosité récemment développé au CERN a été adapté aux scénarios d'irradiation typiques du cyclotron Arronax.

Title : Radioprotection aspects associated to radionuclides for medical applications

Keywords : Medical radionuclides, radioprotection, transport packages, waste management

Abstract : The protection of the workers and the public is of primary importance in all the phases of the radionuclides production chain, from the collection to the shipment, but also in the management and the disposal of the waste. This thesis works explore some aspects of those steps. The phases of the collection in the CERN-Medicis facility have been studied and the first idea of the collection chamber has been outlined.
In the transport sector The International Atomic Energy Agency (IAEA) establish strict rules to respect for the design of new packages. Moreover when the activities produced exceed some limits imposed by the regulation per each radionuclides, specific containers shall be used for the transport. They must insure optimal protection in normal and accidental conditions of transport and are called type B. The core of this PhD study is the design of a new transport container to move the irradiated samples from the place of production to the radiopharmacies.
The design makes use of several techniques, as Monte Carlo calculations for radiosafety analysis and finite element techniques to foresee the performance of the package under the testing conditions. A prototype has been realized and the homologation procedure started.
For some radionuclides the transportation limits are not tabulated and general values are used to limit the activity to transport. A method making use of Monte Carlo calculations has been put in place to recalculate those quantities depending on their real hazard. The method shows the possibility to increase the transport limit for a list of isotopes used in the field of nuclear medicine.
The process of radionuclides' collection has as main consequence the production of highly activated materials to be treated and disposed as waste. A tool for a proper definition of the level of hazard recently developed at CERN has been customized for irradiation scenarios typical of the Arronax cyclotron.